Immunochemical and Chromatographic Methods for Two Anthropogenic Markers of Contamination in Surface Waters: Caffeine and Coprostanol

Dissertation
zur Erlangung des akademischen Grades
doctor rerum naturalium
(Dr. rer. nat.)
im Fach Chemie
eingereicht an der
Mathematisch-Naturwissenschaftlichen Fakultät I
der Humboldt-Universität zu Berlin
von

Apotheker José João Dias Carvalho

Präsident der Humboldt-Universität zu Berlin
Prof. Dr. Jan-Hendrik Olbertz
Dekan der Mathematisch-Naturwissenschaftlichen Fakultät I
Prof. Dr. Andreas Herrmann

Gutachter/innen:

1. Prof. Dr. Ulrich Panne
2. Priv.-Doz. Dr. Michael G. Weller
3. Priv.-Doz. Dr. Rudolf J. Schneider

Tag der mündlichen Prüfung: 12.04.2011

This page intentionally left blank.

Die vorliegende Arbeit wurde im Zeitraum von Oktober 2006 bis März 2010 im Arbeitskreis von Prof. Dr. Ulrich Panne, Institut für Chemie, Humboldt-Universität zu Berlin durchgeführt.

This page intentionally left blank.

Dedicated to my great-uncle José Fernando Coelho de Sousa,

whom I never met.

This page intentionally left blank.

Zusammenfassung

Koffein (1,3,7-Trimethylxanthin) und Coprostanol (5β-cholestan-3β-ol) wurden im Berliner Oberflächenwasser nachgewiesen. Ihre Konzentrationen korrelierten mit dem Verunreinigungsgrad der Proben, was nahelegt, dass sie sich als Marker für menschliche Aktivität eignen. Bemerkenswerterweise wurde Koffein in jeder einzelnen Oberflächenwasserprobe oberhalb der Bestimmungsgrenze von 0,025 µg/L gefunden.

Um Oberflächenwasserproben in größeren Serien zu untersuchen, war die Entwicklung zweier neuer Methoden erforderlich: ein Immunoassay, basierend auf einem monoklonalen Antikörper für Koffein und eine dispersive flüssig-flüssig Mikroextraktionsmethode (DLLME), gefolgt von Flüssigkeitschromatographie gekoppelt mit Tandem-Massenspektrometrie (LC-MS/MS) für Coprostanol.

Der entwickelte Koffein-Immunoassay zeigt die beste je erhaltene Nachweisgrenze für Koffein (0,001 µg/L), erlaubt Hochdurchsatz-Analysen und erfordert keine Probenvorbereitung. Der Assay wurde auch erfolgreich für die Messung von Koffein in Getränken, Haarwaschmitteln, Koffeintabletten und menschlichem Speichel angewendet.

Antikörper gegen Coprostanol sind nicht kommerziell erhältlich. Eine neue Strategie Anti-Coprostanol-Antikörper zu generieren wurde erarbeitet, die eine analoge Verbindung – Isolithocholsäure (ILA) – als Hapten verwendet, mit der eine Gruppe von Mäusen immunisiert wurde. Ein polyklonales Anti-ILA-Serum wurde produziert, welches Coprostanol bindet, aber die niedrige Affinität erlaubte nicht den Aufbau eines Immunoassays, der die Messung von Umweltkonzentrationen des Anayten (im Bereich ng/L) zulässt. Spezifische Anti-ILA-Immunglobuline G wurden auch in den Faeces der Mäuse gefunden.

Coprostanol wurde in den Wasserproben durch die Verwendung einer neuentwickelten LC-MS/MS-Methode unter APCI-Ionisation (atmospheric pressure chemical ionisation) gemessen. Konzentrationen oberhalb von 0,1 µg/L wurden nach Voranreicherung der Probe mittels DLLME bestimmt. Diese Extraktionsmethode erwies sich auch als geeignet für die Anreicherung von Coprostanol-ähnlichen Verbindungen wie Cholesterol, Cholestanol, Cholestanon, Ergosterol und Stigmasterol.

This page intentionally left blank.

Abstract

Caffeine (1,3,7-trimethylxanthine) and coprostanol (5β-cholestan-3β-ol) were detected in samples of Berlin's surface water. Their concentrations correlated with the contamination status of the samples, suggesting their usefulness as markers of human activity. Remarkably, caffeine concentrations were always well above the limit of quantitation of 0.025 µg/L.

In order to screen surface water samples in larger series, the development of two novel methods was required: a monoclonal antibody-based immunoassay for caffeine and a dispersive liquid-liquid microextraction (DLLME) method, followed by liquid chromatography tandem mass spectrometry (LC-MS/MS) for coprostanol.

The caffeine immunoassay developed shows the best analytical limit of detection (LOD) obtained so far for caffeine (0.001 µg/L), allows high-throughput analysis, and does not require sample pre-treatment. The assay was also successfully employed to measure caffeine in beverages, shampoos, caffeine tab-lets, and human saliva.

Antibodies to coprostanol are not commercially available. A new strategy to generate anti-coprostanol antibodies was elaborated using an analogous compound as hapten – isolithocholic acid (ILA) – and immunizing a group of mice. A polyclonal anti-ILA serum was produced, which binds coprostanol but the low affinity did not permit setting up an immunoassay to measure environmental concentrations of the analyte (in the range of ng/L).

Specific anti-ILA immunoglobulin G were also found in the faeces of the immunized mice.

Coprostanol was quantified in the water samples using a newly developed LC-MS/MS method using atmospheric pressure chemical ionisation (APCI). Concentrations above 0.1 µg/L were determined after sample preconcentration using DLLME. This extraction method also proved to be successful for enrichment of coprostanol-related compounds such as cholesterol, cholestanol, cholestanone, ergosterol, and stigmasterol.

This page intentionally left blank

.

Contents

This page intentionally left blank

Abbreviations and acronyms

Ab	Antibody
Ag	Antigen
APCI	Atmospheric pressure chemical ionisation
BALB/c	Bagg Albino (inbred research mouse strain)
BSA	Bovine serum albumin
CAS	Chemical abstracts service
CE	Capillary electrophoresis
^{13}C-NMR	13 Carbon nuclear magnetic resonance spectroscopy
COP	Coprostanol
CV	Coefficient of variation
CZE	Capillary zone electrophoresis
DCC	Dicyclohexylcarbodiimide
DLLME	Dispersive liquid-liquid microextraction
DMF	N,N-Dimethylformamide
DMSO	Dimethyl sulfoxide
DOF	Degrees of freedom
DSC	Differential Scanning Calorimetry
e.g.	*Latin: exempli gratia* (for example)
EDTA	Ethylenediaminetetraacetic acid
EEA	European Environment Agency
EIA	Enzyme immunoassay
ELISA	Enzyme-linked immunosorbent assay
EMeA	European Medicines Agency
EMIT	Enzyme modulated immunotest
EPA	Environmental Protection Agency (U.S.A.)
ESI	Electrospray
EU	European Union
Fab	Antigen-binding fragment
Fc	Crystalizable (constant) fragment
FCS	Fetal calf serum
Fv	Variable fragment
GC-MS	Gas chromatography-mass spectrometry
H chain	Heavy chain (immunoglobulin)
HAT	Hypoxantine, aminopterin and thymidine medium (Hyb selection medium)
HILIC	Hydrophilic Interaction Chromatography
^{1}H-NMR	Proton nuclear magnetic resonance spectroscopy
HRP	Horseradish peroxidase
Hyb	Hybridoma
i.e.	*Latin: id est*. (that is)
IA	Immunoassay
IC50	Inhibition concentration. Concentration that is required for 50% inhibition *in vitro*
IEF	Isolelectric focusing
Ig	Immunoglobulin
ILA	Isolithocholic acid
L chain	Light chain (immunoglobulin)
LA	Lithocholic acid
LC-MS/MS	Liquid chromatography-tandem-mass spectrometer
LDC	Limiting dilution cloning
LLE	Liquid-liquid extraction

MAb	Monoclonal antibody
MALDI	Matrix-assisted laser desorption ionisation
NHS	N-hydroxysuccinimide ester
NSB	Non-specific binding
o/n	Over night
OD	Optical density
OVA	Ovalbumin, albumin from egg-white
OWCs	Organic wastewater contaminants
PAb	Polyclonal antibody
PBS	Phosphate buffered saline
PEG	Polyethylene glycol
PPCPs	Pharmaceutical and personal care products
QC	Quality control
RIA	Radioimmunoassay
RSD	Relative standard deviation
RT	Room temperature, 20°C
SD	Standard deviation
SPE	Solid phase extraction
SPME	Solid phase microextraction
STP	Sewage treatment plant
STW	Sewage treatment works – same as STP
TBS	Tris buffered saline
TMB	3,3',5,5'-tetramethylbenzidine
TOF/MS	Time-of-flight mass spectrometry
USGS	United States Geological Survey
vs.	*Latin: versus* (against, turned)
WFD	Water framework directive
WTP	Water treatment plant
WWTP	Wastewater treatment plant

1. Introduction

"The history of men is reflected in the history of sewers (…) it has been a sepulchre, it has served as asylum, crime, cleverness, social protest, the liberty of conscience, thought, theft, all that the human law persecute or have persecuted is hidden in that hole"

Victor Hugo, Les Misérables, 1892

1.1. Pharmaceuticals in surface water

1.1.1. Brief historical review

Civilizations have always formed around water supplies. The importance of water quality for drinking and other purposes was clear to our ancestors, although an understanding of water quality had neither been well known nor documented.[1] One of the first written recommendations in the field of water treatment dates from approximately 4000 B.C., with text in Sanskrit and Greek advising filtration through charcoal, sunlight exposure, boiling and straining.[2] At that time, visible turbidity was the treatment driving force since many waters contained particulates which imposed an objectionable taste and appearance to water.

Several improvements in water treatment have been made through the centuries until the early 1800s, when slow sand filtration began to be used regularly in Europe.[2,3] The turn of the 18th to the 19th century represented a major breakthrough for humankind – the industrial revolution. Major changes in agriculture, manufacturing, mining, transport, health and technology had a profound effect on the peoples' life, mainly in Europe and North America. The concentration of population in and around the cities brought about major progresses in water supplies, waterborne diseases awareness and water treatment. The London cholera outbreaks in 1831, 1848 and 1854 represent the starting point for enormous changes in water treatment technology and water distribution improvements.[4] The inhabitants of the Victorian London were supplied by water pumped out from different locations of the Thames.[5] It took more than 10 years until the epidemiologist John Snow was able to correlate the number of cholera cases with some particular pumps, like the famous one in Broad Street (currently Broadwick

Street), which was responsible for the most deaths during the 1853 outbreak.[5,6] Snow could thus demonstrate that cholera was being spread through contaminated water collected from locations on the Thames' river banks where wastewater was being discharged upstream. Ten thousand people died[7] and many others left London, which provoked a wave of panic described by the German poet Heinrich Heine from Paris during the 1831-32 epidemics: "It was as if the end of the world had come. The people fell on the victims like beasts, like maniacs."[8,9]

It was then clear that a waterborne organism was the cause of such mortality and that water treatment needed to be improved far beyond the good taste, good appearance and visible characteristics. The widespread use of the microscope and the "germ theory" of Louis Pasteur (~1880s), which explained how microscopic organisms could transmit diseases through water, opened the way to the use of disinfectants such as chlorine.[3] Turbidity was no longer an exclusive aesthetic problem: particles in source water, such as faecal matter, could harbour pathogens. Additionally to sand filtration, chlorination started to be used in the early 1900s in Europe and in the USA.[1] The concerns about drinking water quality during the early twentieth century were mostly focused on disease-causing microorganisms in water systems and disinfection methods using chlorine and ozone.[2] Disinfectants have been largely applied ever since to prevent the distribution of diseases and to improve water quality.

Combining filtration with chlorine, which supposedly eliminated waterborne enteric disease, had an unfortunate consequence: the quality of the water source was something of less importance, succumbing to the expedient of developing lower-cost polluted river sources and providing thereafter filtration and chlorination. Most industrial cities at that time started to pump out water from the nearby water sources, despite having better-quality options within a reasonable distance, though at higher costs.[10] As microorganisms causing enteric disease were under control and cancer as well as reproductive dysfunction were not well-known and understood, major concerns regarding water quality lay dormant until the chemical revolution.

The technical improvements during World War II brought about a chemical revolution: thousands of synthetic organic compounds were designed with the aim to be toxic to biota but also long lasting after their application. The fact that these compounds could reach environmental waters was at that time unknown and had been slowly recognised.[10]

The discovery of the insecticidal effect of DDT (dichlorodiphenyltrichloroethane) by Paul H. Müller in 1939, marks the beginning of the modern chemical industrial revolution and a turning point in public health, agriculture and (later recognised) environmental sciences.[11] The immediate success of DDT in controlling typhus, malaria and yellow fever during World War II was a stunning example of what humans could exercise over disease. Malaria alone claimed more than 50 million lives during the first half of the twentieth century. Synthetic pesticides became a symbol of progress during the post-war years and provided a level of control over environmental risk. Their benefits were easily recognised by the number of lives saved, the crop yields increase, the soil loss decrease and the economic growth.[11] Their setbacks were only disclosed years later after another revolution in chemistry: the analytical one.

"To only a few chemicals does man owe as great a debt as to DDT... In little more than two decades, DDT has prevented 50 million human deaths due to malaria, that otherwise would have been inevitable."

National Academy of Sciences (USA), Committee on Research in the Life Sciences, 1970

The commercialisation of HPLC and GC instruments in the 1960s and 1970s was the decisive contribution to identifying some synthetic compounds like pesticides and the disinfection by-products resulting from water treatment.[12]

The pioneer works of the botanist Mikhail Tsvet (also known as Tswett) in the beginning of the 20th century founded the basis of what is known nowadays as liquid chromatography.[13,14] It took more than 60 years until the first commercial instrumentation was presented to the scientific community during the 5th Symposium on “Advances in Chromatography” (Miami, 1969).[12] Two years later, the first book on HPLC was published by Wiley[15] and the 1970s witnessed a milestone in analytical separation and the beginning of a successful story – the widespread use of HPLC.

Gas chromatography (GC) has a similar story.[16] Albeit that the first experiments with GC had been already performed in the 1950s (James and Martin, 1954),[17] only in the late 1970s the first insights on disinfection by-products in treated drinking water came to light.[18] Achievements have been done ever since until the rather recent recognitions of their hazard to human health,[19,20] their effects on abortion[21] and fertility.[22]

"An essential condition for a fruitful research is to have at one's disposal a satisfactory technique. Any scientific progress is progress in the method."

Mikhail Semyonovich Tsvet (Tswett), The life and scientific works of Michael Tswett, 1972[14]

The last documented revolution was the sociological one. The 1960s was the decade of the rock' n' roll affirmation, the sexual revolution, the birth control pill and the articles by the American marine zoologist Rachel Carson. First published in an article of the New Yorker in June 1962,[23] Silent Spring rang the bell about the impact of DDT on human health and the environment. Published as a book the same year, Silent Spring[24] was a bestseller at the time and it is still a mandatory book for environmental scientists. It brought environmental questions to the public agenda, gave the forewarning in global warming, led to the ban of DDT in the USA and made Rachel Carson an environmental icon. The beginning of an intense research field had just been started – the fate of pesticides residues in the environment.

"Can anyone believe it is possible to lay down such a barrage of poisons on the surface of the earth without making it unfit for all life? They should not be called insecticides but biocides." (About the DDT spraying).

Rachel Carson, Silent Spring, 1962[24]

The recognition of the impact of the birth control pill (containing estrogens) as well as other pharmaceuticals on the environment only started in the early 1980s. This story began when grossly hermaphrodite (intersex) fish were found in the settlement lagoons of two sewage treatment plants (STPs) in England (unpublished observations).[25] These settlement lagoons were receiving effluent from a major STP, prior to entering a river, thus suggesting that exposure to effluents could have profound effects on fish. It was later shown that STP effluent was estrogenic to fish.[26] These observations initiated a new research field in the 1980s about the effects of effluents in sex determination and partial or complete sex change in aquatic organisms.[25,27] Androgenic activity of effluents was firstly observed by Howell *et al.* in Florida mosquitofish (Gambusia affinis) in the late 1970s.[28,29] They observed that all female fish were strongly masculinised, displaying both physical

secondary character and reproductive behaviour of males. The effluent was from a paper mill and only 20 years later, laboratory studies showed – using an androgen-dependent bioassay – that exposure to paper mill effluents induced androgenic activity.[30] Yet, the compound or mixture of compounds responsible for this androgenic activity still remains unknown.[31]

From the first observation of imposex in molluscs attributed to the aquatic environmental contamination (caused by tributyltin) in 1970[25] until the observations of alligators feminisation in some lakes in Florida,[32] 30 years of research were invested.

"All females are strongly masculinised, displaying both physical secondary sex characters and reproductive behavior of males. Males exhibit precocious development of physical sex characters and reproductive behavior. This constitutes the first report of possible environmental-induced masculinization involving a total natural population of vertebrates"

Mike Howell et al., Copeia, 1980[29]

The detection of salicylic acid and fibric acid (a metabolite of several lipid regulating agents) in Kansas city in 1977 showed that pharmaceuticals and their residues could be found in municipal sewage treatment plant (STP).[33] But evidence that they could reach the aquatic environment only started to be given in the beginning of the 1980s with the investigations conducted by the UK Water Research Centre and the Thames Water Authority.[34,35] Even though the exact concentrations were never mentioned, the studies revealed that drugs were present in surface waters in concentrations up to 1 µg/L.

Finally, in 1996 Thomas Heberer and co-workers from the TU Berlin presented in Vienna[36] the conclusion of their studies on surface and groundwater in Berlin: they found several pharmaceutical residues up to 1.9 µg/L (being diclofenac, ibuprofen, propiphenazone and clofibric acid the most frequently detected ones). They analysed 30 representative surface waters from rivers, lakes and channels in Berlin and a few groundwater samples used for drinking water production, where some polar pharmaceutical residues were also found.[36,37]

Almost simultaneously – the investigation was performed between 1995 and 1997 – Thomas Ternes studied the occurrence of 32 drug residues (less than 1% of the pharmaceuticals approved for human medical treatment in Germany at that time)

from different pharmacotherapeutic groups, as well as some metabolites in German municipal STP discharges, rivers and stream waters.[38] His data showed that STP were unable to efficiently remove some of these compounds, having found concentrations in the ng/L range in surface waters but in some cases reaching 3 mg/L (bezafibrate). The stability of some pharmaceuticals, their metabolites and also conjugation products (from phase II metabolism), was shown and a new race in environmental chemistry had just started – the search for pharmaceuticals in environmental waters.

Albeit several groups were conducting research in the field of pharmaceutical residues at that time, it was the study from the United States Geological Survey (USGS), published in 2002,[39] that gave the alert and boosted this new research field. The study from Kolpin *et al.* showed for the very first time the ubiquitous presence of 95 organic wastewater contaminants (OWCs), including pharmaceutical residues, in 80% of the 139 water streams, across 30 American states (Figure 1), sampled during 1999 and 2000.

The most frequently detected compounds were coprostanol (faecal steroid), cholesterol (plant and animal steroid), N,N-diethyltoluamide (insect repellent), caffeine (stimulant), triclosan (antimicrobial disinfectant), tri(2-chloroethyl)phosphate (fire retardant), and 4-nonylphenol (non-ionic detergent metabolite). Caffeine was detected in 62% of the samples with concentrations ranging from 0.015 µg/L to 6.0 µg/L (average concentration: 0.081 µg/L); and coprostanol in 85% with concentrations ranging from 0.005 µg/L to 150 µg/L, (average concentration: 0.088 µg/L).

Figure 1. Location of the 139 stream sampling spots used in the USGS study, published in 2002. Adapted from Kolpin et al., Environ. Sci. Technol. (2002) 36: pp 1202-1211.[39]

"The primary objective of this study is to provide the first nationwide reconnaissance of the occurrence of a broad suite of 95 OWCs, including many compounds of emerging environmental concern across the United States"

Dana K. Kolpin et al., Environ.Sci. Technol., 2002[39]

A major conclusion from the USGS study was that almost no data were available concerning pharmaceuticals metabolites to fully understand the fate and transport of OWCs in the hydrologic system as well as their ultimate overall effect on human health and the ecosystem. Ever since, the number of publications covering the presence of pharmaceuticals and their metabolites has increased sharply as displayed in Figure 2.

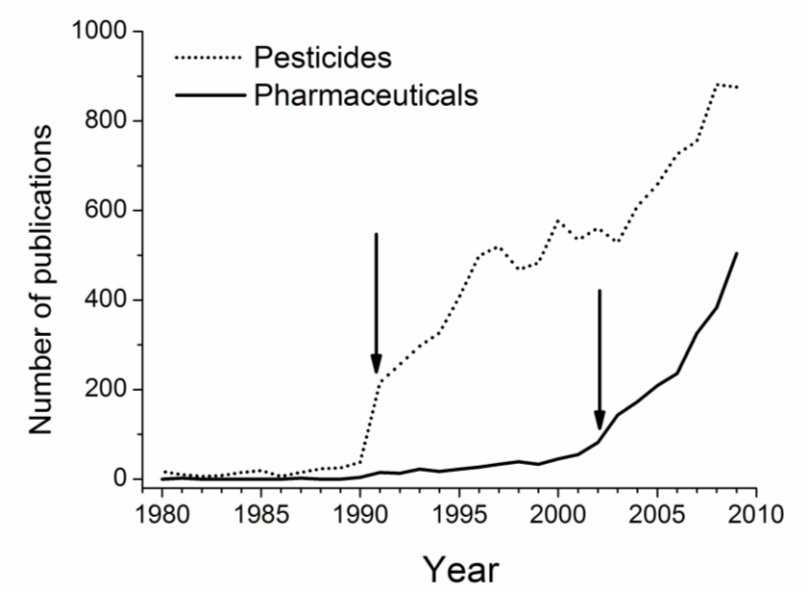

Figure 2. Number of publication per year (1980-2009) when searching the on-line database ISI Web of Knowledge[40] for "pesticides in water" (doted line) and "pharmaceuticals in water (bold line). The arrows represent an exponential increment in the publications number when compared to the previous year: 1991 (+450% publication in pesticides) and 2002 (+75% publication in pharmaceutical). The data was obtained on September 22nd 2010.

It did not take a long time until pharmaceuticals and personal care products (PPCPs) were detected in drinking waters all over the world: Germany,[41-43] South Korea,[44] USA,[45,46] Australia,[47] Japan,[48] Italy,[49]Thailand[50] and many others.

The reason why research concerning the detection of pharmaceuticals in water samples did not follow the trend of the research on pesticides is because the scientific community and regulators realised very soon the problems they would face and maybe we all have learned some lessons from the past. Closing the pump like during the cholera outbreaks is not possible this time and banning some pharmaceuticals based on ecological data will raise other question, i.e. it will be very difficult, for example, to withdraw the efficient anti-tumour drug cisplatin from the market based on some still unconvincing ecological data.[51-53] Additionally, the number of molecules used in human and animal's therapeutics surpasses by some thousands the number of pesticides in use.

1.1.2. Analytical challenge and regulations

Currently, Germany has about 50,000 drugs registered just for human use, 2700 of which represent 90% of the total consumption (900 different active substances).[54,55] Are analytical chemists able to develop methods for all these compounds and their metabolites? It is certainly feasible. Are environmental toxicologists able to provide data about the impact of these substances, metabolites and conjugates on the ecosystems? Maybe… Are epidemiologists able to show the impact of these compounds and the synergistic effect of their mixtures in human health? It would certainly take a large effort in terms of money, time and manpower to accomplish such tasks and to produce consistent data.

If Queen Victoria had waited until *Vibrio cholerae* had been identified as the cause of the deaths during the London cholera epidemic, thousands of more human lives would have been lost. Indeed, as soon as the contaminated pumps were identified, she demanded their immediate closing, a kind of measure that cannot be taken with pharmaceutical residues.

The European Union, which is leading the process in term of legislation, released in 2006 an important guideline asking for environmental risk assessment (ERA) studies for every new medical product designed for human use.[56] Pharmaceutical companies submitting a new marketing authorisation application to the European Agency for Medicines (EMeA), now have to provide an environmental risk assessment report. Nonetheless, thousands of compounds already present on the market are not affected by this regulation.

Most EU countries are simply performing the minimum required risk assessments, but some have gone further. With the program START[a], Germany has brought together pharmaceutical companies, researchers, politicians and others in order to explore ways to reduce contamination of waterways.[57,58] In an effort to reduce pharmaceutical impact on the environmental, Sweden created a database for physicians where pharmacologically active substances are classified according to their potential environmental hazards. At the moment of prescribing a treatment to their patients, Swedish physicians can select a “greener” alternative – when available – with similar pharmacological effect.[59]

[a] *START - Strategien zum Umgang mit Arzneimittelwirkstoffen in Trinkwasser. (Management Strategies for Pharmaceutical Residues in Drinking Water)*

Additional measures were proposed by Ternes from the German Federal Institute of Hydrology (BfG) and Joss and Siegrist from the Swiss Federal Institute for Environmental Science and Technology (Eawag).[60] They proposed four measures including for example the separation of hospital wastewater systems from the domestic ones, and a separate system for collecting the urine[61] – as most of pharmaceutical residues are excreted via urine. They concluded however that such measures require strong political decisions, acceptance from the population, money for new infrastructure, and decades to be implemented.

In the meantime, other solutions are needed to tackle the problem posed by PPCPs in environmental waters:

1) Selection of specific PPCPs for the water monitoring programs;[62,63]

2) Computer-based modelling for environmental fate prediction;[57,63-66]

3) Use of chemical markers from human, hospital and pharmaceutical industry wastewater input in waters.[67-70]

Using source-specific chemical markers presents some advantages over the two other options. Computer-based modelling, although very useful, only allows for environmental predictions based on known, sometimes very old, information regarding the physico-chemical properties of the compounds and their metabolism in humans, animals, and *in vitro* experiments. These models also assume that similar substances would have similar effects on the environment, which is not always true.[71] And similarity is a very imprecise concept in ecotoxicology. In brief, several risky assumptions have to be made prior to use modelling programs, like the following ones[65]: metabolism or breakdown of the drug within humans or the sewage system do not occur; an average 10-fold dilution of sewage effluent in river water, pharmaceuticals do not adsorb to organic or inorganic colloidal material or bacterial biomass in STPs or natural waters.

Selecting specific PPCPs for the water monitoring programs is proposed by many authors[62,63] but, also here some issues are of concern and questions need to be answered. Which PPCPs should be monitored? The most frequently detected ones? The most concentrated ones? The less biodegradable ones? The most toxic? And toxic to whom, the ecosystem or to humans?

Drugs such as diclofenac (anti-inflammatory), ibuprofen (anti-inflammatory), carbamazepine (anti-epileptic), clofibic acid (metabolite of several blood lipid regulators) are present in quantifiable concentrations (ng/L to the µg/L range).

Others such as cyclophosphamide and cisplatin (cytostatic agents), being very toxic and passing unchanged through the STPs, are mostly undetected in the environment due to their low concentrations.[62]

An additional drawback of this option is how to launch a future European regulation for the entire EU: while in Germany 900 compounds represent 90% of the market, the UK has about 3000.[54,55] And consumption patterns, even for the same molecule, are different. Nimesulide, an anti-inflammatory drug that has been present on the market for 25 years is a good example for a comparison at the European level. Even though the polemic regarding fatal liver damage is still going on, nimesulide was already withdrawn from the market in Sweden, Ireland and Germany. But it remains available in most EU countries and Switzerland, and the European Agency of Medicines released a communiqué in 2007 and again in 2009 supporting the use of nimesulide.[72,73] It is true that nimesulide cannot be purchased from a neighbourhood pharmacy in Germany, but it can quickly be bought over the internet.

By the facts exposed, it is easily comprehensible why the EU did not hitherto include any pharmaceutical in the list of priority substances[74] appended to the Water Framework Directive of 2000.[75] An agreement on which substances should be included in it is likely to take some years.

Source-specific chemical markers have been suggested for tracking OWCs in natural waters, including PPCPs.[76-81] They have even been proposed as a more reliable alternative to microbiological indicators.[82-85] Indeed, once released in rivers with strong anthropogenic activity impact, like the Seine for example, microbiological indicators disappeared relatively rapidly due to mortality (protozoan grazing, lysis) or loss of cultivability induced by stress conditions (sunlight effect, nutrient concentration, temperature).[83] Chemical markers offer in addition to stability, and what is maybe their biggest advantage over biological indicators, a shorter analysis time when compared with the typical microbiology culturing techniques, which can take between 18 to 96 h.[86] Caffeine[67] and coprostanol[87-89] are two of these chemical markers and were the ones selected for this PhD project and thus discussed in detail in the next pages.

1.2. Caffeine and coprostanol as anthropogenic markers for pharmaceuticals input in environmental water

1.2.1. Caffeine and coprostanol as markers

Caffeine (1,3,7-trimethylxanthine) is the most widely used psychoactive substance in the world today.[90] It can be found in a variety of sources, the most well-known being coffee, tea, cocoa, soft-drinks, energy drinks, pills and chocolate.[91-93] Nowadays, it can also be met in beers, shampoos, anti-headache formulations,[92] seawater[94], surface water,[67] drinking water,[46] and rainwater.[95]

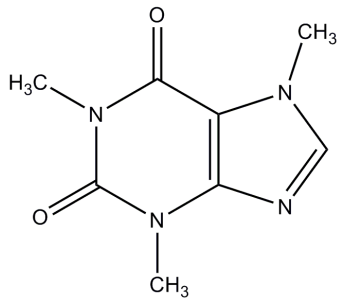

Figure 3. Caffeine (1,3,7-trimethylxanthine).

The high consumption of caffeine by most of the world's nations, especially in urban areas, lead to caffeine becoming an environmental marker of human contamination.[67,68,82,96,97] The presence of caffeine and elevated nitrate concentrations has been shown to be associated with anthropogenic input around population centres,[98] whereas some bacterial indicators did not correlate to these chemical indicators and appeared to have non-human sources.[67,82] Furthermore, its presence in urban areas was linked to faecal coliform abundance[84,96] and some authors have been suggesting the use of caffeine as an indicator for drinking and recreational water quality since the use of bacterial indicators requires a time-consuming culture test.[82]

In the past decade, the identification of pharmaceuticals in surface,[38,99,100] ground[101] and drinking water[37,49,99] raised attention from the environmental chemistry community and it was a reminder that people's drinking water was once another community's wastewater.[102] The USGS study conducted to evaluate the presence of these compounds[39] exposed two important facts: the presence of several pharmaceuticals in watersheds is widespread; and the difficulties that laboratories and national agencies responsible for water quality would face if they intended to monitor thousands of these active substances in a water body. Caffeine was found in most of the studies where pharmaceuticals were monitored: in wastewater effluents,[68,103-106] surface waters,[107,108] groundwater,[98,109] drinking water,[110] alpine mountain spring water, rainwater,[49] untreated[46] and treated

drinking water.[49] Consequently, caffeine seems to be a serious candidate to become a chief marker for pharmaceuticals input in natural waters.[67,68]

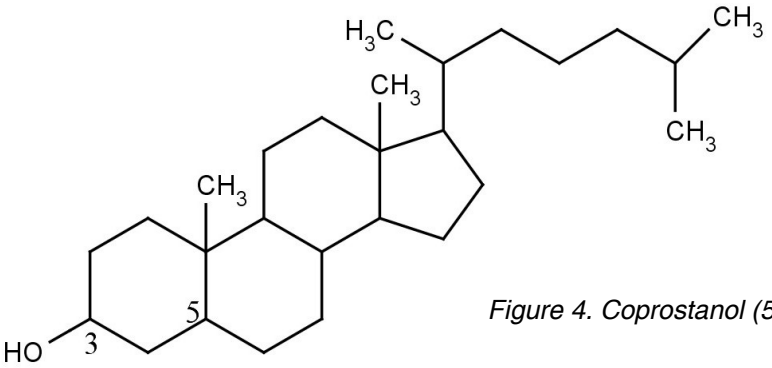

Figure 4. Coprostanol (5β-cholestan-3β-ol).

Opposite to caffeine, the use of coprostanol (5β-cholestan-3β-ol) as a marker of anthropogenic contamination is not newfangled.[76,111,112] It has been in use since the 1960s[113] mainly to access human input in marine and coastal waters,[77,112,114] extreme conditions making it difficult to use bacterial growth as contamination marker.

Recently, it has been revived as a marker for OWC due to some restriction in using faecal bacteria indicators. Because the ecological and survival characteristics of bacterial, viral and parasitic pathogens vary under environmental conditions, the use of faecal indicators such as coprostanol is an uprising alternative.[82,83,113,115] Like caffeine, coprostanol is a source specific indicator but not exclusive for humans. As a product of the cholesterol metabolism in mammals,[116,117] coprostanol also allows to track cattle farming in receiving waters.[79,88,118] The combined use of caffeine and coprostanol could be useful to distinguish between solely human from mammals' input into the waters.

Cholesterol is a widespread sterol in nature and its presence in waters does not necessarily mean contamination.[119] Only its faecal metabolite coprostanol, which is a result of enzymatic conversion by some bacterial microflora exclusively present in mammals gut does.[116]

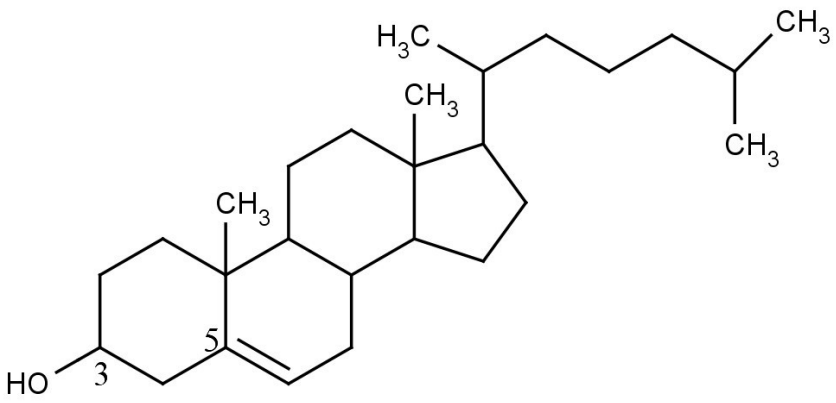

Figure 5. Cholesterol (5-cholesten-3β-ol).

1.2.2. Analytical methods to quantify caffeine – state of the art

Several methods have been proposed to detect and quantify caffeine, mostly in beverages: capillary zone electrophoresis,[120] gas chromatography coupled with mass spectrometry[121,122] or nitrogen-phosphorous detector,[123] liquid chromatography with UV detection[124] or mass spectrometric detection,[125] Fourier transform infrared spectrometry,[126] solid-phase Fourier transform–Raman spectrometry,[127] solid-phase ultraviolet sensing,[128] square-wave voltammetry[129,130] and a caffeine selective electrode.[131] The major concern seems to be matrix effects and therefore almost all of the described methods make use of sample preparation techniques with different degrees of complexity, associated costs and time requirement. It seems that an Enzyme-Linked Immunosorbent Assay (ELISA) has never been proposed to quantify caffeine in water samples without requiring any previous clean-up or extraction step.

For water samples, achieving low limits of detection seems to be the driving force when an analytical method is being developed. Solid-phase extraction (SPE) followed by liquid chromatography tandem-mass spectrometry[39,44,104,125,132-134] or gas chromatography[68,84] are the most widely used methods to determine caffeine in water samples. The limits of detection achieved are in the order of 0.002 µg/L, when an enrichment factor of 1000 is used for pre-concentration of the samples.[67]

A radioimmunoassay was developed in the 1970s to measure caffeine in plasma and saliva in concentrations higher than 25 µg/L.[135] An automated enzyme immunoassay (EMIT) became commercially available in the 1980s (from Syva) and

showed a cross-reactivity of 28% of paraxanthine (caffeine's main metabolite) in the range 0.5-155 mg/L.[136] Despite the high cross-reactivity, the assay seemed to be suitable for clinical purposes and the results correlated well with those obtained by HPLC in the mg/L range tested.[136,137] Some other assays have been developed ever since but all of them aimed at biological samples containing microgram to milligram per litre of caffeine.[138-141]

In the present work, a new immunoassay for caffeine is described using a commercially available antibody selected from one polyclonal and two monoclonal antibodies, and a *de novo* synthesised enzyme tracer.

The reference SPE-LC-MS/MS method for caffeine is just briefly described (6.7 - Reference method for caffeine, page 83) as it brings no major improvements to published works.[44,134,142,143]

1.2.3. The stanols analytical challenge

Coprostanol and related stanols are analytically challenging when compared to caffeine and related xanthines. They are non-polar, do not absorb in the UV/Vis range, lack fluorophore groups as well as easily ionisable ones required for ESI mass spectrometry (MS) detection.

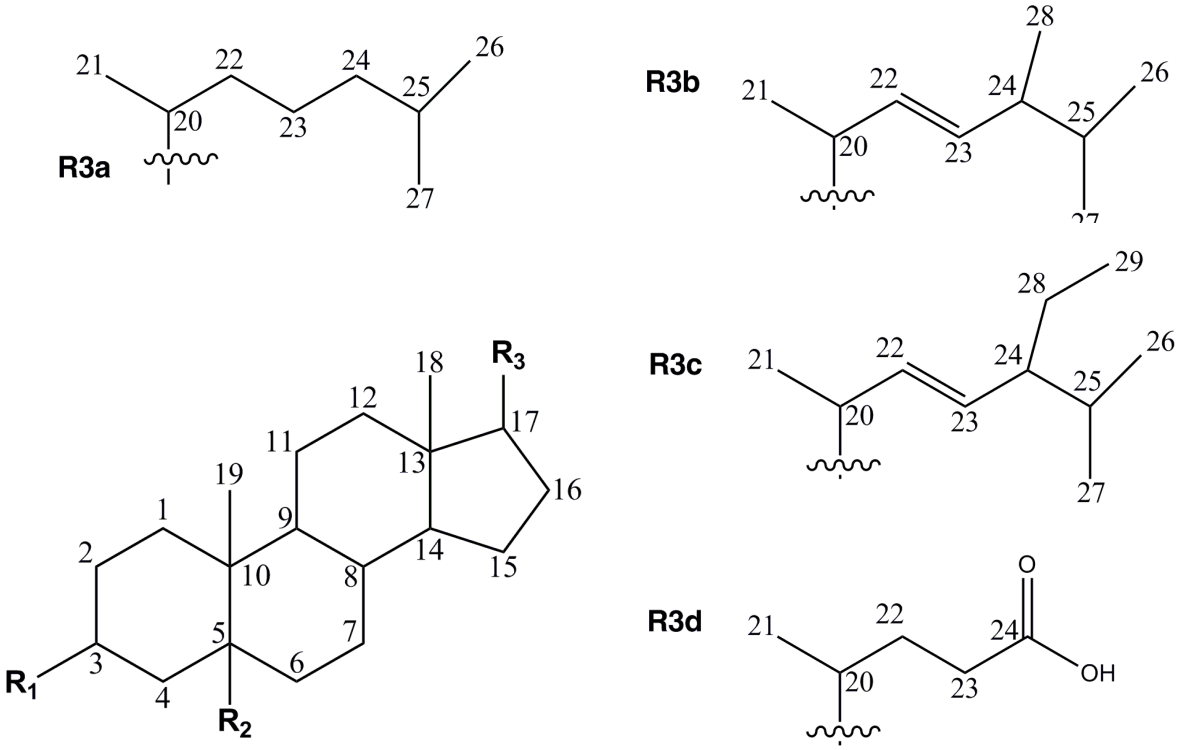

Compound	R1 (C3)	R2 (C5)	R3 (C17)	C-C Double bond(s) position
Coprostanol	β - OH	β - H	β – R3a	-
Cholestanol	α - OH	β - H	β – R3a	-
Cholesterol	β - OH	-	β – R3a	C5 – C6
Ergosterol	β - OH	-	β – R3b	C5 – C6 C7 – C8 C22 – C23
Stigmasterol	β - OH	-	β – R3c	C5 – C6 C22 – C23
Isolithocholic acid	β - OH	β - H	β – R3d	-
Lithocholic acid	α - OH	β - H	β – R3d	-
Cholestanone	O	β - H	β – R3a	-
Cholestan	H	β - H	β – R3a	-

Figure 6. Chemical structures of the sterols, stanols and bile acids referred to within this thesis.

The most used instrumental technique for analysing faecal sterols in environmental waters,[144-146] animal faeces,[88] soils,[147] food materials,[148,149] and sewage[144,150] is still gas chromatography (GC) with mass detection (MS).[88,144,147,149-151] Flame ionisation detection (FID)[149] and electron-capture detection[152] have also been successfully applied. In all cases, a derivatization of the hydroxyl groups of the analytes to their respective trimethylsilyl (TMS) esters is compulsory. In order to achieve µg/L detection level, an extraction step is additionally required to pre-concentrate the analytes,[145] making the entire procedure very laborious and time-consuming, e.g. sometimes taking more than 24h to analyse a sample.[153]

Several extraction methods have been reported including supercritical fluid extraction,[152] sonication assisted extraction,[153] Soxhlet extraction,[154] liquid–liquid extraction (LLE),[88,144,149,155] solid phase extraction (SPE),[148,156] and even recently (2010) in-tube solid-phase microextraction (IT-SPME).[145]

The analytical options for coprostanol offered by the literature are poor. This fact seems to be related with the field of application of the methods: food chemistry,[148,149] biological samples like animal faeces[88] and sewage analysis.[144,150] Sensitivity was therefore not an issue as very high concentrations of coprostanol were always present.

Contrary to caffeine, it is very difficult to assert a detection range for coprostanol by analysing the literature. It seems plausible that an instrumental limit of detection (without extraction) around 1 mg/L is achievable.[149] Methods' detection limits between 0.2 µg/L[149] and 1 µg/L in water samples have been reported[144] after sample pre-concentration. The literature is confusing regarding the way authors claim their limit of detection (LOD), an example is an extremely low detection limit of 2 ng/L after liquid-liquid extraction of surface water samples (10,000-fold concentration) with dichloromethane.[151] The limit of detection is also presented as being the same for several compounds analysed (including coprostanol, testosterone, estrone and estradiol-17β), determined by using 3 injections, by GC-MS and coprostanol was not derivatized.

One of the first HPLC methods reported for coprostanol, using a C18 column, goes back to year 2000.[156] It suggested a less laborious derivatization technique to allow its detection as coprostanyl-p-nitrobenzoate using a diode array detector (DAD) but does not mention a limit of detection. A chromatogram showing a feeble peak was however presented, obtained after injecting 25 µL of 200 mg/L coprostanol, but a

signal scale is absent, thus not allowing a proper judgment of the method sensitivity.

An LC-APCI-MS/MS method was published in 2007[148] for phytosterols separation in food samples after supercritical carbon dioxide extraction. Coprostanol was not measured but its isomer cholestanol was determined with a reported LOD of 0.13 mg/L and LOQ of 0.37 mg/L based on the peak signal-to-noise ratio of 3 and 10, respectively.

Currently available methodologies involve derivatization of the compound and several enrichment steps, which are time-consuming, expensive, and increase uncertainty in the final result due to multiple manipulations of the sample.

A demand needs to be met for reliable, highly precise and cost-efficient analytical methods to measure coprostanol in surface waters and other environmental matrices.

1.3. Immunochemical methods in Environmental Chemistry

Immunochemical methods encompass a series of analytical tools from the pioneer Radioimmunoassay (RIA)[157] to modern immunosensors[158,159] passing through the Enzyme-linked immunosorbent assay (ELISA).[160] The discussion is here restricted to ELISA with a focus on environmental chemistry and hapten-based assays. As several textbooks are available and good reviews on the state of the art exist,[158,161,162] only a summary of the technique is presented below (1.3.1, page 36). Yet, some considerations regarding immunization, antibody production and hybridoma screening methods for coprostanol are discussed in detail as this background is required to interpret the results.

1.3.1. Enzyme-linked immunosorbent assay (ELISA) at a glance

Immunoassays are based on the binding properties of antibodies (Abs) with antigens (Ags). The Ab-Ag interaction is reversible, as determined by the law of mass action, and is based on electrostatic forces, hydrogen bonding, hydrophobic, and van der Waals Forces.[163] The most commonly used type of antibody in immunoassays is the immunoglobulin G (IgG).

Enzyme-based immunoassays (EIA) offer numerous advantages over other immunotechniques because their signal is amplified by forming a large number of product molecules. They are widely used for environmental purposes, especially those based on heterogeneous conditions, such as ELISA.[163,164] The most commonly used enzymes for producing the tracer are horseradish peroxidase (HRP) and alkaline phosphase (AP).[163]

ELISAs may be carried out by using different formats, being competitive assays the most frequently used in environmental chemistry.[165,166] They can be performed in different ways, such as the analyte and the enzyme tracer competing for a limited number of antibody binding sites (direct), or the analyte and the immobilised ligand (analyte coupled to a protein) competing for a limited number of binding sites (indirect).[164] For competitive ELISA, the higher the analyte concentration in the sample, the weaker will be the observed signal. In the direct assay the analyte is coupled to the enzyme (tracer) while in the indirect one, a secondary antibody (anti-IgG) is usually labelled with the enzyme and binds to the analyte-binding antibody (immobilised). Figure 7 illustrates the two formats used within this thesis.

Many different materials can be used as support for the antibodies/antigens, from 96-wells microtitre plates[167] and aminosilane slides[168] to compact discs (CDs).[169]

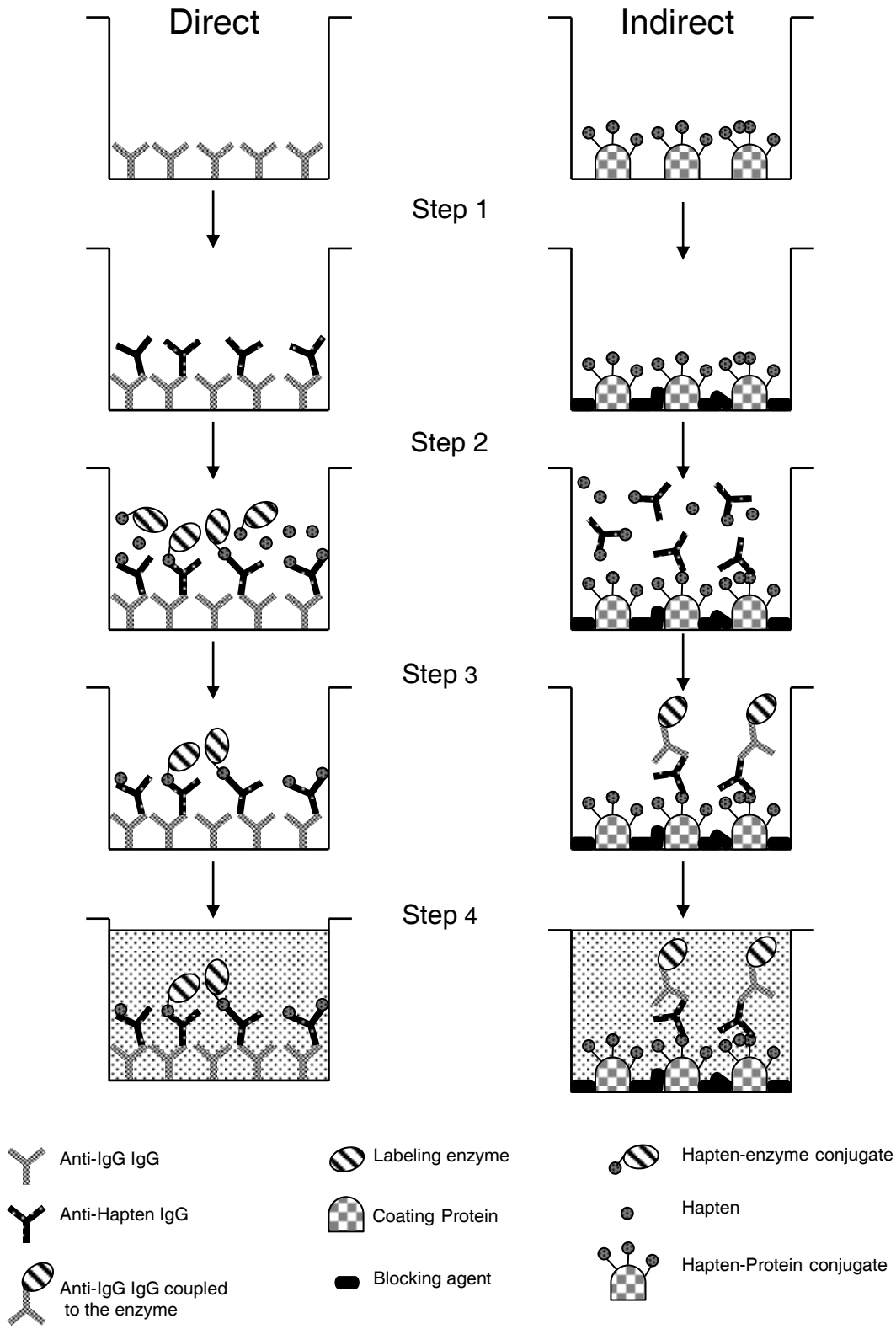

Figure 7. Competitive ELISA formats, direct (left) and indirect (right), used in this thesis. The reservoir (squared-like shape) represents a microtitre plate well.

The anti-hapten IgG (Figure 7) in the direct form can also be immobilised directly on the microtitre plate surface, as it was the case of the polyclonal anti-caffeine ELISA presented in this work. Monoclonal antibodies (mAbs) however bind only weakly to the surface and thus the plate is usually coated with an anti-IgG immunoglobulin (coating antibody or secondary antibody).[163] Assays with mAbs do not necessarily require a secondary antibody. However, when they are used, a lower concentration of the mAb is then needed, lowering the overall analytical costs.

1.3.2. ELISA – state of the art

The claim for the development of immunoassays (IAs) comes from two research groups: the first one was developing an immunoassay for insulin (Yalow and Berson, 1970)[157] while the second group was working on a binding assay to thyroxine in human plasma (Ekins, 1970).[170] Only the work of Yalow and Berson[157] is normally credited for IAs development, probably because Ekins[170] used a thyroxine binding protein (naturally occurring) instead of an antibody.

Both assays, designed for clinical applications, made use of radiolabelling (Radioimmunoassay, RIA). It took approximately 10 years until Enzyme labelling assays were proposed (EIA).[171] Clinical and medical chemistry are still today the major application fields for IAs, as a brief search on ISI Web of knowledge[40] by looking for the keywords “immunoassay” or “ELISA” for the period 2000-2010 showed.

Table 1. Number of publications per research field obtained on ISI Web of knowledge[40] on the 4th of November 2010. The keywords “Immunoassay” or “ELISA” were used for the search covering the last decade (2000-2010).

Research field	N. of Publications	% of the total
Clinical and Medical	54817	79
Chemistry multidisciplinary (incl. analytical)	9239	13
Environmental sciences and Agriculture	2177	4
Physical-Chemistry, Biophysics and Material Sciences	1710	3
Food and plants science	1704	3

Although the analysis was not extensive and details are not given here, it is certain that IAs are still mostly used for clinical purposes. Environmental and food chemistry applications seemed to be driven by compounds such as pesticides,[164,172,173] estrogens,[174,175] and toxins.[176] IAs were successfully used in

the past[177,178] to detect pesticides and estrogens and are still being developed and proposed today.[179,180]

High antibody cross-reactivities, which discouraged the commercial use of IA in the past, are being advantageously used today to detect multiple analytes as well as structurally related compounds using a single assay.[164,181,182] This is particularly interesting in the case of pharmaceutical products and their related metabolites in waters, some of them being still unknown.[181,182]

Another issue in setting pesticide immunoassays was the relatively small offer of commercial antibodies.[158,183,184] Most environmental chemists had to produce their own antibodies (Abs), which represents a laborious and costly process that often involved external partners, since animal breeders and cell-culture facilities are usually unavailable in environmental chemistry labs. On the contrary, antibodies for pharmaceutical products are widely available thanks to their previous use in clinical chemistry, e.g. for the monitoring of active substances and metabolites in biological fluids. This was for example the case for numerous pharmaceutical products like diclofenac,[185] ibuprofen,[159] sulphonamides,[186] carbamazepine,[160] and now caffeine,[167] that were quantified in different environmental waters in the ng/L range using ELISA.

As the bottleneck caused by the availability of suitable antibodies is widening and since an increasing number of universities and companies are now able to produce antibodies for small molecules (haptens),[184] immunochemistry is evolving to set multianalyte assays (multiplex),[187,188] on-line systems,[158,189] portable devices to be used in the field[190] and more sensitive detection methods.[158,180,191]

Contrary to caffeine, coprostanol does not possess the typical features to be an easy candidate for the development of an immunoassay. First of all, there is no available antibody for coprostanol – or related compounds – in the market. Coprostanol is nonpolar, has a low solubility in water[192,193] and it lacks groups believed to be important for the interaction analyte-antibody, e.g. amines and carbonyls.[163] A gap of available antibodies for coprostanol, and related stanols, is thus the main obstacle for developing immunochemical-based methods for these compounds.

1.3.3. Antibody production

A description of the murine immune system is too complex to be encompassed here. Nevertheless, some key concepts are necessary to understand the technology behind antibody production. The most important ones are briefly reviewed in the following pages, with a focus on immunochemistry. Some basic concepts are provided in an appendix (13.2 – Appendix II – A brief Immunological Glossary page 257) to increase readability for non-immunologists. For further reading, two text books are suggested in the bibliography.[194,195]

1.3.4. Antibody structure and function

The antibodies used in immunochemistry are the circulating antibodies, also called immunoglobulins. Immunoglobulins (Igs) are soluble glycoproteins. The protein part consists of two identical heavy chains (H) of 55 kDa and around 450 amino acids, two identical light chains (L) of 25 kDa and around 220 amino acids. They are linked together by non-covalent interactions and stabilised by interchain disulfide bonds. The N-terminal domain of each light and heavy chain are highly variable in their amino acid sequence, and are referred to as the variable regions (V_L and V_H, respectively) – both variable regions form the antigen-binding site.[195] The C-terminal domains of the light and heavy chain together form the constant regions (C_L and C_H, respectively), which determine the effector function of the immunoglobulins (in vivo) and the immobilization of Igs on solid supports in immunoassay (like the microtitre plates).

Murine Igs, like Igs from other mammals, can be divided into five classes: IgG, IgA, IgM, IgD and IgE. They differ in function, size, charge, amino acid sequence and carbohydrate content.[194]

Igs are expressed as 1) membrane-bound receptors on the surface of B cells[b]; 2) circulating (soluble) molecules in the serum and tissue fluids. Contact between the B cell receptor (antibody on the membrane) and the antigen it recognises, produces a B cell activation and differentiation into a plasma cell, which secrete large amount of circulating antibodies. The secreted antibody has the same binding specificity as the original B cell receptor.[196]

[b] *Please refer to the glossary on page 257 for further clarification of the term.*

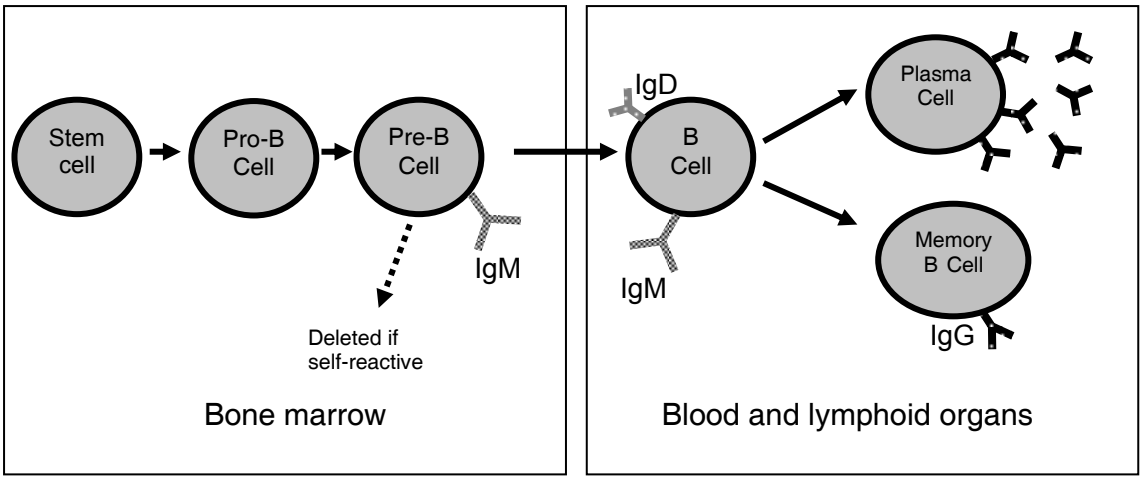

Figure 8. B cell maturation scheme. B cells are produced by a series of maturation steps from precursors in the bone marrow. Simplified version of a scheme from Playfair and Bancroft (2004).[196]

The soluble immunoglobulin G (IgG) accounts for 70-75% of the total serum Ig pool. Therefore, it is the most used in immunochemistry techniques. IgG is a monomeric four-chain molecule with 146-170 kDa. IgA is the predominant immunoglobulin in seromucous secretions and accounts for 15-20% of the serum Ig pool.[196]

Each immunoglobulin is bifunctional (except IgD), having:

1) A part that recognises and binds the antigen (V_L and V_H domains – variable). It contains the antigen binding site and it is usually referred to as the Fab region[b].

2) Another part that promotes the killing and/or removing of the immune complex formed through the activation of effector mechanisms (conserved in each isotype). It is the effector part, usually referred to as the Fc region[b].

Within the variable regions (V_L and V_H domains) some polypeptide segments show a very high variability and are named hypervariable regions. They are involved in the antigen binding by creating an interaction site that is complementary in shape, charge and hydrophobicity to the epitope/hapten[c] they bind. For this reason, they are also referred to as complementary determining regions (CDR1, CDR2 and CDR3). Their variability is a result of an extensive gene recombination process and somatic mutations, which results in a high variable specificity within the antibody pool.[196]

[c] *Please refer to the glossary on page 257 for further clarification of the term.*

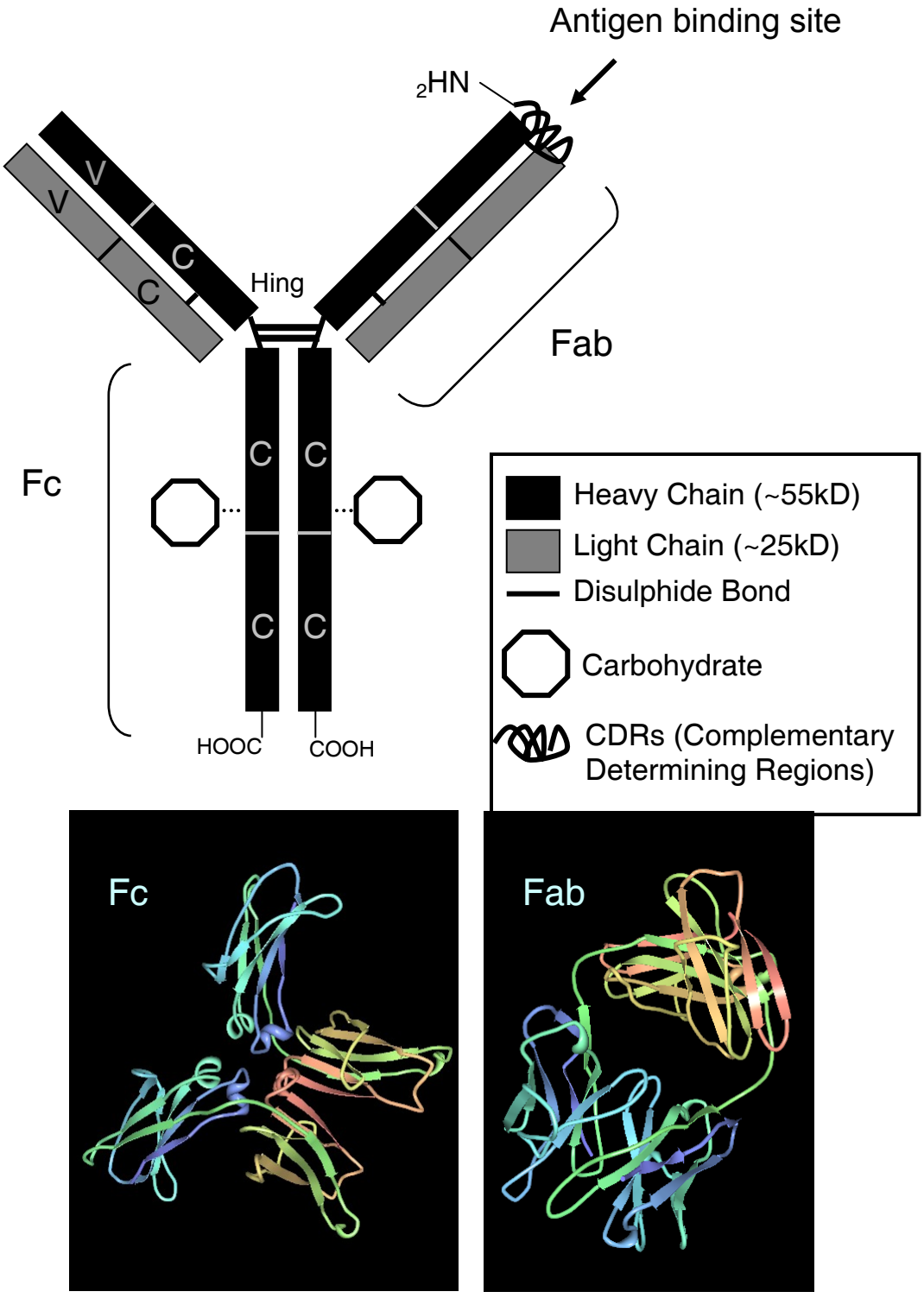

Figure 9. Top: Schematic representation of an IgG. Bottom: Murine IgG Fc fragment and Fab fragment obtained from the Protein Data Bank (PDB) based on the works from Feige et al. (Fc fragment)[197] *and Banfield et al. (Fab fragment).*[198]

1.3.5. Triggering the immune system for a *self* molecule

The immune system has generally the ability to distinguish endogenous (self) from exogenous molecules (non-self), this mechanism is called self and non-self discrimination. The immune system usually reacts only against non-self molecules, but it can however be manipulated in either ways: by suppressing its response towards a non-self (e.g. the immunosuppressors used during organ transplantation) or by triggering it so that it reacts against a self, as it is shown in this thesis and auto-immune diseases are a naturally occurring example of such.[196]

Small molecules like coprostanol are unable to elicit an immune response (non-immunogenic), they are called haptens. A molecule with less than 1000 Da is usually unable to stimulate the immune system and does not induce a secondary antibody response.[199]

Anti-hapten antibodies can however be raised by several strategies: the most popular one is to couple the hapten to an exogenous macromolecule (non-self) and immunize the animal with the hapten-macromolecule conjugate (antigenic). Proteins are widely used for that purpose but some synthetic polymers were also successfully employed.[200] To obtain murine anti-hapten antibodies, the most commonly employed proteins are albumins from other species[201,202] – bovine serum albumin (BSA) and ovalbumin (OVA) – and keyhole limpet hemocyanin (KLH), a highly immunogenic protein from a giant keyhole limpet (a marine gastropod). KLH induces indeed a stronger immune response in mice than mammals-related albumins (BSA and OVA)[203] but has some well-known drawbacks: The first of them is the low purity and high heterogeneity of the KLH supplied (heterogeneously glycosylated and made up of several subunits).[204] The immune system can indeed react not only against the hapten-KLH conjugate (antigen) but also to unknown impurities in the injected antigen. A second drawback is its dimension: while BSA has about 66 kDa, KLH is supplied with a molecular size between 4,500 kDa and 13,000 kDa, which may cause problems when a conjugate hapten-KLH has to be characterised by MALDI-TOF/MS.[204]

BSA is supplied with high purity and it is easily characterised by mass spectrometry based techniques such as MALDI-TOF/MS and ESI-MS.

1.3.6. *In vivo* Immunization

An important feature of the immune response is that it demonstrates memory. It "remembers" if it has “seen” an antigen before and it reacts to secondary exposures to the same antigen in a different manner than after a primary exposure (1st immunization). Generally, only an exposure to the same antigen will elicit this memory response. While in the primary response (after 1st immunization), the major class of antibody produced is IgM, in the secondary response (re-immunization, also boost) it is IgG (also IgA and some IgE).[196] The antibodies that persist after the secondary response are mainly from the IgG type, and they can be in circulation for weeks, months or years (the principle of vaccination). A number of re-immunizations (boosts) were performed in this project to enhance the production of high titre of IgG and to create memory effect. Worth to be mentioned: if there are specific IgG in the serum, every new exposition to the antigen will result, in addition to new IgGs expression, in a rapid immune elimination of the complex antibody-antigen.[194]

The antibody affinity (binding strength) to the antigen is theoretically increased during the secondary response and multiple boosts lead to higher affinities while reducing affinity towards related antigens – affinity maturation.[202] The affinity maturation occurs as a result of somatic mutation in the hypervariable regions and subsequent selection and proliferation of B cells, which bind antigen with higher affinity.[194] Antibodies with high affinity bind the antigen with a greater stability in a shorter time than those with low affinity and are preferable for immunochemical techniques.

1.3.7. Polyclonal and monoclonal antibodies

The used BSA-hapten conjugate, like most antigens *in vivo*, presents numerous epitopes that are recognised by a large number of circulating B cells. Each B cell is activated to proliferate and differentiate into plasma cells, and the resulting antibody response is polyclonal. In contrast, monoclonal antibodies (mAbs) are antibodies produced by a single B cell clone.[205]

PAbs can be generated more rapidly, at less expense, and with less technical skill than is required to produce mAbs. One can reasonably expect to obtain pAbs within a couple of months, whereas the generation of hybridomas and subsequent

production of mAbs can take up to a year or longer, therefore requiring considerably more expense and time.[206]

The principal advantages of mAbs are their homogeneity and the fact that they can be produced endlessly.[167] Once the desired hybridoma has been generated, mAbs can be generated as a constant and renewable resource, theoretically for ever. In contrast, pAbs generated to the same antigen using multiple animals will differ among immunized animals, and the obtained antibodies will be different from one batch to another. The quantity of pAbs obtained is therefore limited by the size and lifetime of the animal used. Rabbits, goats and sheep are the most common hosts.[206,207]

1.3.8. Challenge in hapten(-self)-specific antibodies

"… scientists have come up with solution to certain problems only to find that the biological world got there first."

Ray Paton, Artificial immune system, 2002[208]

The production of antibodies or anti-serum to coprostanol was never reported.

Structurally related compounds were looked at before drawing the experimental protocols for the immunization. The most studied of them is cholesterol, which shares the 3β-OH with coprostanol but has one double bond in the B ring (C5-C6). Thus, the resulting conformations of coprostanol and cholesterol molecule are different as discussed in the results section (10.1.1 - Hapten selection, page 174). In any case, precedent experiments using cholesterol as a hapten provide very useful information for the production of mAbs.[209,210]

Karl Landsteiner and co-workers first suggested that sterols can be immunogenic when attached to large carrier proteins[211] (~1936) and in the 1960s, Bailey *et al.*[212] showed that anti-cholesterol activity can be induced in serum by immunizing with cholesterol-albumin conjugates. Anti-cholesterol antibodies (AChA) were also found to be induced by inoculation of liposomes containing 71% cholesterol.[209] The liposome formulation was also used to generate mAbs to cholesterol but only from the IgM type.[213]

Only recently two anti-cholesterol mAbs IgG were claimed to have been produced.[214] They bind free cholesterol (adsorbed directly on the microtitre plate

surfaces) as well as the three serum lipoproteins containing bound cholesterol (VLDL, LDL and HDL). No inhibition curves are presented to free cholesterol, impeding a proper judgement about the affinity of the obtained mAbs. Interesting is the mAbs selectivity presented, which confirms others authors' works: the hydroxyl group in C3 is critical for the cholesterol recognition and for the binding Ab-cholesterol.[214,215] Cholesterol-related compounds, containing the 3β-OH, bind to the antibodies while others lacking the OH group do not. Moreover, bile acid containing the 3-OH do not bind, stressing the importance of the double C5-C6 bond and the rings conformation for the recognition.[214,216] Peculiar is the fact that besides IgM, only IgGs from the subtype IgG3 were obtained. IgG1 and IgG2 were not found.[214,216]

Studies have also reported the presence of naturally occurring anti-cholesterol antibodies (autoantibodies) in a variety of experimental animals and man.[217,218] To date, the biological effects of antibodies to cholesterol, whether naturally occurring or induced, are unknown.[216,219]

Vaccines against cholesterol have been tried out but it seems that the anti-cholesterol IgG does not remain in circulation for a long time.[209,220] Despite some studies showing a reduction in atherosclerosis platelets after immunizations using cholesterol liposomes and protein conjugates, the effect is not long lasting and after 9 month there are no differences between non-immunized and immunized individual.[212,221] This together with the fact that most induced antibodies seemed to be from the IgM type (primary immune response), raises some questions about the possibility of producing IgGs to endogenous molecules using in vivo systems.

Another non-endogenous compound, made exclusively from carbon and hydrogen, also seems to induce an immune response – squalene.[222] Anti-squalene antibodies were found in American veterans who fought during the Gulf War and were immunized with an anthrax vaccine containing squalene.[223] The Gulf War syndrome was thought for some years to be caused by these anti-squalene antibodies in the serum.[224,225] As squalene is used as adjuvant in a lot of vaccines (including the seasonal influenza vaccine), pharmaceutical companies suggested lately that anti-squalene antibodies are present at low levels in the serum of individuals who were never immunized with squalene-containing formulations.[226-228] Additionally, the study from Novartis seems to show that administering squalene-containing vaccines neither induced anti-squalene antibodies nor enhanced preexisting antisqualene antibody titers.[226]

Lately, an antibody was proposed for capture proteins bound to the bile acid lithocholic acid (2008).[229] The reported mAb was however produced to bind to the immobilized hapten-protein and not to the hapten alone in solution.

Here, the antibody production for coprostanol assumes the following concepts:

- Coprostanol has only a possible functional group to attach it to a carrier protein: C3-OH. From previous works, this group seem to be crucial for the antibody recognition and therefore should be available as epitope.[214]

- The lack of a coupleable group in the side chain (C17) led to a search for possible candidates which, sharing the same conformation of coprostanol and possessing the C3-OH, have additionally an amine or carboxylic acid terminal group.

- The cyclopenta[a]phenanthrene skeleton is able to work as an epitope and generate hapten-specific antibodies.[222,224]

- Because the selected hapten was an endogenous bile acid (isolithocholic acid), it has to be assumed that it is possible to raise antibodies (or enhance the production of autoantibodies) against self molecules.[194]

- Due to the diversity of B cell present in the spleen it is possible to obtain an anti-coprostanol mAb using a structurally-related hapten in the immunogen.

"The studies discussed have a bearing upon the question of the lipoid nature of alcohol soluble haptens since, granting the accuracy of the data presented, these haptens and chemically known lipids are the only material that appear to acquire antigenicity by the addition of proteins. It is not evident, however, why substances chemically so dissimilar as sterols and phosphatides should have a special property in common."

Karl Landsteiner, The specificity of serological reactions, 1936

1.3.9. Production of mAbs – The hybridoma technology

MAbs can be obtained using either *in vivo* or *in vitro* techniques. An *in vivo* technique was used in this project as *in vitro* techniques for haptens still present some drawbacks[230] and have been mainly applied to obtain humanised and chimeric mAbs for human use – as therapeutic agents.[231-233]

The generation of mAbs for immunoassays still relies largely on the traditional hybridoma technology (Köhler and Milstein, 1975).[234]

Each B cell secretes one specific antibody directed to a specific epitope. This B cell secreting the desired anti-hapten antibody has to be selected out of millions of cells. Unfortunately, secreting B cells can only replicate a limited number of times, therefore rendering production of mAbs by their cultivation all but impossible.[235] Immortalising them is thus required. This can be accomplished using the hybridoma technology[234]: fusing the somatic B cell with a myeloma (tumour) cell line from the same mouse strain, and generating an immortal hybrid – B cell and myeloma – called hybridoma.

Hybridomas have the antibody secreting capacity (from the B cell) and they are able to divide perpetually when cultivated in permissive conditions (from the myeloma cells).[236]

The B cells to fuse are usually obtained from the mouse spleen (~$1x10^8$ cells) and the somatic fusion is accomplished by co-centrifuging the spleen cells with myeloma cells in polyethylene glycol (PEG), which allows cell membranes to fuse.[202] A slightly modified method, using additionally an applied voltage, seems to improve the fusion yield – electrofusion.[237,238] The yield is a critical issue in the whole process since it is not truly clear how many B cells do indeed fuse. Fusion performed with the help of polyethylene glycol (PEG) or Sendai virus have recognised shortcomings: relatively low yield of hybrids, loss of viability and secretory properties.[239] Electrofusion is believed to increase the yield but exact figures were not found in the literature.[239,240]

Efforts to improve efficiency and stability of monoclonal antibody-producing cell lines have not brought about substantial progress since the invention of the hybridoma technology.[207,240]

These shortcomings make it necessary to seek new approaches for the generation of hybridomas or alternative approaches to by-pass the hybridoma technology as suggested and patented by Pasqualini and Arap.[241,242] The proposed hybridoma-free generation of monoclonals consists of generating immortal splenocytes (spleen B cells) by-passing the somatic fusion. To do so, Pasqualini and Arap created a transgenic mouse with a mutant temperature-sensitive simian virus large tumour antigen under the control of a murine major histocompatibility promoter from which splenocytes were derived. At a permissive temperature (33°C) the splenocytes were immortalised and became capable of

secreting monoclonal antibodies into the culture medium. The authors claimed that immortal splenocytes showed a higher genetic stability in comparison to that of hybridomas.[241] Yet, the technology does not seem to be effective at saving costs and time needed for monoclonal antibody production.

1.3.10. Hybridoma selection

After the somatic fusion, the hybridomas have to be separated from the non-fused myeloma cells (which could overgrow and restrain the hybridomas expansion). This is achieved using a metabolic pathway deficit of the myelomas used: they lack the enzyme hypoxanthine guanidine phosphoribosyl transferase (HGPRT), which holds a key role in the synthesis of guanidine tri-phosphate (GTP) in the nucleotide synthesis salvage pathway. These cells are still able to synthesise their nucleotides via the main pathway, but when cultivated in the presence of aminopterin, an inhibitor of dehydrofolate reductase (DHFR), an enzyme that produces tetrahydrofolate – a key co-factor in the synthesis of thymidine tri-phosphate (TTP) – these cells can not replicate. Since each of the pathways leading to the production of nucleotides is non-functional under such conditions, myeloma cells are unable to grow in HAT (hypoxanthine-aminopterin-thymidine) medium.[243]

B cells from the spleen have a functional HPRT enzyme and are able to survive in the presence of aminopterin. But, as somatic cells, they can only replicate a few times before dying naturally.

Only fused clones (hybridomas) that have inherited the ability to replicate indefinitely from the myelomas and the functional HPRT expression from the B cells will grow for a number of generations in the presence of aminopterin.[199,235]

The selection of the secreting hybridomas (clones) is normally carried out using limiting dilution cloning (LDC).[244] Although being labour intensive and having low throughput, it is still widely used owing to its relative simplicity and low cost. LDC involves dispensing a low-density hybridoma suspension into a microtitre plate and allowing them to grow. Periodically, supernatants from the wells are analysed for the presence of the desired antibody by using a suitable assay system, normally an ELISA.[245] The cells from wells producing the desired antibody are further diluted until eventually some wells will contain clones of a hybridoma derived from a single cell producing a monospecific antibody. If the cells remain viable and proliferate then a monoclonal antibody-secreting hybridoma has been isolated.[246]

The screening of the supernatant is the recognised process bottleneck[245,247]: microplate-based ELISAs are the most widely used methods for hybridoma screening, mainly using the indirect format (with immobilisation of hapten-protein conjugate).[245,248] The process is laborious, time-consuming[207] and has many pitfalls as briefly described beneath.

About 10 microtitre plates (~1000 wells) have to be screened within a day using a volume of 100 µL from the cells supernatants. Hundreds to thousands of different cells are present in each well, including secreting and non-secreting Hybridoma.[249] The replication pattern of hybridomas varies from clone to clone as well as does the protein (antibody) expression capacity among secreting ones. Thus, a risk of a faster growing by non-secreting hybridomas (consuming the medium nutrients) is of concern as secreting ones can as a result die in culture. It is therefore critical to select by LDC secreting-hybridomas as soon as possible to isolate them from non-secreting ones.[250] And due to the small amount of excreted antibodies into the medium, the risk of losing the desired hybridoma, by not detecting the excreted antibody, is indeed very high.[250]

Indirect ELISA (hapten-protein conjugate immobilised) offers an advantage over the direct one (anti-IgG antibody immobilised): better sensitivity as it generates higher signal-to-noise ratios.[247] However the risk of false positives is elevated when the indirect format is used. Cervino *et al.* reported up to 50% of false positive clones when the indirect format is used against 1% when using the direct one,[245] confirming thus the results from Weller in the early 1990s.[251] Still the indirect format seems to be the standard procedure in hybridoma screening.[207,248]

Alternative methods have been proposed to reduce the workload and time needed for the screening and to increase the detection sensitivity. The BIAcore screening,[252] flow-based kinetic exclusion immunoassay (KinExa),[250] time-resolved fluorescence assay,[253] and microarrays[168] have been suggested as practical options. Although being less laborious and time-saving, they still rely on the indirect format using the immobilised antigen. Recently, Rieger *et al.* reported an alternative microarray screening method but based on the direct format (immobilised antibody).[247]

The use of microarrays is very promising as besides allowing high-throughput screening, it requires only a few nanoliters of the hybridoma supernatant.[168,247] The low volumes required permit: 1) screening for antibodies against different antigens/hapten simultaneously; 2) to establish inhibition curves (competitive

assay) from the very beginning of the process. In microtitre-plate based ELISAs this is not possible – the dilution of the 100 µL supernatants increases the risk of false negatives.[245,247]

Another interesting alternative is the plating of hybridomas in a semisolid medium (methylcellulose based). The secreted antibodies will be immobilised in the proximity of the hybridoma secreting cell and are detected using a fluorophore-labelled hapten.[254] The main advantage of this technology (Genetix Clone Pix Fl) is that it allows for earlier identification and subsequent isolation of the secreting hybridoma.

Flow cytometry and cell sorting was also recently proposed.[255] The technique has a high throughput and it reduces the overall costs and workload. The proposed method is based on the binding of secreted monoclonal antibodies to an affinity matrix assembled (anti-(Fc-)IgG-mouse antibody from a goat) immobilised on the outer cell membrane of hybridomas. Hybridomas are allowed to secrete into a viscous medium and secreted antibodies are then detected using a monoclonal antibody, specific to the Fab fragment of mouse IgG, conjugated to a fluorophore. Fluorophore-bound secreting cells are finally selected via flow-cytometric cell sorting according to the their surface fluorescence.[255] It is however assumed the homogeneity in the distribution of the affinity matrix on the hybridomas outer membranes and that diffusion phenomena of secreted antibodies are avoided by the use of a viscous medium, i.e. antibodies from a secreting-hybridoma do not diffuse in the viscous medium and thus cannot bind to a non-secreting clone nearby.

To summarise, currently used hybridoma screening methods strongly rely on microtitre-plate based ELISAs, which are recognised to both overreporting (false positive clones) and underreporting (false negative clones) of secreting hybridomas. More systematic studies, like the one from Cervino *et al.,*[245] comparing the different formats are useful in order to establish a proper judgement about the best practices to employ. Improvements in automation and multiplex screening are necessary to overcome the process bottleneck.

2. Objectives

The objectives of this thesis were:

1. To develop an inexpensive and high-throughput immunochemical method to quantify caffeine in environmental waters,

    1.1. avoiding time-consuming sample preparation techniques;

    1.2. comparing polyclonal serum and monoclonal antibodies commercially available for caffeine and producing a de-novo synthesised tracer;

    1.3. validating the developed assay for surface waters and comparing its performance with a reference method (LC-MS/MS).

2. To create the first immunoassay for coprostanol.

    2.1. producing an immunogen that could stimulate a murine immune response against coprostanol;

    2.2. generating a polyclonal serum and monoclonal antibodies using *in vivo* immunization and hybridoma technology;

    2.3. developing a new extraction method for coprostanol and related compounds that allows their quantitation in unfiltered surface waters;

    2.4. developing a new LC-MS/MS method to quantify coprostanol and related compounds in surface waters.

3. To demonstrate the suitability of the new developed analytical methods for surface water monitoring.

3. Thesis structure

The work presented results from research on two different analytes with the aim to develop immunoassays for caffeine and coprostanol. They share the same final practical application – surface waters monitoring – but their analytical state of the art started at two different stages: caffeine is a polar and well-studied analyte in several matrices while coprostanol quantitation in waters represents a major challenge, even when using chromatographic techniques. Antibodies to caffeine are widely available while for coprostanol they had to be raised, with all the shortcomings described in the introduction. As a result, the caffeine immunoassay has a major focus on validation issues and suitability to use it within different applications (*PART 1*). The second part (*PART 2*) addresses the complexity of coprostanol and related compounds' analytics as well as some hints for future antibody production targeting stanol-related molecules. The two analytes are discussed together during the surface water monitoring campaigns (*PART 3*).

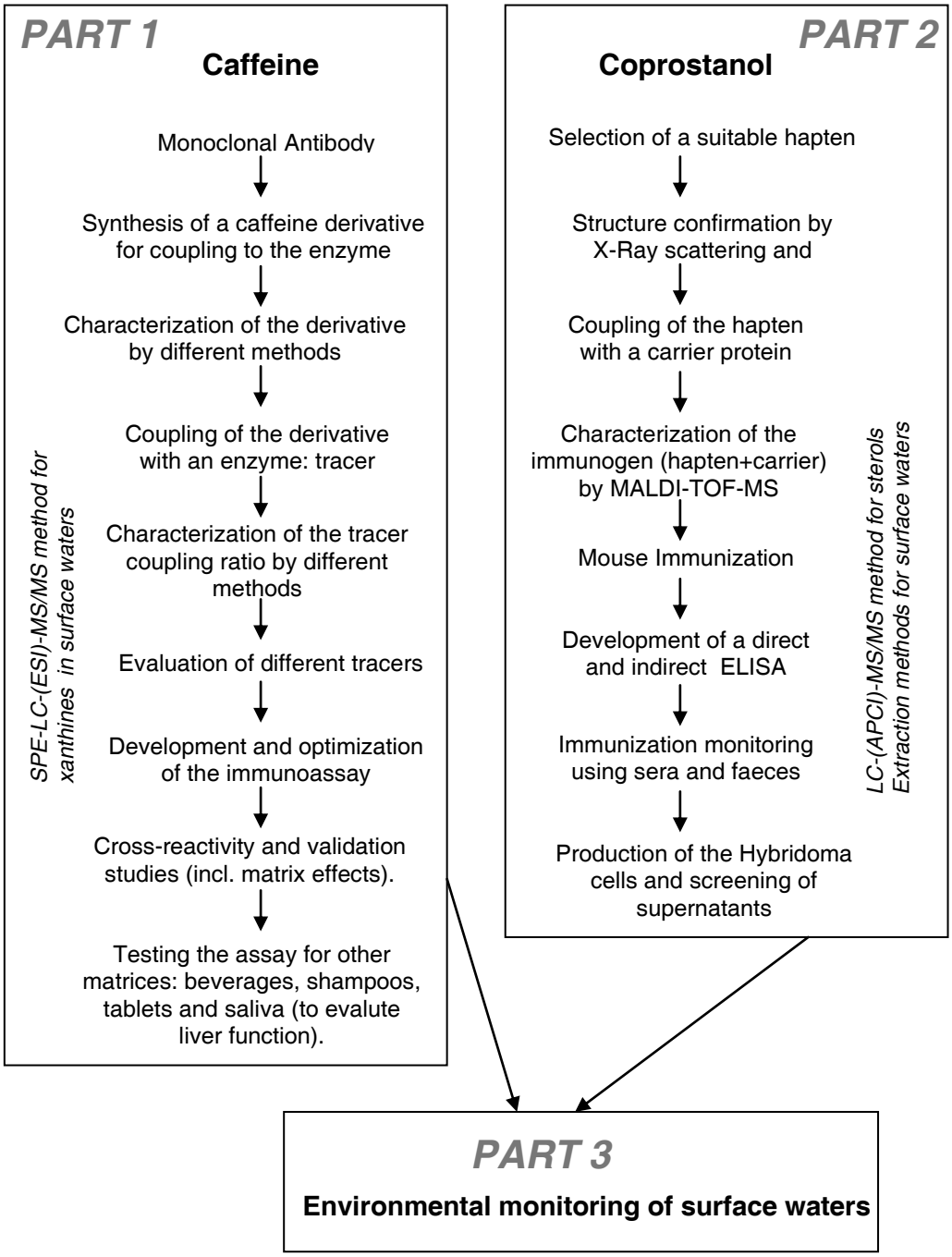
PART 1
Caffeine
Monoclonal Antibody
Synthesis of a caffeine derivative for coupling to the enzyme
Characterization of the derivative by different methods
Coupling of the derivative with an enzyme: tracer
Characterization of the tracer coupling ratio by different methods
Evaluation of different tracers
Development and optimization of the immunoassay
Cross-reactivity and validation studies (incl. matrix effects).
Testing the assay for other matrices: beverages, shampoos, tablets and saliva (to evalute liver function).
SPE-LC-(ESI)-MS/MS method for xanthines in surface waters
PART 2
Coprostanol
Selection of a suitable hapten
Structure confirmation by X-Ray scattering and
Coupling of the hapten with a carrier protein
Characterization of the immunogen (hapten+carrier) by MALDI-TOF-MS
Mouse Immunization
Development of a direct and indirect ELISA
Immunization monitoring using sera and faeces
Production of the Hybridoma cells and screening of supernatants
LC-(APCI)-MS/MS method for sterols Extraction methods for surface waters
PART 3
Environmental monitoring of surface waters

4. Equipment and common materials

4.1. General instrumentation

4.1.1. Liquid chromatography-mass spectrometry (LC-MS/MS)

The LC-MS/MS experiments were carried out using an Agilent 1100 liquid chromatography system from Agilent Technologies (Waldbronn, Germany) and an API 4000 triple-quadrupole mass spectrometer from Applied Biosystems (Darmstadt, Germany). Both instruments were controlled by Analyst™ software (v 1.4.2, Applied Biosystems).

4.1.2. Immunoassay equipment

The microplate spectrophotometer used was a SpectraMax Plus384 from Molecular Devices (Ismaning, Germany) controlled by SoftMax® Pro software (v 5.2, Molecular Devices). The plate shaker was a Titramax 101 (Heidolph, Schwabach, Germany) set at 750 rpm. Plates were washed using an automatic 96-channel plate washer, ELx405 Select™ from BioTek Instruments (Bad Friedrichshall, Germany).

4.1.3. Extraction equipment

Solid-phase extraction (SPE) was performed using an automatic SPE workstation, AutoTrace™, from Dionex (Idstein, Germany). Extracts evaporation was achieved by using a benchtop nitrogen stream evaporator, SLS 02 Evaporator from SLS-Labor (Bad Münstereifel, Germany).

Dispersive liquid-liquid microextraction (DLLME) was performed using an orbital shaker – circular gyrating motion – KS 501 from IKA Labortecnik (Staufen, Germany).

4.1.4. MALDI-TOF/MS

MALDI-TOF mass spectra were acquired using a Bruker Reflex III MALDI mass spectrometer from Bruker-Daltonik (Bremen, Germany) operated with a nitrogen laser and at 20 kV acceleration voltage.

4.1.5. Capillary electrophoresis

A capillary electrophoresis (CE) system with DAD (diode array detector), HPCE 3D™ (Hewlett Packard) was used for all the CE experiments. Instrument control and data acquisition were performed using the HP ChemStation software (version B.03.01, Agilent).

4.1.6. Chromatography columns

Table 2. HPLC columns used within this thesis.

Column name	Description	Supplier
Prot RP 18S	Protein reversed-phase column, UltraSep ESD 300, 125 mm x 3 mm	SepServ, Berlin, Germany
Phen	C18 reversed-phase column, UltraSep ES, 250 mm x 2.1 mm, 5 µm	SepServ, Berlin, Germany
Phen1	C18 reversed-phase column, UltraSep ES, 250 mm x 3 mm, 5 µm	SepServ, Berlin, Germany
Sep	C18 reversed-phase column, 100 mm x 4 mm, 5 µm	SepServ, Berlin, Germany
HILIC	Zorbax HILIC Plus, 4.6 x 100 mm, 3.5 um	Agilent, Waldbronn, Germany
Monolithic	Monolithic column C18, Onyx 50 mm X 2.0 mm	Phenomenex, Aschaffenburg, Germany
Purospher	C18 reversed-phase column, 250 x 3 mm, 5 µm	VDS Optilab, Berlin, Germany

4.2. Software

Origin™ 8.0 Software (OriginLab, Northampton, USA) was used for most of the displayed graphs.

ChemBioDraw Ultra (v 11.0.1) and ChemBio3D Ultra (v 11.0.1), from CambridgeSoft (Cambridge, United Kingdom) were used for drawing the chemical structures, the reaction mechanisms and 3D representations.

MarvinSketch 2010 (v.5.3.0.1) from ChemAxon, University of Kentucky, USA) was also used to drawn some chemical structures.

4.3. Proteins

Horseradish peroxidase (HRP), EIA grade, from horseradish was obtained from Roche Applied Science. According to the producer, the lyophilised enzyme, salt-free, comprises more than 90% of the isoenzyme C (HPLC), carbohydrates content: 12.0-14.5% (w/w), amino groups: 2-3 moles/mole of enzyme and, a Rz number (Reinheitszahl) of 3.0-3.5 (A_{403}/A_{275}). Specific activity is approximately 3,500 U/mg lyophilizate (25°C, tetramethylbenzidine, H_2O_2).

Bovine serum albumin (BSA) – as immunogenic carrier protein. The lyophilised albumin fraction V (min. 99%, receptor grade) used for preparing the conjugates – including the immunogens – was purchased from Serva Electrophoresis. The BSA used as buffer additive, min. 98%, was from Sigma.

Ovalbumin (OVA), lyophilised albumin from hen egg white, min. 95%, was obtained from Fluka.

4.4. Buffers

Table 3. Buffers used within this thesis. All buffers were prepared in Milli-Q water unless other solvent is mentioned.

Solution name	Composition	pH
Carbonate buffer	15 mM sodium carbonate 35 mM sodium hydrogenocarbonate 3 mM sodium azide	9.60
PBS buffer	10 mM sodium dihydrogen phosphate 70 mM disodium hydrogen phosphate 145 mM NaCl	7.60
Sodium bicarbonate buffer	0.13 M sodium bicarbonate	8.10
Substrate buffer	220 mM potassium dihydrogen citrate 0.5 mM sorbic acid potassium salt	4.00
Substrate solution[256]	540 µL TMB solution and 3 mM hydrogen peroxid in 21.5 mL of substrate buffer	-
TMB solution (Tetramethylbenzidine)	40 mM tetramethylbenzidine and 8 mM tetrabutylammonium borohydride in *N*,*N*-dimethylacetamide	-
Tris buffer	10 mM tris-(hydroxylmethyl)-aminomethan 15 mM NaCl	8.50
Tris-NaCl buffer	10 mM tris-(hydroxylmethyl)-aminomethan 150 mM NaCl	8.50
Washing buffer	0.05% (v/v) tween™ 20 in PBS buffer pH 7.6.	7.60

4.5. Materials

Transparent microtitre plates with 96 flat-bottom wells possessing high protein binding capacity (MaxiSorp™) were purchased from Nunc (Thermo Scientific). UV-transparent 96 wells microtitre plates, UV-Star™, were purchased from Greiner bio-one (Frickenhausen, Germany).

PD-10 columns containing Sephadex G-25 were obtained from GE Healthcare (Munich, Germany). Grade 288 paper filters for water sample filtration were from Sartorius (Goettingen, Germany). Folded-paper filters grade 292, 110 mm, 87 g/m^2 were also supplied by Sartorius. Polypropylene tubes (1.5 mL) were purchased from Eppendorf (Hamburg, Germany). Zeba™ Micro Desalt Spin Columns were from Pierce (Thermo Scientific).

Surface water's samples were collected using 1 l brown glass bottles from Schott (Duran, Schott AG, Mainz, Germany). Samples for element analysis were collected in half-liter plastic flasks treated with nitric acid, directly supplied by Dr. Lueck's laboratory (Metal analysis, Inorganic Reference materials, BAM, Berlin).

4.6. Chemicals and buffer salts

Guardian™ (peroxidase conjugate stabiliser/diluent) was purchased from Thermo Scientific (Schwerte, Germany). 3,3',5,5'-Tetramethylbenzidine (TMB), research grade, and Tween™ 20, pure, were purchased from Serva (Heidelberg, Germany). Ultrapure Sinapic matrix for MALDI was supplied by Protea Biosciences (Nîmes, France).

Buffer salts (sodium phosphate dibasic dihydrate, sodium phosphate monobasic dihydrate, potassium phosphate monobasic, potassium dihydrogen citrate, sodium chloride, sodium carbonate, sodium bicarbonate) were of Fluka "ultra" quality (Sigma-Aldrich). Tris(hydroxymethyl)-aminomethan (p.a. for buffer), trifluoroacetic acid (for protein sequence analysis) and calcium nitrate tetrahydrate (ACS) were purchased from Merck (Darmstadt, Germany).

Hydrogen peroxide 30% Trace select®, *N,N*-dimethylformamide (puriss.), *N,N'*-dicyclohexylcarbodiimide (puriss.), *N*-hydroxysuccinimide (purum), sorbic acid potassium salt (p.a.), ammonium acetate (puriss., LC-MS additive) and calcium

sulphate dehydrate (puriss.) were also from Fluka. Sulphuric acid 95-97%, and hydrochloric acid 32%, were of “Baker analysed grade”, methanol and acetonitrile were HPLC gradient grade (Mallinckrodt Baker, Griesheim, Germany).

N,N-Dimethylformamide, anhydrous, 99.8% was from Aldrich; potassium carbonate, Biochemika Ultra, anhydrous, >99.0% and sodium hydroxide, Biochemika Ultra, >98,0%, were from Fluka. Hydrochloric acid, reagent grade, 37% and magnesium sulfate, anydrous, Reagent Plus, >99.5%, were supplied by Sigma-Aldrich.

Ultrapure reagent water (hereafter referred to as Milli-Q water) was obtained by running demineralised water (by ion exchange) through a Milli-Q® water purification system, Millipore Synthesis A 10 (Millipore, Schwalbach, Germany).

.

PART I
Caffeine Immunoassay

5. Additional materials (PART I)

5.1. Chemicals

Caffeine (puriss.), theophylline (>99.0%), xanthine (puriss. >99%), guanine (puriss.), adenine (purriss.) and adenosine (>99%) were purchased from Fluka. Theobromine (min. 99.0%) and paraxanthine (approx. 98%) were supplied by Sigma-Aldrich. Deoxyadenosine triphosphate (dATP) and deoxyguanosine triphosphate (dGTP) were supplied by Fermentas (Vilnius, Lithuania). Phosphoric acid (85%), *N,N*-dimethylacetamide (puriss.), sodium azide (>99%), ethyl 6-hexanoate (>97%, GC) and ethylenediaminetetraacetic acid disodium salt dihydrate (EDTA, >99%) were purchased from Sigma-Aldrich. 6-Bromohexanoic acid ethyl ester, purum, >97,0% was purchased from Fluka and Chloroform, HPLC grade, >99,9% from Aldrich.

5.2. Antibodies

The anti-caffeine monoclonal antibody (mouse IgG 2b, catalogue number C0110-06, clone 1.BB.877, lot L0251502M, 1.37 mg/mL) was purchased from USBiological Inc. (Swampscott, MA, USA). The other tested anti-caffeine monoclonal antibody (mouse IgG1, catalogue number 10-C05, clone M94128, lot 334, 4.7 mg/mL) was purchased from Fitzgerald Industries International (Concord, MA, USA).

The anti-caffeine polyclonal serum (BT17-1040-04, Lot D991007, serum from sheep, 50 µL) was obtained from BIOTREND Chemikalien GmbH (Cologne, Germany). According to the company's information the anti-serum was obtained after immunizing a sheep with a conjugate of ovalbumin (OVA) and 7-(5-carboxypentyl-)1-3-dimethyl-xanthine. The received 50 µL were divided into 5 µL aliquots and stored at -20°C until used. Once an aliquot had been thawed, it was stored at 4 °C.

The secondary (capture) antibody, a polyclonal anti-mouse IgG whole molecule (R12569, Lot 20243, 2.2 mg/mL), from sheep, was obtained from Acris Antibodies GmbH (Herford, Germany).

5.3. Mineral waters

The mineral waters were purchased from local supermarkets and retail stores in Berlin (Kaufland, Galeries Lafayette and Galão). The beverages, coffee and teas were purchased in a local supermarket (Kaufland). The caffeine tables were acquired in a local pharmacy and the Nespresso® coffee capsules acquired via internet.

5.4. Cartridges and filters

Strata-X™ cartridges (200 mg, 6 ml, 33 µm) were supplied by Phenomenex, (Aschaffenburg, Germany) and C18 Bakerbond (500 mg, 6 mL) obtained from J.T.Baker (Deventer, The Netherlands). Vivaspin 500® filters, cut-off of 3 kDa were supplied by Sartorius.

6. Methods (PART I)

6.1. Caffeine derivative synthesis

The caffeine derivative (CafD) was produced based on a synthesis described by Cook[257] with major modifications as described described below.

3.2 g of theophylline (17.8 mmol) was dissolved in 70 mL of anhydrous *N*,*N*-dimethylformamide (DMF). 2.9 g potassium carbonate (21 mmol) was added under continuous stirring. 3.58 ml of 6-Bromohexanoic acid ethyl ester (20.2 mmol) was added and the mixture stirred at 60 °C for 14 h. The reaction was monitored using thin-layer chromatography (TLC). The suspension was filtered using a folded paper filter, and the potassium carbonate retained on it was washed several times with small amounts of DMF. These washing fractions were added to the filtrate and the solvent evaporated using a rotary evaporator (p = 16 mbar, T = 48 °C). The residue (a light-red powder) was dissolved in chloroform at 40 °C and dried over magnesium sulfate, after cooling to room temperature, and filtered afterwards. Chloroform was evaporated (p = 440-450 mbar and T = 48 °C) and 2.25 g (7 mmol) of the obtained product (7-ethoxycarboxypentyl-1,3-dimethylxanthine) was dissolved in 70 mL DMF. 40 mL NaOH (10%) were added. This mixture was refluxed at 115 °C for 30 minutes to cleave the ethyl ester (the reaction was again monitored using TLC). The solvents were evaporated on a rotary evaporator at 50

°C ($p_{(H2O)}$ = 76 mbar; $p_{(DMF)}$ = 10-20 mbar) and the remaining residue dissolved in water. HCl 30% (m/v) was added (pH 4) to protonate the carboxylic group. The product, 7-(5-carboxypentyl)-1,3-dimethyl-xanthine, was extracted by liquid-liquid extraction into ethyl acetate, after adding sodium chloride into the water phase. The CafD was recrystallised from ethyl acetate to obtain colourless needles.

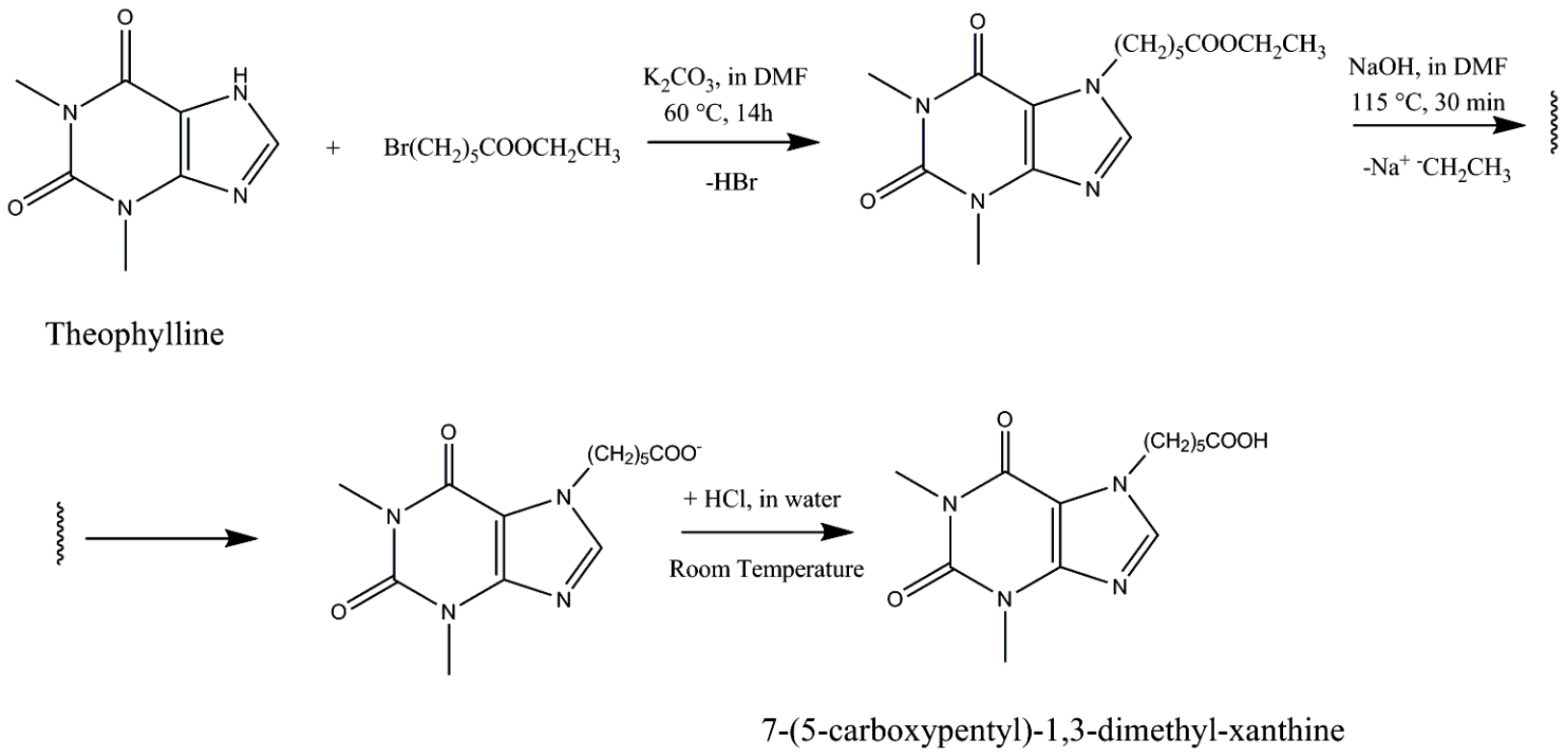

Figure 10. Caffeine derivative (7-(5-carboxypentyl)-1,3-dimethyl-xanthine) synthesis. A detailed description of the synthesis is provided in the text (page 64).

6.2. Caffeine derivative characterisation

6.2.1. Differential scanning calorimetry (DSC)

The melting point was determined using a differential scanning calorimeter (Diamond DSC, PerkinElmer, Waltham, MA, USA). The amount of substance used was 0.75 mg and the temperature rise from 80 °C to 150 °C (at 10 K/min).

6.2.2. LC-MS/MS

Table 4. LC-MS/MS method for the characterisation of the caffeine derivative.

Chromatographic parameters		
Column	Purospher RP-C18, 250 x 3 mm, 5 µm	
Guard column	Purosphere RP-C18, 10 x 3 mm, 5 µm	
Oven temperature	35 °C ± 2°C	
Mobile phase A	5 mM ammonium acetate + 0.01% acetic acid in water	
Mobile phase B	Methanol	
Gradient	t (min)	%B
	0	30
	5	30
	15	90
	16	30
	25	30
Flow rate	0.400 mL/min	
Injection volume	20 µL	
MS parameters		
Ionisation	ESI+	
Acquisition mode	Scan from 50.0 to 600.0 a.m.u.	
Curtain gas	20 psi (138 kPa)	
Ion source gas #1	50 psi (345 kPa)	
Ion source gas #2	45 psi (310 kPa)	
Source temperature	410 °C	
Entrance potential	10 V	
Declustering potential	75 V	
Ion spray voltage	4.5 kV.	

The separation was performed according to the method summarised below in Table 4. Ten milligram of each substance to be analysed, theophylline, intermediate ester

and the final acid, were dissolved in ten millilitres of a mixture of water:methanol 1:1 (v/v), i.e., a final concentration of 1 g/L.

6.2.3. X-ray crystallography

Crystals of 7-(5-carboxypentyl)-1,3-dimethylxanthine monohydrate were grown by solvent evaporation from ethyl acetate at room temperature. The single crystal X-ray data collection was carried out on a Bruker AXS SMART diffractometer at room temperature using Mo K-alpha radiation (lambda = 0.71073 Å), monochromatised by a graphite crystal. A total of 10307 reflection intensities were measured with an exposure time of 30 s per frame. The data reduction was performed by using the Bruker AXS SAINT and SADABS packages.[258] The structure was solved by direct methods and refined by full-matrix least squares calculation using SHELXTL.[259]

6.2.4. ^{1}H and ^{13}C NMR (Nuclear Magnetic Resonance)

NMR spectra have been recorded under standard conditions on a Bruker Avance 600 NMR spectrometer, operating at 400 MHz. The substance was dissolved in hexadeuterodimethyl sulfoxide (DMSO-D6, isoptopic purity 99.96 atom% D, Aldrich).

6.3. Enzyme tracer synthesis

CafD was coupled to horseradish peroxidase (HRP), using the NHS/DCC activated ester method.[182,260] The coupling occurs in two steps: first, a reactive intermediate (highly electrophilic) is produced – the activated ester – which is thereafter coupled to terminal amines ($-NH_2$) of lysine residues on the protein, under slightly basic pH conditions.[261]

To couple a carboxylic acid (CafD) to terminal lysine residues of a protein, the oxygen of the carboxylic group must be first converted into a better leaving group. This was achieved by using carbodiimide chemistry. The oxygen (nucleophile) from the carboxylic will attack the central carbon of *N,N'*-dicyclohexylcarbodiimide (DCC), producing an unstable and electrophilic o-acetylisourea intermediate, which can by itself react with terminal amino groups (from the protein) to form an amide bond (not

shown in Figure 11.). Yet, this unstable intermediary can also form a non-reactive diamide by Beckmann rearrangement[262] if the nucleophile (amine residues on the protein) is not present or if it is not provided fast enough in the reaction mixture. Additionally the intermediate is susceptible to hydrolysis when water is present, regenerating the original acid. The addition of *N*-hydroxysuccinimide (NHS) improves the stability[263] of the intermediate and enhances the yield of the linkage up to 15-fold.[264] NHS converts the amine-reactive ester to an amine-reactive NHS ester, which is sufficiently stable to permit a two-step cross-linking procedure, allowing the carboxylic groups on the protein/enzyme to remain unaltered.

The reaction to obtain the active ester should occur in a completely water-free environment. Thus, the reaction was carried out in anhydrous dimethylformamide (DMF) and under a nitrogen atmosphere. The solvent should be polar enough to dissolve the hapten (CafD); less polar solvents (like tetrahydrofuran) were tried and the conjugation was not successful. A reaction pathway is summarily presented in Figure 11 and a detailed mechanism covering the carbodiimide activation of the acid is given in Appendix I – Detailed mechanism of the conjugation using a carbodiimide Page 255).

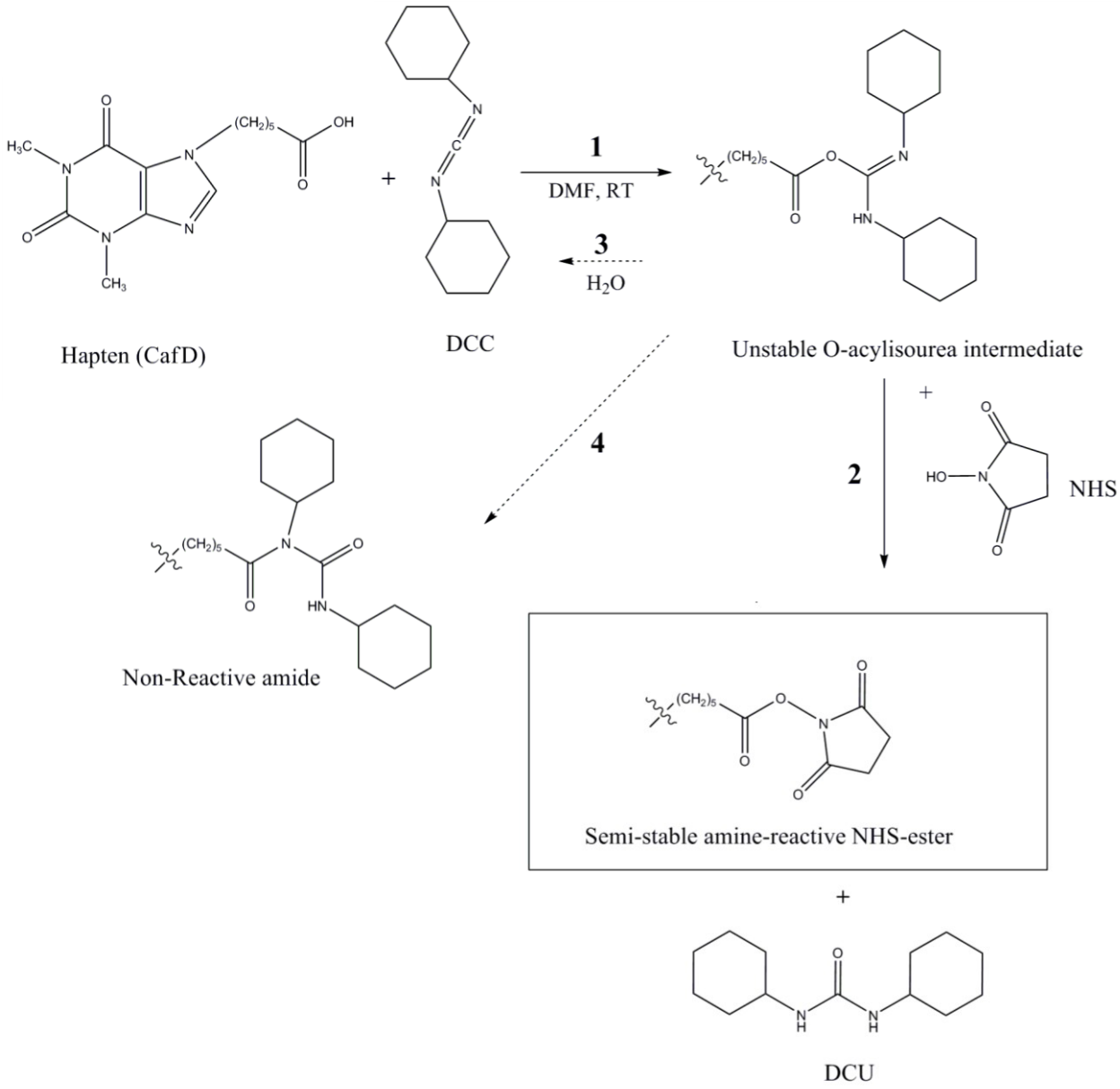

*Figure 11. Production of an active NHS ester using the NHS/DCC method. 1). The terminal carboxylic group of the hapten is converted into an unstable O-acylisourea intermediate by DCC (N,N'-dicyclohexylcarbodiimide). 2) The unstable intermediate reacts with NHS (*N*-hydroxysuccinimide) to produce a more stable amine-reactive ester. 3) Hydrolysis of the o-acylisourea occurs if water is present 4) As an alternative route a non-reactive amide can be formed by rearrangement, in case NHS is not present; the unstable O-acylisourea intermediate can also be coupled directly to the protein/enzyme*

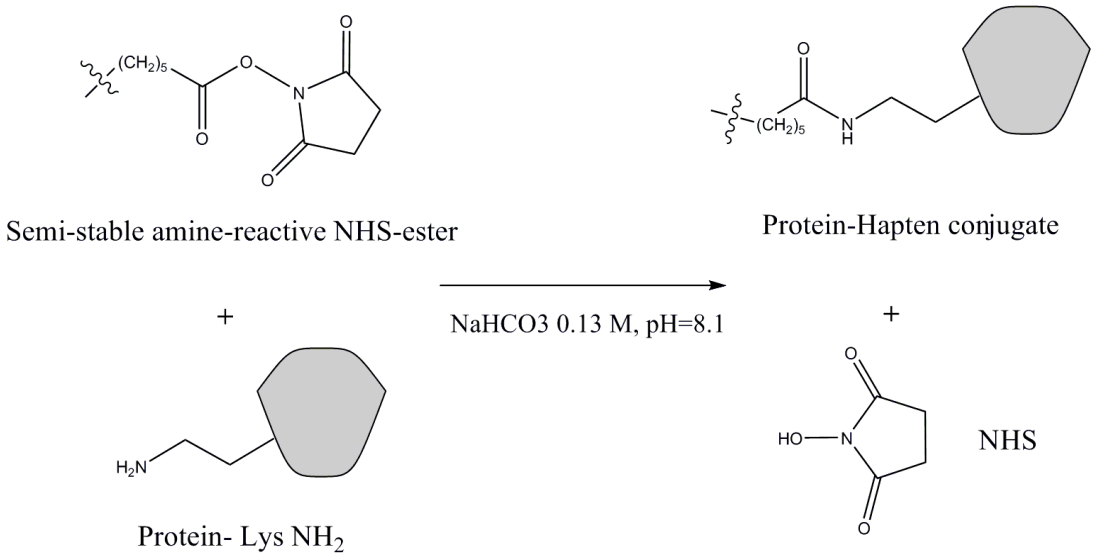

Figure 12. Protein-hapten conjugate synthesis. The amine-reactive ester is coupled to amine groups of the protein in aqueous medium and slightly basic pH (8.1). The amine groups of an amino acid will attack the carbonyl carbon and initiate the addition of the hapten followed by elimination of NHS.

Conjugation Protocol:

3.123 mg (10 µmol) of CafD was dissolved in 120 µL anhydrous DMF and 1.151 mg (10 µmol) of N-hydroxysuccinimide (NHS) was added while gently stirring. After total dissolution of the NHS, 2.063 mg (10 µmol) of N,N'-dicyclohexylcarbodiimide (DCC) was added and the mixture stirred at 500 rpm, using a 5 mm magnetic stir bar, overnight at room temperature (RT) and protected from light. The mixture was centrifuged at 15 °C, 15,000 x g for 10 minutes and 4.64 µL supernatant added to a solution containing 0.340 mg HRP (0.00773 µmol) in 300 µL sodium bicarbonate 0.13 M buffer (pH 8.1). The mixture was stirred for 4 hours (RT, protected from light), and thereafter purified by GPC (gel permeation chromatography) on a PD-10 desalting column using PBS buffer (1mM sodium phosphate, 0.015 M NaCl, pH 7.6) as the eluent. Two drops (~ 100 µL) were collected in each well of a microtitre plate and after reading the absorbance at 405 nm, the volumes of the three wells with highest absorbance were pooled (Figure 13) and the concentration determined photometrically at 405 nm using HRP dilutions to set up a calibration curve. The pooled fractions were mixed with an equal volume of Guardian™ peroxidase conjugate stabiliser and stored at 4 °C. Because Guardian™ contains bovine serum albumin and other unknown additives, a small aliquot of the conjugate without stabiliser was kept for MALDI-TOF/MS analysis. The native HRP was carried

through the conjugation procedure too (without the CafD), and used as reference value for HRP mass.

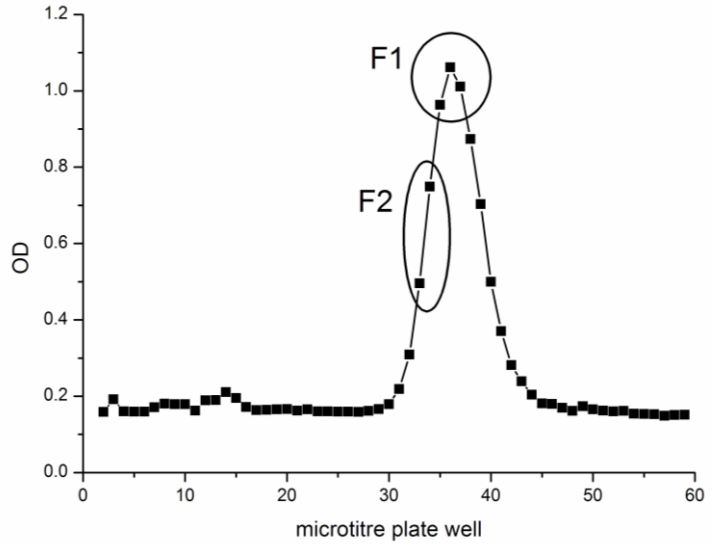

Figure 13. Tracer recovery after clean-up on a Sephadex PD-10 column. The microtitre plate is read at 405 nm and the top fraction (F1) is recovered into an Eppendorf tube; a second fraction (F2) was also recovered and can be used as a reserve.

Remark: The above-described protocol corresponds to a molar reaction ratio of 1:50 (Hapten:Enzyme). For lower or higher ratios the pipetted volume of supernatant, containing the activated ester (4.64 µL in the above-described case), should be adapted to the desired coupling ratio. All the remaining protocol stays as described.

6.4. Tracer characterisation

The characterisation of protein/hapten coupling ratios is currently a very active field of research and no unswerving method for such purpose has been described insofar. Several techniques have been employed, both individually or by combining more than one, such as MALDI-TOF/MS, LC-MS(/MS) Gel Electrophoresis,[201] Capillary Zone Electrophoresis (CZE)[265,266] and Isoelectric Focusing electrophoresis (IEF),[266] either using a gel or a capillary (cIEF). The gel-based techniques were dismissed from the very beginning because they do not allow quantitation, they use relatively high volumes of sample (which are mostly not available), and they require complex staining techniques as well as the pernickety preparation of native gels (acrylamide is a potent neurotoxin and agarose gels rarely provide a uniform pore size).[267] The others abovementioned techniques were tested and the obtained results are presented here except for the capillary

isoeletric focusing (cIEF) method. The developed cIEF method lakes robustness and samples repeatability was an unresolved issue. Consequently it is omitted here.

6.4.1. UV spectroscopy

The HRP conjugates and "native" HRP standard dilutions (HRP as supplied) (calibrators) were measured in a UV-Star™ microtitre plate by UV-Vis (280 nm and 405 nm) using 200 µL of each solution against a blank of PBS buffer.

6.4.2. MALDI-TOF/MS

MALDI-TOF mass spectra were acquired on a Bruker Reflex III MALDI mass spectrometer (Bruker-Daltonik, Bremen, Germany) operated with a nitrogen laser and at 20 kV acceleration voltage. 10 µL of each, native HRP and HRP conjugates, were loaded onto a Zeba™ Micro desalt spin column, centrifuged for 90 seconds at 10,000 rpm, eluted with 10 µL water and mixed with 50 µL of matrix. Sinapic acid matrix was freshly prepared as a 10 g/L aqueous solution, containing 50% acetonitrile and 0.1% trifluoroacetic acid. The sample target was precoated with a droplet of 0.5 µL of matrix solution and dried for 5 minutes. Then 0.5 µL of protein sample was added onto the same spot and air-dried for one hour. Data was processed using Origin 8.0. The mass peaks were fitted with a Lorentzian function and the centres of the fitting curves assigned to the native HRP and the conjugate masses.

6.4.3. LC-MS/MS

The tracers characterisation was performed according to the method summarised in Table 5. The tracers were diluted 1:5 in Milli-Q water directly before analysis.

Table 5. LC-MS/MS method for the enzyme tracer characterisation.

Chromatographic parameters		
Column	Protein reversed-phase column, Prot RP 18S, UltraSep ESD 300, 125 mm x 3 mm	
Guard column	-	
Oven temperature	30 C ± 2°C	
Mobile phase A	0.1% trifluoroacetic acid in Milli-Q water	
Mobile phase B	0.1% trifluoroacetic acid in methanol	
Gradient	t (min)	%B
	0	60
	3	60
	12	90
	25	90
	25.1	60
	35	60
Flow rate	0.450 mL/min	
Injection volume	10 µL	
DAD acquisition		
Wavelengths	from 190 to 900 nm	
Step width	2.0 nm	
MS parameters		
Ionisation	ESI+	
Acquisition mode	Scan from 200.0 to 3000.0 a.m.u.	
Dwell time	2 sec	
Curtain gas	30 psi (207 KPa)	
Ion source gas #1	50 psi (345 kPa)	
Ion source gas #2	50 psi (345 kPa)	
Source temperature	500 °C	
Entrance potential	10 V	
Declustering potential	70 V	
Ion spray voltage	5.0 kV.	

Tracer concentrations were determined after extracting the chromatograms at the wavelengths 405 nm (for the heme group) and 280 nm (the apoenzyme). Peak comparison was performed both by area and height, as discussed afterwards in detail (Results section: 7.2.2.ii - LC-UV and LC-MS, page 105).

The coupling ratios were determined after extracting the m/z range 1400-2800 and thereafter applying the Bayesian Protein Reconstruction, using the Bio tools extension of Analyst™ software (starting mass: 20,000 Da; stop mass: 70,000 Da; step mass: 1 Da; S/N threshold: 20; 20 iterations). The concentrations were determined using the heme trace at m/z = 607 and the trace of the m/z range of 1500-2800 for the apoenzyme. The calibration curve was obtained using six HRP standards, from 0.1 mg/mL to 1.5 mg/mL.

6.4.4. Capillary zone electrophoresis – UV-Vis

The separation was carried out at 25 °C using a fused silica capillary (polyimide coating), 50 µm I.D. from Polymicro Technologies (Phoenix, Arizona, USA), pre-coated with the polymer HPMC (hydroxypropyl methylcellulose), 2% in background electrolyte (BGE): phosphate buffer 50 mM pH 7.0 containing 0.25% HPMC as dynamic coating agent. Detection was performed at fixed wavelengths: 214 nm, 280 nm and 405 nm.

Samples were injected into the capillary by pressure – 30 mbar for 5 sec – and a positive voltage applied to obtain a constant current of 40 µA.

All solutions, including samples and BGE, were filtrated using 0.45 µm circular syringe filters (25 mm diameter) supplied by Nalgene Nunc international. When used for the first time the capillary was rinsed with the following solutions: 1 M NaOH (10 min), 0.1 M NaOH (20 min), Milli-Q water (40 min), 2% HPMC in BGE (5 min), BGE (5 min).

Peak integration was performed both by height and area. For the determination of enzyme tracers' concentrations, the current was increased to 60 µA to minimise the peak broadening caused by the coupling ratios interval within each tracer.

6.5. Polyclonal Antibody (pAb) immunoassay

The direct competitive ELISA was entirely performed at room temperature. The transparent high-binding microtitre plates were coated directly with the anti-caffeine polyclonal sheep serum diluted 75,000-fold in PBS buffer, covered with Parafilm® and incubated 2 hours on the plate shaker at 750 rpm. The plates were then washed three times with washing buffer.

The caffeine standards and samples were added to the plate (100 µL per well) and incubated for 30 minutes, thereupon the tracer (0.015 µg/mL in PBS buffer, 100 µL per well) was added and incubated for 30 minutes with permanent shaking. The caffeine calibration standards were prepared in Milli-Q water from a caffeine stock solution of 1.000 g/L in methanol. The calibration curve was established using 7 calibrators, from 0.01 µg/L to 1000 µg/L.

After washing away standards/samples and unbound tracer, 200 µL of substrate solution was added into the wells and incubated for 30 minutes while shaking. The reaction was stopped using 1 M sulphuric acid, 100 µL per well. The optical density was measured at 450 nm using 650 nm as reference.

For quantitation purposes the calibrators were fitted with a logistic model curve (sigmoidal). Both calibrators and samples were determined in triplicate on each plate.

6.6. Monoclonal antibody (mAb) immunoassay

An identical *modus operandi* was used for all the samples: water, beverages and human saliva. A lower calibration range – from 0.025 µg/L – was used for quantifying caffeine in the water samples (lower concentration of the calibrators, anti-caffeine antibody and tracer) and a higher range – from 1 µg/L and 2.5 µg/L for the beverages and saliva samples, respectively.

All assays were performed using the direct competitive format at room temperature. Tris-NaCl buffer pH 8.50 was used for all steps except the substrate. The plates were coated with polyclonal anti-mouse IgG (H&L, “whole molecule”) serum (1 mg/L in Tris-NaCl buffer, 200 µL per well), covered with Parafilm® and incubated overnight (~ 18 hours) at 750 rpm. The caffeine calibration standards were prepared in Milli-Q water from a caffeine stock solution of 1 g/L in methanol. From the substrate adding onwards the same protocol used for the polyclonal was applied (6.5 - Polyclonal Antibody (pAb) immunoassay, page 75).

6.6.1. Immunoassay procedure

For the lower-concentration range, the anti-caffeine monoclonal antibody was diluted to 0.0137 µg/mL (200 µL per well), added to the pre-incubated plate and shaken for 90 min. The caffeine standards and samples were incubated (100 µL per well) together with the tracer (0.0027 µg/mL, 100 µL per well) for 40 minutes with permanent shaking. The calibration curve was established using 10 calibrators, from 0.010 µg/L to 1 µg/L.

The same procedure was used for the upper-range except for the concentrations of anti-caffeine antibody (0.137 µg/mL), tracer (0.008 µg/mL), and the standards used to establish the calibration curve: from 1 µg/L to 100 µg/L.

6.6.2. Cross-reactivities

The immunoassay selectivity for caffeine with respect to related xanthines was tested by assaying an aqueous dilution series of theophylline, theobromine, paraxanthine, xanthine, caffeine-*trimethyl*-^{13}C, the caffeine derivative synthesised (CafD) and caffeine itself. Additionally several purines, structurally related to the xanthine ring, were tested: adenosine, adenine, guanine, deoxyadenosine triphosphate (dATP) and deoxyguanosine triphosphate (dGTP).

The cross-reactivity was calculated as the ratio of mass concentrations at the inflection points (midpoints, parameter C in the 4 parameters logistic (PL) curve ~ half maximum inhibitory concentration (IC50)) of the corresponding calibration curves and expressed in percent relative to the caffeine midpoint (Equation 1) as described elsewhere.[160,175]

$$CR = \frac{C_{Caffeine}}{C_{Test}} \times 00 \quad \text{(Eq. 1)}$$

CR describes the cross-reactivity in percent; $C_{caffeine}$ is a parameter of the 4PL giving the caffeine concentration at the inflection point and C_{Test} refers to the concentration of the cross-reacting compound at its inflection point.

6.6.3. Matrix effects

A previous experiment, hereunder described, forecasted a major interference by the sample mineral content. This experimental part was thus designed to tackle with that particular setback.

i. Previous experiment

The first study on matrix effects was performed using three surface waters (from the Teltowkanal – a water channel in southern Berlin), a tap water, two mineral waters (with low and high mineralisation), and Milli-Q water spiked with 0.5 µg/L caffeine. All samples were analysed by ELISA and SPE-LC-MS/MS.

ii. Effect of the sample mineralisation

Eleven mineral waters from different origin in Europe and with different mineralisation (the waters' composition and origin are provided in Table 6) were spiked with 1 µg/L caffeine and analysed by ELISA and by LC-MS/MS (direct injection). Caffeine recovery was correlated with the waters composition data.

Table 6. Composition of the mineral waters used to study the matrix effects. The parameters pH, electric conductivity at 20°C and Total Dissolved Solids (TDS) at 180 °C were measured according to standard procedures for water analysis.[268] The remaining parameters were provided by the water suppliers in the bottle banderole.

Water	Origin	mg/L								
		$[Ca^{2+}]$	$[Na^{+}]$	$[HCO^{3-}]$	$[Mg^{2+}]$	$[SO_4^{2-}]$	$[Cl^{-}]$	$[F^{-}]$	$[K^{+}]$	$[NO^{2-}]$
Voss	Norway	0.8	1		0.6		9		0	
Fastio	Portugal	1.3	4.1	8		1	4.2		0.6	
Celtic	France	10.5	1.1	48	4	6	<5	<0,10	1.9	2.1
Llanllyr	UK	12	14	68	6	17	30		2	
Lausitzer	Germany	12.5	4.1	44.8	2.2	4.8				
Saskia	Germany	29.1	13.2		3	42.7	31			<0.5
Aquarel	Belgium	61.3	13.7	198	4			0.1		
Apollinaris	Germany	90	30	1800	120	100	130		30	
Vittel	France	91	7.3	258	19.9	105				
Voeslauer	Austria	110.3	11.4	255	43.3	229	21		1.8	
Quézac	France	241	255	1685	95	143	38	2.1	50	<1

Water	pH	Elec.conductivity 20°C (µS/cm)	TDS(1), (mg/L)
Voss	6.76	79.2	22
Fastio	5.8	34.6	34
Celtic	7.64	88.1	46
Llanllyr	5.55	182	84
Lausitzer	6.32	97.8	36
Saskia	6.94	243	192
Aquarel	7.98	352	249
Apollinaris	6.62	1788	1855
Vittel	7.52	557	397
Voeslauer	7.71	764	599
Quézac	6.86	2680	521

(1) TDS Total dissolved solids at 180 °C

iii. Effect of the calcium concentration

The effect of calcium was evaluated using a low mineralised bottled water (Lausitzer, 12.5 mg/L Ca^{2+}, 97.8 µS/cm, 36 mg/L of total dissolved solids) spiked with different calcium concentrations (0, 5, 25, 50, 100, 150, 250, 500, and 1000 mg/L Ca^{2+}, using $CaCl_2$) and the same amount of caffeine, 1 µg/L. The spiked solutions were analysed by ELISA and by LC-MS/MS (direct injection). A mineral water was used instead of Milli-Q water as the latter lacks buffer capacity: pH variations could lead to misinterpretations. The pH difference between all the spiked samples was not significant: 7.46 ± 0.17 pH units.

iv. Effect of EDTA addition

To all mineral waters spiked with different levels of calcium (using calcium chloride) and 1 µg/L caffeine, the same amount of EDTA disodium salt dihydrate was added (51 mmol/L). The samples were mixed and left on the bench for 2 h before analysis.

v. Calcium effect vs sample mineralisation

From the aforementioned Lausitzer mineral water, three different samples were prepared: Lausitzer 1 (spiked with 1000 µg/L Ca^{2+}, 1756 µS/cm); Lausitzer 2 (spiked with NaCl to a conductivity close to the one of sample 1, 1746 µS/cm) and Lausitzer 3 (without additions). All samples were analysed using the immunoassay.

6.6.4. Temperature effect

The assay was performed at three different temperatures: 4°C, 20°C (room temperature), and 37°C. The assay buffers and calibration standards were placed overnight at the temperature to be tested. All the incubation steps were performed at the temperature tested.

6.6.5. Operator influence

The operator influence was assessed by assaying 20 water samples from the Teltowkanal, on the same day, by three different experienced operators: 1. A PhD student with some experience performing ELISA; 2. A training student with 2 month of experience doing ELISA; 3. A specialised technician with several years performing immunoassays.

6.6.6. Fitting models for binding assays

A 4-parameter sigmoidal fitting is the most commonly used in immunoassay. Several other fitting models were tested to evaluate if (1) the sum of the residuals decreases; (2) precision is improved and (3) better accuracy achieved.

The fitting models tested are described in Table 7. Overall, a total of 16 different calibration curves were tested for comparing the different models.

Table 7. Fitting models tested for the calibration curves in ELISA. (†) Only used for the upper-range calibration curve; (‡) only used for the lower-range of the calibration.

Function	Number of parameters	XX	YY	Equation
Hyperbolic (generalised hyperbole function)	4	[x], Log [x]	OD	$y = A - \frac{B}{(1 + Cx)^{1/D}}$
One-parameter Power function(†)	1	[x]	OD	$y = x^{A}$
Symmetric Power Function with offset(‡)	4	[x]	OD	$y = y0 + A\left\|x - c_c\right\|^{p}$
Sigmoidal – Logistic function	4	[x], Log [x]	OD	$y = \frac{(A - D)}{1 + \left(\frac{x}{C}\right)^{B}} + D$
Sigmoidal – Botzmann function(‡) (or dose-response curve)	4	[x], Log [x]	OD	$y = \frac{(A1 - A2)}{1 + e^{\left(\frac{x - X_0}{dx}\right)}} + A2$
Allometric 1 (also known as Classical Freundlich Model)	2	[x]	OD	$y = Ax^{B}$
Exponential Decay 1st Order	4	[x]	OD	$y = y_0 + Ae^{-\frac{x}{T}}$
Exponential Decay 2nd Order	6	[x]	OD	$y = y_0 + A_1 e^{-\frac{x}{T_1}} + A_2 e^{-\frac{x}{T_2}}$
Exponential Decay 3rd Order	8	[x]	OD	$y = y_0 + A_1 e^{-\frac{x}{T_1}} + A_2 e^{-\frac{x}{T_2}} + A_3 e^{-\frac{x}{T_3}}$
Linear Transformation	2	Log [x]	-Log (OD)	$y = Ax + B$

6.6.7. Validation

The limit of detection (LOD) and limit of quantitation (LOQ) were calculated independently of one another. There is some consensus on the LOQ definition and methods to calculate it.[269-272] The same cannot be said about the LOD; its definition is to some extent clear but the methods and statistics used to calculate it still raise discussions,[174,270-278] making the concept rather woolly.

The LOQ was calculated using the calibration precision profile[279] after selecting the calibration range – which was configured to include the expected concentration of the real samples. A maximum allowable relative error of 20% for a determined concentration was selected as criterion to establish the LOQ, using ten calibration curves obtained on different days. This value was thereafter experimentally confirmed by measuring 18 times the LOQ concentration (in Milli-Q water) and calculating the measurements' standard deviation. Preferably a surface water sample – without the analyte – should be spiked at the LOQ level to provide unequivocal evidence, but such analyte-free sample could not be found. Therefore, surface water samples containing caffeine concentrations close to the LOQ were repeatedly analysed (within the same day and on different days) and their standard deviation represents a reasonable evidence of the LOQ figure presented.

The LOD was determined using an experimental approach rather than a probabilistic one. Several caffeine concentrations which provide a signal different from the blank were assayed 18 times against 18 blanks within the same plate. The LOD was defined as the concentration which results in the 18 signals are lower than the 18 signals of the blanks. This is a very conservative approach and the calculated LOD is most likely too high when compared with other methods, though this approach minimises the occurrence of both α and β errors.[274,275]

Intraday and Interday precisions were obtained by repeat measurements of several real samples, on the same day and over three days (three replicates per day), respectively. Six water samples were selected on the basis of their caffeine concentration, in order to cover the full calibration range. All the beverages were used for the intraday and interday precision studies.

6.7. Reference method for caffeine

6.7.1. LC-MS/MS method for xanthines quantitation

The final method is summarised in Table 8. The final chromatographic conditions allow for the separation of theophylline and paraxanthine, which share the same MRM transitions.

Table 8. LC-MS/MS method for quantitation of several xanthines.

Chromatographic parameters		
Column	Phen, UltraSep ES, C18 reversed-phase 250 mm x 2.1 mm, 5 µm	
Guard column	Phen, UltraSep ES, C18 reversed-phase 10 mm x 2.1 mm, 5 µm	
Oven temperature	50 °C ± 2°C	
Mobile phase A	5 mM ammonium acetate in Milli-Q water	
Mobile phase B	Methanol	
Gradient	t (min)	%B
	0	25
	7	25
	14	95
	20	95
	20.1	25
	30	25
Flow rate	0.450 mL/min	
Injection volume	30 µL	
MS parameters		
Ionisation	ESI+	
Acquisition mode	Static mode, MRM 2 transitions per compound	
Dwell time	0.1 sec	
Curtain gas	30 psi (207 KPa)	
Ion source gas #1	50 psi (345 kPa)	
Ion source gas #2	70 psi (480 kPa)	
Source temperature	500 °C	
Entrance potential	10 V	
Cell exit potential	10 V	
Declustering potential	80 V	
Ion spray voltage	5.0 kV.	

The quantitation was performed using the peak area of the most intense MRM transition (MRM1) and the second one (MRM2) was used for confirmation purposes. The compounds were identified based on the presence of both MRM transitions and the retention time. The mass spectrometry conditions for the individual compounds as well as theirs retention times are summarised in Table 9.

Table 9. Mass spectrometry conditions for MS-acquisition of several xanthines in MRM mode.

Compound	Exact Mass [a.m.u]	Precursor ion (*m/z*)	Collision Energy [eV]	Product ions (*m/z*)	RT [min]
Non-retained solute					2.12
Xanthine	152.03	153.0	28	110.0 (MRM 1) 135.7 (MRM 2)	3.61
Theobromine	180.06	181.0	27 30	163.0 (MRM 1) 138.0 (MRM 2)	4.96
Paraxanthine	180.06	181.0	35	124.0 (MRM 1) 96.0 (MRM 2)	6.28
Theophylline	180.06	181.0	35	96.0 (MRM 1) 124.0 (MRM 2)	6.94
Caffeine	194.08	195.0	30	138.0 (MRM 1) 110.0 (MRM 2)	12.7
Caffeine-trimethyl-^{13}C	197.09	197.8	30	139.8 (MRM 1) 111.5 (MRM 2)	12.7

6.7.2. Solid-phase extraction for xanthines

The SPE was carried out using a polymeric reversed phase, Strata-X™ (200 mg, 6 ml, 33 µm), in an automatic SPE workstation, AutoTrace™. The cartridges were preconditioned using two times 10 mL methanol followed by 20 mL Milli-Q water and loaded with 400 mL sample. Afterwards the cartridges were dried by a nitrogen stream (purity 5.0) for 15 minutes and caffeine eluted by 10 mL methanol. The methanol extract was evaporated to dryness using a nitrogen stream and the residue reconstituted in 400 µL Milli-Q water (concentration factor of 1000-fold). Although a C18 reversed phase, Bakerbond (500 mg, 6 mL), provided similar recoveries, the polymeric phase cartridge was selected in order to include additional compounds (more polar) in the same SPE procedure. Caffeine-*trimethyl-*

^{13}C was used as internal standard (75 µg/L) but the recoveries were not corrected since they were higher than 90% for all samples.

6.8. Monitoring caffeine in water samples

Surface water samples (approximately 1 L) were collected close to the surface, in brown glass bottles, stored at 4°C and analysed within 2 days. The water samples were filtered using folded-paper filters prior to SPE enrichment. Ten surface water samples were collected at different locations within Berlin: Teltowkanal (a river-linking channel) (3 samples), Großer Wannsee (large lake, actually part of a slow-running river) (2 samples), Schlachtensee (small lake, but not a completely closed system) (1 sample), Spree (Berlin's inner city river) (3 samples), and Nikolassee (medium-sized lake) (1 sample). For more information on the locations along Berlin's waterways refer to Heberer, 2002.[280]

6.9. Monitoring caffeine in saliva samples

The immunoassay procedure was the same described earlier (6.6.1 - Immunoassay procedure, page 77) but using 9 calibrators to construct the calibration curve, from 2.5 µg/L to 150 µg/L.

6.9.1. Saliva collection

Sixty samples from ten individuals were collected every hour for five hours, after the intake of 200 mg caffeine. The group was composed by regular caffeine consumers, five women and five men, three smokers and seven non-smokers, five were between twenty and thirty years-old, three between thirty and forty, one between forty and fifty and one over fifty. The saliva samples were collected directly into 2 mL Eppendorf tubes, vortexed, centrifuged (15 °C, 15,000 x g, 5 minutes) and placed overnight at 4 °C until extraction.

6.9.2. Samples pre-treatment

To remove proteins and cells from the samples two methods were tested:

1) Ultrafiltration (diafiltration) using filters with a cut-off of 3 kDa (Vivaspin 500®, Sartorius);[281]

2) Protein precipitation using an organic solvent – acetonitrile.[282,283]

Twelve (12) different saliva samples from different individuals were spiked with 10 mg/L of caffeine-*trimethyl*-$^{13}C_3$ (1.5 mL saliva + 15 µL of 1000 mg/L of caffeine-*trimethyl*-$^{13}C_{3)}$ and the proteins removed using both methods. From each spiked sample, 2 aliquots of 200 µL were passed through a Vivaspin 500® filter and centrifuged for 20 minutes, 15,000 x g (16,000 rpm) at 6 °C; 2 other aliquots with the same volume were placed into Eppendorf tubes and 1000 µL acetonitrile were added prior to centrifugation, under the same conditions. All the 4 aliquots were centrifuged simultaneously. The filtrates were diluted 100-fold in Milli-Q water prior to LC-MS/MS analysis and the acetonitrile extracts diluted 20-fold in Milli-Q water. For calculation purposes, the dilution factor for the acetonitrile extracts was obtained considering the thermodynamic properties of the mixtures water + acetonitrile at 20.0°C (293.15K) and atmospheric pressure.[284,285]

After comparing the methods, all samples were extracted using acetonitrile and analysed by ELISA and LC-MS/MS on the same day, using the same calibration standards. The samples, as well as the control sample extracts, were evaporated until dryness under nitrogen stream and reconstituted in equivalent volumes of Milli-Q water. Thereafter the extracts were diluted to fit the calibration range.

6.9.3. Spiking experiments

One saliva sample (t = 180 min) from each individual (n = 10) was spiked with caffeine and caffeine-trimethyl-$^{13}C_3$ ($^{13}C_3$-CAF), at approximately half the caffeine concentration found in the original sample.

6.9.4. Quality control samples

The saliva samples were divided in batches of 10 elements, one batch per each sample time collection. The following control samples were included in each batch: Milli-Q water spiked with caffeine to obtain a final concentration of 75 µg/L (calibration curve middle concentration) and passed through all the process steps;

Milli-Q water was also extracted to serve as a blank control; a control standard of 75 µg/L (prepared independently from the one used for calibration) was analysed together with each batch to evaluate the fit of the calibration curves. Noteworthy to mention is the fact that the antibody does not distinguish between caffeine and caffeine-trimethyl-^{13}C ($^{13}C_3$-CAF) and therefore the sample could not be spiked with the latter. The matrix effects were evaluated using the spiking experiments described before (6.9.3 Spiking experiments, page 86).

6.10. Monitoring caffeine in beverages, shampoos and caffeine tablets

Coca-Cola®, Coca-Cola® Zero® (without sugar), Coca-Cola® caffeine-free, Club-Mate, Becks beer Level 7 (supplemented with caffeine), and Red Bull Energy Drink were degassed using argon. The espresso coffee was prepared using a black capsule (“Ristretto”, ~ 5 g ground coffee) in a Nespresso™ coffee machine (Delonghi EN90). The final espresso volume was 20 mL. The filter coffee was obtained by dripping 250 mL water on to 15.2g coffee (“Auslese”, Melitta), using a coffee maker (Ideen Welt, Rossman, Germany). The tea samples (black, green, Earl Grey, and raspberry tea) were obtained by placing a teabag into 300 mL boiling hot water for 10 min. The caffeine tablet (0.450 g, 200 mg caffeine) was dissolved for 3 h, with stirring, in 1 L Milli-Q water pH ~ 3. The shampoo (0.510 g) was dissolved in 1 L of Milli-Q water. Most samples were diluted 1:1000, 1:10,000, or 1:100,000 in Milli-Q water; Coca-Cola caffeine-free was analysed directly, raspberry tea diluted 1:10 and the shampoo diluted 1:100.

7. Results and discussion (PART I)

7.1. Caffeine derivative (CafD) characterisation

The chemical name of the derivative is 7-(5-carboxypentyl)-1,3-dimethylxanthine monohydrate and the systematic name 6-(1,3-dimethyl-2,6-dioxo-2,3,6,7-tetrahydro-1H-purin-7-yl) hexanoic acid monohydrate.

7.1.1. Differential scanning calorimetry (DSC)

The thermodynamic melting point of 7-(5-carboxypentyl)-1,3-dimethylxanthine monohydrate is 124 °C (major peak) and a second peak was observed at 106 °C corresponding to the loss of crystal water. Ladenson *et al.*[286] reported the same caffeine derivative – used to produce a new recombinant anti-caffeine antibody – with a different melting point: 129 °C. Yet, no further details are given by the authors regarding the synthesis, besides being based on the same reference[135] and outsourced to a private company (Daniel Fine Chemicals, Edmonton, Alberta, Canada). Furthermore, information regarding the substance clean-up, crystallisation and detailed procedure for the melting point measurement are not described in their work. Melting point determinations following *Pharmacopoeia* procedures – capillary method – produce slightly high melting points (MP_{pharm}) than the thermodynamic melting point (MP_{therm}), which is the one here reported. This could explain the difference obtained by Ladenson et *al.* Additional data about the derivative purity, collected during this thesis (LC-MS/MS, crystal structure, H- and C-NMR), gives confidence in the MP_{term} obtained, 124 °C.

7.1.2. LC-MS/MS

The mass spectrum of theophylline (the starting material), acquired in scan mode, shows only 2 peaks at: m/z 181 (100%) corresponding to the protonated molecular ion $[M+H]^+$; and m/z 124 (37%) resulting from the loss of a methyl group and retro-Diels Alder (RDA) rearrangement of the ring system,[287,288] $[M-OCNCH_3+H]^+$. The loss of a methyl isocyanate group (57 a.m.u) is in fact a characteristic aspect of some xanthine derivatives such as theophylline and paraxanthine.[289]

Neither the intermediate ester (1g/L) nor the acid (1g/L) spectrum show the ion m/z 181 at 5.50 min, theophylline retention time; even when the acquisition was

performed in SIR mode. The ester (ethoxycarboxypentyl-1,3-dimethylxanthine) eluted at 14.92 min and the acid (7-(5-carboxypentyl)-1,3-dimethyl-xanthine) at 12.62 min. Two chromatograms are shown in overlay in Figure 14: theophylline acquired in scan mode, after extracting m/z 181 and the acid after extracting m/z 295.

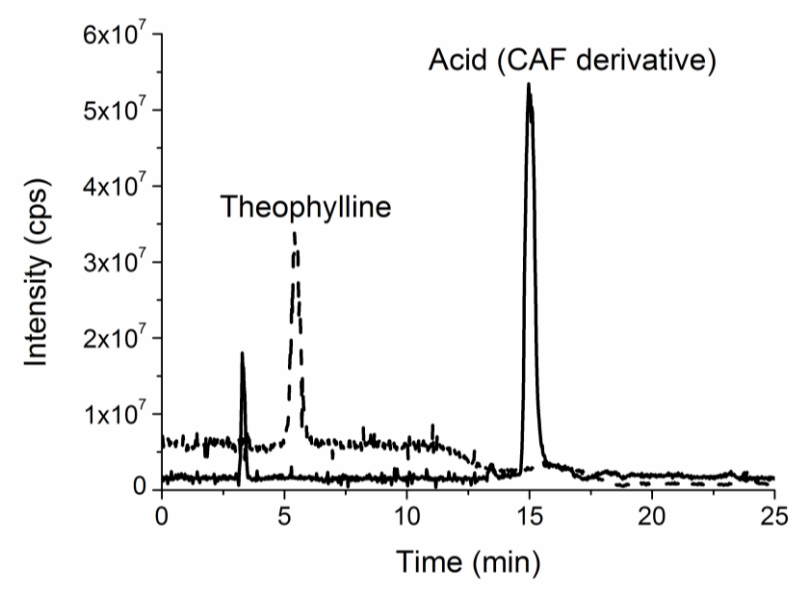

Figure 14. Chromatogram of theophylline (extracted m/z 181, Scan mode) – dashed line and the final acid (extracted m/z 295, Scan mode) – bold line.

The ESI+ spectra of the ester and the final acid are shown in Figure 15. They were obtained from the respective peak apex after subtracting the background noise (between 7 and 8 min).

The ester spectrum shows almost equal intensities of three ions: the molecular ion (m/z 323.1), the sodium adduct (m/z 345.0) and the fragment m/z 277.3 while in the acid spectrum the molecular ion (m/z 295.3) is clearly the predominant one. All the m/z found in the MS spectra are summarised and associated with the correspondent ion structure in Table 10, providing additional confidence of the chemical structure and purity of the synthesised derivative.

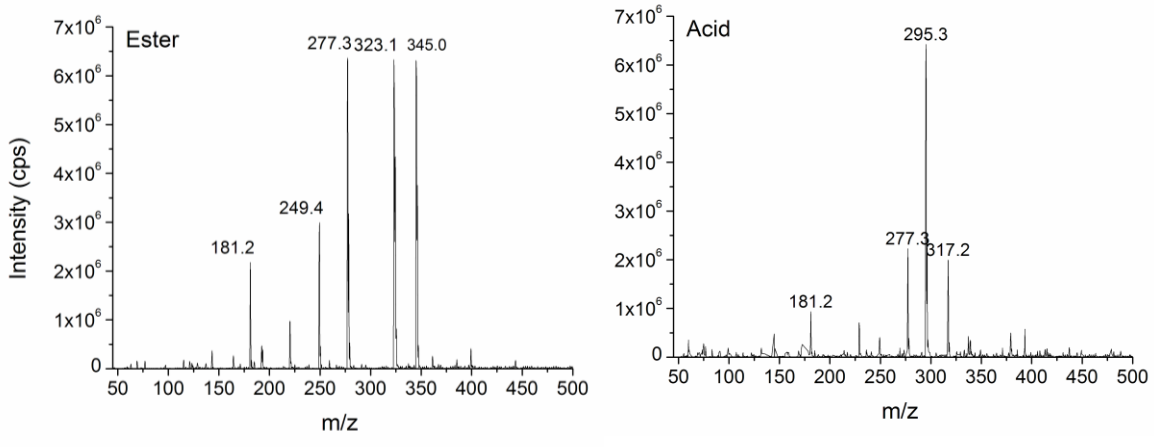

Figure 15. Scan spectrum of the ester (left) and of the final acid (right). The ions corresponding to the recorded m/z are summarised in Table 10.

Table 10. Summary table of the products obtained during the caffeine derivative synthesis. The m/z mentioned here were obtained from the mass spectra displayed in Figure 15.

	Ester	Acid (final product)
Chemical name	Ethoxycarboxypentyl-1,3-dimethylxanthine	7-(5-Carboxypentyl)-1,3-dimethyl-xanthine
R on C7	$(CH_2)_5COOH$	$(CH_2)_5COOCH_2CH_3$
Molecular formula	$C_{15}H_{22}N_4O_4$	$C_{13}H_{18}N_4O_4$
Exact mass	322.1641	294.1328
ESI+ m/z		
Molecular ion	323.1 $[M+H]^+$	295.3 $[M+H]^+$
Sodium adduct ion	345.0 $[M+Na]^+$	317.2 $[M+Na]^+$
Fragment ions	277.3 $[M-CH_3CH_2O]^+$ 181.2 $[M-(CH_2)_5COOCH_2CH_3+H]^+$ 249.4 $[M-COOCH_2CH_3]^+$ 220.1 $[M-CH_3CH_2O-OCNCH_3]^+$	277.3 $[M-H_20+H]^+$ 181.2 $[M-(CH_2)_5COOH+H]^+$

7.1.3. Crystal structure (X-ray)

The crystal structure was reported for the first time based on data produced within this PhD work,[290] helping to understand the binding of the ligands to the monoclonal anti-caffeine antibody. The average C—N, C—C and C—O distances (Figure 16) are in good agreement with those in the caffeine molecule[291,292] and comparable compounds, as theophylline, for example, data taken from the Cambridge Structural Database (CSD, version 5.27).[293,294] Analysis of the crystal structure shows that the molecules are linked via hydrogen bonds to result in a layer structure. As illustrated in Figure 17, intermolecular O—H···N and O—H···O hydrogen bonds, involving O atoms of aqua ligands and the N atoms of imidazole, and a carboxylic O atom contributed to the formation of hydrogen bonds. The center-to-center (DC) and the center-to-plane (DP) distances between two neighboring almost parallel (interplanar angle α = 0.62°) imidazole and adjacent pyrimidine rings are 3.545 Å (DC), 3.341 and 3.336 Å, revealing the existence of π-π stacking interactions, which further stabilise the structure. Further details regarding the crystal data, including bond lengths and angles, can be found in the tables published.[290]

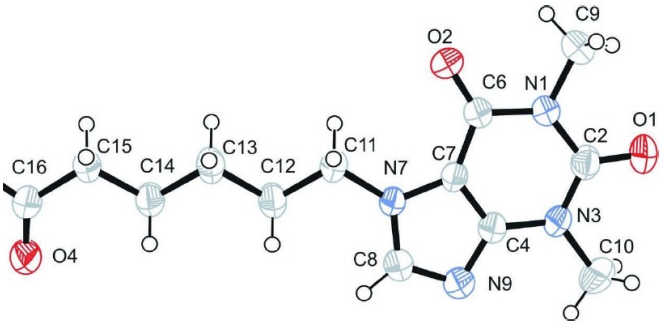

Figure 16. (top) ORTEP-3 representation of 7-(5-carboxypentyl)-1,3-dimethylxanthine with the atomic labelling of the asymmetric unit and coordination sphere, shown with 50% probability displacement ellipsoids.

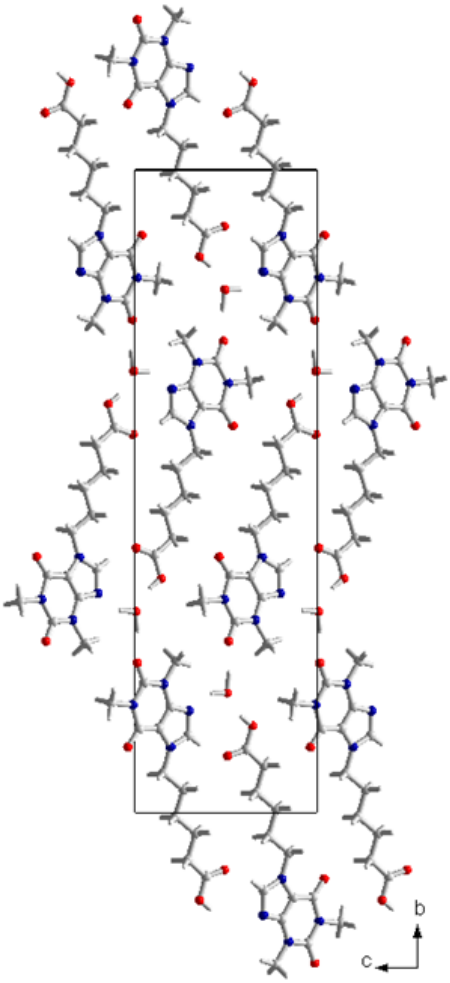

Figure 17.(left) View of the layer array of 7-(5-carboxypentyl)-1,3-dimethylxanthine, formed via strong hydrogen-bonding interactions.

Table 11. Crystal data and structure of 7-(5-carboxypentyl)-1,3-dimethylxanthine.

Molecular formula	$C_{13}H_{18}N_4O_4*H_2O$	$C_{13}H_{18}N_4O_4*H_2O$	Unit cell dimensions	a = 4.370(4) Å b = 34.55(4) Å c = 9.960(9) Å alpha = 90° beta = 93.21 (3)° gamma = 90°
Formula weight	312.33	312.33		
Space group	P 21/c (no. 14)	P 21/c (no. 14)		
Volume	1501.44(3) $Å^3$	1501.44(3) $Å^3$		

7.1.4. ^{1}H- and ^{13}C-NMR (Nuclear Magnetic Resonance)

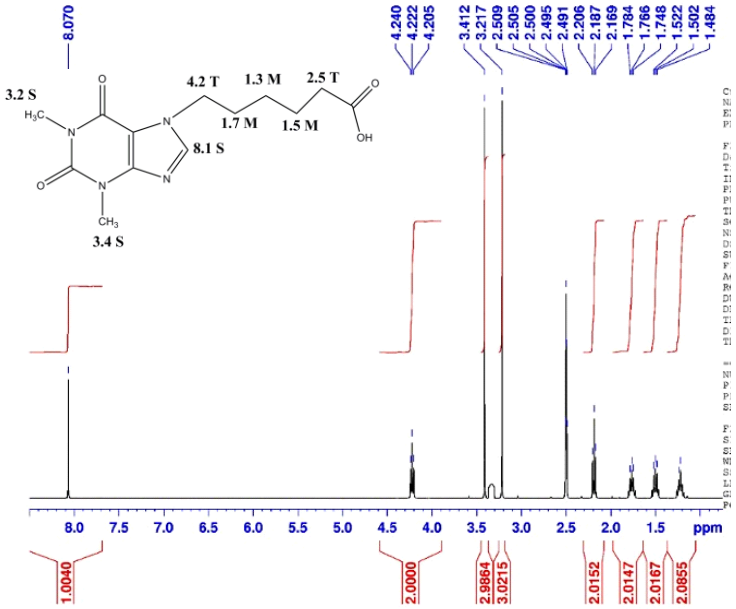

Figure 18. ^{1}H-NMR spectrum of 7-(5-carboxypentyl)-1,3-dimethylxanthine.

The ^{1}H-NMR spectrum (400 MHz, solvent DMSO) shows the following signals: δ = 1.3 (2H, multiplet, CH2), 1.5 (2H, multiplet, CH2), 1.7 (2H, multiplet, CH2), 2.5 (2H, triplet, CH2), 3.2 (3 H, singlet, CH3), 3.4 (3 H, singlet, CH3), 4.2 (2H , triplet, CH2), 8.1 (1 H, singlet, CH).

The ^{13}C-NMR spectrum (400 MHz, solvent DMSO) shows the following signals: δ = 23.8 (CH2), 25.1 (CH2), 27.6 (N-CH3), 29.4(CH2), 33.4 (N-CH3), 39.8 (CH2), 46.0 (CH2), 105.9 (C-C-N), 142.4 (C-H), 148.4 (N-C-N), 151.0 (Amid-C=O), 154.3 (amide C=O), 174.3 (COOH).

7.2. Tracer characterisation

7.2.1. Coupling ratio

The characterisation of enzyme/hapten coupling ratios was achieved using several techniques: MALDI-TOF/MS, LC-MS and CZE-UV. The results are presented by individual technique within this section and summarily compared at its very end (7.2.1.iv - Summary – Coupling ratios, page 102)

i. MALDI-TOF/MS

The main advantage of the MALDI interface is that it allows the detection of the "full" molecule, i.e., the soft ionisation causes little or no fragmentation of the analytes, allowing the detection of the molecular ion. In such way, the enzyme mass as well as the conjugates can be directly obtained from the spectra without further treatment, as opposite to electrospray ionisation where protein reconstruction software is needed.

A typical MALDI-TOF/MS spectrum is shown for the unmodified peroxidase (native HRP) and a coupled one (tracer) in Figure 19. The molecular ion was always the most intense peak, followed by two minor ones: a double-charged molecular ion – with half the molecular ion m/z value – and a cluster of two molecular ions, with a double m/z value.

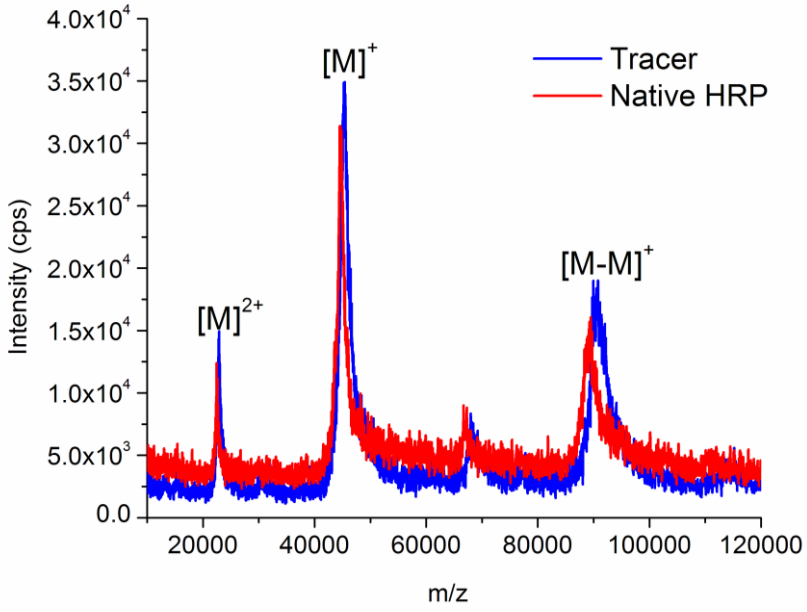

Figure 19. MALDI-TOF/MS spectra of native HRP (unmodified horseradish peroxidase) – red line; and a tracer (conjugated HRP) – blue line. Three major ions are found in each spectrum: The molecular ion $[M]^+$, a doubled-charged molecular ion $[M]^{2+}$ and a cluster of two molecular ions $[M\text{-}M]^+$.

The differences on the masses between the tracer and the HRP can be calculated from any of the spectrum peaks. No significant differences were found when the coupling ratios were calculated based on any of these three different peaks and therefore the most distinct one – the molecular ion – was chosen for the calculation.

The tracer coupling ratios were calculated after fitting the MALDI-MS spectrum with a Lorentz function (m/z fitting range: 30,000-60,000), and taking the apex of the peak. Additional information about the distribution of the coupling ratios, i.e. the coupling ratio range can also be obtained when the minimum and the maximum masses are taken into account (Figure 20). From the figure mass values, an average coupling ratio – for the represented tracer – can be determined as 2.4 molecules of hapten per molecule of peroxidase (the mass difference is 706 a.m.u. divided by the hapten mass, 294.4). Using the minimum and the maximum from both peaks, an interval of coupling ratios can be obtained starting at 0.4 and having the maximum at 4.1 hapten molecules per molecule of HRP. The minimum and the maximum mass values were obtained at 3-fold the signal of the baseline (taken at 35,000).

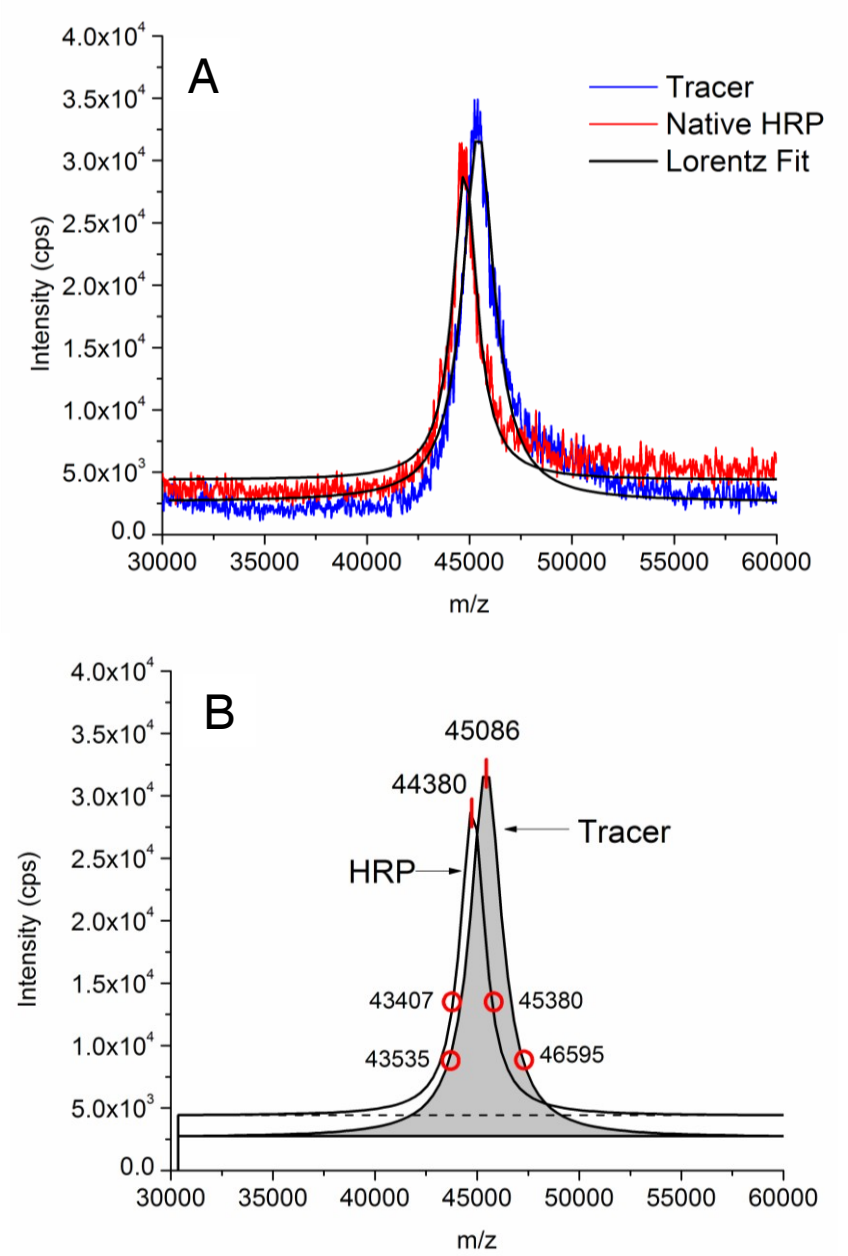

Figure 20. Detailed view of the m/z interval (30,000 – 60,000) illustrating the obtained raw spectra for tracer and native HRP and the Lorentz fitting (A); the calculations were performed using the fitted curves (B) by taking the peak apex and the beginning and end of the peak at 3 times the signal of the respective peak baseline intensity (illustrated by the red circles). The area under the tracer curve is filled in grey for better visualisation.

The coupling ratios for all the produced tracers are summarised in Figure 27 (page 103) together with the LC-MS and CZE-UV results.

ii. LC-MS

The supremacy of LC-MS over MALDI-MS is the fact that the first permits a previous separation of the analytes. As a reversed-phase column for protein separation was used (Prot RP 18S), requiring an organic solvent for the elution, the enzyme is (partially) unfolded during the chromatographic run and what is more, it looses the heme group and the two calcium ions. The unfolding has no practical implications on the final mass, except for the downwards mass-shift caused by the dislodgement of the heme group and the two calcium ions.

A typical chromatogram of HRP (0.5 mg/mL) is shown in Figure 21 after extracting the m/z range 600 to 2900. The peak of the heme group elutes at 9.9 min whereas the apo-enzyme[d] elutes at 13.3 min. The respective UV spectra are represented to show the maximal wavelength and also that a minor amount of enzyme molecules still keep the heme group, as proved by the absorption of the apo-enzyme peak at ~400 nm (RT = 13.3 min).

The mass spectrum of the peak at 13.3 min was taken for both, the different tracers and HRP and it is depicted in Figure 22-A. Observably, the obtained multicharged ions show already obvious differences between the tracer's ion masses – shifted to higher masses – and the ones of native HRP. When the spectra are reconstructed, using the *Bayesian Protein Reconstruction* add-in feature from the Analyst™ software, the protein mass range can be determined as illustrated in Figure 22-B. The mass peaks were fitted using the Lorentz function and analysed the same way as the MALDI ones: taking the peak apex, the minimum and the maximum (at 3-fold the baseline signal).

[d] *apo-enzyme should be used exclusively for the protein part of the enzyme, without the prosthetic group. In this case, as some of the molecules retain the heme, a mixture of species exists: the apo-enzyme and the holoenzyme.*

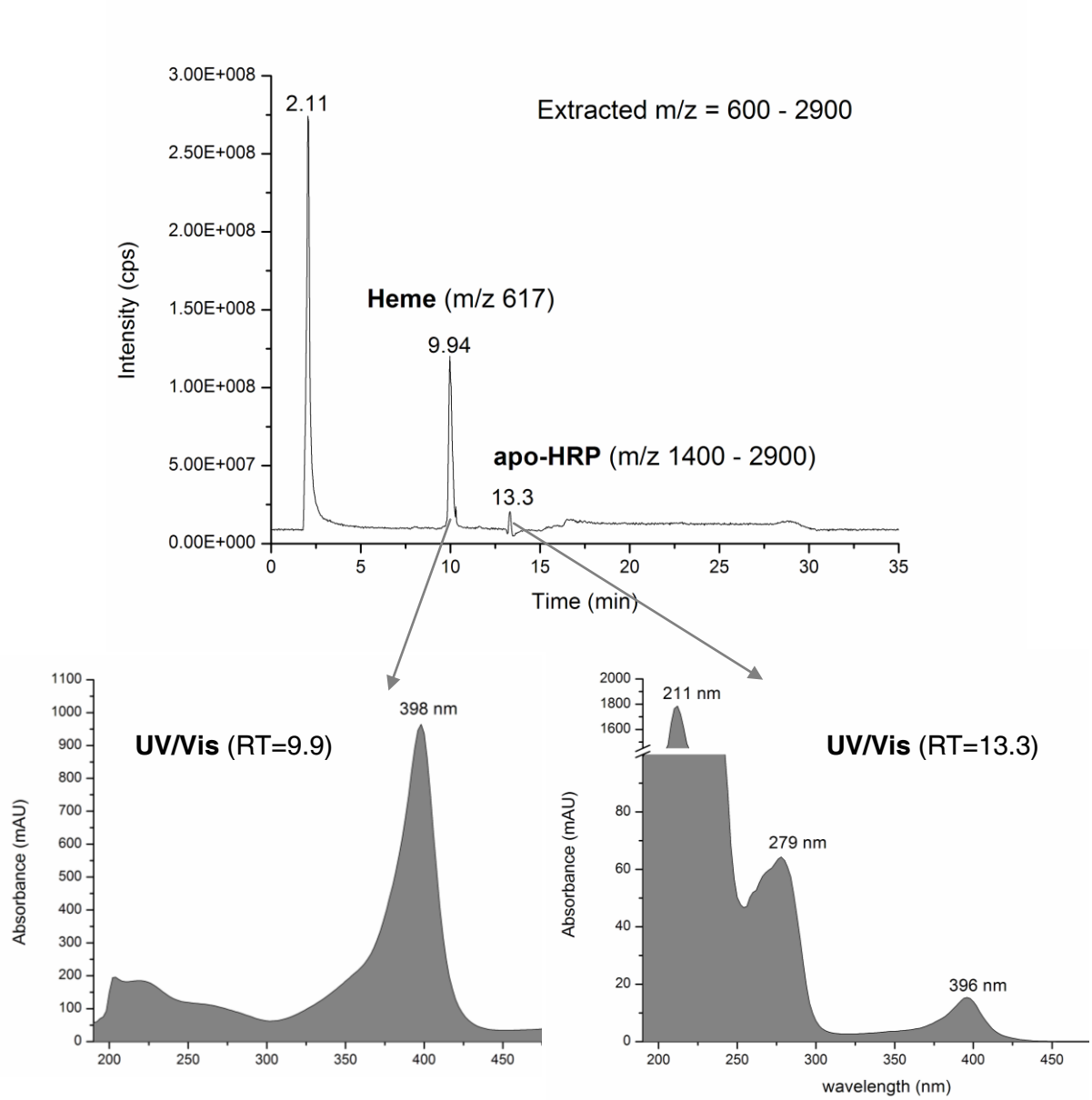

Figure 21. Top: Chromatogram of 10 µL HRP 0.5 mg/mL. The chromatogram was obtained after extracting the m/z range 600 to 2900 from the full scan spectrum. The first peak at 2.11 min corresponds to unretained solutes and the solvent front; the heme group elutes at 9.94 min and the apo-HRP at 13.3 min. Bottom: The UV spectra were taken at the apex of the peak, from the DAD spectra, and are depicted on the right-hand side.

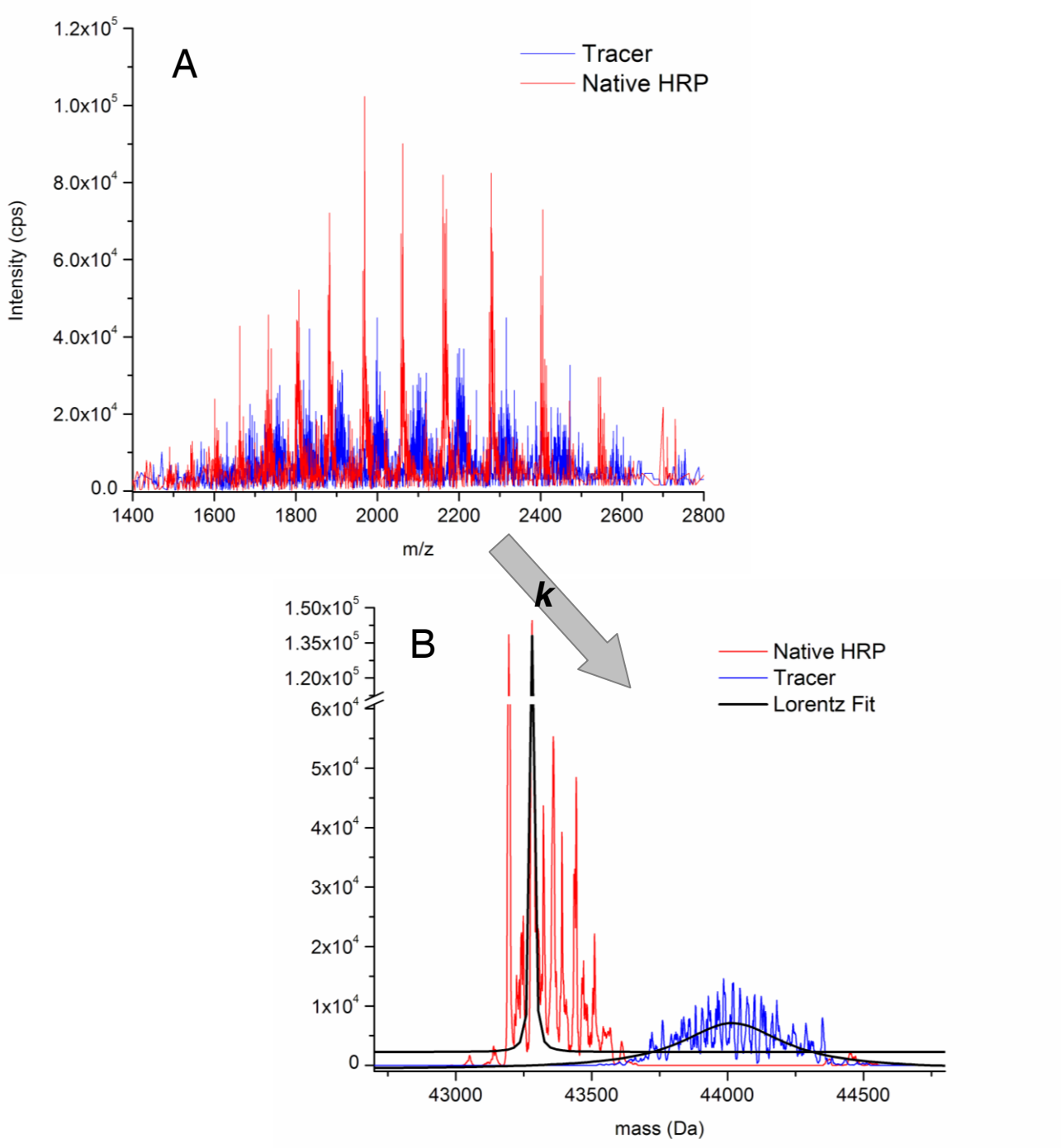

Figure 22. (A) Mass spectra of a tracer and the native HRP (at 13.3) showing the region m/z 1400 to m/z 2800. (B) Reconstructed tracer and HRP masses, from the spectra represented in A, after Bayesian Protein Reconstruction (k). The tracer is represented by the blue line while HRP spectrum is depicted in red. Lorenztian fitting is in both cases pointed up by the black line (B).

Albeit the spectra being analysed likewise the MALDI ones, more information about the coupling ratios distribution can be obtained due to the chromatographic separation. The conjugated peroxidase (tracers) elutes a few seconds later than the native HRP (Figure 23) and the peaks of the tracer are broadening as the coupling ratio interval increases, revealing the different species inside the tracer mixture. The mass spectra for the tracers were thus obtained from the entire peak – to encompass all the coupling ratios – starting and finishing at 3-fold the signal of the baseline. The final reconstructed tracers' spectra as well as the ones from different concentrations of HRP are represented by. The mass broadening caused by the different coupling ratio intervals is evident: the higher the peak broadening, the higher the coupling ratio interval.

Remark: The masses correspond to the apo-HRP and the apo-Tracer, without the heme group and the calcium ions.

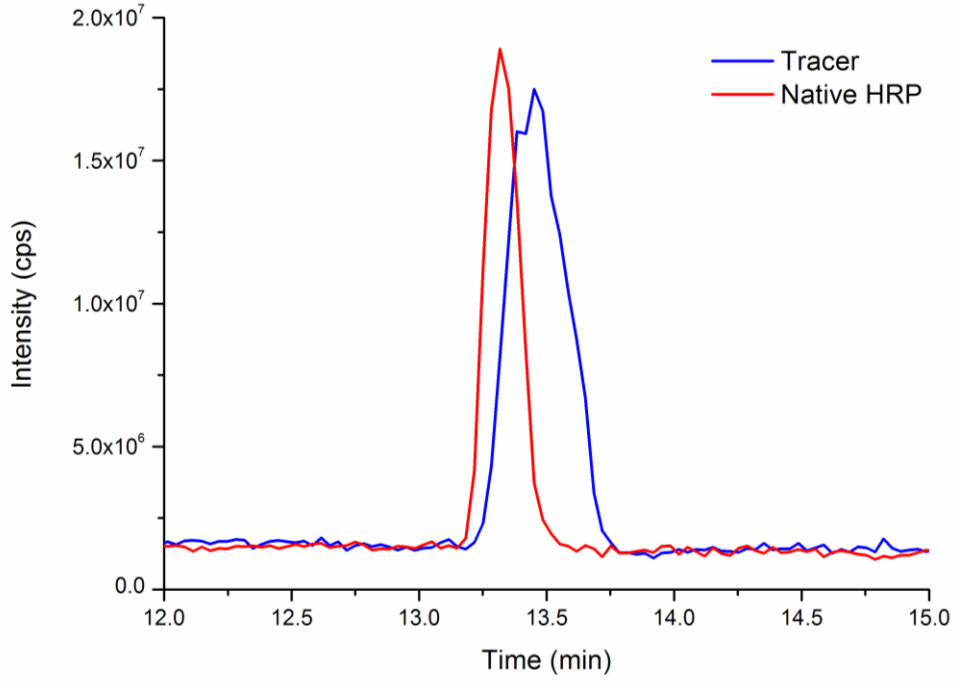

Figure 23. Chromatograms obtained after extracting m/z range 1400-2800. The red line represents the native HRP (0.5 mg/L) and the blue line a tracer dilution to obtain approximately the same concentration of HRP, both using a 10 µL injection.

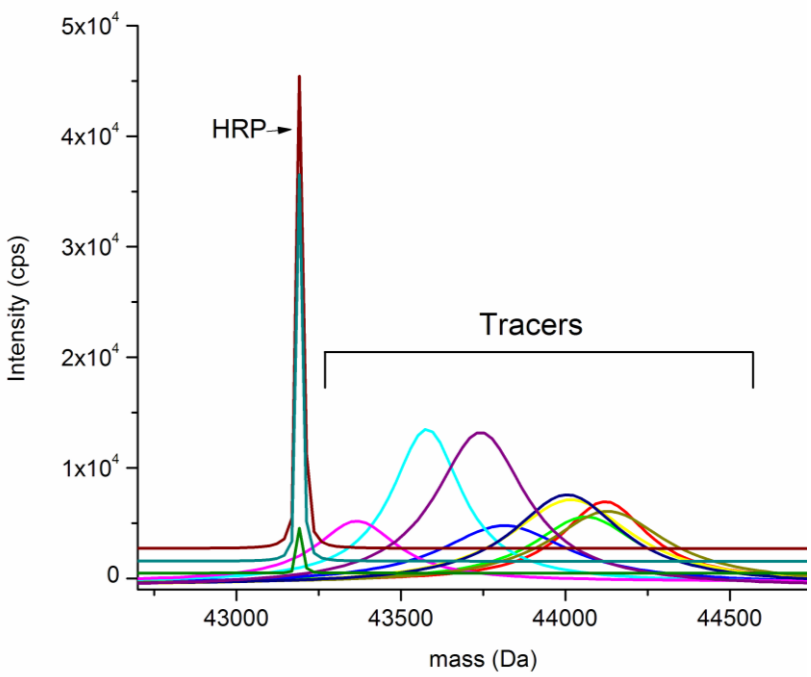

Figure 24. Reconstructed mass spectra from LC-MS, for different concentration of HRP and the different tracers synthesised.

iii. Capillary Zone Electrophoresis (CZE)

The different coupling ratios formed during conjugation could be separated, even if not baseline-resolved, and the resulting peaks integrated. The peak areas could therefore be compared, providing additional information vis-à-vis the coupling ratio interval and roughly the relative amount of each of them in the mixture (Figure 25).

The tracer represented in Figure 25, has a coupling ratio interval between 1 and probably 4. No unconjugated HRP can be "seen" in this tracer – the migration time of a coupling ratio zero (0:1) is equal to the one of the native HRP. The coupling ratio 1:1 could only be assigned to peak 1 because MALDI-MS and (or) LC-MS data was available, showing that the interval of masses starts just about the value of 1 hapten molecule per molecule of peroxidase.

Although very valuable, CE-UV data cannot stand alone for the determination of coupling ratios; it requires previous mass data from MALDI-MS or LC-MS.

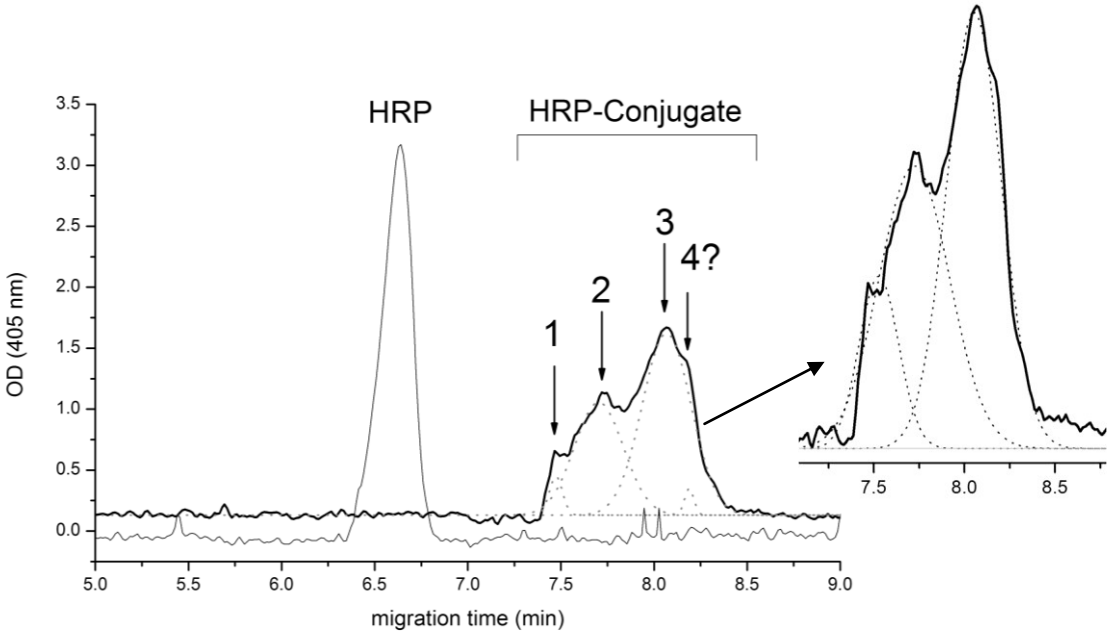

Figure 25. Electropherograms of native horseradish peroxidase (HRP) and a tracer (HRP-conjugate) using detection at 405 nm. The HRP-conjugate shows several peaks, possibly 3 or 4, and the integration of 3 of them is shown in detail on the enlargement represented on the right-hand side. Three peaks can be clearly seen and a fourth one could not be fitted inside the curve, though the specie might be present in a very low concentration. The migration times of the peaks are the following, with the relative area indicated under brackets: peak 1: 7.5 min (16%); peak 2: 7.7 min (37%); peak 3: 8.1 min (47%).

Using the electrophoretic migration time together with the MALDI-MS and LC-MS data, it is possible to approximately determine the relative amount of each coupling ratio within the same tracer, i.e., to know the coupling ratio distribution present in each tracer. For that, the peak areas of each coupling ratio (Figure 25) are calculated as a percentage of the total peaks' areas and, a distribution like the ones represented in Figure 26, is obtained.

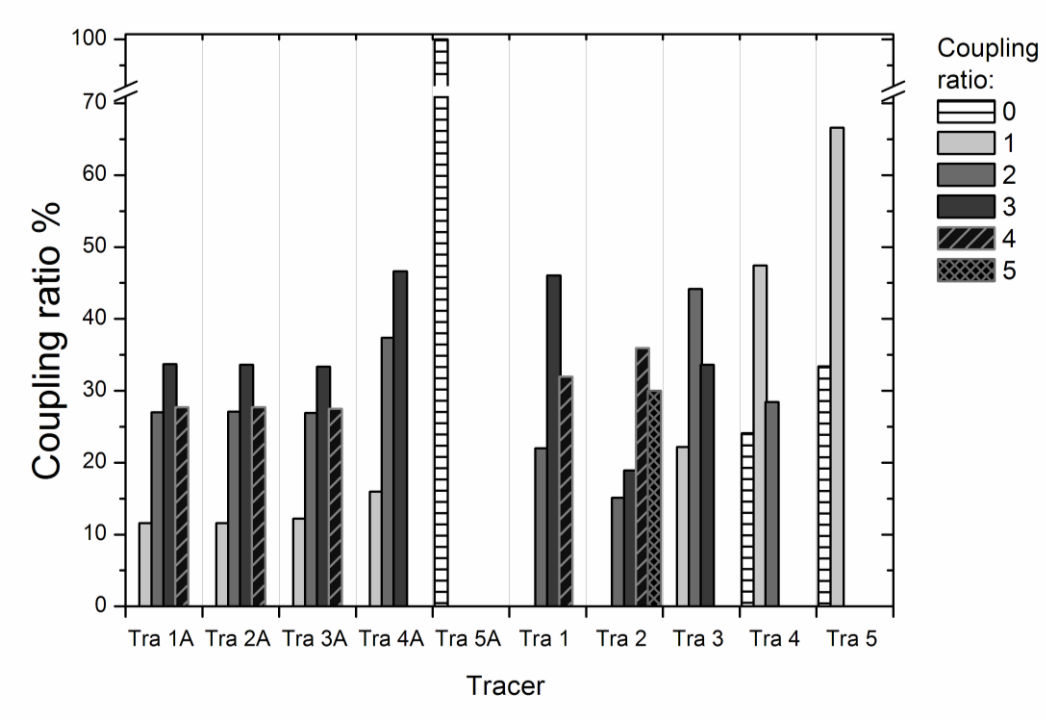

Figure 26. Distribution of the different coupling ratios within each of the tracer preparations. The bars represent the relative area of the peak and their sum equal to 100% for each individual tracer. Tracers represented by TraXA were obtained by the NHS-DCC method whereas the TraX were obtained using the mixed-anhydride method. The stoichiometric coupling ratios used for the syntheses were 1:100 (Tra1, Tra1A); 1:50 (Tra2, Tra2A); 1:20 (Tra3, Tra3A); 1:5 (Tra4, Tra4A) and 1:0 (Tra5, Tra5A).

iv. Summary – Coupling ratios

The coupling ratios obtained from all the methods are very alike, with the MALDI-TOF/MS outcome showing broader coupling intervals (Figure 27). The reason for this can be the absence of a previous separation and also, the difficulty in finding exactly the same “concentration” of HRP and tracer in the spots of the sample slide. In any case the results disclosed in Figure 27 reveal a good correlation between the methods employed and permit the use of just one of them in future works.

Either method seems equally effective for the coupling reaction and in producing conjugates with equivalent coupling ratios. Yet, some minor differences can be deducted from Figure 27: The mixed-anhydride method generates tracers with coupling ratios average of ~ 3 for the three trials with stoichiometric ratios of 1:100, 1:50 and 1:20, whereas the NHS/DCC method seems to required, at least an excess of 50-fold of the hapten to generate the same coupling ratio. The synthesised tracers present enough coupling ratio variability to test for its influence in the overall immunoassay performance.

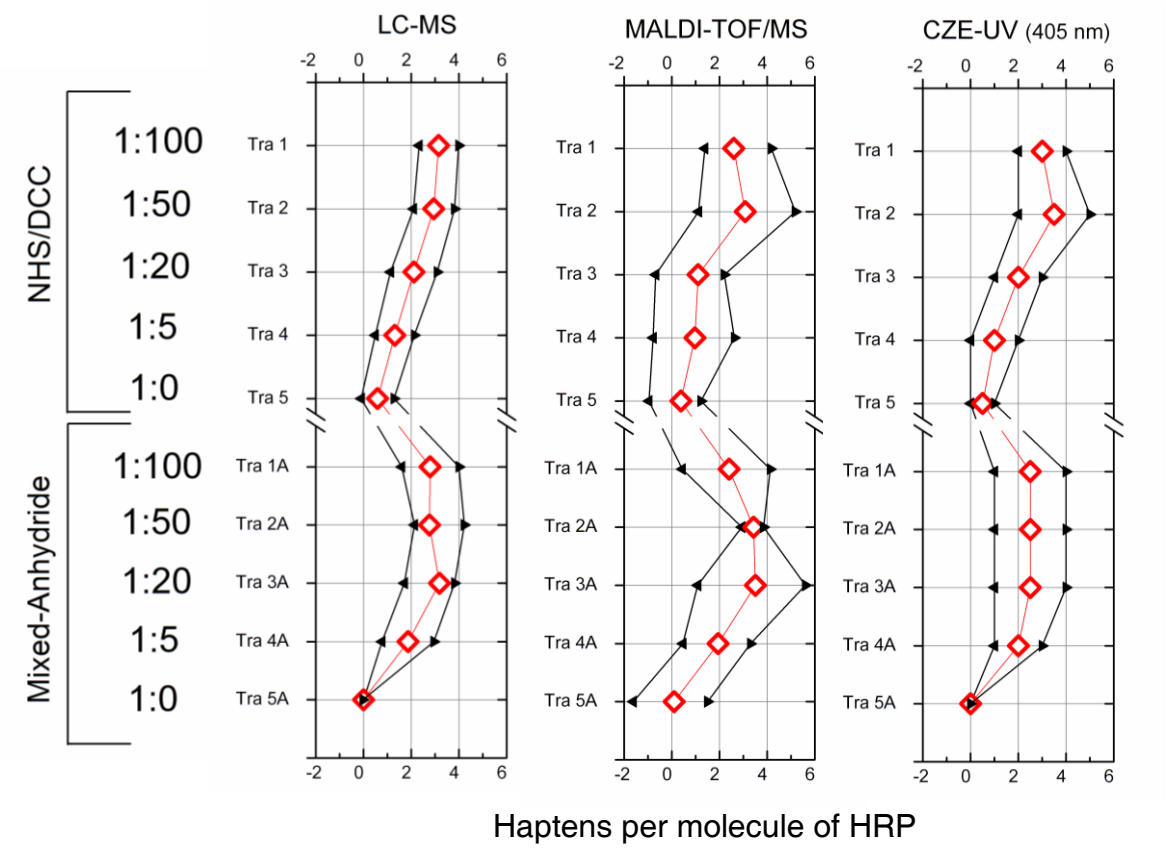

Figure 27. Coupling ratios obtained for 10 different tracers using three different analytical tools: LC-MS, MALDI-TOF/MS and CZE-UV. The tracers produced are divided into two groups according to the conjugation method used: NHS/DCC and the mixed-anhydride; the stoichiometric reagent ratios, used in the coupling reaction, are mentioned on the first column from the left, decreasing from 1:100 until 1:0 (without the hapten).

7.2.2. Determination of the concentration

A number of previous considerations must be made for a good understanding of the problem complexity:

– Protein concentrations are usually determined either by the Bradford method[e] or by reading the absorbance at 280 nm.[295] The last one is very common when small volumes are available as, after reading, the solution can be easily recovered and reused. The concentration of a protein solution can be therefore calculated either by the Lambert-Beer law (at 280 nm) or by an external standard calibration curve, with the same protein as standard or another similar to the one being quantified.[295] For this work this was not possible because the coupled hapten has its maximum absorption at 275 nm. Nevertheless, the data obtained at 280 nm was analysed and it is presented here as it provides useful information about the coupling ratios.

[e] *Based on the pH-dependent binding of a dye (coomassie brilliant blue G-250) to the protein: absorbance max. at 595 nm.*

– Having a heme group with a maximal absorption at 405 nm, HRP conjugates (tracers) could be easily quantified using this wavelength, if only the UV-spectral behaviour would not change during the conjugation and tracer purification steps. Changes were perceived for the blank tracers (Tra5 and Tra5A) spectra when compared to the native HRP ones, in the same buffer (PBS). Mostly, the ratio A405/A280 – usually referred to as the *Reinheitszahl* number, RZ – is much lower in the HRP passed throughout the conjugation process, i.e. in the blank tracers, than in the native HRP. Since the hapten is not present in solution, a likely phenomenon which might explain this RZ decrease is the effect of the organic solvent on the displacement of the heme group in HRP molecules. In any case, measuring the tracers at 405 nm means measuring the active enzyme in the solution, which for the aim of this work – comparing different tracers on the ELISA performance – is the gist.

i. CZE-UV

Using capillary zone electrophoresis (CZE), the tracer protein concentrations were quantified at two different wavelengths: 280 nm and 405 nm, using either the peak height or the peak area. The method used for determining the coupling ratio was slightly modified here (higher current) to minimise the peak broadening – caused by the different coupling ratio intervals inside each tracer mixture.

The concentrations obtained using absorbance values at 280 nm were always higher than concentrations obtained at 405 nm, except for the blank tracer – without the hapten coupled – as for the HRP standards when read as unknown samples in the calibration curve. This means that the higher absorbance at 280 nm is most likely caused by the absorbance of the coupled hapten. Indeed, the higher the coupling ratio, the higher the difference between the concentrations obtained at both wavelengths. And a linear correlation between coupling ratio average and the relative differences between the two wavelengths gave a correlation coefficient of 0.80.

Integration by peak height led always to lower concentrations than when the peak area was used, irrespectively of the wavelength employed. This expected effect is caused by the coupling ratio distributions as illustrated by Figure 28, where the tracer's electropherograms are plotted together with HRP standard solutions.

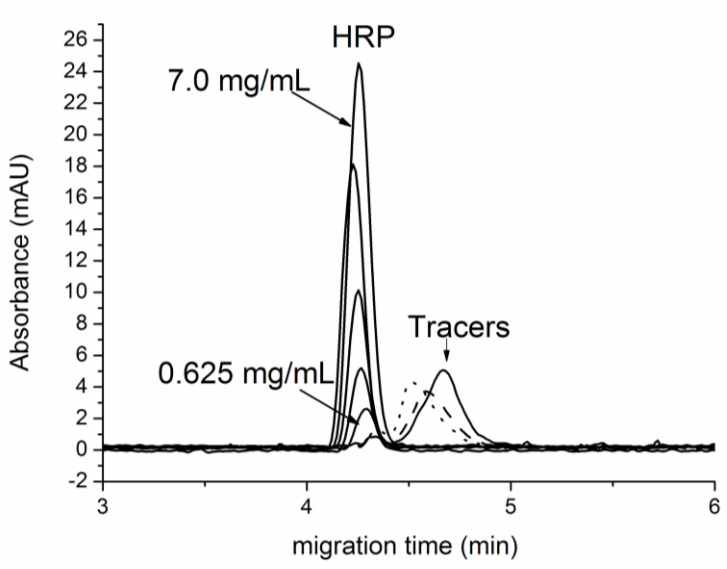

Figure 28. Electropherograms of HRP standards (from 0.625 mg/L up to 7.0 mg/L) and three tracers, illustrating the quantitation by CZE-UV (405 nm).

ii. LC-UV and LC-MS

The presence of acetonitrile in the mobile phase causes the heme group displacement in a concentration-dependent mode. Such occurrence was positively used to quantify the tracer's concentration alongside with the remaining enzyme part, the hereafter called "apo-tracers".

The free heme group could be detected using UV (both 280nm and 405 nm) and mass spectrometry, either using the m/z value of the molecular ion (m/z 607) or its cluster (m/z 1232). When UV detection was used, whichever peak integration mode was chosen, the obtained tracer concentrations were always the same. Mass detection gave slightly lower values in most of the cases but not in all of them. In any case the differences are very acceptable as shown in Figure 30 (page 107).

Opposite was the outcome when the apo-tracers were used, which undergo similar problems with the coupled-hapten absorption as the ones afore-described for the CZE. The UV detection at 280 nm generates very high concentrations when compared with the other methods, in fact it turned out the highest concentrations registered. Likewise CZE, the peak broadening caused by the different coupling ratios inside the same tracer solution, leads to a difference when the calibration is based on peak areas or peak heights. Yet, less noticeable than in the CZE case, as the separation resolution between the species is also less powerful with reversed-phase chromatography. When the detection is performed by mass, extracting the m/z range 1500-2800, the obtained concentration are rather comparable to the

ones found using the heme mass. Figure 29 represents the chromatograms obtained using the m/z range 1500-2800 (apo-tracers) and the heme group m/z, and aims to show that the heme group peak has similar shape and retention time for all the tracer while some differences can be observed in the apo-tracer ones, due to different coupling ratios.

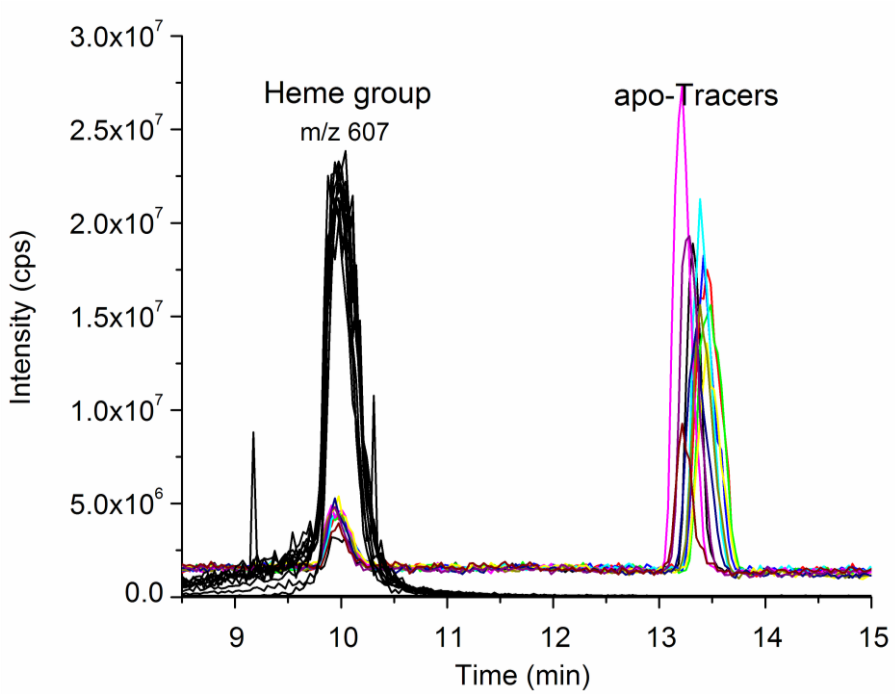

Figure 29. LC-MS chromatograms for all the tracers. The coloured chromatograms were obtained after extracting the m/z range: 1500-2800 whiles the black ones where obtained via extraction of the m/z 607 ion (heme group).

iii. UV-Vis spectroscopy

The tracers were also measured directly in PBS buffer in a UV-Star™ microtitre plate by UV-Vis (280 nm and 405 nm) and as expected the concentration obtained at 280 nm were also considerably higher.

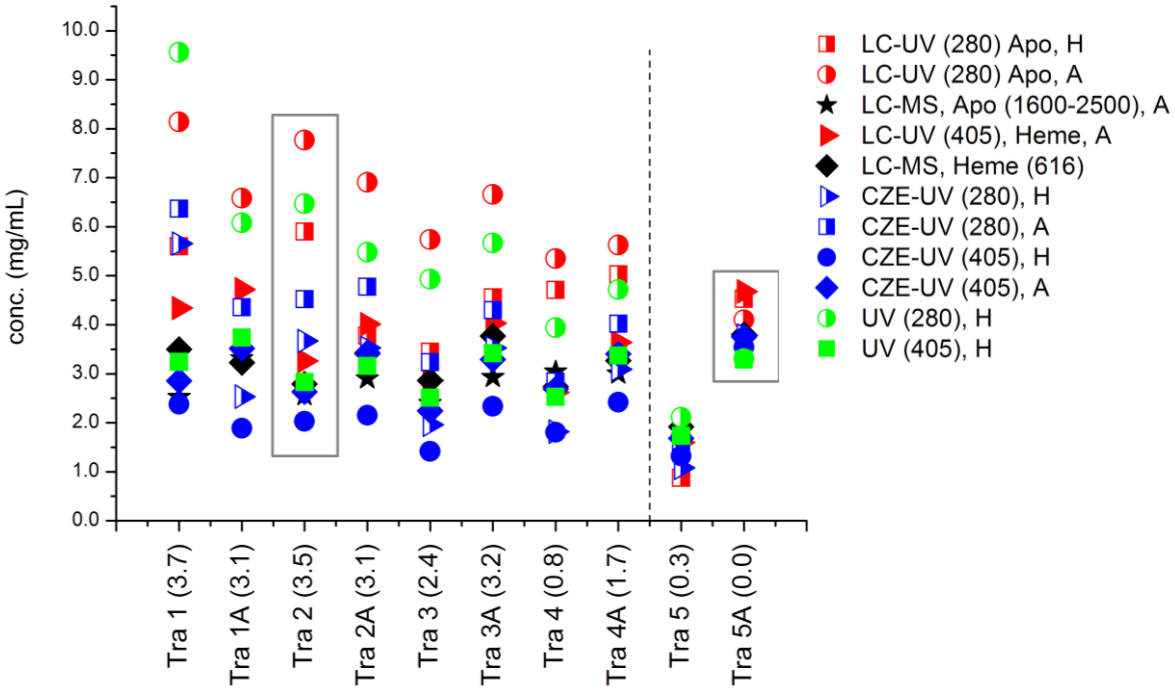

Figure 30. Final concentration found for the produced tracers using different analytical techniques and detection modes. The legend is presented on the right-hand side, where each analytical technique is represented by a different colour and detection at 280 nm is always represented by half-filled symbols while at 405 nm by bold ones. Mass detection is represented by bold black symbols. The wavelengths or the m/z are represented within brackets and the letter after the comma is the peak integration mode: area (A) or height (H). The dashed-line separates the hapten-conjugated tracers (left) from the ones without the hapten – blank tracers (right). Two grey-lined squares were included to show the variability of concentrations in a tracer with a high coupling ratio (Tra1A) in comparison with a zero-coupled blank tracer (Tra5A).

The numbers inside brackets in the x-axis are the average coupling ratio, of the respective tracer, obtained by MALDI-TOF/MS.

Some redundant data was excluded from the picture: LC-UV of the heme at 280 nm (peak integration by area and height) and at 405 nm (integration by peak height) have similar results to the represented LC-UV (405), heme, A (bold red right-triangle); the cluster of the heme group by MS has the same outcome as the heme molecular ion itself and was therefore omitted (LC-MS, heme, 616).

To sum up:

Determination of HRP-based tracers should be preferentially performed at 405 nm or using mass spectrometry detection, based on the released heme group.

7.2.3. Tracer coupling ratio influence on ELISA

When the tracers were diluted to obtain equal concentrations (using the concentration values obtained at 405 nm, heme group, by LC-MS), no differences were found neither in the enzyme activity nor on the ELISA sensitivity. As Figure 31 shows, the different tracers give similar curves and the C-values (indicative value for sensitivity) are not significantly different. This systematic study of the tracers was performed after recognizing in previous experiments that the coupling ratio hapten/enzyme did not seem to play an important role on the assay performance. Though some more studies are required, the obtained data strongly advice against such extensive and time-consuming studies in future ELISA development processes.

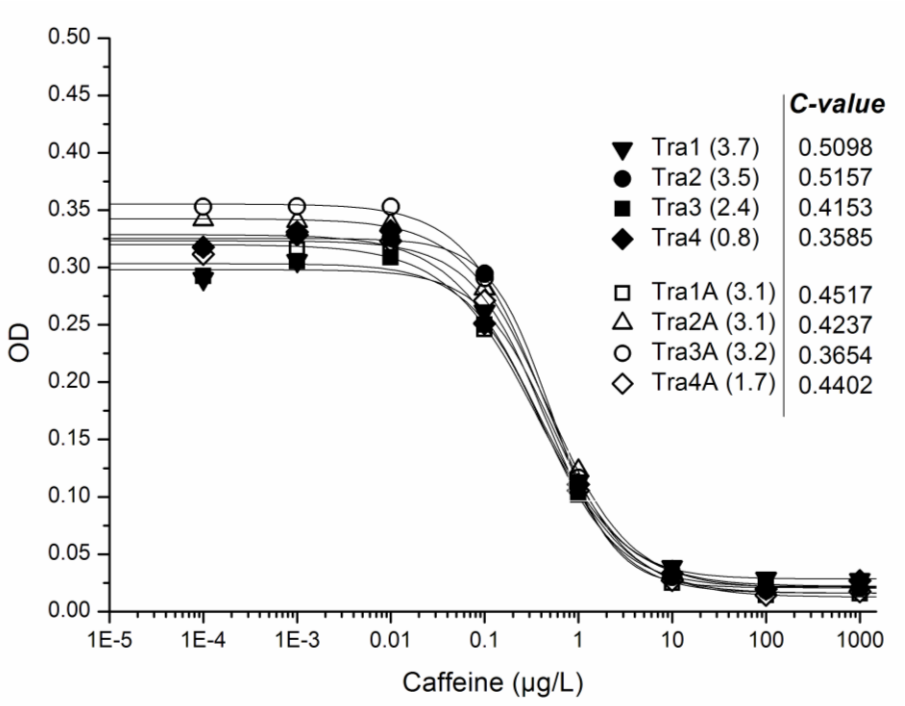

Figure 31. ELISA calibration curves for the synthesised tracers. The bold-symbols represent the tracers obtained using the NHS/DCC method whereas the open-symbols the mixed-anhydride coupling. The MALDI-TOF/MS average coupling rates are indicated within brackets, after the tracer designation. Blank tracers (Tra5 and Tra5A) are not represented since they do not bind to the antibody, as expected. The C-values, obtained from the logistic fitting curve are indicated on the right side of the legend to allow sensitivity comparisons.

The coupling ratio hapten/peroxidase does not seem to influence the overall sensitivity of the newly developed caffeine immunoassay.

7.3. Polyclonal antibody immunoassay

The immunoassay setup and optimisation using the anti-caffeine polyclonal serum from sheep was extensively discussed in a diploma thesis.[296] Therefore, the details regarding the optimisation of the assay – which follow the same procedures used for the monoclonal antibody – are omitted here.

After testing several buffers (carbonate, Tris, PBS) as well as different pH during the different steps of the assay, the best C-value (best sensitivity) was achieved by using PBS buffer pH 7.6 during the anti-serum and the tracer incubation steps. Carbonate buffer did not even permit the establishment of a calibration curve.

Anti-caffeine serum and tracer dilution were optimised to provide an acceptable A-value (maximal absorbance) between 0.5 and 1 and thereafter the best C-value. A 75,000-fold dilution for the anti-serum and a 10,000 fold dilution for the tracer were found to be the optimal conditions. Typical C-values range from 1.8 to 9 µg/L using the aforementioned conditions. The sensitivity could have been further optimised, same manner as for the monoclonal antibody (7.4 - Monoclonal antibody (mAb) immunoassay, page 114), but the encountered matrix effect when real samples were measured discouraged such a time investment. A typical routine calibration curve is depicted in Figure 32, with a resulting C-value of 7.5 µg/L.

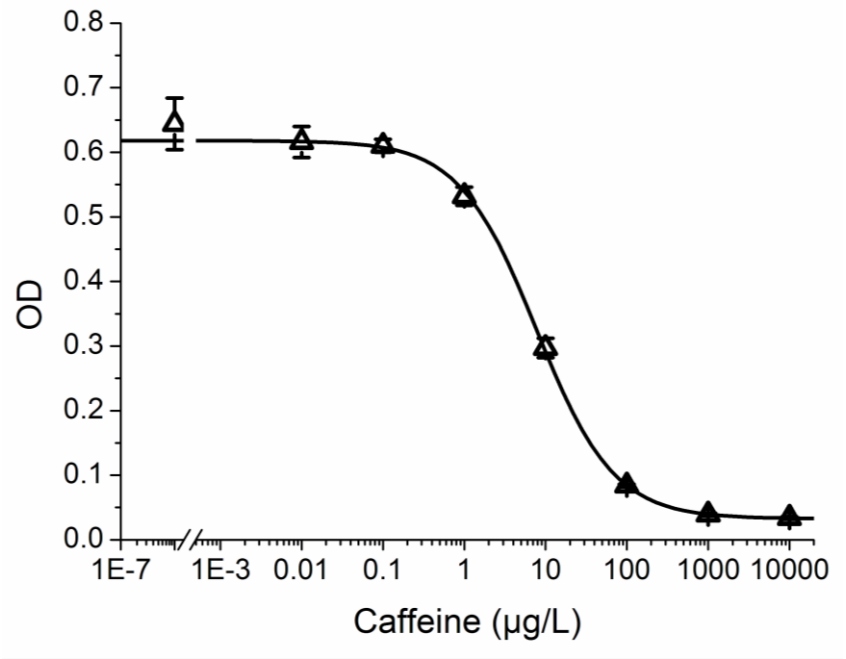

Figure 32. Calibration curve obtained with the anti-caffeine polyclonal serum from sheep. The curve parameters are: A = 0.618, B = 0.914, C = 7.5, D = 0.020, R^2 = 0.9998.

7.3.1. Surface water samples monitoring

Three surface water samples collected from the Teltowkanal in Berlin-Adlershof (Lat.: 52°25'33.8232''; Long.: 13°31'36.5046'') were analysed using the polyclonal immunoassay and compared with the reference method afore-described (6.7 - Reference method for caffeine, page 83). The outcome is summarised in Table 12.

Table 12. Caffeine concentration in surface water samples from Teltowkanal (Berlin-Adlershof) collected on the 27th August 2007 and analysed using the polyclonal (pAb) immunoassay and a reference method: SPE-LC-MS/MS.

Sample	pAb Immunoassay	Reference method (SPE-LC-MS/MS)
	Caffeine [µg/L]	
Teltow 1	12	0.062
Teltow 2	3.5	0.080
Teltow 3	3.4	0.13

An overestimation is evident from the table values. Some cross-reactant was suspected to be the cause and hence several related compounds were tested as described beneath.

7.3.2. Cross-reactivities (pAb)

The caffeine-related xanthines presented relatively low cross-reactivities: Paraxanthine (0.23%), theophylline (4.5%), theobromine (2.3%) and xanthine (<0.008%) as well as other chemically similar compounds the cross-reactivities of which are detailed jointly with the ones from the monoclonal antibody assay in Table 14 (page 116). Moreover, the concentrations of the other xanthines in surface water are relatively low to justify such overestimation. To illustrate the unlikeliness of xanthines causing such an effect, Table 13. was produced. Xanthines' concentrations in the tested water samples are not sufficiently high to explain such overestimation. Interesting is the fact that the compound with the highest cross-reactivity (theophylline) is the one found in lower concentrations in the analysed waters and the highest concentrations were found for the lowest cross-reactant (xanthine).

Table 13. Concentrations of several xanthines in water samples from the Teltowkanal, Berlin, measured by SPE-LC-MS/MS. (*) These values were obtained by multiplying the concentration of the compound in the sample by the compound cross-reactivity. By doing such, an estimate value of the expected overestimation could be obtained.

	Cross-reactivity [%]	Teltow 1 [µg/L]	Teltow 2 [µg/L]	Teltow 3 [µg/L]
Caffeine	100	0.062	0.080	0.13
Paraxanthine	0.23	0.010	0.010	0.022
Theophylline	4.5	<0.005	<0.005	0.005
Theobromine	2.3	0.016	0.021	0.054
Xanthine	<0.0008	0.23	0.27	0.32
Expected concentrations given as caffeine equivalents(*) in µg/L				
Paraxanthine		2.3E-05	2.4E-05	5.0E-05
Theophylline		< 2.3E-04	< 2.3E-04	2.3E-04
Theobromine		3.8E-04	4.8E-04	0.001
Xanthine		1.8E-06	2.1E-06	2.5E-06
Sum		6.3E-04	7.4E-04	0.0015

A vast number of compounds present in water, known and unknown ones, would have had to be tested in order to find the cross-reactant(s). The most evident substances were tested, like the purines guanine and adenine (nucleic bases). By sharing the xanthine ring and conceivably being present at high concentration in an aquifer – DNAs and RNAs – it would be reasonable expecting them to be the overestimation cause. Yet, insignificant cross-reactivities were found with some exceptions from the tri-phosphate forms, particularly guanosine-5'-triphosphate (GTP) with a cross-reactivity of 0.18%.

GTP besides presenting a carbonyl function on the same position as caffeine, which adenosine itself lacks, has the residual sugar bonded to the purine ring via C7, i.e. the same position used for conjugating the CafD with the enzyme and producing the tracer – via a carbon chain spacer and an amide bond. The CafD cross-reactivity is 1100%, meaning that it is binding more effectively to the antibody than caffeine itself – as expected, given that it was the immunogen used for raising the antibody.

7.3.3. The calibration range

In addition to the cross-reactivity, the calibration curve was also checked as a possible reason for the deviation on caffeine concentration.

Typically, immunochemists use a 4-parameter sigmoidal curve to fit calibrators with a 10-fold concentration difference between them, over a range of concentrations wider than at least 8 orders of magnitude (e.g. from 0.01 to 1000 µg/L). Taking into account that for establishing such a calibration, six calibrators were used and for the reference method (LC-MS/MS) the same number of calibrators is used to cover a shorter calibration range (typically from 5 to 100 µg/L), a question can be posed regarding the calibration itself. This was checked by establishing an immunoassay calibration using 7 calibrators (Figure 33-A) and 16 calibrators (Figure 33-B), all of them read on the same plate (same absorbance), and analyzing 10 aliquots from a surface water sample and 10 aliquots of the same sample spiked with 20 µg/L caffeine. The native sample had a concentration of 4.47 µg/L (± 9.4%) using curve A and 4.85 µg/L (± 9.8%) using B; and the spiked sample 24.6 µg/L (± 7.3%) using curve A and 26.2 µg/L (± 6.6%) using B.

Although the results are not different enough to justify the overestimation found for the polyclonal serum, they are significantly different to illustrate how important the range selection is for the final result accuracy. Using curves like the one represented by A (Figure 33) should be progressively abandoned in quantitative environmental chemistry.

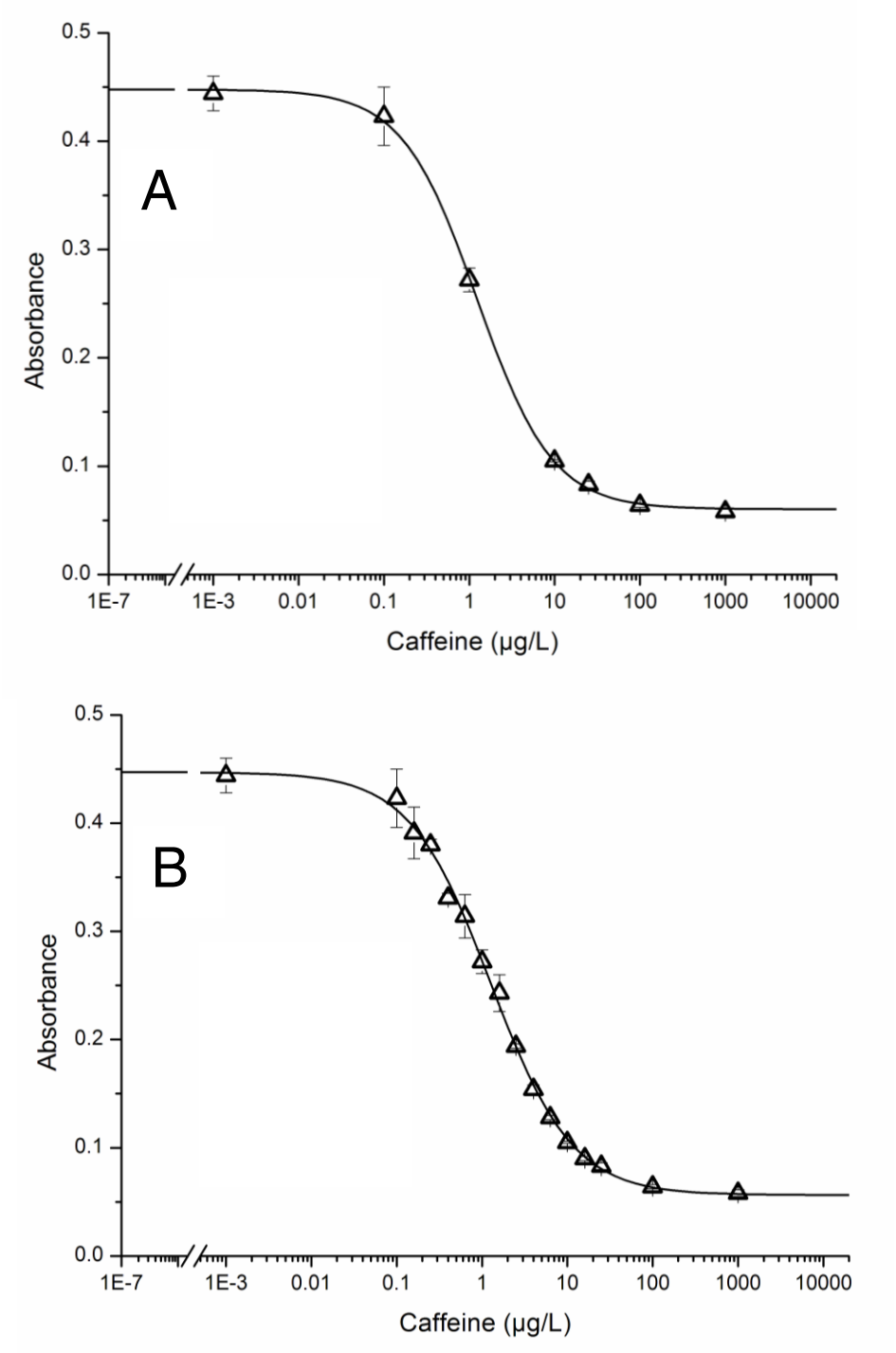

Figure 33. Calibration curves obtained using the frequently used calibration standards in ELISA (A) and using a larger amount of calibrators within the quantitation range (B). Curve (A): A = 0.448, B = 0.991, C = 1.3, D = 0.060, R = 0.9992; and (B): A = 0.447, B = 0.914, C = 1.3, D = 0.056, R^2 = 0.9974.

7.4. Monoclonal antibody (mAb) immunoassay

The foremost results obtained using the monoclonal antibody were already published[167] and are here described in more detail.

7.4.1. Antibody selection

Two monoclonal antibodies were tested. One did not bind to the synthesised tracer. Relying on the information provided by the antibodies suppliers, no difference is found regarding the immunogen chosen to produce anti-caffeine antibodies, in fact all suppliers state to have used keyhole limpet hemocyanine (KLH) coupled with 7-(5-carboxypentyl-)1,3-dimethyl-xanthine,[297] the same caffeine derivative used to produce the tracer. If this information was trustworthy, the produced tracer should bind to all the antibodies available on the market.

After testing the antibody supplied by Fitzgerald (Ab2 in Figure 34) an extensive analysis to all the antibodies available in the market was done and it was found that even though they assert to have used the same immunogen, they present different values of cross-reactivities. From that information, obtained from the antibodies datasheets, two general groups of monoclonal antibodies can be established: a group where the caffeine derivative (7-(5-carboxypenthyl-)1,3-dimethylxanthine) was synthesised from theophylline, i.e., the same used for the tracer synthesis; and another group where the derivative was probably produced using paraxanthine as major building block, a possible 3-(5-carboxypenthyl-)1,7-dimethyl-xanthine derivative. The USBiological antibody (Ab1 in Figure 34) belongs to the first group, while the Fitzgerald (Ab1 in Figure 34) to the second one. The major xanthine cross-reacting with the first group of antibodies is theophylline, while with the second one is paraxanthine. This means that if a caffeine derivative is produced using paraxanthine as building block, instead of theophylline, the resulting tracer would probably bind to the second group of antibodies (to which the Fitzgerald antibody belongs).

Further experiments were not conducted in this field because: 1) being paraxanthine the major caffeine metabolite, the antibody with the lowest cross-reactivity towards paraxanthine was selected; 2) paraxanthine is very expensive when compared with theophylline, which creates some restriction when large amounts of tracer are to be produced, relevant for the prospective commercialisation of the assay.

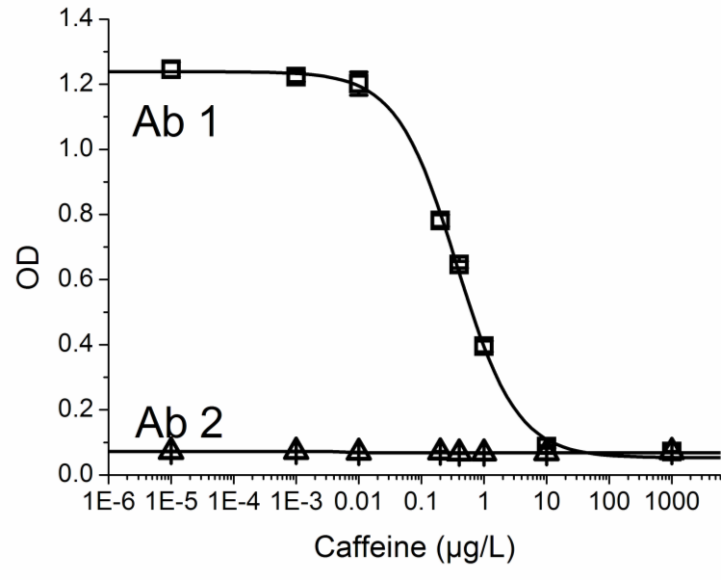

Figure 34. Binding of the tracer to two antibodies: the one used in the immunoassay (Ab1) supplied by USBiological and the first antibody tested (Ab2), which does not bind to the tracer, supplied by Fitzgerald.

7.4.2. Cross-reactivities (mAb)

The monoclonal antibody (mAb), from USBiological, and the polyclonal antibody (pAb) were tested for cross-reactivity with compounds structurally related to caffeine. The cross-reactivity results for both are summarised in Table 14 to provide comparison readability. Paraxanthine, the major liver metabolite of caffeine, advantageously presented a very low cross-reactivity of 0.08%, for the mAb. Furthermore the cross-reactivities for all compounds structurally related to caffeine are well below 5% when this antibody is used.

Table 14. Cross-reactivities (molal), in percent, for several compounds in two caffeine immunoassays using a commercial mAb and pAb, respectively. (*) Adenine, guanine and deoxyadenosine triphosphate (dATP) show the same low cross-reactivity as xanthine and therefore they were not included in the table.

Substance	CAS number	Structure	pAb	pAb
Caffeine (1,3,7-Trimethylxanthine)	58-08-2	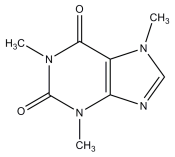	100%	100%
Theophylline (1,3-Dimethylxanthine)	58-55-9	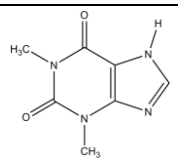	12.4 ± 2.2%	4.48 ± 0.4%
Theobromine (3,7-Dimethylxanthine)	83-67-0	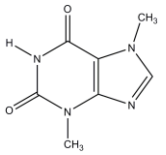	0.13 ± 0.06%	2.33 ± 0.16%
Paraxanthine (1,7-Dimethylxanthine)	611-59-6	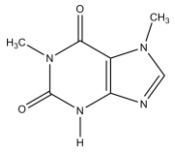	0.08 ± 0.01%	0.23 ± 0.01%
Xanthine(*)	69-89-6	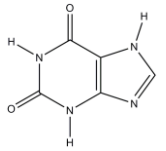	<0.002%	<0.008%
Caffeine-trimethyl-^{13}C	78072-66-9	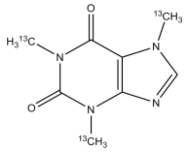	93.1 ± 1.9%	100.3 ± 6.2%
Caffeine derivative (7-(5-Carboxypentyl)-1,3-dimethylxanthine)	61444-23-3	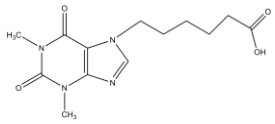	218 ± 10.0%	1108 ± 138%
dGTP	2564-35-4	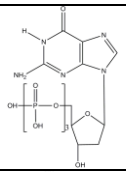	0.04 ± 0.003%	0.18 ± 0.02%
Adenosine	58-61-7	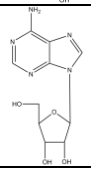	0.03 ± 0.01%	<0.008%

7.4.3. Matrix effects

In initial experiments (6.6.3.i – Previous experiment, page 78), low recoveries were observed for the Teltowkanal samples (43%), the tap water (56%), and the highly mineralised water (59%), whereas Milli-Q water (102%) and a low-mineralised mineral water (96%) showed acceptable caffeine recoveries by ELISA. In contrast, the SPE–LC–MS/MS results showed good recoveries for all samples (above 80%) hinting for an effect of the sample mineralisation on the ELISA rather than on the analyte itself. Consequently 11 mineral waters (with different mineralisation and spiked with 1 µg/L caffeine) were analysed and a significant correlation was found between caffeine recovery and calcium concentration (R^2 = 0.974), electric conductivity (R^2 = 0.936) and the total dissolved solids at 180 °C (TDS, R^2 = 0.966), as illustrated in Fig. 1, which shows the calcium concentration as an example of such correlations[f]. Sodium (R^2 = 0.019), chloride (R^2 = 0.204), the pH (R^2 = 0.340), and to some extent also sulphate (R^2 = 0.608) did not show a significant effect on the assay performance in the ranges tested (for details please refer to Table 6, page 79, under section 6.6.3 - Matrix effects).

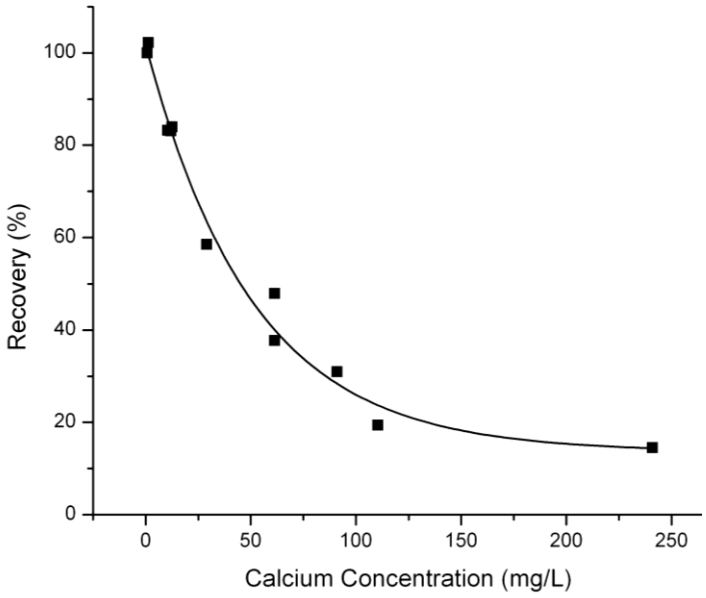

*Figure 35. Correlation between the calcium concentrations in different mineral waters and the caffeine recovery in the respective sample. The points were correlated using a 1st order exponential decay fitting: Caffeine Recovery = 88.2*e^(-[Ca2+]/50.9) + 13.6; R^2 = 0.984.*

[f] *The statement reports to an observation, being clear that a sample with a high mineralization will consequently have a high electric conductivity and a high content in TDS.*

7.4.4. Calcium effect

The spiking experiments with calcium using a low mineralised water (Lausitzer, 12.5 mg/L Ca^{2+}, 97.8 µS/cm) (6.6.3.iii – Effect of the calcium concentration, page 79) are summarised as a bi-histogram in Figure 36, and clearly show the inverse correlation between the calcium concentration/sample mineralisation and caffeine recovery (R^2 = 0.910). Yet, again the caffeine recoveries measured by LC–MS/MS were reasonably constant, irrespective of calcium concentration/sample salinity (R^2 = 0.264).

Two possibilities have been envisaged to overcome this assay drawback:

1) Removing the calcium by adding excess of EDTA to the sample (described in 6.6.3.iv – Effect of EDTA addition, page 80). The results summarised in Figure 36 show a positive effect on the recovery when 51 mM EDTA is added, with the exception of the highest concentrations: 500 and 1000 mg/L (~12.5 mM and 25 mM, respectively). For these concentrations the opposite effect was observed.

2) Increasing the buffer salinity by adding NaCl (tenfold more concentrated than in regular Tris buffer). When the concentration of NaCl in the Tris buffer (10 mmol/L Tris, 15 mmol/L NaCl) was increased to 150 mmol/L, the aforementioned drawback was overcome, as illustrated by the recoveries in Figure 36. It was also interesting to observe that the ELISA signal (OD) and sensitivity were considerably enhanced when the NaCl concentration was increased (data not shown). For higher concentrations of Tris no improvement was observed. The final buffer has a pH of 8.5 and an electric conductivity of 15.7 mS/cm . The highest electric conductivity found in the surface waters analysed was 1.8 mS/cm.

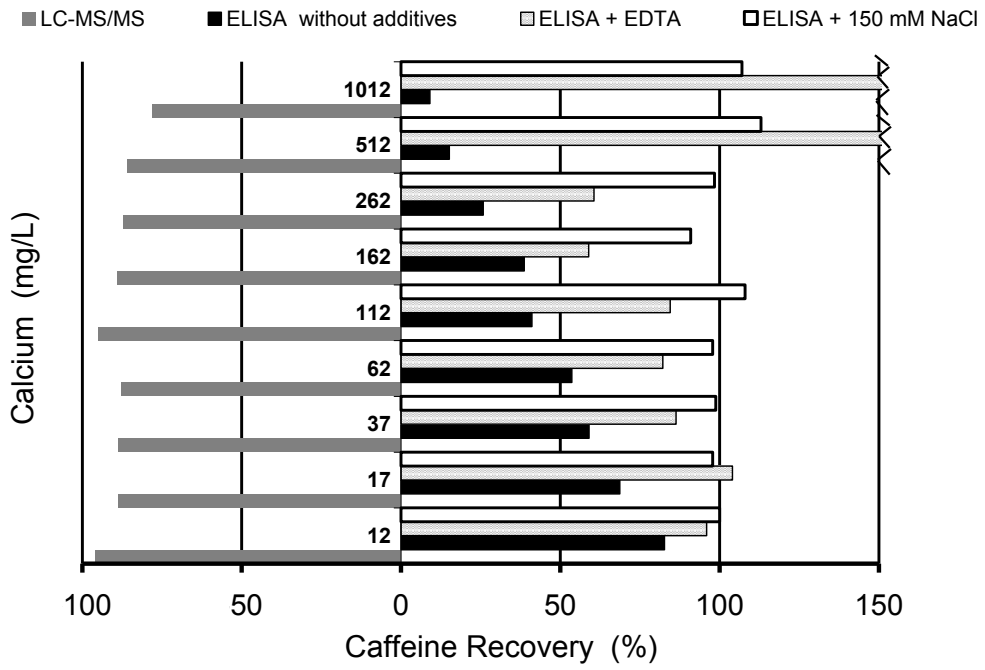

Figure 36. Bi-histogram representing caffeine recovery (in %) in a mineral water spiked with different calcium concentration and a constant amount of caffeine (1 µg/L), when measured by LC-MS/MS and ELISA. The bars on the left-hand side represent the recoveries obtained by LC-MS/MS and the ones on the right-hand side the recoveries obtained by ELISA: without additives adding to the Tris buffer (black bars); when 51 mM EDTA was added (hatched bars) and after adding 150 mM NaCl (open bars). The calcium concentration, in mg/L, is indicated by the numerals between the LC-MS/MS recovery bars, left to the y-axis.

In the last experiment described in the methods section (6.6.3.v – Calcium effect vs sample mineralisation, page 80) concerning the calcium concentration/sample mineralisation, in sample Lausitzer 1 (1000 mg/L Ca^{2+}, 1756 µS/cm) only, a low caffeine recovery was obtained (40%); Lausitzer 2 (12 mg/L Ca^{2+}, 1746 µS/cm) despite the high salinity shows 86% recovery, which is closer to the value obtained with the control sample, Lausitzer 3 (96%). These results suggest an effect of calcium on the immunoassay when solutions with low buffering capacity are used. This effect was not observed when the high-salinity buffer was used.

7.4.5. Temperature effect

The assay was performed at three different temperatures: 4°C, 20°C (room temperature), and 37°C. It was observed that the higher the temperature, the higher the signal. Likewise the C-value and D-value increase by increasing the temperature. Each calibration standard was analysed in triplicate and the mean

relative standard deviation (RSD, %) of all signals also increases with the temperature: 4 °C (1.7%), 20 °C (2.7%) and 37 °C (4.9%). The curves are summarised in Figure 37 and the sigmoidal curve's parameters are described in the respective caption. Room temperature (20°C) was selected because besides providing acceptable results it is less bothersome for routine use.

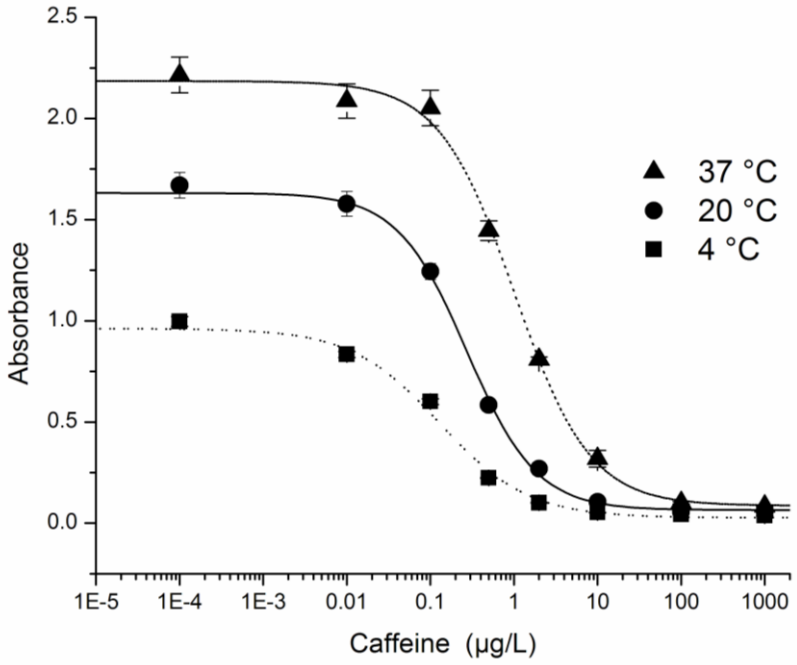

Figure 37. Incubation temperature effect on the ELISA. Obtained values for the curves at [37 °C]: (A) = 2.184, B = 0.964, C = 1.016, D = 0.087; [20 °C]: A = 1.657, B = 1.011, C = 0.264; D = 0.061; and [4 °C]: A = 0.966, B = 0.906, C = 0.145, D = 0.033.

7.4.6. Calibration curves

The water samples were measured using the "lower-range" calibration (Figure 38-A) and the beverages quantified by using the upper range (Figure 38-B). The saliva samples were measured with the calibration starting at 2.5 µg/L instead of 1 µg/L.

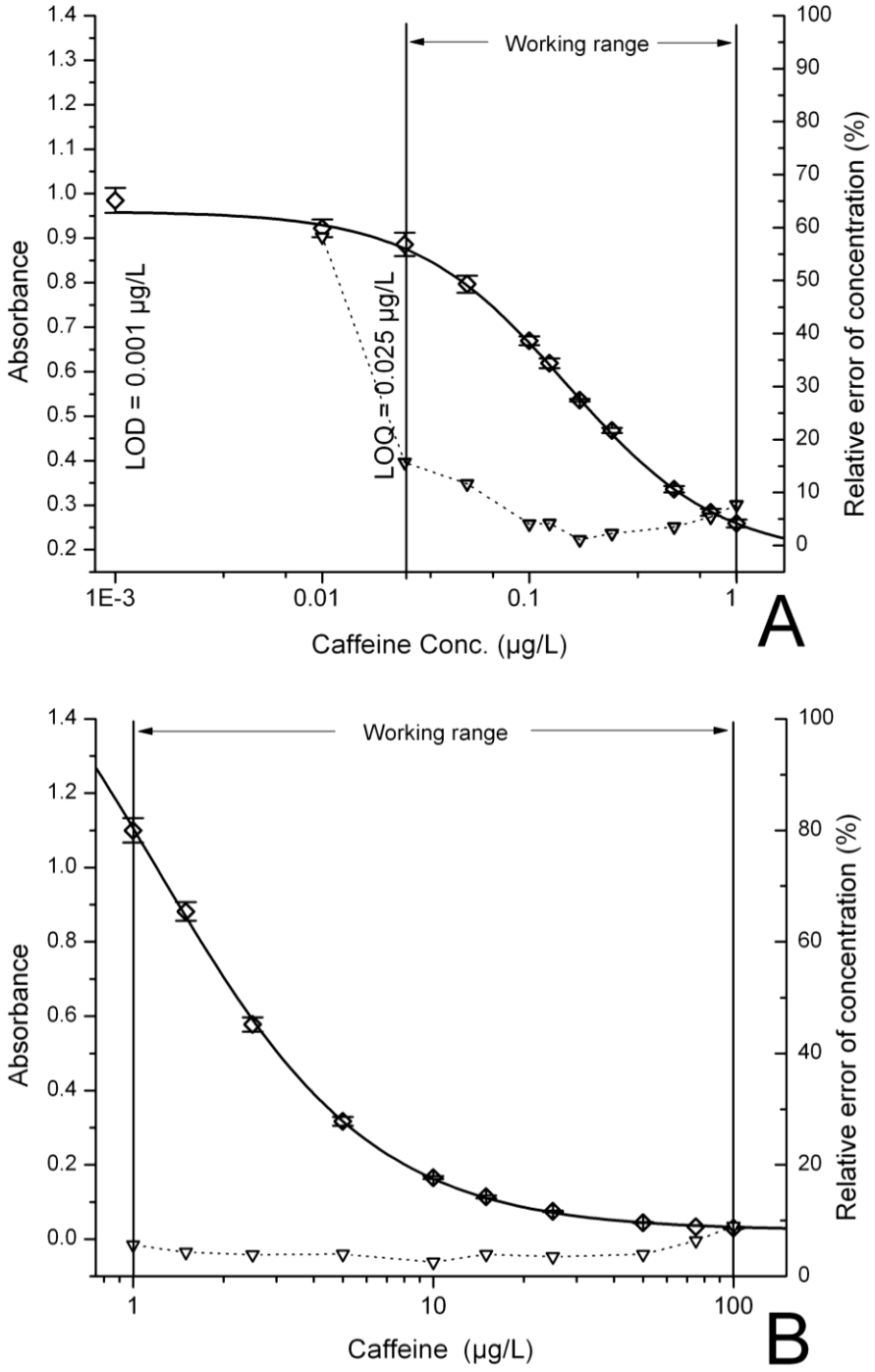

Figure 38. Calibration curves for the lower-range (A) and upper-range (B). (A) ELISA calibration curve – lower range – used to quantify the water samples. The first standard shown is the method LOD (0.001 µg/L) which is not included in the calibration fitting. The LOQ – 0.025 µg/L, is the first standard of the working range which reaches until 1 µg/L. The C-value is 0.180 µg/L and R^2 = 0.9987. (B) Calibration curve – upper range – used to quantify the beverages, shampoo and caffeine tablet solution (R^2 = 0.9995). The right axis in both graphs represents the relative error of concentration calculated from the precision profile;[279] the obtained points are represented by the open triangle.

7.4.7. Fitting models for binding assays

The calibration curve model used in immunoassays has been seen almost as an axiom: in the past two decades the sigmoidal fitting has been widely used assuming it to be the most apt one. The reason seems to be a mixture between historical practice and the function usefulness itself.

Several fitting models (6.6.6. - Fitting models for binding assays - Table 7, page 81) were tested to endorse the sigmoidal fitting (logistic function) because the topic has not drawn proper attention being the literature on this field pretty scarce.[298-301] Two calibration working ranges were tested for the best fitting: a lower-range (from 0.010 µg/L to 2.5 µg/L) and an upper-range (from 2.5 µg/L to 200 µg/L, here called extended range; and a reduced upper range until 150 µg/L).

i. Upper-range fitting

Hyperbolic, allometric and sigmoidal logistic functions, as well as exponential decay functions of 2nd and 3rd orders seem to fit properly the calibrators of the upper-range, while the sigmoidal Boltzmann dose-response curve and the exponential decay function of 1st order can only be used if the range is reduced, for example by starting at 10 µg/L instead of 2.5 µg/L (Figure 39). The power curve is inappropriate for use in the assays. Nineteen calibration curves were analysed and Figure 39 shows an archetype of such curves.

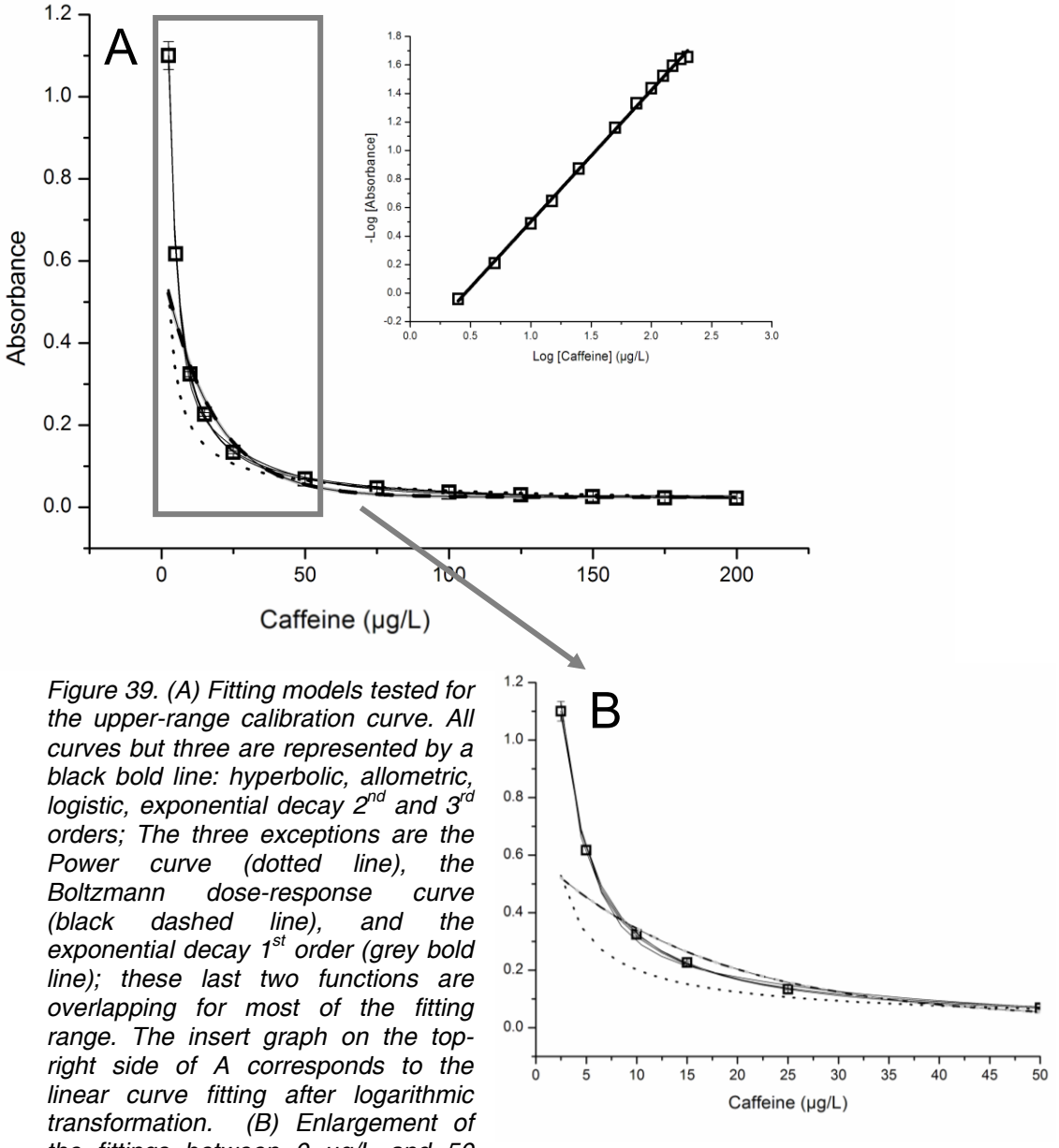

Figure 39. (A) Fitting models tested for the upper-range calibration curve. All curves but three are represented by a black bold line: hyperbolic, allometric, logistic, exponential decay 2nd and 3rd orders; The three exceptions are the Power curve (dotted line), the Boltzmann dose-response curve (black dashed line), and the exponential decay 1st order (grey bold line); these last two functions are overlapping for most of the fitting range. The insert graph on the top-right side of A corresponds to the linear curve fitting after logarithmic transformation. (B) Enlargement of the fittings between 0 µg/L and 50 µg/L caffeine.

One would anticipate a better fitting to provide better accuracy. In fact that is entirely true when functions with unsatisfactory fitting are compared to suitable ones, but within the latter, differences in accuracy do appear. Apparently equivalent fitting models generated different sample concentrations and consequently differences in accuracy. Several samples (saliva) and extra-calibration standards (control standards) were analysed by ELISA and LC-MS/MS, the latter providing the reference values for accuracy calculation purposes. The differences were calculated for each sample as percentages, and are plotted in Figure 40: (A) using

the range 2.5 µg/L – 200 µg/L and (B) using the reduced upper-range 2.5 µg/L – 150 µg/L.

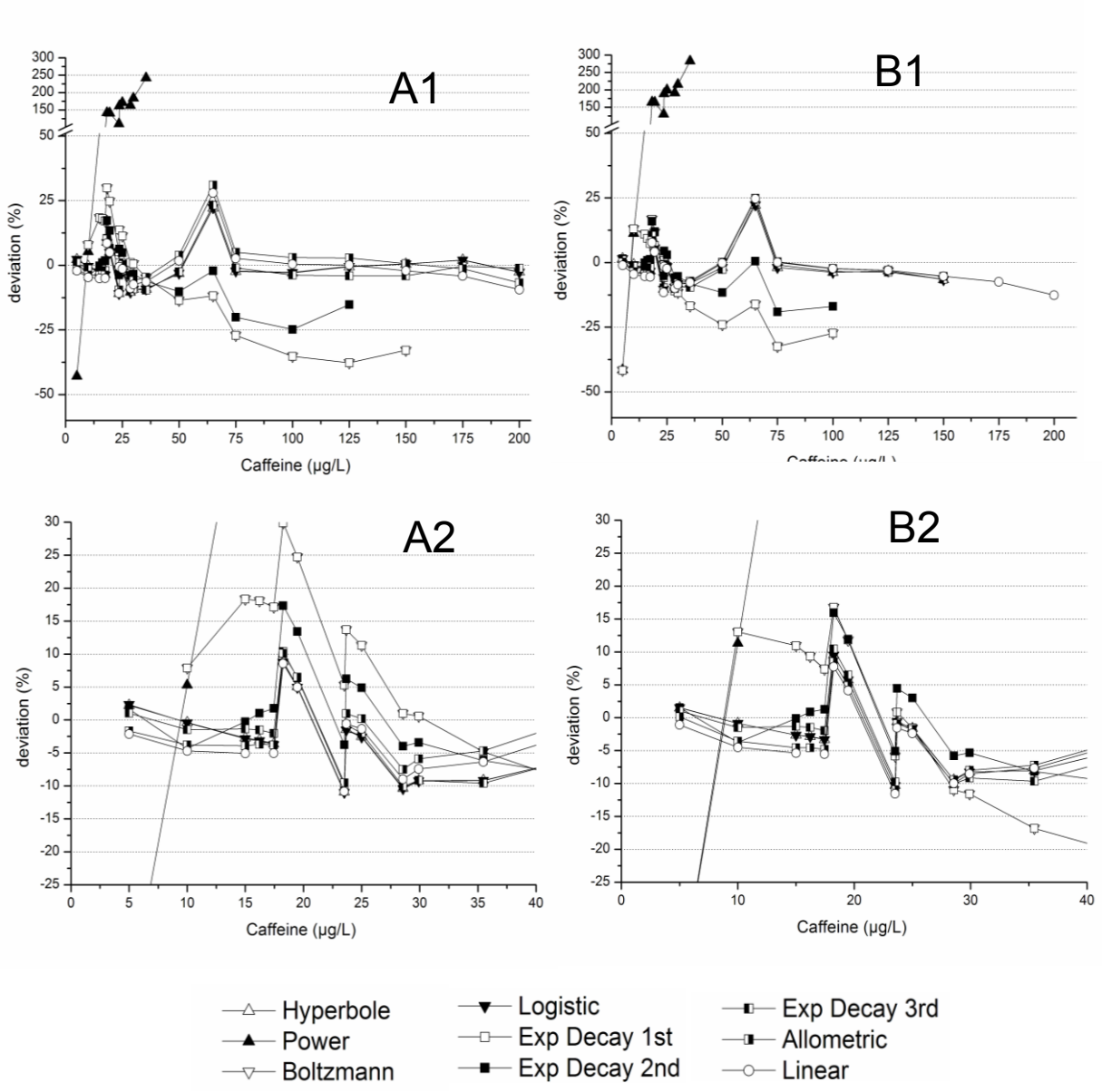

Figure 40. Deviation between the concentration obtained by ELISA using several fittings and the reference value by LC-MS/MS. A1 and A2: Using the calibration upper-range 2.5 µg/L – 200 µg/L and showing an amplified view of the concentrations below 40 µg/L (A2); B1 and B2: Using the reduced upper-range 2.5 µg/L – 150 µg/L and showing an amplified view of concentration below 40 µg/L (B2).

A first glance at Figure 40 is enough to dismiss the Power curve, which provides enormous deviations from the reference values; even when the calibration range is reduced (B1).

Exponential decay 1st order and sigmoidal Boltzmann fitting results overlapped one another and, for concentrations above 75 µg/L (in the Figure 40 example) or 100 µg/L in other curves, the deviations are higher than 25%.

Exponential decay 2nd order shows a better performance with all the results allocated within the ± 25% deviation; yet this fitting is still poorer than most of the others and does not allow quantitation above 125 µg/L or 150 µg/L depending on the curve. For concentrations below the 40 µg/L threshold, this curve can however be used without major accuracy concerns.

Hyperbolic, exponential decay 3rd order, and sigmoidal logistic curve fitting always provided similar results in the 19 curves analysed, as evidenced by Figure 40-A1 and A2.

The allometric function and linear transformation showed relevant differences in 6 of the 19 curves analysed. The advantage of using a linear transformation is that it allows to roughly estimate an out-of-range sample, i.e., above the last calibrator concentration, which can be helpful to establish a suitable dilution for samples after a first run.

Reducing the calibration range by removing the two highest calibrators improved significantly the accuracy, as can be seen in Figure 40-B1 and B2, when comparing them with A. Interesting are the overlapping results obtained for all the curves with better fittings – hyperbolic, allometric, exponential decay 3rd order, linear transformation and sigmoidal logistic model – when the range is reduced. This shows that, by reducing the range, the nature of the fitting model became less significant.

Some differences in precision can also be observed for the different fittings, as illustrated by the error bars in Figure 41. Each point corresponds to an average of 3 replicates of the same sample and the respective standard deviation of the concentration, represented by the error bar. The power curve shows the lowest precision, followed by the Boltzmann curve, exponential decay 1st order and exponential decay 2nd order. Hyperbolic, logistic, linear, allometric and exponential decay 3rd order offer the best precision among the tested models. A

correspondence between the LC-MS/MS results and the different ELISA fittings can also be inferred from Figure 41 by the more or less pronounced skewness of results around the line y = x, i.e., the ideal correlation.

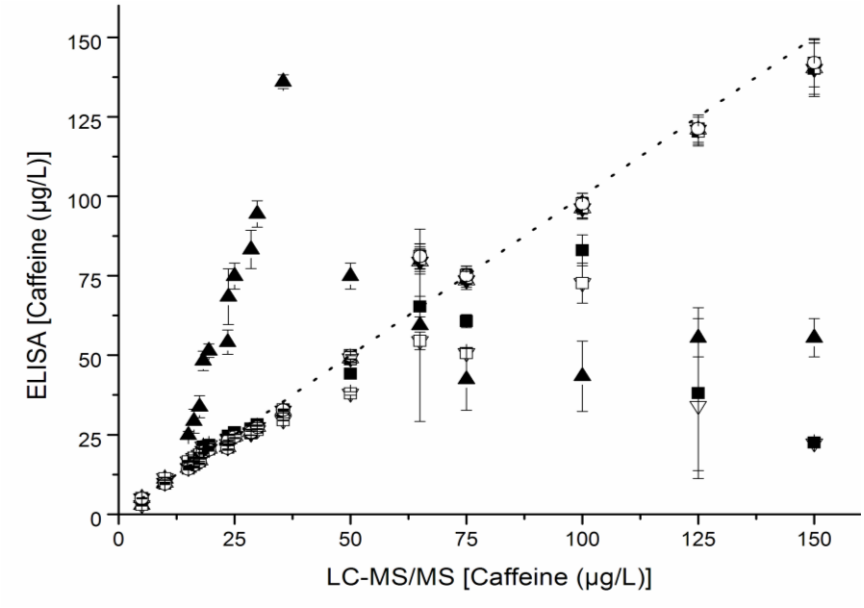

Curve	Slope	R^2	N
Hyperbolic	0.960	0.994	20
Power curve	4.291	0.972	14
Boltzmann	0.663	0.986	18
Logistic	0.960	0.994	20
Exp Decay 1st	0.706	0.960	20
Exp Decay 2nd	0.817	0.991	18
Exp Decay 3rd	0.960	0.994	20
Allometric	0.975	0.994	20
Linear	0.975	0.994	19

Figure 41. Correlation between caffeine concentrations obtained by LC-MS/MS (Linear calibration) and by ELISA using several fitting models. Each point corresponds to a concentration average of three sample replicates and the error bar the respective standard deviation. The dotted-line is the ideal correlation, (y = x). Remark: the absorbance were only read once and on the same microtitre plate, being the only difference the fitting model used to establish the calibration.

The table on the right-hand side shows the slopes of the linear regression between ELISA and LC-MS/MS and the respective coefficient of correlation (R^2); N represents the number of samples used for the correlation. Please note that not all the fitting models enable quantitation of the entire batch of 20 samples.

i.a. Residual analysis, Chi-Square (goodness-of-fit) test and coefficient of correlation (R^2)

For the nineteen independently obtained calibration curves – nine fitting models were used for regression analysis over nineteen independent datasets – the sum of the residuals, the chi-square and R^2 were determined and plotted as shown in Figure 42 and Figure 43.

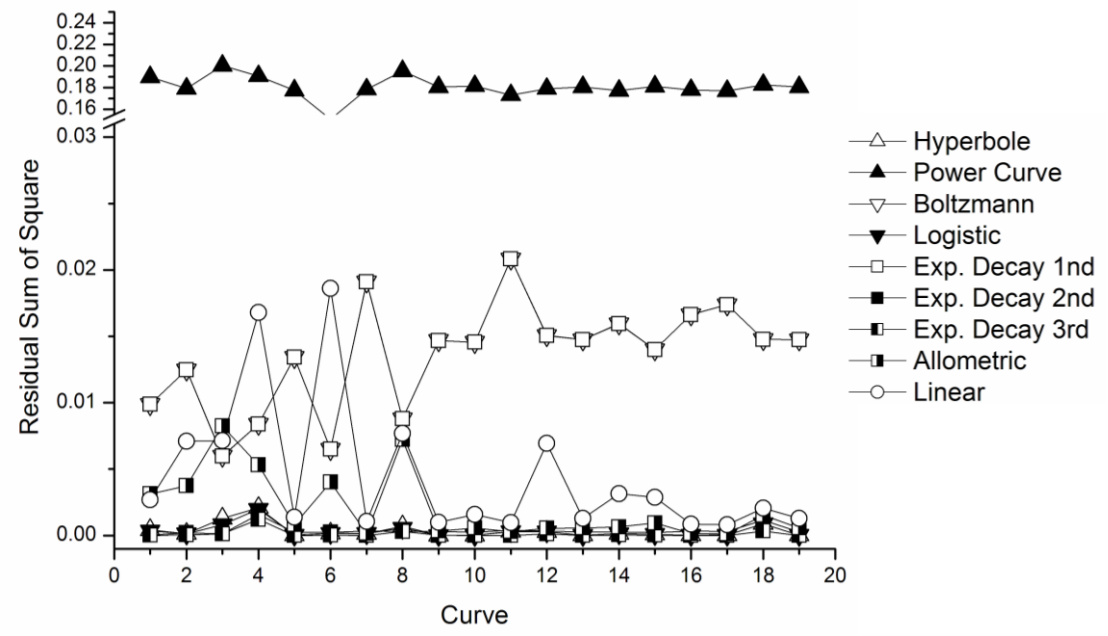

Figure 42. Residual sum of the square for 19 calibration curves using 9 different fitting models. The chi-square test values gave similar results (data not shown).

Again, the power curve can be immediately dismissed due to the residual sum of the squares, shown in Figure 42. Boltzmann and exponential decay 1st order (overlapping) functions also presented significantly higher sums of the residuals than the curves seen at the bottom of the graph (hyperbolic, exponential decay 2nd and 3rd order and logistic). The linear transformation and allometric appear in intermediate position between these last two groups described.

Statistical analysis was performed for all the fitting and shows significant differences ($p = 0.05$) of the mean of the distributions (one-way ANOVA, 9 factor levels) as well as in the variances (homogeneity of variance test) using Levene's Test (both, absolute deviations and squared deviations) and the Brown-Forsythe Test ($p = 0.05$ level, 19 degrees of freedom, DOF). Normality of the distributions was assumed from the results of the Kolmogorov-Smirnov test (0.05 level, 19 DOF). Moreover,

Shapiro-Wilk and Lilliefors tests for normality lead to the same outcome if outliers are removed. Since the aim of this study was to select the best fitting curve for use in routine, all curves obtained were used for the calculation.

A reduced graphical analysis was performed by evaluating exclusively the best-fitting curves. The detailed view of these four functions is given in Figure 43 and shows no significant differences between them. The same statistical treatment was produced and, for the $p = 0.05$ confidence level, no differences were found between the four distributions.

The F-test, comparing two-by-two and using the logistic function as the reference, suggested that no significant differences existed between the distribution variances. Interpretation of the data must be done carefully because the different functions have a different number of parameters involved (please refer to Table 9, page 84, in 6.6.6 - Fitting models for binding assays): looking at the residual sum of squares (Figure 43-A), not taking the number of parameters used in the function into account, apparently the exponential decay 3rd order (8 parameters) fitting is much better than the 4-parameter functions (hyperbolic and logistic). This difference almost vanishes when Chi-square is analysed (Figure 43-B), as taking into account the number of function parameters it reduces the degrees of freedom. In this case, over-parameterised functions such as the exponential decay 3rd order show less impressive performance.

The curves number 4 and 18 (Figure 43) were obtained using data sets of lower quality but are represented to show that in such cases, the goodness-of-fit outcome is the same as for the rest of the calibrations data.

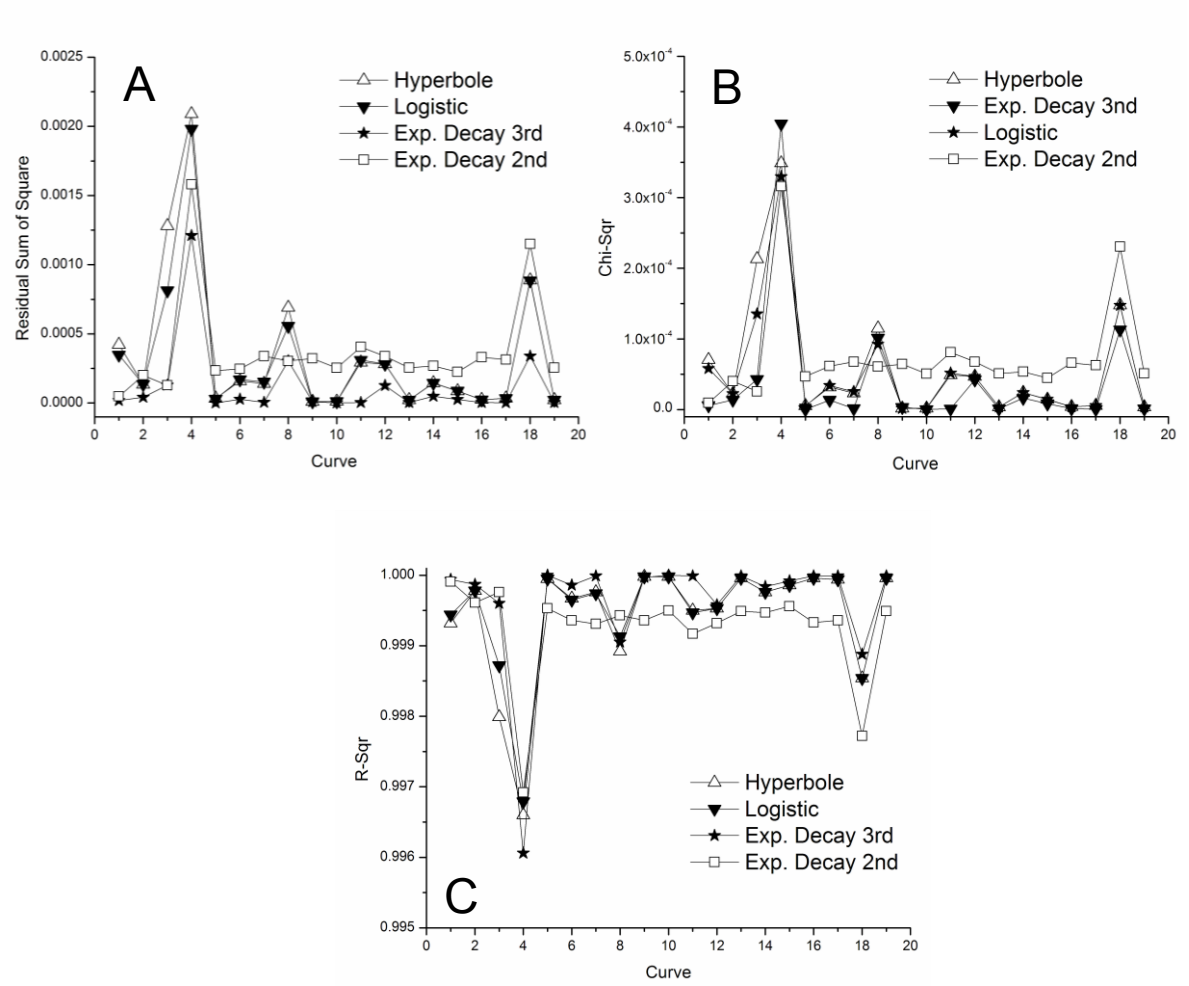

Figure 43. Detailed view of Figure 42, showing the best-fitting curves: Hyperbolic, Logistic, Exponential decay 2nd and 3rd order. (A) Residual sum of squares; (B) Chi-squared value; (C) R-squared value.

To sum up:

The 4-parameter functions, hyperbolic and logistic seem to be suitable for fitting the upper-range calibration curve and increasing parameterisation (exponential decay 2nd and 3rd other) does not seem to improve the precision of the concentration results.

Remark: During the analysis of the fitting data, several statistic tools were considered and tried out. Some softwares, like the one used here (Origin 8), make use of the F-test and the Akaike criterion test[302] to compare different fitting models. The use of the latter, though possibly useful in other situations, is strongly discouraged in the analysis performed here. When the Akaike criterion was applied

to the tested functions, misleading results were produced, suggesting for example that the Power curve offers a much better fitting than the logistic one. The reason for this odd outcome is the different numbers of parameters between the different fitting models. And the Akaike criterion takes into account and favoured functions with less parameters, generating wrong interpretation when too different functions, regarding the number of parameters, are to be compared.

ii. Lower-range fitting

The same procedure was used for the lower-range of the calibration (from 0.010 µg/L to 2.5 µg/L) with a rather different outcome: the linear and the allometric function proofed not to be fit-for-purpose for the fitting in the lower concentration range.

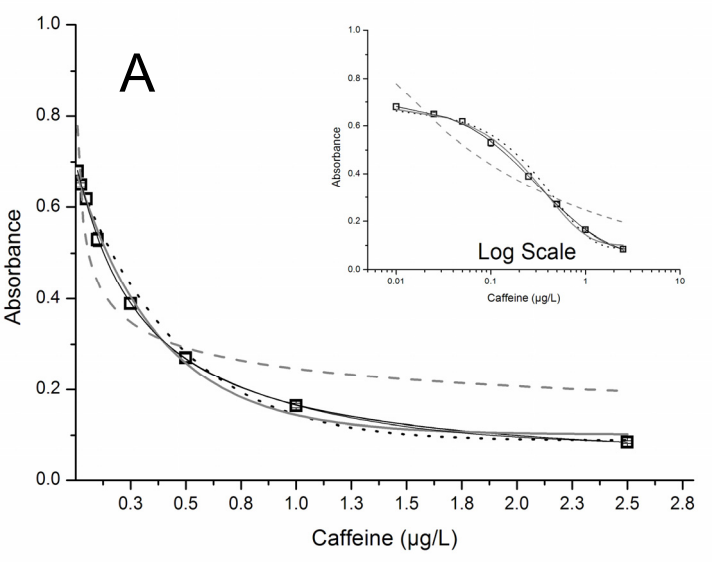

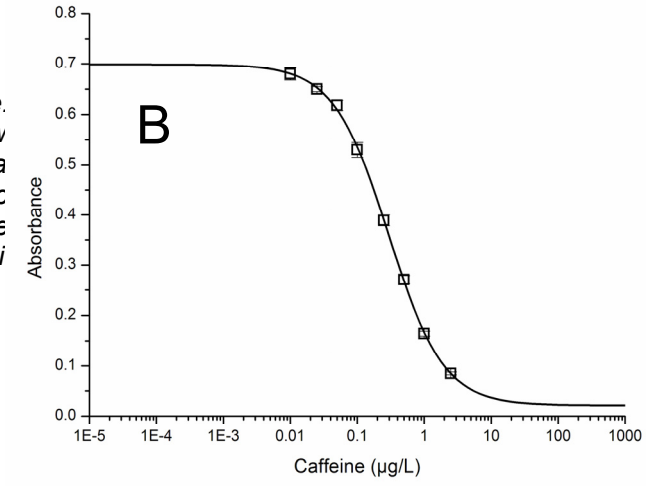

Figure 44. (A) Fitting models tested for three are represented by a black bold line. orders; The three exceptions are the Pov curve (black dashed line), and exponentia on the top-right side of A corresponds to represented in A but using the log scale curve represented in most immunochemi 0.021; R^2 = 0.9994).

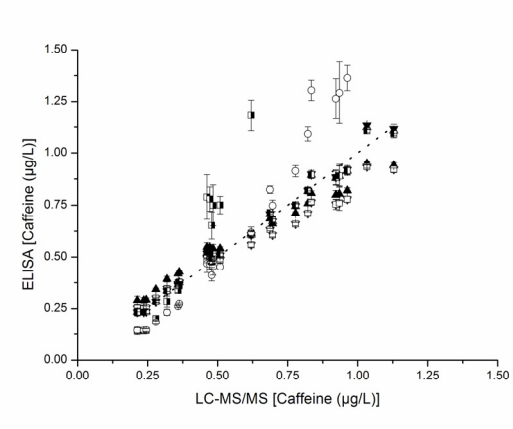

Curve	Slope	R^2	N
Hyperbolic	0.973	0.992	24
Power	0.725	0.989	24
Boltzmann	0.739	0.991	23
Logistic	0.985	0.992	24
Exp Decay 1st	0.739	0.991	23
Exp Decay 2nd	0.967	0.993	24
Exp Decay 3rd	0.967	0.993	24
Allometric	3.177	0.969	15
Linear	1.983	0.964	24

Figure 45. Correlation between caffeine concentrations obtained by LC-MS/MS (Linear calibration) and by ELISA using several fitting models. Each point corresponds to a concentration average of three sample replicates and the error bar to the respective standard deviation. The dotted-line is the ideal correlation, when LC-MS/MS results are plotted on the ordinate, i.e., the curve y = x. The table on the right-hand side shows the slopes of the correlations and the respective squared correlation coefficient; N represents the number of samples used for the correlation.

A good correlation – analysing the slope values – was obtained when using hyperbolic, logistic and the exponential decay 2nd and 3rd order functions.

Allometric (slope = 3.2) and linear (slope = 2.0) functions provide unacceptable results, showing an overestimation of concentrations, especially marked for samples containing higher caffeine concentrations (Figure 45). Though the correlation between the data is good for these two curves (acceptable correlation coefficients), the correspondence between the two datasets (ELISA and LC-MS/MS), as shown by the curves slopes, is very poor. Additionally with the allometric function only 15 out of 24 samples could be quantified.

Exponential decay 1st order and the Boltzmann function showed an overall concentration underestimation as can be observed in the graph (Figure 45) and numerically by their curves' slopes (0.74).

The deviations between the results obtained by LC-MS/MS and the ELISA, using the best-fitting function are represented beneath (Figure 46). Only results obtained using the best fitting curves were included, for avoiding scale-distortion generated by the highest deviations and to illustrate the equivalent outcome when hyperbolic, logistic or exponential decay 2nd and 3rd order functions are used.

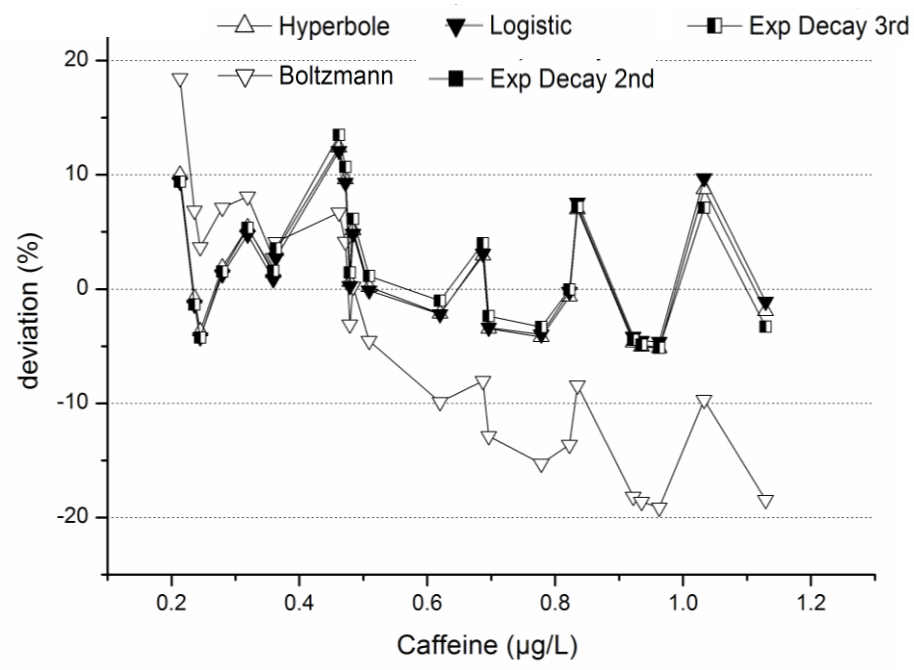

Figure 46. Deviation between the concentration obtained by ELISA using several fittings and the reference value by LC-MS/MS.

ii.a. Residual analysis, Chi-Square (goodness-of-fit) test and coefficient of correlation (R^2)

The residual sum of squares as well as the chi-square test is presented in Figure 47. They show a very similar trend to the ones obtained for the upper-range (7.4.7.i.a, page 127), here with the inclusion of the Boltzmann model.

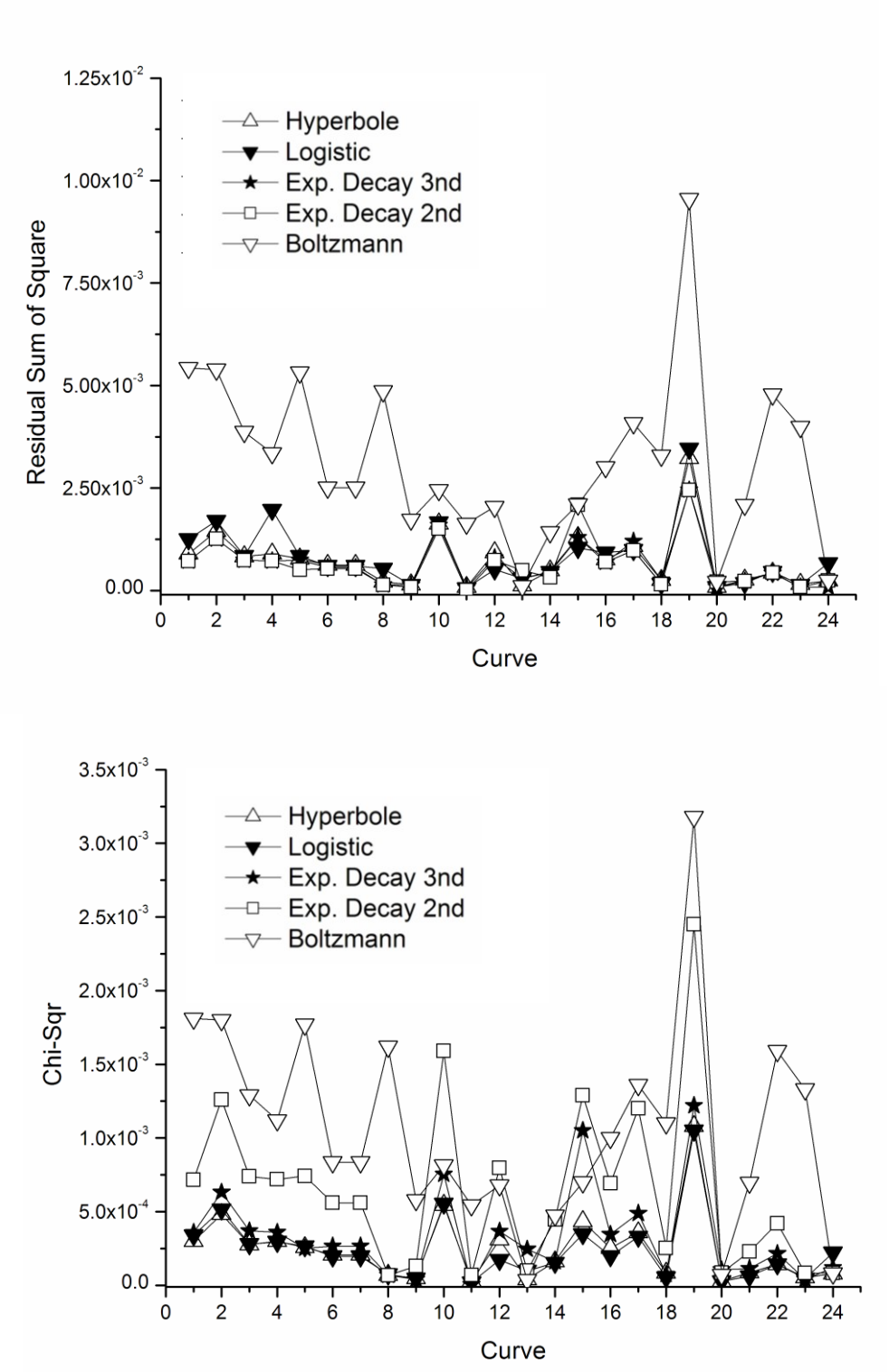

Figure 47. Residual sum of the squares (top) and chi-square (bottom) for 24 calibration curves using the 5 best-fitting models for the lower-range calibration curve.

Statistical analysis of the data was performed as for the upper-range (page 127) and significant differences were found between the models represented in Figure 47 (calibration curve no. 19 was removed before statistical analysis).

Performing one-way ANOVA (p = 0.05) and homogeneity of variances test for the sum of residues, significant differences were found between the models represented in Figure 47. Removing the Boltzmann function from the statistical analysis, no significant differences were found between the means and the variances of the sum of the residues between the four remaining distributions. Yet, when chi-square values are compared using the same statistical tools, the exponential decay 3rd order exhibits a significant difference (p = 0.05 level), both in the mean and in the variances. A summary of the results is graphically represented as box-plots in Figure 48 for the 5 fitting models tested.

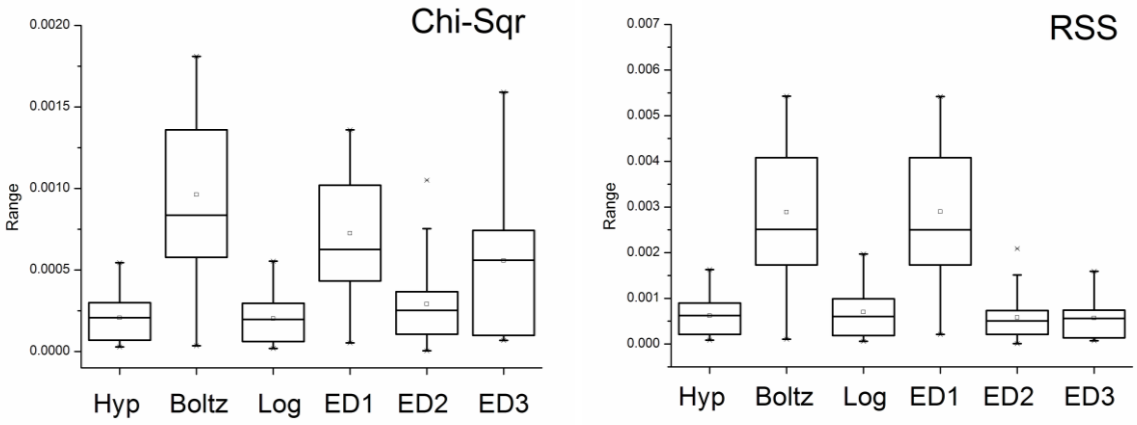

Figure 48. Box-plots of the Chi-squared (left) and Residual sum of squares (RSS, right) showing the mean value and the distribution dispersion around that mean, n = 23. Note: data from one calibration curve (n° 19) was left out as it completely distorts all distributions. Abbreviations: Hyp–hyperbolic, Boltz–Boltzmann, ED1, ED2, ED3–exponential decay of 1st, 2nd, 3rd order, respectively.

As for the upper-range, hyperbolic, logistic and exponential decay 2nd order can equally be used to fit the data. The first two functions have the advantage of making use of only 4 parameters against 6 of the exponential decay 2nd order.

Regarding the presented data, one can say that a 4-parameters function is required to properly fit the data and it seems worthless to increase the number of parameters above four..

To sum up:

The 4-parameter logistic function or the hyperbolic function can be used for both calibration ranges studied.

Advantageously, the hyperbolic function does not required a log transformation of the x-axis and also – as it is a well-know mathematic model – it facilitates further calculations like uncertainty determination or calculation of the limits of quantitation.

Increasing the number of parameters above 4 does not seem to bring any benefit, considering the (limited) amount of data analysed.

Remark: The 4-parameter logistic function approximate the hyperbolic function in *ideal* assay conditions, i.e. when the D-value tends to zero and the B-value approximates one, which is valid for much of the curve analysed here.

7.4.8. Operator influence

A major concern when performing ELISA is the operator influence on the final result. Three operators with different experience in the technique assayed the same batch of 20 surface waters within the same day and equal conditions. Operator 1 was an average-experienced analyst (a PhD student); Operator 2 a student in training with 2 months experience in performing the technique and, Operator 3 a specialised technician with several years experience.

As Figure 49 shows most of the points are superposing one another, which suggests a feeble influence of the operator on the assay when a standard operational procedure is available to an analyst with some previous training on the technique. The average of the sample concentrations (n = 20) and average of the relative standard deviations (%) between the three does not differ significantly: 0.533 µg/L (0.040%); 0.536 µg/L (0.052%); 0.539 µg/L (0.024%) for operator 1, operator 2 and operator 3, respectively.

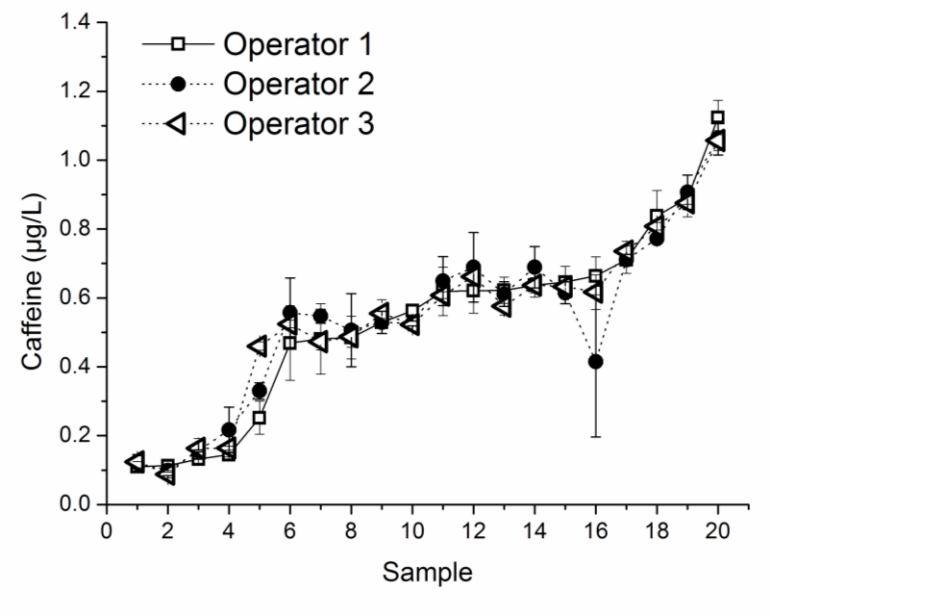

Figure 49. Operator influence on the ELISA. Operator 1 (open squares): middle-experienced analyst; 2 (filled circles): little experienced analyst "novice"; Operator 3 (open triangles): experienced analyst (specialist). The samples were sorted by caffeine concentration.

7.4.9. Limit of quantitation (LOQ) and limit of detection (LOD)

The LOQ was estimated on the basis of two premises: (1) the concentrations of caffeine expected in surface water samples, which defined the calibration lower-range used, and (2) the precision profile[279] obtained for that calibration (Figure 38-A). The LOQ thus assigned (0.025 µg/L) was then experimentally verified by assaying 18 times a standard with that concentration; a standard deviation of 14.8% was obtained.

The LOD was determined experimentally after recognizing that some statistical approaches, mainly those using the standard deviation of the blank, are prone to yield an inconsistence result. In such cases the LOD is subject to statistical fluctuation based, for example, on the number of replicates used to calculate the standard deviation rather than the intrinsic assay sensitivity itself. The approach used here most likely leads to a higher (thus less impressive) LOD but it places the analyst on safe ground. The results of three standards are shown in Figure 50 — 0.005, 0.002, and 0.001 µg/L, the lowest one being the method LOD. None of the signals obtained with the eighteen replicates of the 0.001 µg/L standard overlaps with the range of the blanks.

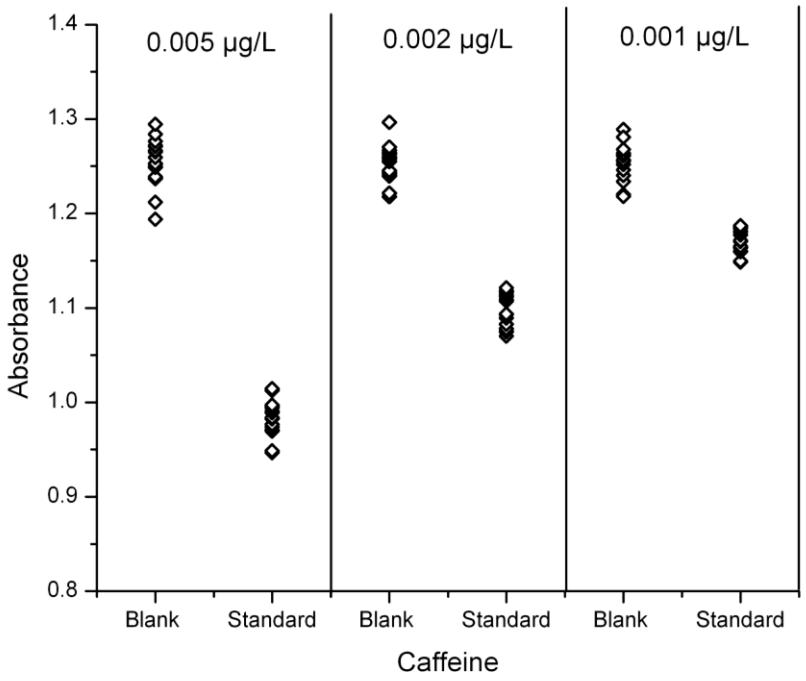

Figure 50. Experimental determination of the LOD. Three standards: 0.005 µg/L, 0.002 µg/L and 0.001 µg/L were analysed 18 times against 18 replicates of a blank sample (Milli-Q water), in the same plate. Each symbol represents a replicate analysed.

7.5. Reference method for caffeine

An LC-MS/MS method was developed for caffeine and related xanthines (paraxanthine, theophylline, theobromine and xanthine). Caffeine-(3-methyl-^{13}C) was used as internal standard.

The MS acquiring conditions were optimised by injecting individual solutions of each compound (0.5 mg/L) and acquiring in scan, parent scan and finally MRM mode for quantitation purposes. Because the amount of available literature, regarding xanthine quantitation by LC-MS/MS is satisfactory[44,125,133,134], only the highlights of the method development are described here.

7.5.1. Product ion scan

Xanthines have a relatively low number of ESI+ fragments contrariwise to sterols, for example. Typically, their product scans spectrum shows one main fragment which clearly outstands the others (more than at least 70% more intense than the second one). To illustrate this fragmentation pattern the caffeine product scan is

shown in Figure 51, with the main fragment m/z = 137.8 (100%), the parent ion m/z = 194.9 (36%) and a second fragment at m/z = 109.7 (21.4%). The main fragment results from a cleavage of the xanthine ring between N1-C2 and N3-C4 (m/z 137 and 57) and the second one from the cleavage C2-N3 and C5-C6 (m/z 109 and 85). Minor fragments (<10%) are included in Table 15.

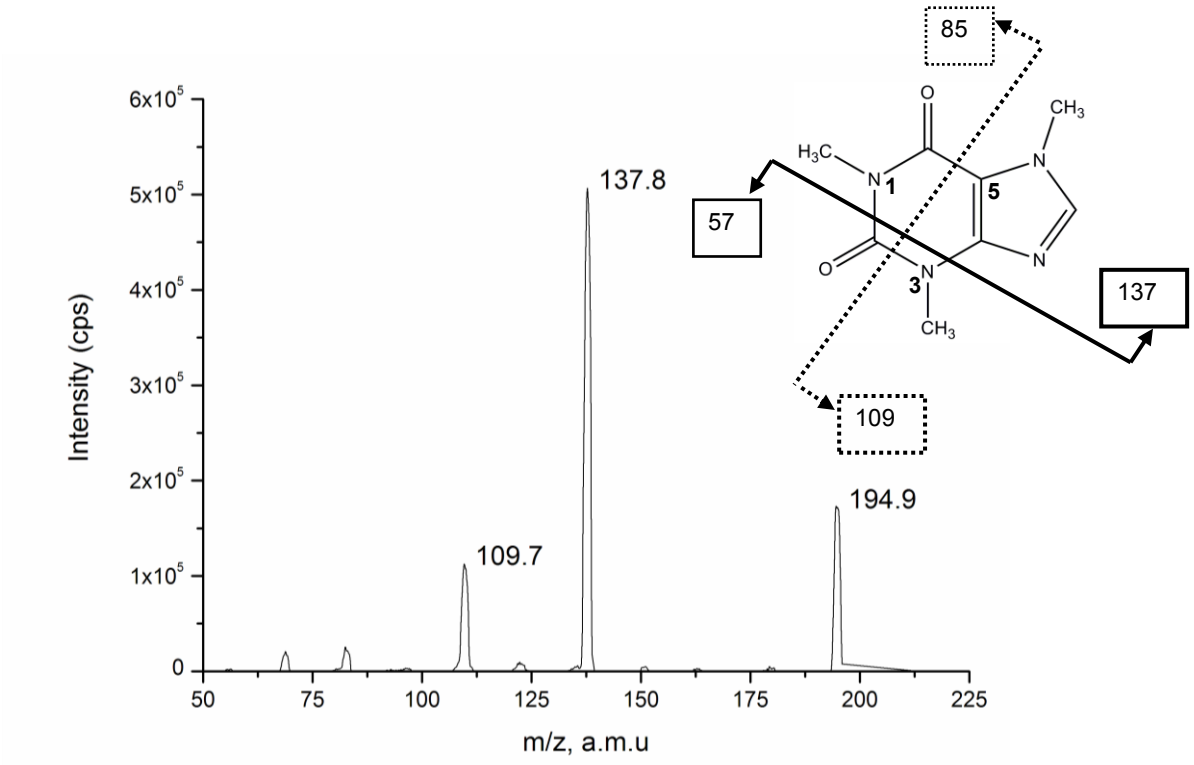

Figure 51. Caffeine product scan obtained after applying a collision energy of 30 eV and the corresponding fragmentation pattern (insert, right).

The same collision energy was applied to all the methylxanthines (30 eV) to allow a comparison between the fragmentation patterns. Theobromine shows the highest number of fragments among the methylxanthines and shares the major fragment m/z with caffeine. Paraxanthine and theophylline present the most interesting results as both shares the major fragments – yet different fragmentation patterns – demanding thus a proper chromatographic separation. Nevertheless, their differences become noticeable if the collision energy is increased to 35 eV: paraxanthine retains the m/z 123.6 as its major fragment while in theophylline's spectrum the m/z 95.7 is markedly increased and can be used for quantitation purposes. Additional differences are visible in Table 15, like the number and relative intensity of fragments obtained using equal collision energy (30 eV).

Table 15. Fragments of methylxanthines after applying a collision energy of 30 eV. The relative intensity of each fragment is indicated in brackets.

Compound	Precursor ion (m/z)	Collision Energy (eV)	Obtained product ions (m/z)
Theobromine	181.0 $[M+H]^+$	30	137.5(100%); 180.9 (88%)*; 162.5 (52.0%); 109.8 (50.1%); 134.9 (36.7%); 107.5 (33.0%); 68.9 (20.7%); 82.3 (20.0%); 96.2 (18.7%); 122.3 (12.7%).
Paraxanthine	181.0 $[M+H]^+$	30	123.6(100%); 180.9 (25.6%)*; 95.9 (7.3%); 141.7 (4.9%); 69.0 (2.5%); 163.2 (1.2%).
Theophylline	181.0 $[M+H]^+$	30	123.6(100%); 180.8 (31.6%)*; 95.7 (28.9%); 69.0 (10.0%); 136.7 (5.3%); 108.1 (2.6%); 149.0 (1.6%); 162.8 (1.6%); 82.9 (1.4%).
Caffeine	195.0 $[M+H]^+$	30	137.8(100%); 194.8 (36.0%)*; 109.7 (21.4%); 82.9 (6.2%); 69.0 (4.0%); 122.3 (2.0%).

7.5.2. Chromatographic separation

The best separation was obtained using a C18 reversed-phase column, 250 mm x 2.1 mm, 5 µm (Phen) after testing two other columns: Purospher RP-C18, 250 x 3 mm, 5 µm; and a Zorbax HILIC column, 4.6 x 100 mm, 3.5 µm.

Caffeine is easily separable from the other xanthines whichever column was used. Contrary, paraxanthine and theophylline were not baseline-resolved but when the Phen column was employed. The gradient ammonium acetate 5mM/methanol was also optimised to allow for separation of these two methylxanthines (Figure 52).

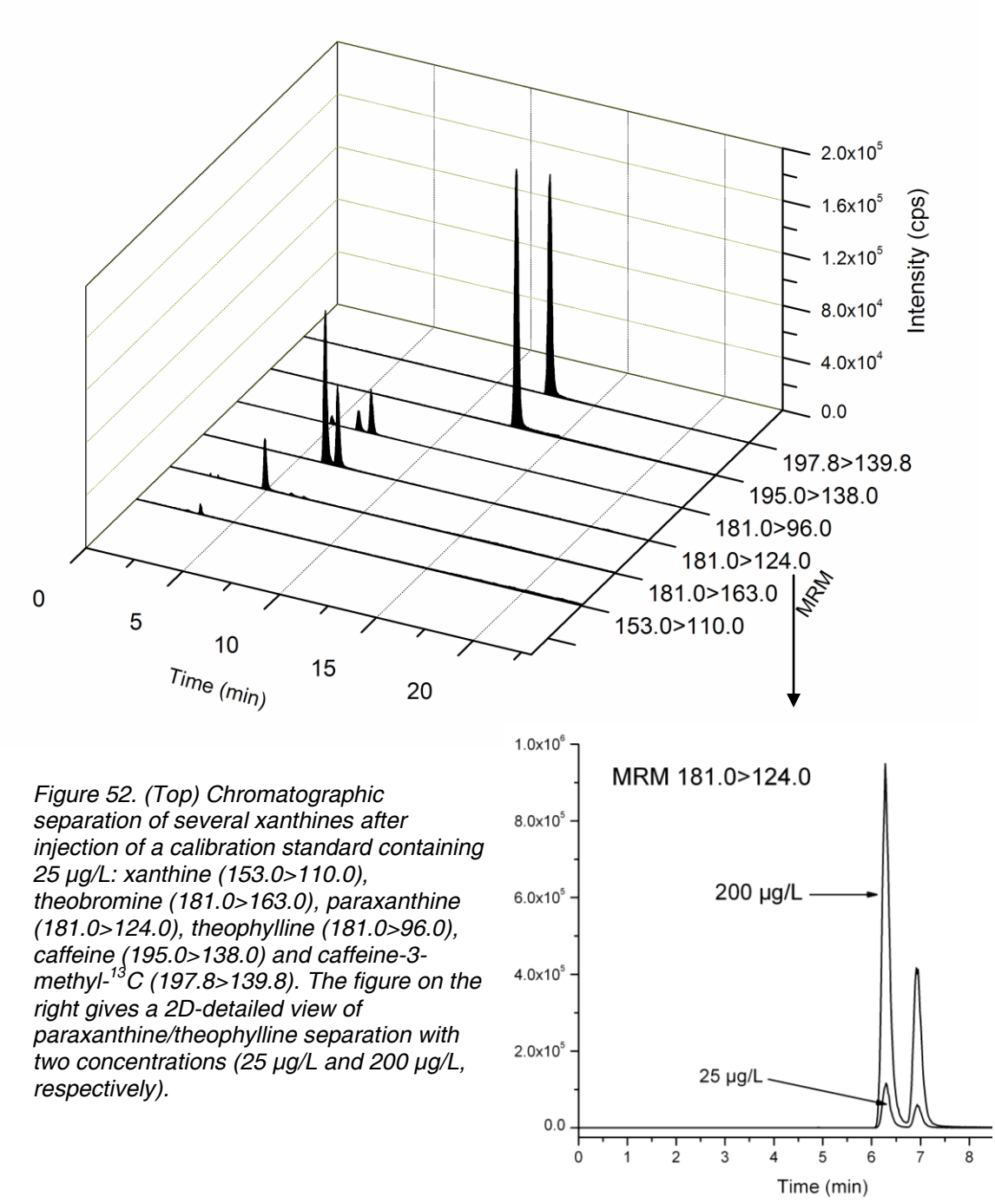

Figure 52. (Top) Chromatographic separation of several xanthines after injection of a calibration standard containing 25 µg/L: xanthine (153.0>110.0), theobromine (181.0>163.0), paraxanthine (181.0>124.0), theophylline (181.0>96.0), caffeine (195.0>138.0) and caffeine-3-methyl-^{13}C (197.8>139.8). The figure on the right gives a 2D-detailed view of paraxanthine/theophylline separation with two concentrations (25 µg/L and 200 µg/L, respectively).

The chromatogram – Figure 52, top – also allows to compare the signal intensities, being caffeine peak (195.0>138.0) the most intense one and xanthine the weakest (153.0>110.0). Hence, different individual quantitation limits were obtained: 25 µg/L xanthine, 10 µg/L theobromine and theophylline, 5 µg/L paraxanthine and caffeine 2.5 µg/L caffeine.

7.6. Monitoring caffeine in water samples

The concentration of caffeine in surface water samples was determined by directly measuring the sample – without any pre-treatment – using ELISA.

The ELISA results were compared with those obtained by SPE-LC-MS/MS for different surface waters in Berlin[g]. Even though the ELISA is dealing with concentrations 1000-fold lower than the LC–MS/MS ones (without enrichment), the correlation between both methods is very good, as shown in Figure 53 by the curves slope. Fifty two surface water samples were used to establish this correlation, during several sampling campaigns, locations and times; with caffeine concentrations ranging from 0.030 to 4.0 µg/L.

Because the number of samples with concentrations higher than 1 µg/L is scarce and could bias the slope of the curve, a second correlation was performed using only concentrations below that value, with the results being presented on the right-hand side of Figure 53. The obtained slopes were the same (1.005) but the correlation coefficient shows a higher dispersion for concentrations below 1 µg/L (0.908 vs. 0.961 for the entire batch of samples). The reason for this deviation is discussed in detail in the water screening section (11.1.3 - Teltowkanal, from page 240) and is mainly attributed to a sampling spot directly influenced by wastewater treatment effluent discharge into the Teltowkanal. It was observed that the assay overestimates the caffeine concentration in treated wastewaters.

---

[g] *The samples are described in detail in the Water sampling campaigns part (11.1 - Surface waters, page 229).*

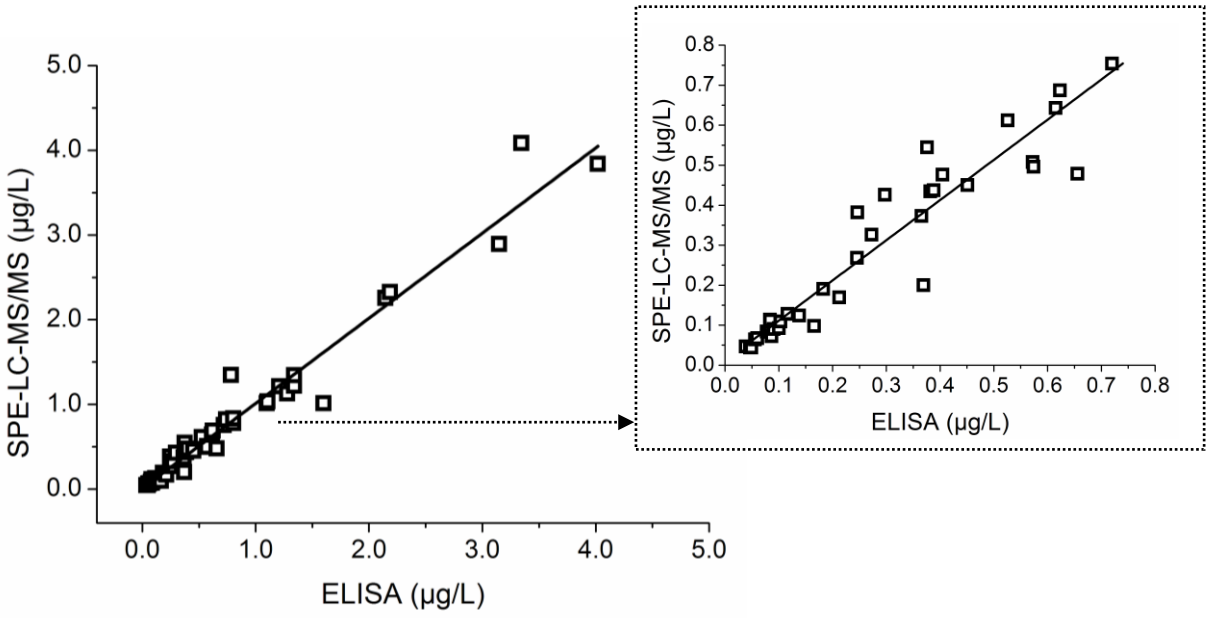

Figure 53. Correlation between the surface water samples' results (n = 52) obtained by ELISA (x-axis) and SPE–LC–MS/MS (y-axis). Each point represents a sample and the data was fitted by using a linear function: [Caf]SPE-LC-MS/MS = 1.005×[Caf]ELISA+0.002; R^2 = 0.961. The slope of the curve depicts the correlation between the methods. The figure on the right-hand side shows the correlation between samples with concentration below 1 µg/L (n = 40) and the obtained correlation curve slope is [Caf]SPE-LC-MS/MS = 1.0046×[Caf]ELISA+0.007; R^2 = 0.908.

7.6.1. Intraday and interday precision

ELISA intraday and interday precision for surface water samples is shown in Table 16. Intraday and interday variations were lower than 12% and 17.0%, respectively. One water sample (containing 0.510 µg/L caffeine) was also measured 25 times in the same microtitre plate and the standard deviation was 7.2%. A water sample with a caffeine concentration of about the LOQ (0.030 µg/L) shows the method precision at this concentration level (~17%).

Table 16. Intraday and interday precision for several water samples by ELISA. Water sample 5 (0.510 µg/L caffeine) was additionally measured 25 times in the same plate and the standard deviation was slightly higher – 7.2%. Water sample 1 has a caffeine concentration about the LOQ (0.030 µg/L) and can accordingly show the method precision at this concentration level (~17%).

	Intraday precision n = 5, same plate		Interday precision n = 9, over 3 days	
Water samples	Sample concentration (µg/L caffeine)	RSD	Sample concentration (µg/L caffeine)	RSD
Sample 1	0.030	9.4%	0.033	16.9%
Sample 2	0.058	12.0%	0.061	14.7%
Sample 3	0.093	3.5%	0.093	15.5%
Sample 4	0.160	9.2%	0.162	11.8%
Sample 5	0.510	1.2%	0.590	11.9%
Sample 6	1.74	1.8%	1.72	2.6%

7.6.2. Spiking experiments

Neither a reference material nor an intercomparison proficiency test was available for caffeine in water samples. To overcome this shortcoming, a surface water sample was spiked at different caffeine levels (0.05, 0.10, 0.25, 0.5, and 1.0 µg/L) for further analytical quality assurance. Recoveries between 92% and 102% were obtained (Table 17). Although the data do not represent proof of accuracy, they give extra confidence about the assay performance.

Table 17. Results from the spiking experiments with a surface water sample (sample 2 from Table 16), at different caffeine concentration levels. (*)The unspiked sample has a caffeine concentration of 0.058 µg/L.

Sample	Spiking level [µg/L caffeine]	Caffeine by ELISA, [µg/L]	Recovery ± error [%]
Spiked 0	0	0.06(*)	-
Spiked 1	0.05	0.11	102 ± 30%
Spiked 2	0.10	0.15	95 ± 24%
Spiked 3	0.25	0.33	106 ± 10%
Spiked 4	0.50	0.52	93 ± 8.5%
Spiked 5	1.0	0.97	92 ± 11%

7.6.3. Analyte stability and sample handling

Surface water samples from two water screening campaigns (n = 19) were randomly selected to test for analyte stability in the matrix, under controlled storage conditions – dark-glass vials at 4°C. The samples were analysed at t = 0 (sampling day), and at different times thereafter until 65 days, as indicated on the axis in Figure 54.

Landwehrkanal has no wastewater input (at least officially reported ones) – samples marked as LWK, while Teltowkanal samples were collected downstream (TKA) and upstream (TKB) of a treated wastewater discharge point. Certainly, these three situations do not cover the broader range of surface water types but they do suggest that caffeine is relatively stable in the matrix, at least for 50 days, when stored at 4°C and protected from the direct light. The graphics present in Figure 54 shows a mixed trend, with some samples showing increasing concentrations while for some others they seem to be decreasing. Sample handling, including homogenisation, cooling and heating cycles, aliquotation and reproducibility itself should be considered as important contributions to the concentration fluctuations.

Similar results were obtained in spiked surface water sample from lakes in Switzerland: no degradation of caffeine was found for 40 days – maximum time of the published study – except in samples exposed to sunlight, where caffeine undergoes photodegradation with an half-life of 12 days.[67]

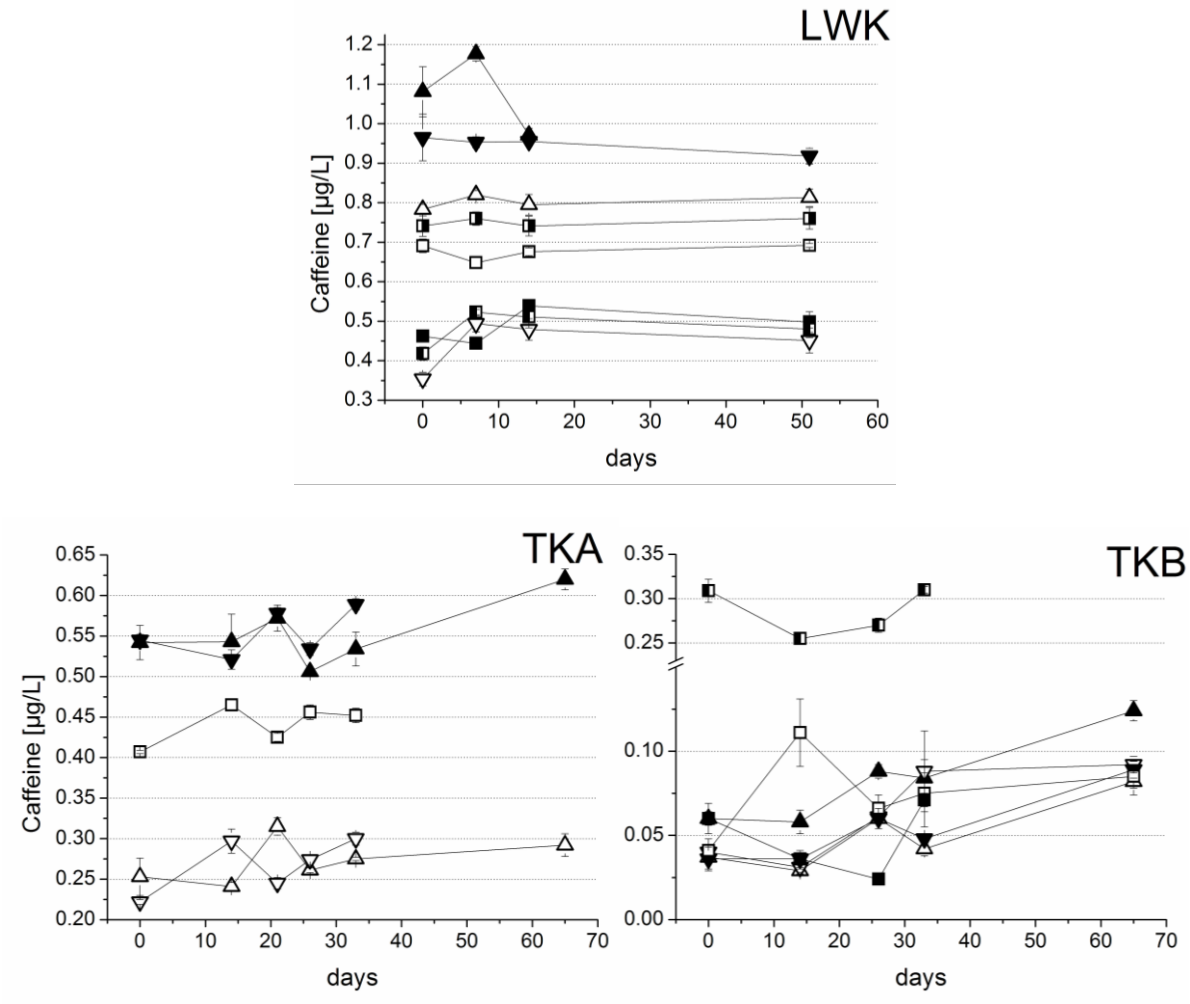

Figure 54. Stability of caffeine in surface water samples: from Landwehrkanal (LKW), Teltowkanal downstream of a wastewater treatment plant discharge point (TKA), and upstream of the wastewater treatment plant discharge point (TKB).

Comparing the means of 15 samples at t = 0 and t = 14 days, no differences were found at the p = 0.05 confidence level and 14 DOF (paired sample *t*-test). The population variances are also not significantly different (0.05, 14 DOF, two-sample test for variance). Interesting is the fact that the centre of the distribution at t = 14 (0.326 ± 0.282) is slightly higher than the one at t = 0 (0.313 ± 0.277), suggestive of an increment of the concentration instead of a decline. The sample handling is probably the reason for this increment.

The number of samples is clearly insufficient to conclude about stability differences between the three surface waters tested, and one should be careful when looking at the data presented in Figure 54: samples collected upstream of the wastewater treatment plant discharge point (TKB) have apparently more variability throughout the time but this apparent higher differences are more likely related to the lower concentration of caffeine in these samples than the analyte stability in the matrix.

7.7. Monitoring caffeine in saliva samples

7.7.1. Sample pre-treatment methods

The main concern during saliva samples preparation is to remove the proteins and enzymes, mainly peroxidases, without removing the analyte. Two methods were compared for such purpose: protein precipitation by using an organic solvent (acetonitrile) and diafiltration (with a 3 kDa cut-off microfilter).

Acetonitrile extraction shows slightly better recovery of $^{13}C_3$-CAF in both saliva samples and Milli-Q water (Figure 55). A major pitfall of the method seems to be the relatively higher dispersion and skewness of the data as illustrated by the box plots in Figure 55. The minimum of the acetonitrile distribution is clearly an outlier (84.5%) but it was not removed as the plot-shape does not change significantly by doing so.

Moreover, the differences between the methods are not significant when one looks at the absolute recovery values: 84.5 – 99.8% for acetonitrile and 87.6 – 95.3% for the filtration method.

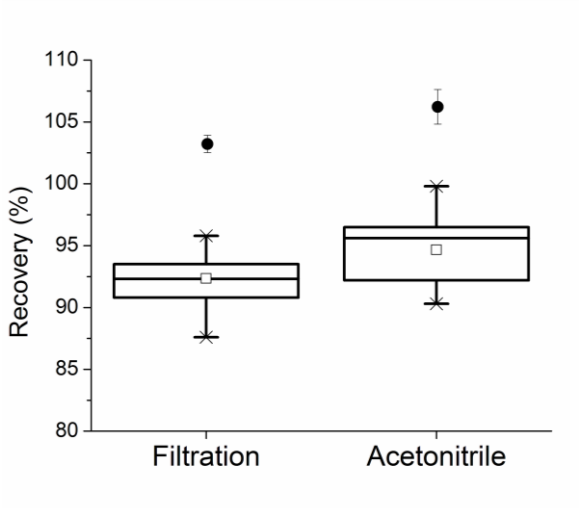

Figure 55. Box plot representing the $^{13}C_3$-CAF recovery in 12 saliva samples using filtration or acetonitrile to remove proteins/enzymes and cells. The black dots represent the recovery obtained in Milli-Q water (n = 3) to serve as a reference point.

Caffeine concentrations were also compared and the results are presented in Figure 56. The same outcome is observed; slightly higher values were obtained when acetonitrile is used, as illustrated by the slope of the correlation curve (1.06). The replicates' standard deviations (n = 3), for the same sample, seems to follow the same trend as for $^{13}C_3$-CAF (data not shown): acetonitrile extraction seems to generate slightly lower standards deviations than the filtration method.

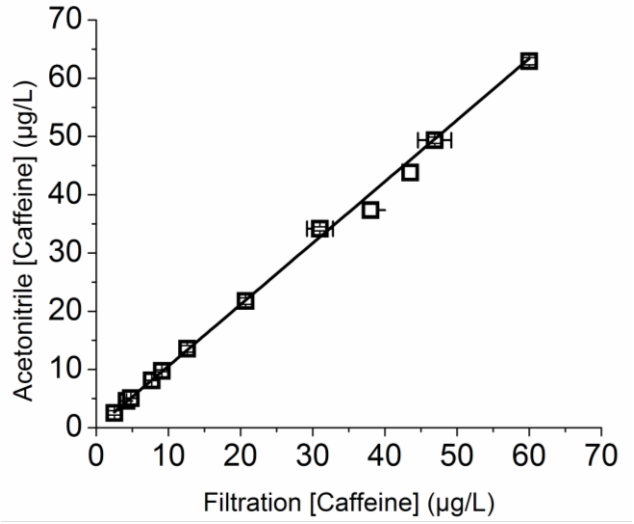

Figure 56. Concentration of saliva samples (uncorrected for the dilution factor) in a batch of 12 saliva samples, extracted by the two methods.Concentrations determined after acetonitrile precipitation are plotted on the abscissa and the filtration ones as the ordinate. Regression line: y= 1.0555 (± 0.01222)x + 0.0475 (± 0.076); R^2 = 0.99853.

7.7.2. Comparison with reference method

The calibration curve for ELISA was obtained by fitting the standards with a logistic 4-parameter curve (Figure 57). The calibration standards were selected to provide equidistant concentrations between them when a linear curve transformation is used, as illustrated by the insert in Figure 57. The linear transformation was obtained by plotting – log [OD] on the y-axis. The precision profile of the entire range was calculated using the model proposed by Ekins.[279] It shows very low overall errors (< 8%), with the lowest for the two lowest standards (< 2%) and the highest ones for the upper-range calibrators (around 7%).

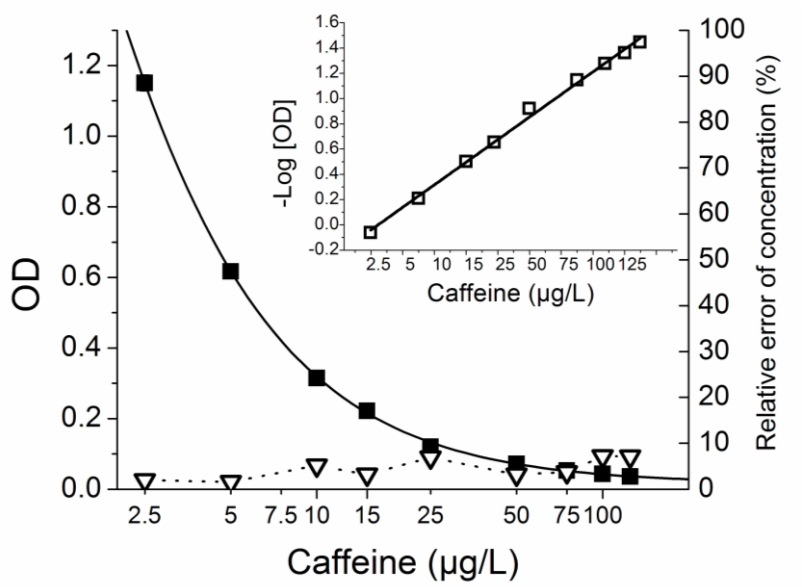

Figure 57. ELISA calibration curve used to quantify the saliva samples. The right axis represents the relative error of concentration calculated from the precision profile,[279] the points obtained are represented by open triangles and connected by a dashed line. The transformation of the calibration curve towards a linear model is represented by the insert on the top-right side.

The results from both methods, after correcting for dilution, were plotted using a Bland-Altman plot – Figure 58. The entire batch but two samples fall within the range of ± 1.96 times the standard deviation of the data, thus providing evidence of good agreement between the methods. The plot also shows a rather equal distribution above and below the 0% line, though a slightly higher number of points fall below that line.

A Student *t*-test (one-tailed) also shows no evidence of a significant difference between the methods for p = 0.05 and 58 DOF [t critical = 0.42; t (table) = 2.00].

The F-test [p = 0.05, n-1 = 59] also shows no evidence of significant differences between the method variances, F-critical = 1.03/ F(table) = 1.54).

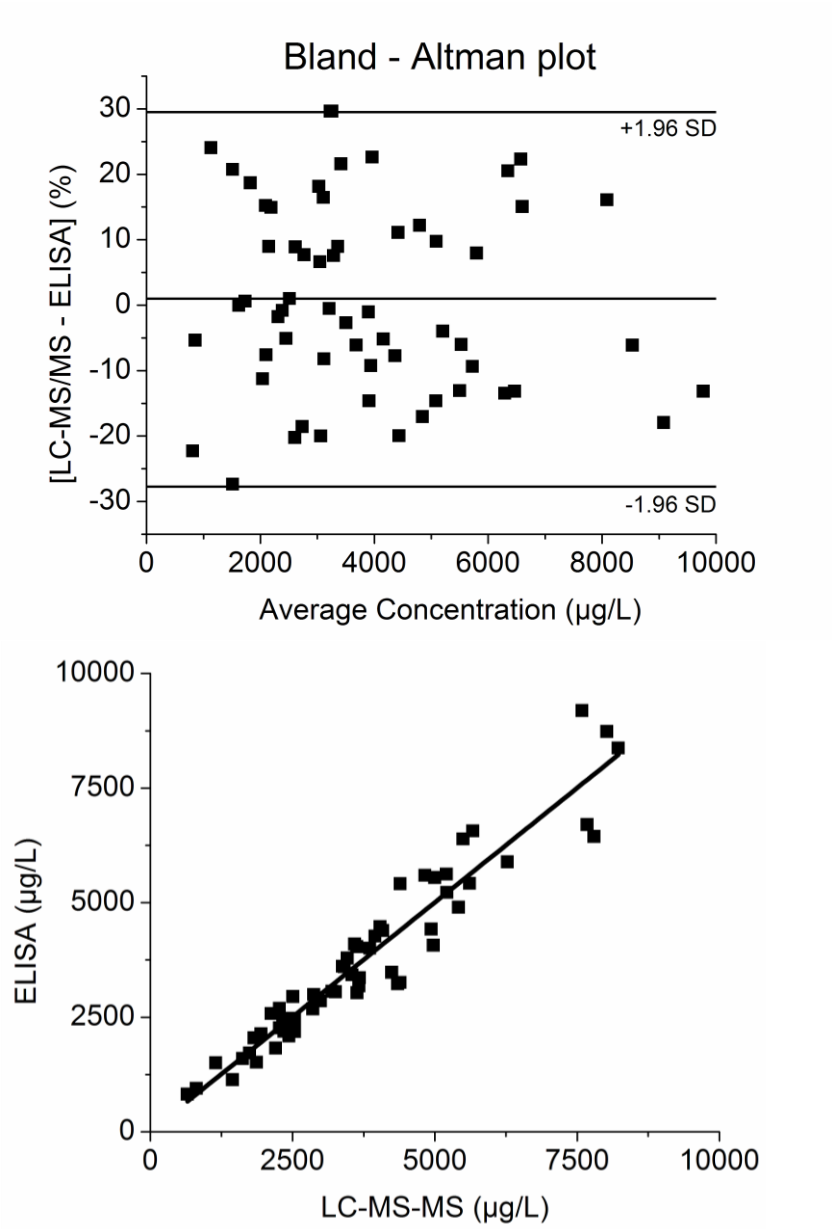

Figure 58. Bland-Altman plot for the saliva samples measured using both methods. The x-axis represents the average concentration of the values obtained using both methods and the y-axis the differences between them, in percent. On the right-hand side the regression representing the same data, correlates the ELISA results (y) with the LC-MS/MS ones (x): y = 0.998x + 13.78 (R^2 = 0.913).

Remark: Bland-Altman plots are the most common way of representing correlation between analytical methods in clinical chemistry. The linear regression is the widespread style to represent such data in analytical chemistry, and it is visually easier to make an overall judgment of methods equivalence by using it.

7.7.3. Spiking experiments and quality control samples

Analyte recoveries higher than 77% were observed when the samples were spiked with $^{13}C_3$-CAF and above 87% for caffeine itself. Table 18 summarises the results and the data provides further confidence regarding the suitability of the acetonitrile-based extraction procedure.

Table 18. Recoveries of caffeine and caffeine-trimethyl-$^{13}C_3$ in ten saliva samples from different individuals (A-J), collected at t = 180 min.

	Caffeine				**$^{13}C_3$ Caffeine**		
Sample	Sample concentration	Spiking level	Concentration determined	Recovery	Spiking level	Final concentration	Recovery
	[µg/L]	[µg/L]	[µg/L]	[%]	[µg/L]	[µg/L]	[%]
A	5002	2500	7033	93.8	2218	2500	88.7
B	3465	1250	4346	92.2	1129	1250	90.3
C	4391	1250	5408	95.9	1103	1250	88.3
D	3592	1250	4575	94.5	1084	1250	86.8
E	2539	1250	3283	86.6	1031	1250	82.5
F	3255	1250	4221	93.7	1120	1250	89.6
G	1150	500	1497	90.7	395	500	79.1
H	2127	1000	2872	91.8	779	1000	77.9
I	4244	1250	5304	96.5	1054	1250	84.3
J	2270	1000	3130	95.7	765	1000	76.5

Milli-Q water spiked showed recoveries between 96% and 104% and the control standard of 75 µg/L caffeine variation between -7.1% and 1.4%. Caffeine was not detected in any blank samples.

7.7.4. Caffeine profile evaluation in saliva

As illustrated by Figure 5, the caffeine metabolic profile can be achieved using the developed ELISA. An extra LC-MS/MS analysis was performed (2 inj.) seven days later (the extracts were frozen at -20 °C during this interval) to show the differences between the two LC-MS/MS analysis (by comparing with the 1st injection).

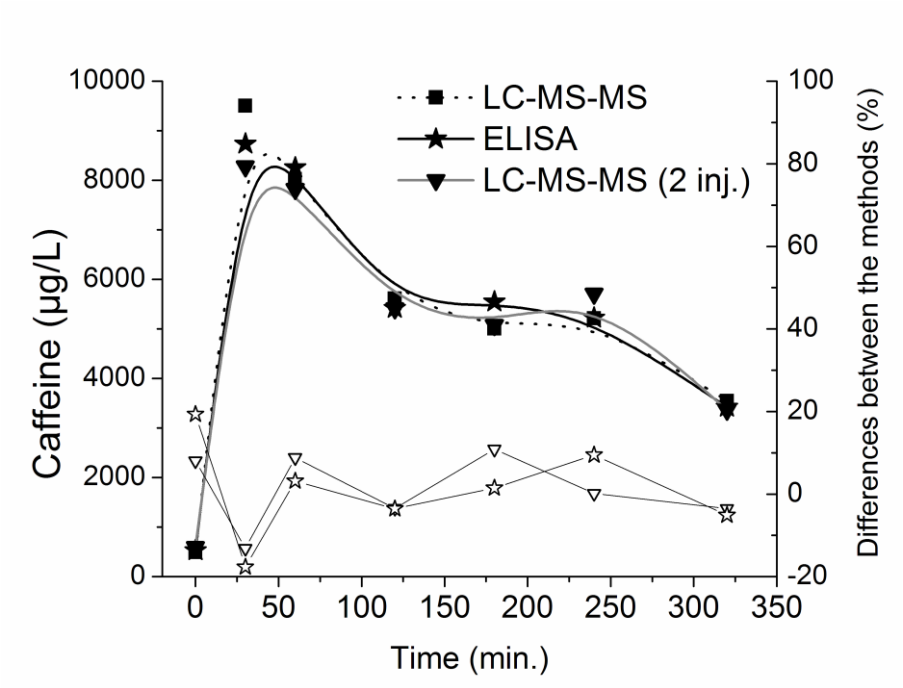

Figure 59. Caffeine salivary concentration over time using ELISA (filled stars), LC-MS/MS (filled squares) and a second LC-MS/MS analysis performed on another day (filled triangles). The lines connecting the bold symbols represent the caffeine decay with time: bold line for ELISA, dashed line for LC-MS/MS, first (black) and second (grey) analysis. The open symbols represent the deviation, in percent, of caffeine concentrations obtained by ELISA (open stars) and the second LC-MS/MS analysis (open triangles); using the first LC-MS/MS results as reference values.

Adult hepatic microsomal function can be assessed by a simple caffeine clearance test.[303,304] In fact, it has been shown that caffeine clearance is a more sensitive indicator of structural liver disease than conventional liver function tests, especially for alcoholic liver disease.[305] Several authors have unveiled the equivalence between salivary and plasma concentration of caffeine in hepatic liver function assessment,[135,303,306,307] and it seems that the salivary sampling alone has become accepted.[308] Some authors even suggested a single-point measurement to evaluate cirrhotic dysfunction.[304,309] A single caffeine concentration in saliva – total

overnight salivary caffeine assessments (TOSCA) – has been proposed as a useful diagnostic tool for cirrhotic patients and eventually also helpful for discriminating between the cirrhosis types.[309]

AS Figure 60 shows, the metabolism of 200 mg/L (*per os*) in 10 healthy voluntaries over a 5 hours period can be evaluated using the developed immunoassay. Even thought the samples were anonymous, important individual data can be obtained from the metabolic profiles: for example, individual A is most likely the shortest individual of the group while G, J and H are the tallest ones; Individual I ingested coffee before collecting sample T1(0h); and individual G, I and E are probably the three smokers of the group, since their caffeine metabolism is accelerated when compared with the others[310]. What is more, the post-lunch slowing down on the caffeine metabolism (around T4 and T5, depending on the individual) can be also seen on the metabolic profiles. A saliva sample (individual I, T6) was probably contaminated or something went wrong with the saliva collection, as the concentration is abnormally high, whether by ELISA or LC-MS/MS.

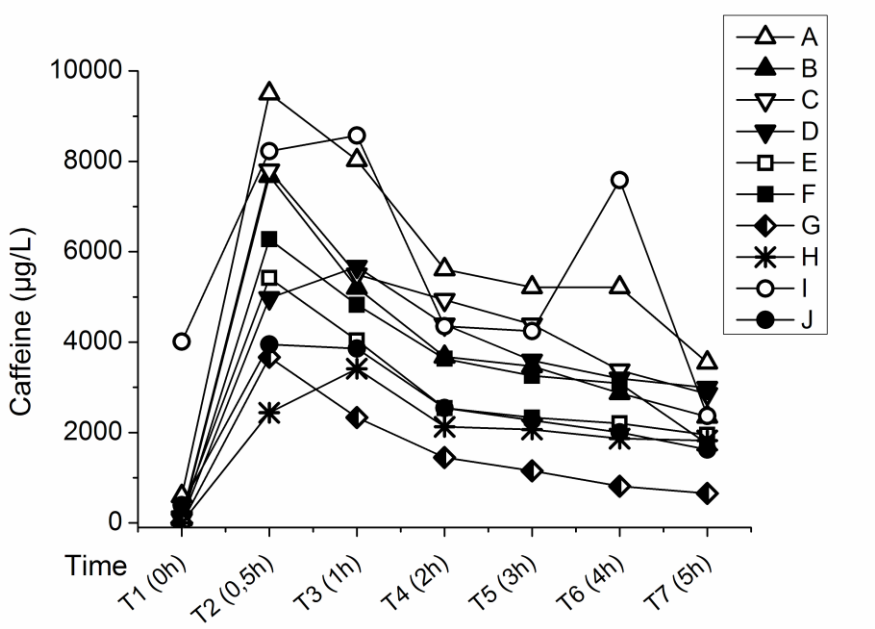

Figure 60. Caffeine concentration in saliva of 10 healthy individuals after injection of 200 mg/L caffeine.

The assay should be further tested by a clinical laboratory, using a cohort containing a statistical significant number (>100) of healthy and non-healthy individuals (with liver malfunction), prior to commercialisation.

7.8. Monitoring caffeine in beverages, shampoos and caffeine tablets

The high caffeine concentration present in most of the beverages requires appropriate sample predilution, prior to analysis by ELISA and direct LC-MS/MS. In this case the upper calibration range (was used for the ELISA and the same calibration standards solutions injected into the LC-MS/MS, thus avoiding calibration-related discrepancies between the methods. The obtained results are summarised in Figure 61 after correcting caffeine concentrations for the dilution factor. When linear regression is used to correlate the data, ELISA and LC-MS/MS results, a curve with a slope of 1.004 and an $R^2 = 0.9946$ is obtained.

Caffeine-free Coca-Cola gave a caffeine concentration of 5.6 ± 0,1 µg/L (n = 3) and Raspberry tea (intense red colour) 14 ± 1.2 µg/L, when measured by ELISA. Caffeine was not detected in both samples by LC-MS/MS and therefore the assay should be cautiously used in direct measurement of complex matrices. When however these samples were diluted 1:10 in Milli-Q, a concentration below 1 µg/L was obtained for both by ELISA. A dilution 1:10 seems thus sufficient to avoid false positive results.

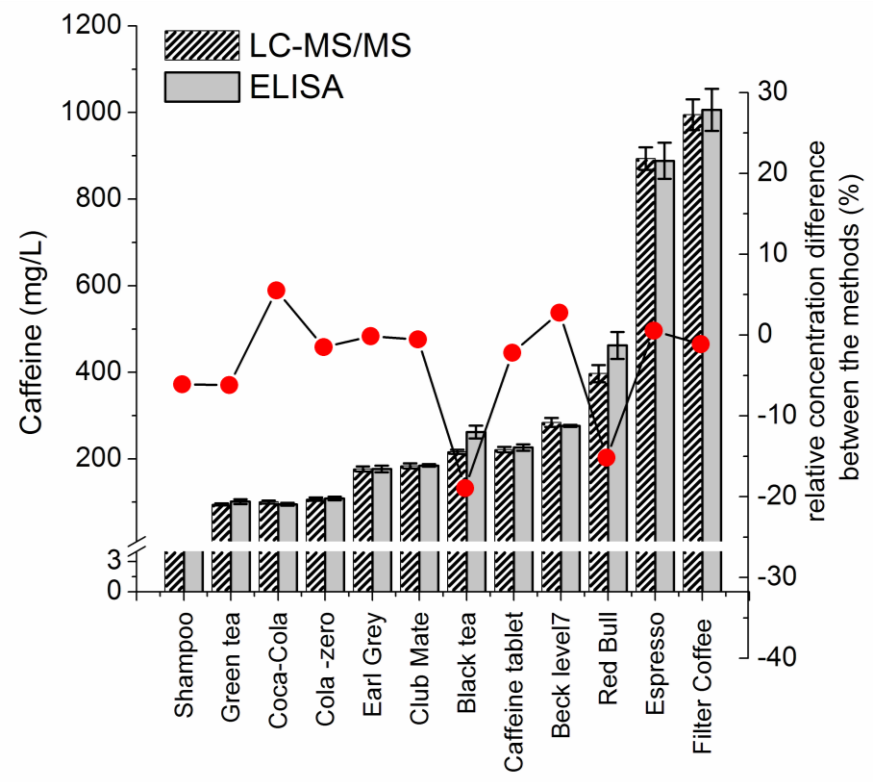

Figure 61. Concentrations of caffeine in several beverages, shampoo, and a tablet. The hatched bars represent the results obtained by LC–MS/MS while the grey bars show the results obtained by ELISA. The difference between both methods is represented by the

circles and can be read on the right-hand y-axis. The shampoo concentration reads 5.1 ± 0.23 mg/L (ELISA) and 4.9 ± 0.16 mg/L (LC–MS/MS)

7.8.1. Intraday and interday precision

The precision of the ELISA for the samples are shown in Table 19. Intraday variations were lower than 5.7% for the beverages with the exception of filter coffee (11.1%) and the interday variation was below 10.4% .The beverages results are presented in the Table 19 as they were obtained from the curve, i.e., before dilution factor correction for better data comparison.

Table 19. Intraday and interday precision for several beverages, shampoo and a caffeine tablet (after dissolution) by ELISA. The results are presented as they were obtained from the curve, i.e., without correction for the dilution factor (indicated within brackets in the first column).

	Intraday precision n = 5, same plate		Interday precision n = 9, over 3 days	
Beverages	Caffeine [µg/L]	RSD	Caffeine [µg/L]	RSD
Black tea (1: 10 000)	2.64	1.5%	2.58	6.6%
Red Bull® (1: 100 000)	4.86	2.9%	4.70	4.6%
Shampoo (1:1000)	4.86	3.2%	4.85	4.3%
Coca-Cola® (1:10 000)	9.81	1.0%	9.85	2.9%
Filter coffee (1:100 000)	11.1	11.1%	10.9	7.8%
Green tea (1:10 000)	15.5	2.9%	15.8	4.9%
Club-Mate® (1:10 000)	18.5	0.7%	18.4	1.7%
Red Bull® (1:10 000)	46.2	3.6%	48.5	6.7%
Espresso coffee (1: 10 000)	88.9	1.2%	86.3	4.7%
Coca-Cola® (1:1000)	94.8	3.7%	95.0	4.5%
Filter coffee (1:10 000)	100.6	4.8%	98.3	8.2%
Green tea (1:1000)	101.3	5.7%	104.3	5.7%
Other matrices				
Caffeine tablet (1:10 000 w/v)	22.6	0.8%	22.6	3.3%
Shampoo (1:100)	52.4	0.3%	47.5	10.4%

7.8.2. Accuracy

Neither a reference material nor an inter-comparison proficiency test is available for caffeine in beverages. Additionally to the good agreement with the LC-MS/MS, for some of the analysed beverages, caffeine concentrations can be found in several tables and therefore used as indicative “reference” values. The values for filter and

espresso-coffee are indicated in Table 20 but they cannot be used as reference values since caffeine final concentrations in those samples depend on the amount of coffee extracted and the volume of water used. As illustrated by the figures in Table 20, a good agreement between the two datasets was achieved.

Table 20. Comparison between the caffeine concentration obtained by ELISA and the indicative "reference" value/interval obtained from previous works.

Sample	ELISA result [mg/L]	Indicative values [mg/L]	Ref.
Coca-Cola® Zero	116	97 108 82 – 124 72 – 161	[311] [312] [313] [91]
Coca-Cola®	97	83 97 130 127 88 – 171 83 – 133	[312] [311] [93] [314] [313] [91]
Red Bull®	460	273 272 320	[314] [312] [311]
Club-Mate®	185	200	[311]
Becks Level 7®	275	250	[315]
Earl Grey tea	177	163 – 333	[316]
Green tea	100	158 – 333 100	[316] [311]
Black tea	264	145–386 187 – 293 199 – 254	[314] [91] [311]
Filter coffee	1110	267 – 1133 748 – 960	[123] [91]
Espresso coffee	983	1000-3500 1690	[123] [317]

To sum up:

The immunoassay is apt to determine caffeine concentration in several matrices including surface waters, human saliva, beverages, shampoos, and dissolved caffeine tablets.

PART II

Coprostanol immunization and stanols reference method

8. Additional materials (PART II)

8.1. Chemicals

Coprostanol ≥ 98%, cholestanol ~ 95%, cholestan ≥ 97%, cholestanone 99%, cholesterol ≥ 99.0%, stigmasterol ~ 95% were supplied by Sigma-Aldrich. Ergosterol ≥ 95.0% and lithocholic acid ≥ 99.0% were purchased from Fluka. Isolithocholic acid ≥ 99% was synthesised by Steraloids (London, United Kingdom).

Acetic acid 100%, ACS/ISO grade, was supplied by Merck and isopropanol, HPLC grade, from J.T.Baker. Ammonium acetate, purriss., eluent additive for LC-MS, was from Fluka. Sodium azide, ≥ 99%, Riedel-de Haën, was purchased from Sigma-Aldrich. Complete protease inhibitor cocktail tablets (cOmplete ULTRA) were from Roche (Mannheim, Germany) and Pepstatin A from Applichem (Darmstadt, Germany). Freund's complete adjuvant was purchased from Difco (Lawrence, KS, USA). Casein sodium salt from bovine milk was purchased from Sigma (C8654). Deuterated chloroform, isotopic purity 99.96 atom % D was from Aldrich.

8.2. Antibodies

Polyclonal anti-IgG sera were obtained from Acris Antibodies GmbH (Herford, Germany): anti-mouse IgG (H&L) whole molecule, from sheep (R1256P, Lot 20243, 2.2 mg/mL); anti-mouse IgG-F(c), from goat, (R1612P, Lot 22712, 3.7 mg/mL). The polyclonal anti-IgA mouse serum (from goat, NB 7501, Lot A23, 1 mg/mL), was obtained from Novus Biologicals via Acris Antibodies GmbH.

The polyclonal anti-IgG (whole molecule) mouse serum-HRP conjugate, from goat, was from Sigma (A4416). The serum supplied was a solution in 0.01 M phosphate buffered saline, pH 7.4 containing 1% bovine serum albumin and 0.01% thimerosal.

8.3. Animals

Three female, three months old BALB/c mice were bred at the Biotechnology Department – University of Potsdam, Golm, Germany.

9. Methods (PART II)

9.1. Antibody production

9.1.1. Hapten selection

The selection of the hapten was made by searching for similar structures to the one of coprostanol in databases such as Scifinder[318] and PubChem.[319] Several compounds were selected and thereafter they were compared to coprostanol using CS Chem 3DUltra (CambridgeSoft). Mainly stereochemistry comparison and calculation of bond lengths and angles were performed.

9.1.2. X-ray crystallography and ^{1}H-NMR

The crystals of isolithocholic and lithocholic acid were grown by solvent evaporation from ethyl acetate at room temperature in a desiccator. The single crystal X-ray data collection was carried out at room temperature. A total of 10307 reflection intensities were measured with an exposure time of 30 s per frame. The data reduction was performed by using the Bruker AXS SAINT and SADABS packages.[258] The structure was solved by direct methods and refined by full-matrix least squares calculation using SHELXTL.[259]

Coprostanol crystals were never obtained. Several solvents and mixtures of solvents were tried out unsuccessfully: Toluol, chloroform, tetrahydrofuran, ethyl acetate, acetone, dimethylformamide, water, methanol, acetonitrile and ethanol.

^{1}H-NMR spectra have been recorded under standard conditions on a Bruker Avance 600 NMR spectrometer, operating at 400 MHz. The substances were dissolved in deuterated chloroform ($CDCl_3$, isotopic purity 99.96 atom % D).

9.1.3. Immunogen synthesis and characterisation

The immunogen was produced by coupling isolithocholic acid (hapten) to bovine serum albumin (BSA) using NHS/DCC chemistry as described for caffeine tracer synthesis (6.3 - Enzyme tracer synthesis, page 68).

Briefly, a 50-fold (conjugate one) and a 100-fold (conjugate two) molar excess of the hapten were conjugated with BSA and purified by GPC (gel permeation chromatography) on a Sephadex PD-10 desalting column using PBS buffer as the eluent. The two produced conjugates were characterised independently by MALDI-

TOF/MS and LC-MS/MS using the same procedure already described for the caffeine tracer (6.4 - Tracer characterisation, page 72).

The final immunogen was obtained by mixing conjugate one and two and the concentration determined by UV-VIS spectroscopy using a BSA set of standards at 280 nm (isolithocholic acid does not absorb at this wavelength). The final immunogen (4.5 mg/mL) was diluted and aliquoted in 40 µL PBS buffer containing 150 µg of the conjugate (3.75 mg/mL). Three fractions of the immunogen were insolubilised using acetonitrile (200 µL) and the precipitated conjugate was dried under a nitrogen stream at room temperature. 50 µg of the insolubilised immunogen was mixed with 100 µL of Freund's complete adjuvant and injected in each mouse.

For the boosts, the 50 µg of insolubilised immunogen was redissolved in 100 µL PBS buffer (for the 1st and 2nd boosts) and thereafter the soluble immunogen was used.

9.1.4. Immunization procedure

The immunization was carried out by a project partner, Hybrotec, UP Transfer (University of Potsdam, Golm, Germany) according to procedures already published by the company members[237,238] and herein briefly described.

Three female, three months old BALB/c mice, were immunised intraperitoneally using 50 µg of the insoluble immunogen (BSA-isolithocholic acid conjugate) at day zero. The animals were boosted regularly, according to the schedule in Table 21, with the insoluble (first 2 boosts) and soluble immunogen (after 3rd boost), 50 µg in PBS buffer. Serum samples were taken – venipuncture from the orbital sinus – around five to seven days after each boost to evaluate the titre and affinity maturation of the hapten-specific antibodies. Faeces were collected 28 weeks after the first immunization. Table 21 summarises the timeline used for the immunization process overall.

Table 21. Immunization timeline for the production of a coprostanol monoclonal antibody.

Days	Description	Remarks
0	Immunization	Insoluble antigen
42	1st boost	Insoluble antigen
49	1st venipuncture	
50	1st serum screening	
89	2nd boost	Insoluble antigen
96	2nd venipuncture	
99	2nd serum screening	
118	3rd boost	Soluble antigen
125	3rd venipuncture	
130	3rd serum screening	
146	4th boost	Soluble antigen
151	4th venipuncture	
156	4th serum screening	
193	faeces collection	
205	5th venipuncture and serum screening faeces collection	Second venipuncture after 4th boost
227	faeces collection	
363	5th boost	
366	spleen removal and fusion	

9.1.5. Immunization monitoring

i. Serum collection and testing

The immunization was monitored by assaying the mice sera for coprostanol-selective antibodies. Blood (~ 100 µL) was collected from the orbital sinus and let stand for 2 h at room temperature. The tubes were then centrifuged (3000 x g, 5 min) and the serum preserved with 0.1% sodium azide. The samples were transported refrigerated to the lab and analysed within the next 5 days. All sera were kept at 4 °C.

The search for specific anti-hapten antibodies was performed using direct competitive ELISA in MaxiSorp plates. The capture antibody was an anti-IgG mouse whole molecule (H&L) from sheep, diluted in PBS buffer pH 7.4 to 1 µg/mL (200 µL per well, o/n). The serum samples were diluted in PBS containing 1% (w/v) BSA: 1:1,000-fold and 1:10,000-fold (after the 1st boost); 1:50,000-fold or 1:100,000-fold (after the 2nd boost).

The standard solutions were prepared in Milli-Q water with the exception of the stock solutions which were prepared in isopropanol. The assays were mostly performed with isolithocholic acid (hapten) but also using coprostanol standards whenever appropriate and the sera volume sufficient. The enzyme tracer – an isolithocholic acid-HRP conjugate[h] – was diluted 1:100,000 in PBS containing 1% (w/v) BSA. OD readouts were interpolated by a 4-parameter logistic function, the C-value representing the inflection point of the sigmoidal curve which is similar to IC50.

The incubation time for the sera (200 µL per well) was not less than 2 h, the standards (100 µL) were incubated for 20 minutes alone and one more hour after adding the HRP conjugate (100µL) to the well. The incubation time for the TMB solution was variable, depending on the colour development; a maximal incubation time of 1 h was used but sometimes the acid (H_2SO_4) had to be added much earlier due to higher antibody titres in the sera.

A pre-immunization mouse serum was used as negative control and the anti-caffeine antibody and respective tracer as a performance control of the assay (no commercial antibody is available neither for coprostanol nor for isolithocholic acid).

ii. Faeces

Faeces extractions were based on previous protocols described by Dion *et al.*[320] The mice faeces were extracted using PBS buffer pH 7.6 containing 1% (w/v) sodium azide supplemented with complete protease inhibitor cocktail tablets from Roche (1 mini-tablet, EDTA-free, per 10 mL buffer). One gram of air-dried faeces was shaken overnight (20 hours) with 10 mL of the aforedescribed buffer. The extract was aliquoted into 2 mL Eppendorf tubes which were centrifuged at 15°C, 15,000 x g, for 5 minutes. The supernatant was diluted 10-fold in PBS buffer prior to perform the ELISA – using the same procedure as described for the sera but incubating the extracts longer, 3 h 30 min.

[h] *The HRP conjugate has an average coupling ratio of 2.3 mol hapten per mol HRP.*

iii. Sterol and stanol levels

The sterol and stanol levels in the sera and faeces were measured using the LC-(APCI)-MS/MS described elsewhere (9.2. Reference method for sterols, stanols and bile acids, page 167) after liquid-liquid extraction (sera) or liquid-solid extraction (faeces).

The sera (2 µL) were extracted by adding 1 mL n-hexane, vortexing and shaking for 2 hours. The Eppendorf tube was centrifuged at 15 °C, 15,000 x g, for 5 minutes and the supernatant transferred into an HPLC vial and evaporated until dryness under a nitrogen stream. The residue was resolubilised using 400 µL isopropanol and diluted appropriately to fit the calibration range (100- to 1000-fold) in mobile phase B (isopropanol:methanol, 1:1, v/v).

Faeces (~ 1 g) were extracted using 10 mL of isopropanol, under continuous shaking, RT, o/n. The tubes were let on the bench until all the solids were sedimented and the supernatant was filtered through a 0.45 µm filter. This filtrate was diluted appropriately (10 – 1000-fold) in mobile phase B prior to LC-MS/MS analysis. The faeces results are expressed per g of dry residue: 1 g of faeces was dried at 102 °C in an oven until constant weight (losses between 12 and 16% of water were registered).

9.1.6. Hybridoma technology

One immunized mouse (mouse 2) was killed by diethyl ether inhalation and cervical dislocation three days after the 5th re-immunization. The abdominal cavity was opened and the spleen removed and placed – under sterile conditions – in a Petri dish filled with 10 mL RPMI 1640 (Roswell Park Memorial Institute medium). The spleen was disaggregated and macerated using a spoon-head sterile spatula and some fat residues were removed out of the Petri dish. The obtained cell suspension was transferred into a 50 mL Falcon tube and the Petri dish washed with 5 mL of RPMI 1641, transferred thereafter into the same Falcon. The tube was then let on the bench for 2 minutes to allow precipitation of debris and ~8mL of the supernatant transferred into a new Falcon tube. After centrifugation (200 x g, 10 min), the residue was resuspended in 10 mL BSS (Balanced Salt Solution) buffer for fusion and the viable cells counted using optical microscopy. The myeloma cell line (X63-Ag8.653), also in BSS buffer, was added to the spleen-cells suspension in a ratio 1:3 (cells/mL). The cell suspension was mixed and then centrifuged (400 x g, 3 min), the supernatant poured off and the pellet resuspended with 0.5 mL BSS

buffer. The cell suspension was mixed and then centrifuged (400 x g, 3 min), the supernatant poured off and the pellet resuspended with 0.5 mL BSS buffer. The cell suspension was subsequently mixed 1:1 with 0.5 mL PEG 8000 solution 25% (m/v) in BSS buffer. The fusion between the B cells and the myeloma cells was performed using a modified electrofusion technique[321,322]: 360 µL of the cellular suspension, containing PEG 8000, were transferred into a 2 mm electroporation cuvette and placed on the electroporator (Fisher, modified by Hybrotec). The electropermeabilization pulse (600-650 V, 25 µS) was then delivered followed by an equilibration time (3 min, RT) before the cells were pulled out and resuspended in an Erlenmeyer flask containing 60 mL of cell culture medium 20% FCS (Fetal Calf Serum supplemented with 1% glutamine and 1% mercaptoethanol, in RPMI). The procedure was repeated until all the cells' suspension volume was away and the Erlenmeyer flask containing the cells placed inside an incubator (37 °C, 7% CO_2) for 2 h.

The Erlenmeyer was filled up to 100 mL with HAT selection medium (hypoxanthine-aminopterin-thymidine) and the final volume supplemented with 1% gentamicin to suppress microbiological growth.

The final cell suspension was distributed in five 96-well microtitre cell culture plates (100 µL/well), to which 100 µL/well of a feeder cell suspension (in RPMI) had been previously added. The plates were then incubated at 37 °C (7% CO_2) and every 3 to 4 days 100 µL/well were poured out and new HAT medium (100 µL/well) added.

Twelve days after the fusion, the HAT medium was replaced by a cell culture medium containing 20% FCS (in RPMI, supplemented with 1% glutamine and 1% mercaptoethanol). Three days later the first tests of the cell culture supernatants for anti-hapten specific antibodies were performed.

The hybridomas whose supernatants tested positive in the screening ELISA were expanded in 24-well or 6-well plates and the supernatants tested again. When positive, the cells were diluted successively in 96-well plates – recloning by limiting dilution – and positive wells transferred into another plate and allowed to grow. The process is fully described in the next section – 9.1.7. Screening procedure – by a flowchart (Figure 62, page 166).

Remark: The described procedure was performed by specialised workers at Hybrotec and not by the author, who was just an assistant during the process.

9.1.7. Screening procedure

The hybridoma supernatants, hereafter HybS, (100 µL) were always tested using direct and indirect ELISA. Per each plate a positive control (immunized mouse 2 serum, 4th boost) and a negative control (non-immunized mouse serum) were included. The controls were diluted 1:100,000 for the direct and 1:10,000 for the indirect ELISA.

i Direct screening

The direct (competitive) ELISA was entirely performed at room temperature.

The transparent high-binding microtitre plates were coated with polyclonal anti-mouse IgG (H&L,"whole molecule") serum (2 µg/mL in PBS buffer, 200 µL per well), covered with Parafilm® and incubated overnight (~ 18 hours) on the plate shaker at 750 rpm.

The plates were then washed three times and 50 µL of a 1% BSA solution in PBS (hereafter, PBS-1% BSA) was added pro well followed by 50 µL/well of HybS or dilution of HybS, whenever appropriate. The plates were incubated for 3 h 30 min under shaking.

A PBS-1% BSA buffer (50 µL/well) was added and then 50 µL/well of the tracer (isolithocholic acid-HRP conjugate) which was previously diluted to 2.0 E^{-6} µg/mL in PBS buffer. The incubation time was one hour, under shaking, and afterwards the plate was washed again. The TMB substrate (100 µL/well) was incubated for a minimum of 40 min and then the sulphuric acid 1 M added (100 µL/well).

When the competitive ELISA was performed to check for inhibition, 50 µL/well of standards (isolithocholic acid or coprostanol) were added before adding the PBS-1% BSA buffer and the tracer. The remaining protocol was kept the same.

ii Indirect screening

The indirect ELISA was performed using the same solutions as in the direct screening with the following exceptions.

The microtitre plate was coated o/n with isolithocholic acid-OVA conjugate in PBS (3.5 µg/L, 100 µL/well). After washing, the plate was blocked with a 0.5% casein solution (in PBS) for 1 hour. The HybS were incubated for 3 h and when testing for

inhibition, the supernatants (60 µL/well) were previously mixed with 60 µL/well of the standards solution in a low-binding plate and 100 µL/well of the mixture transferred into the coated Maxisorp plate. The tracer, an anti-IgG serum (whole molecule)-HRP conjugate was diluted 1:10,000 in PBS (100 µL/well) and incubated for 1 h.

iii Screening flowchart

The hybridoma screening process is resumed using a flowchart (Figure 62) describing the process step-by-step.

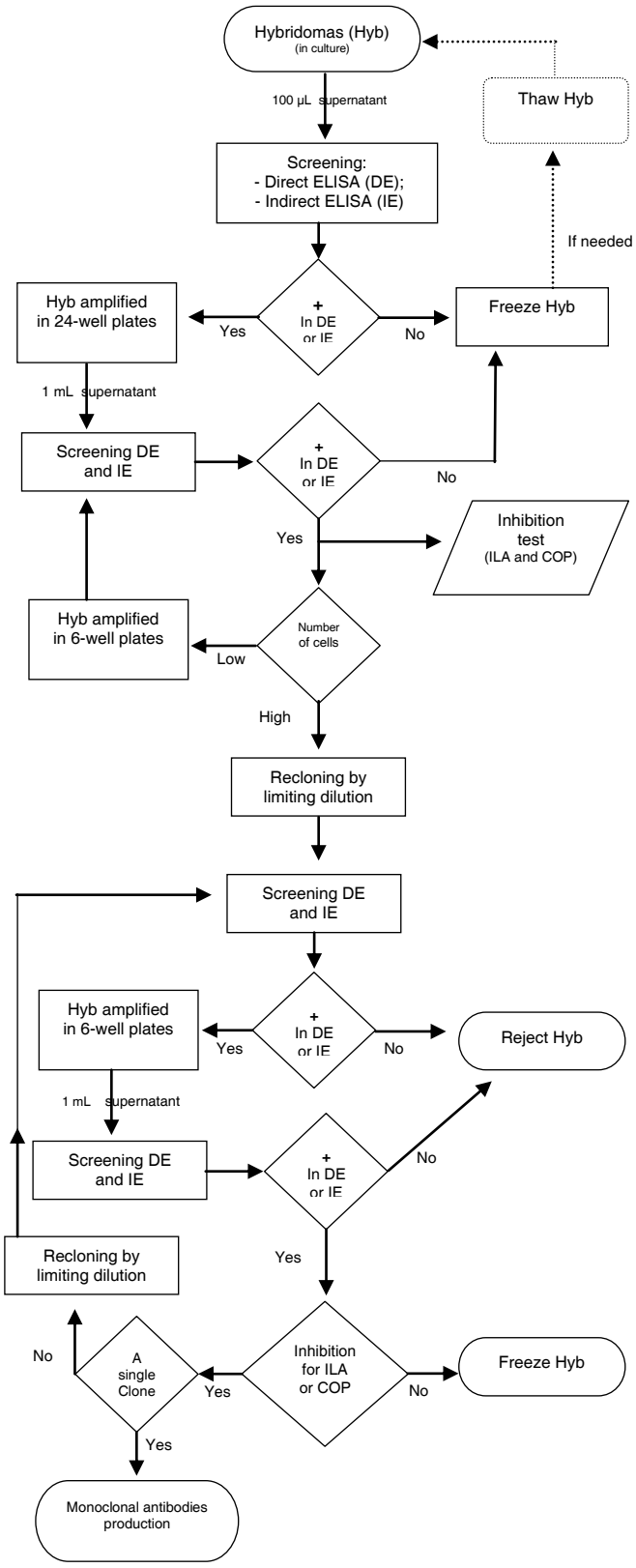

Figure 62.Hybridoma screening flowchart. Hyb (hybridoma), ILA (isolithocholic acid), COP (coprostanol), DE (direct ELISA), IE (indirect ELISA).

9.2. Reference method for sterols, stanols and bile acids

9.2.1. APCI-MS conditions

Each individual standard was injected into the MS via the HPLC system, after reversed-phase chromatography. The atmospheric-pressure ionisation was carried out using chemical ionisation (APCI) after recognizing the inefficiency of electrospray (ESI) ionisation to produce charged ions. All compounds were analysed in positive mode and for each of them a SCAN, a Single Ion Recording (SIR), a product scan (after fragmentation) and several transitions on multiple reaction monitoring (MRM) were obtained. Each standard was injected individually using a solution of 1 mg/L of the compound in methanol.

The optimisation of the MS parameters was done using a multi-compound standard mixture, after chromatographic separation, in both scan and SIR mode. A traditional univariate approach was used by setting up all parameters but one (variable) to fixed standard values: curtain gas (25 psi; 172 kPa), ion source gas 1 (50 psi, 345 kPa), ion source gas 2 (60 psi, 414 kPa), source temperature (450.0 °C), nebulizer current (8.00 µA), dwell time (0.100 sec), declustering potential (50 V) and entrance potential (7.00 V). The collision energy was optimised to allow the presence of precursor ion in the product scan with relative intensity between 20 and 30%.

The quantitation was achieved by using one MRM per compound and the confirmation using at least an additional one and the retention time. Mostly the most intense MRM transition was selected, except in the case another transition presents a better signal-to-noise ratio or it is specific of that compound. The calibration curves were established using the peak areas of a series of multi-compound external standards fitted using a linear regression function and a second order polynomial for cholestanone.

9.2.2. Chromatographic separation

i. Stationary phase and mobile phase

A C18 stationary phase was selected for the separation. The method was initially developed using a longer and narrower column (UltraSep ES Phen1, 250 mm X 3 mm, 5 µm) but the final method made use of a shorter one with a larger diameter (C18 SepServ RP18, 100 mm x 4 mm, 5 µm).

Acetic acid was added to decrease the mobile phase pH until the acid range due to the bile acids isolithocholic and lithocholic acid. Water alone was also tested and

except for the bile acids, it gives the same outcome. Three organic modifiers were tested alone and in mixtures of them: acetonitrile, methanol and isopropanol.

The final chromatographic method used water + ammonium acetate 5 mM + acetic acid glacial 0.05% (v/v) as mobile phase A and a mixture 1:1 of methanol:isopropanol as mobile phase B.

ii. Chromatographic resolution

Compounds sharing the same MRM transition must be well separated prior to their entry in the MS detector. Several gradients, mobile phases, column oven temperatures and organic modifiers were tested to achieve acceptable resolution between these peaks. Resolution was calculated using the "classic" equation (Equation 1)[323,324] and the Purnell equation (Equation 2),[324-326] which besides the retention time and the peak width takes additionally into account the selectivity factor, capacity factor and plate number. A resolution of 1.0 means the two peaks are separated but a value equal or higher than 1.5 is required for a baseline resolved separation.

Equation 1. Chromatographic resolution[323,324]

$$Rs = \frac{2(t_{r2} - t_{r1})}{(w_1 + w_2)}$$

Where *tr* is the retention time and *w* is the peak width at the baseline.

Equation 2. The Purnell equation[324-326]

$$RsP = \frac{N^{1/2}}{4}\left(\frac{\alpha - 1}{\alpha}\right)\left(\frac{k}{1+k}\right)$$

Where N is the plate number, α the selectivity factor and *K* the capacity factor (also known as retention factor). These parameters are calculated according to the following equations.

The number of theoretical plates can be calculated using Equation 3[323,324]

Equation 3. Number of plates

$$N = \frac{t_r^{\,2}}{\sigma}$$

Where σ is the standard deviation of the solute zone. For a symmetric Gaussian peak the standard deviation can be determined from the peak width either at the baseline ($w = 4\sigma$) or at half-height ($w_{1/2} = 2.354\sigma$). Accordingly, the plate height can be written as:

Equation 4[323,324]

$$N = 16\left(\frac{t_r^{\,2}}{w^2}\right) = 5.545\left(\frac{t_r^{\,2}}{w^2_{1/2}}\right)$$

The results presented in the Results section (10.2.2. Chromatographic separation; vi. Chromatographic resolution, page 217) were calculated using the peak width at half-height because it can be measured more accurately than at the baseline, especially in case of peaks with overlapping baselines.

The capacity factor (or retention factor) is the normalised value of the analyte retention that is independent of the column diameter, length and flow-rate. The retention time is normalised to the elution time of a nonretained solute according to the equation:

Equation 5. Capacity factor[323,324]

$$k = \frac{t_r - t_0}{t_0}$$

Where t_0 is the elution time of the nonretained solute and t_r the elution time of the analyte.

The selectivity factor is a measure of the relative affinity of the mobile phase and stationary phase for two adjacent solutes. It is expressed as a ratio between the capacity factor of the two peaks:

Equation 6. Selectivity factor[323,324]

$$\alpha = \frac{k_2}{K_1}$$

Where k_1 is the capacity factor of the first peak and k_2 of the second.

9.2.3. Extraction methods

i. Membrane-assisted liquid-liquid microextraction (MALLME)

The membranes were prepared according to the procedure proposed by the Moeder group.[327] Polyethylene bags were cut out to form several double-faced strips with about 8 mm width and 100 mm length, as illustrated by Figure 63. The open borders were sealed, using a shrink-wrapping device, to produce a closed membrane with exactly 5 mm width, 10 cm length and an aperture on one side. The overlaying foil borders were cut carefully using scissors (the strips were initially 8 mm large) to avoid analytes' absorption onto the crinkles produced by the sealing. Very frequently this cutting step damaged the membrane integrity, though not always macroscopically visible, causing therefore solvent leakage during the extraction step.

Once the membrane is ready, it is filled with isopropanol and immersed in a 40 mL capacity vial containing the same solvent and was shaken for 1 hour at room temperature. Henceforth, the membrane is just handled using metallic tweezers.

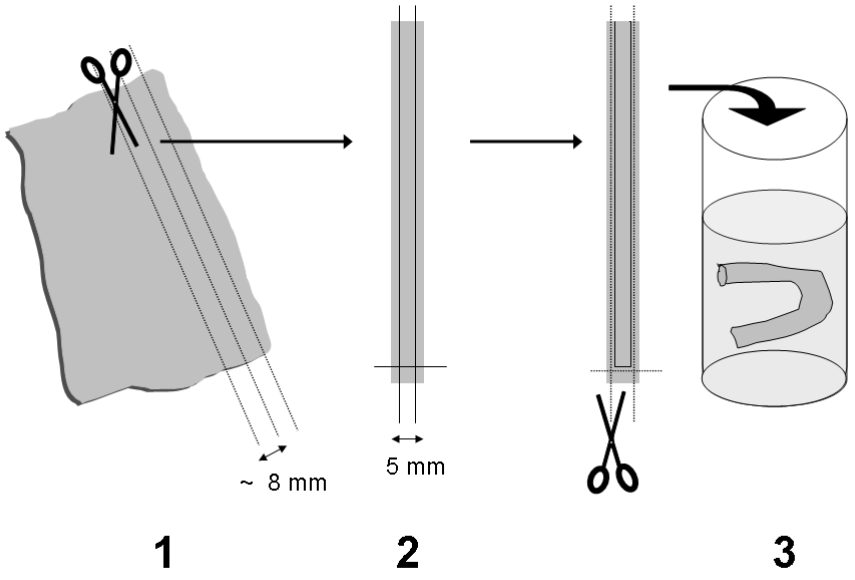

Figure 63. Membrane preparation scheme. (1) The polyethylene bag is cut into double-face strips; (2) Each strip is sealed to produce a 5 mm width membrane and the outer remnants are cut out; (3) The membranes are filled in and immerged in isopropanol.

After the washing step, the membranes are placed in a glass Petri dish and dried in a lab oven, set at 50 °C, until the solvent is entirely evaporated. Using tweezers, the membranes are gripped by the aperture and this time immersed in Milli-Q, preventing water to enter the membrane. Water excess can be removed by wagging the membranes on the air a couple of times. They are after that immersed directly in the samples/standards as illustrated in Figure 64 and the extraction follows the procedure described in the caption.

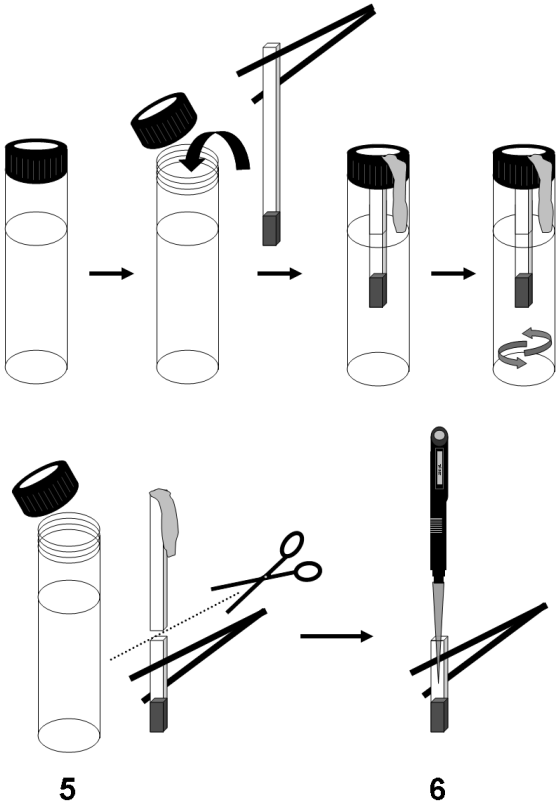

Figure 64. Membrane-assisted liquid-liquid extraction. (1) Twenty mL sample are transferred into a transparent glass vial; (2) The membrane, containing 200 µL isopropanol, is immerged incompletely in the sample; (3) The tube is closed with the Teflon cap, fastening the membrane by its top; (4) The tube containing the hanging membrane is then placed on an orbital shaker (circular gyrating motion) and shaken over-night (~24 h) at 700 rpm, room temperature; (5) Once the extraction is finished, the membrane is removed using tweezers and cut around 2 cm above the isopropanol surface; (6) Finally the isopropanol is removed using a micropipette and transferred into an HPLC vial. After removing the solvent, each membrane was inserted in an HPLC vial and 1 mL isopropanol added to extract possible adsorbed compounds on the outer membrane material.

ii. Dispersive liquid-liquid microextraction (DLLME) – Freezer assisted

The method was based on previous works from Daneshfar[328] and Rezaee.[329] The dispersive solvent, the extraction solvent and respective volumes were optimised to provide the best analytes' recoveries. Two major differences between the herein proposed method and the aforementioned ones are: 1) the extraction solvent used (n-hexane) has a lower density than the sample and 2) the dispersive solvent could not be an alcohol. Further discussion about these differences and the overall method development is given in the Results section – 10.2.3.ii. Dispersive liquid-liquid microextraction (DLLME), page 223. Meanwhile, the optimised procedure for DLLME is provided in Figure 65 and described by the respective caption.

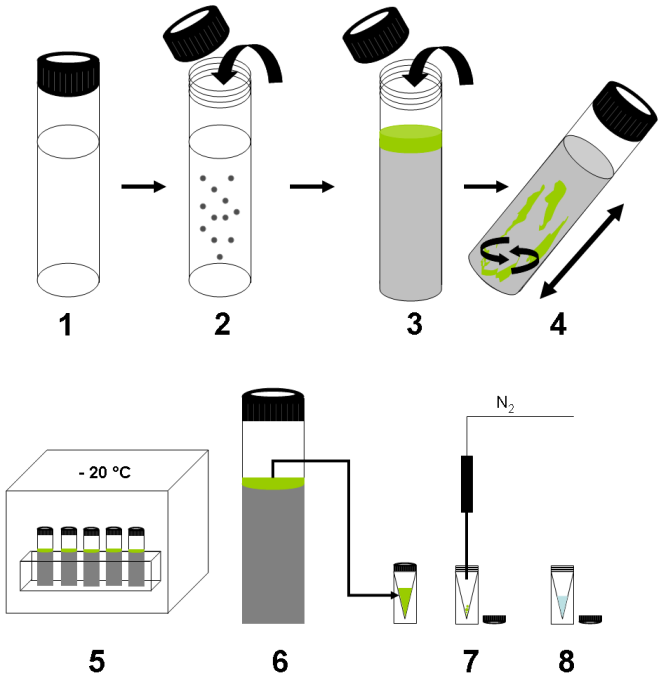

Figure 65. Dispersive liquid-liquid Microextraction procedure. (1) The sample – 10 mL – is placed inside a transparent glass vial; (2) The dispersive solvent (acetonitrile, 50 µL) is added into the sample and the mixture vortexed; (3) The extraction solvent (n-hexane, 200 µL) is added thereafter and the vial closed; (4) Several vials are placed on the orbital shaker in a approximately 45° angle and shaken for 2 hours at 700 rpm, room temperature; (5) Once the extraction is finished, the vials are placed vertically into a freezer at -20 °C until the water-phase is frozen (usually over-night); (6) The n-hexane is recovered from the surface using a 200 µL micropipette and transferred into an HPLC vial; (7) The n-hexane is evaporated till dryness using nitrogen stream and (8) the residue recovered using a mixture of water:methanol/ isopropanol (20:40/40; v:v/v), i.e., the initial composition of the HPLC gradient.

10. Results and discussion (PART II)

10.1. Antibody production

10.1.1. Hapten selection

Coprostanol lacks an available group for coupling it to a carrier protein, except for the hydroxyl group which was believed to play an important role in the compound recognition by the antibody and therefore could not be used for the conjugation.

Different synthetic approaches were studied in order to obtain a similar molecule with a terminal carboxylic acid or amino group at the end of a spacer which would allow for coupling, thus leaving the sterane core (the perhydrocyclopentanophenanthrene ring) and the hydroxyl group "exposed" as part of the epitope for antibody recognition. Finally, a naturally occurring compound was selected to mimic the coprostanol structure in the final immunogen: isolithocholic acid (Figure 66).

Isolithocholic acid is a secondary bile acid produced from cholesterol, via the primary bile acid chenodeoxycholic acid, by a hydratase enzyme from anaerobic bacteria in the intestine of mammals – a dehydroxylation at position C7.[330,331] As other bile acids, isolithocholic acid is reabsorbed from the distal intestine back to the liver via enterohepatic circulation in healthy individuals.[331] Therefore, it is very unlikely to be found, at least in detectable concentrations, in environmental samples. The data available for isolithocholic acid in environmental samples is very scarce.[79,118] and one of the reasons seems to be the insofar analytical shortfall to detect it and also to separate it from its α-isomer, lithocholic acid.[144]

The number of references found in the Scifinder database[318] for isolithocholic acid, when searching by CAS number, was surprisingly low (145 references on 19-06-2009) when compared with other sterols and steroids (1140 for coprostanol, 2650 for cholestanol, 2724 for lithocholic acid, 5780 for ergosterol, 7318 for cholic acid and – not unexpected – 142,439 for cholesterol). This shows that isolithocholic acid has not been yet a main focus of research and consequently most data about it is still to be produced if its metabolism is interesting at all.

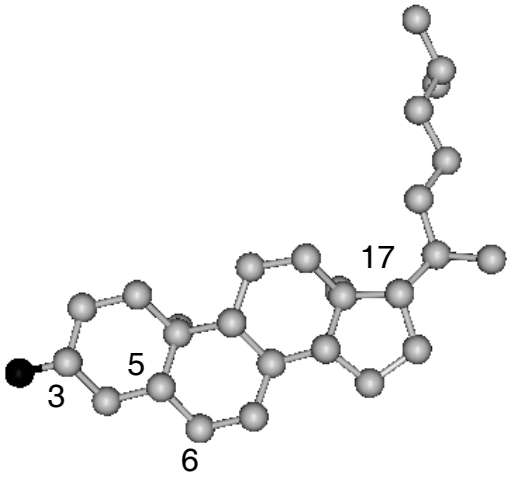

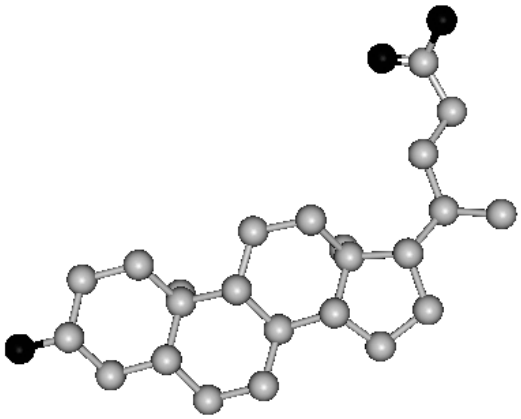

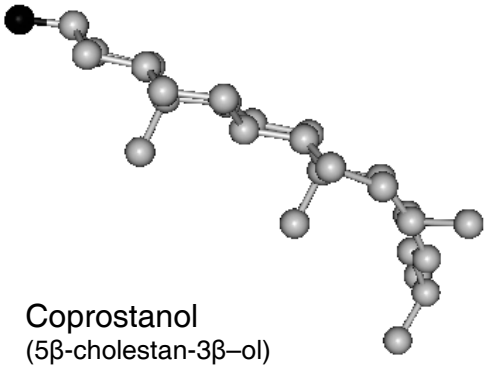

Coprostanol
(5β-cholestan-3β–ol)

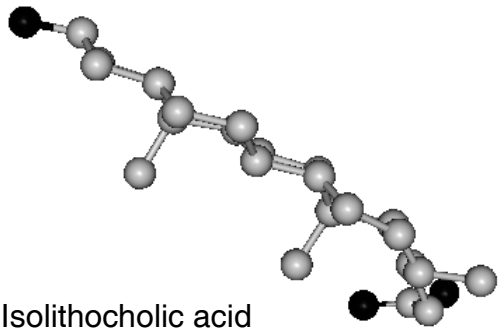

Isolithocholic acid
(5β-cholanic acid-3β–ol)

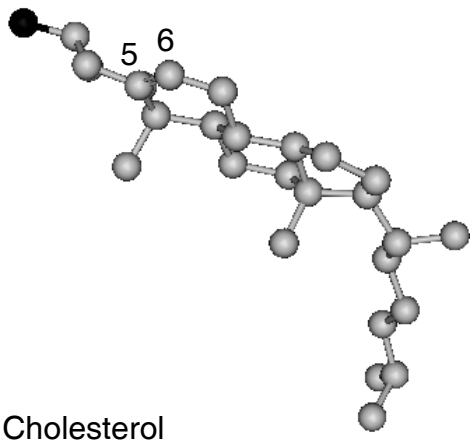

Cholesterol
(cholest-5-en-3β -ol)

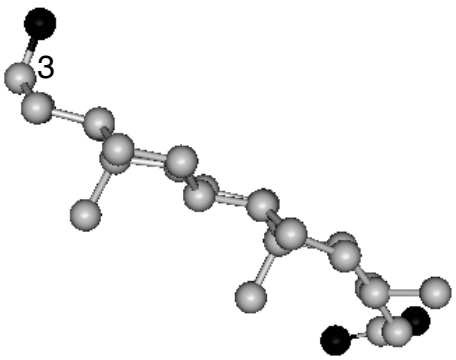

Lithocholic acid
(5β-cholanic acid-3α-ol)

Figure 66. 3D Structures of coprostanol (5β-cholestan-3β-ol), isolithocholic acid (5β-cholanic acid-3β-ol), cholesterol (cholest-5-en-3β-ol) and lithocholic acid (5β-cholanic acid-3α-ol). The structures were drawn using MarvinSpace 5.3.6 (ChemAxon, 2010).

Isolithocholic acid shares the sterane core geometry with coprostanol (Figure 66), as well as the β-hydroxyl group in C3. The difference between the two compounds is located in the side chain at C17, which is shorter for isolithocholic acid and advantageously has a terminal acid group for the conjugation with terminal amino groups in the carrier protein. Whether or not this side chain shortness could play a major role on the antibody specificity towards coprostanol could not be answered at this point, though it is common procedure in immunochemistry to conjugate a hapten with proteins/enzymes via a different side-chain than the one present on the analyte to be measured.[163,182,201]

Lithocholic acid is represented in Figure 66 to show the difference to its β-isomer, isolithocholic acid. Cholesterol is also represented to illustrate the 3D conformation changes on the rings system caused by the double bond between C5 and C6, a common feature of the sterols.

10.1.2. Hapten characterisation

Coprostanol (analyte) and isolithocholic acid (hapten), except for the side-chain on C-17, show the same conformation, atoms distances and bond angles after calculations using CS Chem 3DUltra.

Isolithocholic acid and lithocholic acid crystals were successfully obtained and the x-ray scattering results for isolithocholic acid are presented in Figure 67. Despite several attempts and an extensive list of solvents and solvents mixtures tested, coprostanol crystals were never obtained. An amorphous white powder was the result of all crystal-growing attempts.

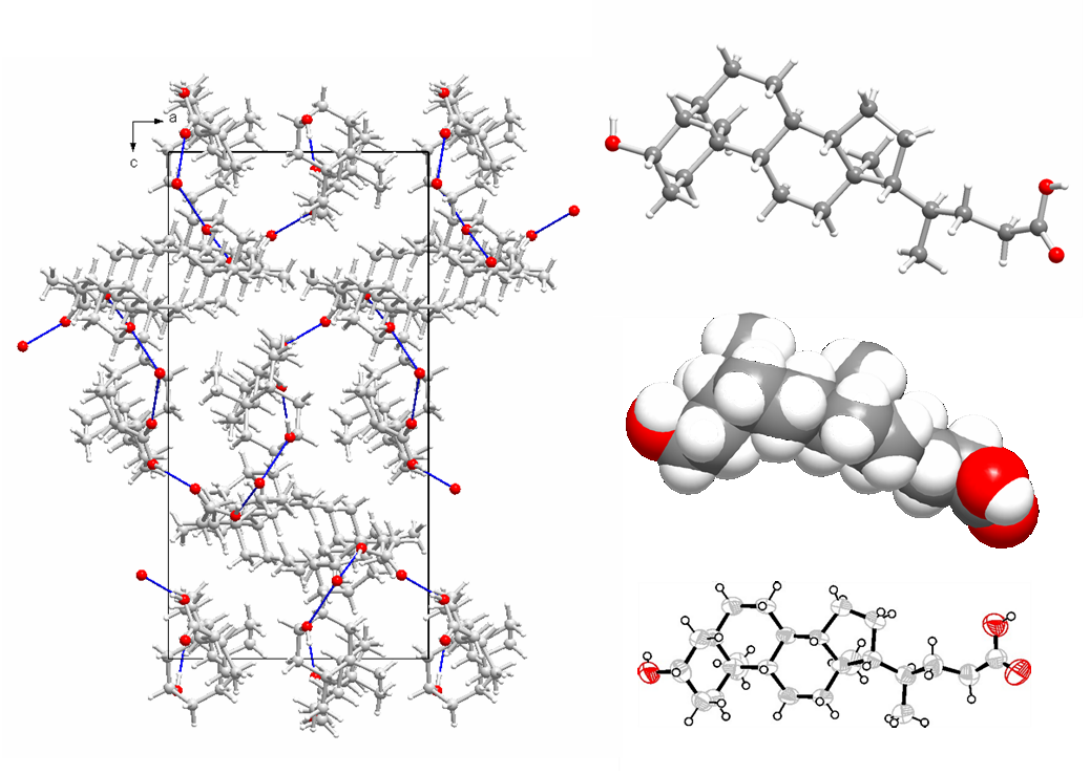

Molecular formula	$C_{24}H_{40}O_3$
Formula weight	376.56
Crystal system	orthorhombic
Space group	P $2_12_12_1$ (no. 19)
Unit cell dimensions	a = 11.939(3) Å b = 16.018(4) Å c = 23.035(6) Å
Volume	4405.10(20) $Å^3$

Figure 67. Crystal data and structure of isolithocholic acid. The hydrogen bonds are labelled with blue lines and the oxygen atoms represented in red.

The ^{1}H-NMR spectra (400 MHz, solvent $CDCl_3$) were obtained for coprostanol, isolithocholic acid and lithocholic acid, and matched the theoretical ones obtained from CS Chem 3DUltra.

10.1.3. Immunogen characterisation

The coupling ratio of the isolithocholic acid – BSA conjugate was characterised by MALDI-TOF/MS. Conjugates with two different coupling ratios had been separately prepared (1:50 and 1:100, mol hapten per mol protein) and afterwards mixed to produce the immunogen (broader distribution of coupling ratios). The first conjugate (1:50) had a coupling ratio interval from 10 to 16 (peak apex 15 mol hapten per 1 mol protein) and the second one (1:100) from 12 to 19 (peak apex 17 mol hapten per 1 mol protein). The MALDI-TOF/MS spectrum of the first conjugate is presented in Figure 68, together with a spectrum of native BSA, to serve as a reference.

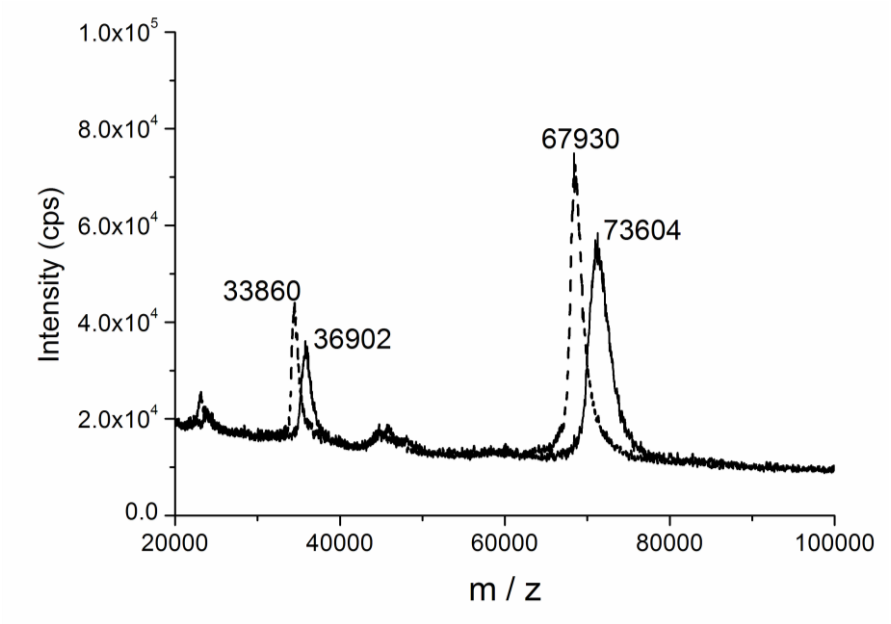

Figure 68. MALDI-TOF/MS spectra of unconjugated BSA and BSA conjugated with isolithocholic acid: average coupling ratio 15.0 mol isolithocholic acid/ 1 mol BSA (coupling range 9.8 – 15.7).

10.1.4. Immunization monitoring

i. Sera

Given that BSA was used as carrier protein in the immunogen, it should be included in the sera dilution and HRP-conjugate (tracer) buffers. Otherwise the anti-BSA antibodies in the sera will produce such a high background that will camouflage the anti-hapten specific IgG, if presented in the sera. Anti-BSA antibodies were detected in all sera from the very beginning, mainly from the 2nd boost onwards (not tested for the 1st boost). When a microtitre plate was coated with 1% (w/v) of different protein solutions (200 µL, o/n), in carbonate buffer pH 8.9, the highest

signals were observed for the wells coated with BSA (Figure 66). The immunized mice sera showed significantly higher signals for BSA than for ovalbumin, which shares some epitopes with BSA. No signal was observed for the pre-immunization serum when the wells where coated with the BSA solution, showing that the anti-BSA antibodies are a results of the immunization.

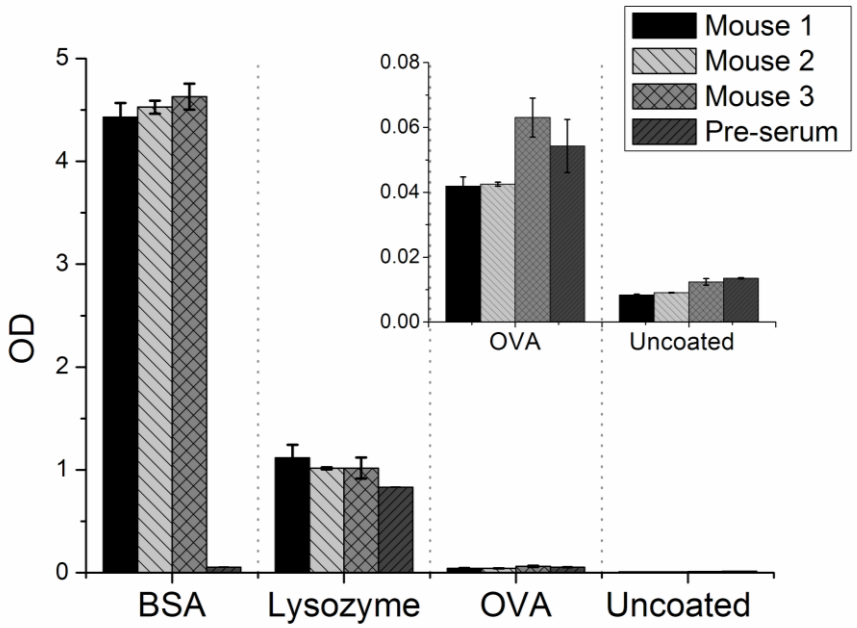

Figure 69. Signals (OD) obtained for a microtitre plate coated with three protein solutions: bovine serum albumin (BSA) 1% in carbonate buffer pH 8.9, lysosyme 1% in carbonate buffer pH 8.9 and ovalbumin (OVA) in carbonate buffer pH 8.9. Several well were left uncoated (only Carbonate buffer) to show the background signal. Sera from the three immunized mice (after 2nd boost) and a pre-serum (non-immunized) were tested – 1:10,000 in PBS (200 µL per well) – using three replicates per each protein to be tested. The anti-IgG mouse-HRP conjugate was diluted 1:5000 in PBS buffer and the colour development stopped after 5 min.

The results (Figure 69) show clearly that BSA has to be added into the buffer before checking the sera for anti-hapten specific antibodies. The results obtained with lysozyme might look awkward at a first glance, as even the pre-immunization serum show very high signals. Lysozyme binding is probably due to its presence and role as hydrolase in the immune system: lysozyme is secreted by mononuclear phagocytes (macrophages) to hydrolyse the glycosidic bond between N-acetylmuramic acid and N-acetylglusosamine in peptidoglycans present in the cell membranes of pathogenic agents. It has a wide distribution in mammals' biological fluids and tissues (e.g. tears, saliva, milk, mucus, egg white, blood), which possibly explains the signals with the pre-immunized serum.

An alternative explanation could be its closeness in sequence and structure to another albumin: alpha-lactoalbumin. Yet, it is unlikely to explain this binding as OVA, a protein closer related to BSA, did not show any binding.

When supplied with the TMB substrate, lysozyme does not catalyse the oxidation reaction, confirming that no peroxidase-like activity is present.

Lysozyme was consequently excluded as a possible protein to be used in the indirect ELISA and ovalbumin was used instead to produce the conjugate protein-ILA to coat the microtitre plates in indirect assays. Lysozyme could be an interesting protein for monitoring humoral immune response in future immunizations, as some difference between the pre-immunized serum and the immunized mice sera, though feeble, seems to be present.

No anti-hapten specific IgGs were detected after the first re-immunization (1st boost). Even when using a low dilution of the serum and a very concentrated HRP-conjugate solution (dilution 1:1000-fold for both), no signal was observed in the ELISA test.

After the second re-immunization (2nd boost), three months after the start of the immunization, the presence of anti-hapten antibodies was revealed by direct ELISA in two of the three immunized mice (Figure 70, left-hand graphs). Mouse 2 and Mouse 3 showed similar anti-hapten titres, evidenced by the OD signals, as well as similar C-values, 41 µg/L and 34 µg/L, respectively.

Only after the 3rd boost, which was performed 19 days after the second one and using the soluble immunogen, anti-hapten antibodies were detected in Mouse 1 (A-value = 0.133; C-value = 43 µg/L). For the other mice – Mouse 2 and 3 – the soluble antigen seems to produce similar effects: it increased the titre by about 30% in both cases and no changes were noticed concerning the C-values (50 µg/L and 44 µg/L, respectively).

The 4th boost, performed 28 days after the third one, using again the soluble immunogen, showed some differences in the immune response between the mice: Mouse 1 had a remarkable rise of the anti-hapten IgG titre (about 500%) while Mouse 2 showed no changes and Mouse 3 a 50% increase on the titre. The C-values remained practically unchanged from the ones obtained in previous boosts (40 µg/L, 52 µg/L and 70 µg/L, for Mouse 1, 2 and 3, respectively). The apparently higher C-value for Mouse 3 is related to the antibody dilution (1:50,000 for all the

sera tested), producing an A-value of 2.4. When this serum was diluted 1:100 000, to produce a similar A-value to mouse 2, a C-value of 43 µg/L was obtained showing that also for mouse 3 no affinity maturation was observed during the immunization process.

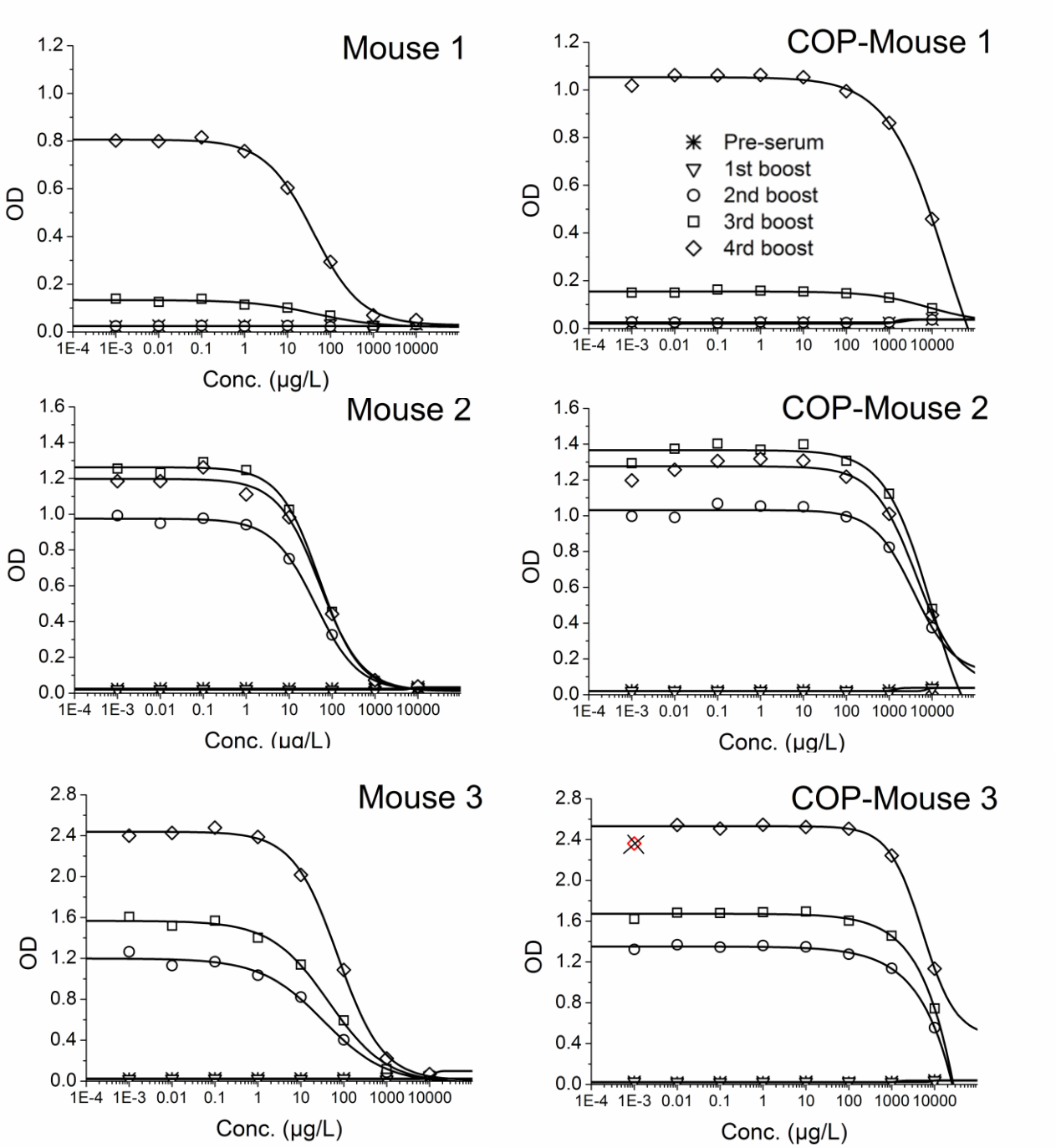

Figure 70. ELISA curves obtained using isolithocholic acid (left) and coprostanol (right) standards. The isolithocholic acid curves were all obtained from the same microtitre plate using sera dilutions 1:50,000. The same sera dilutions were used to obtain the coprostanol curves, all in one microtitre plate.

The pre-immunized serum is represented by a star, the serum collected after the 1st boost by the down-triangle, after the 2nd boost by a circle, after the 3rd by a square and after the 4th by a diamond. The serum from Mouse 1 after the 1st immunization was not included here due to a lack of space on the microtitre plate. Yet, it does not show any differences from the pre-serum, like for mouse 2 and 3. The C- and A-values of the curves are indicated separately in Table 22.

Table 22. Logistic curve parameters: A-value and C-value obtained using several sera and two different standard series: isolithocholic acid and coprostanol. The X indicates no signal on the ELISA test.

Isolithocholic acid (hapten)				
	1st boost	2nd boost	3rd boost	4th boost
C-Value [µg/L]				
Mouse 1	X	X	43	40
Mouse 2	X	41	51	52
Mouse 3	X	34	44	70
A-value (OD)				
Mouse 1	X	X	0.13	0.81
Mouse 2	X	0.98	1.3	1.2
Mouse 3	X	1.2	1.6	2.4
Coprostanol (analyte)				
	1st boost	2nd boost	3rd boost	4th boost
C-Value [µg/L]				
Mouse 1	X	X	7.9E+03	1.3E+04
Mouse 2	X	3.3E+03	5.4E+03	3.8E+03
Mouse 3	X	7.8E+03	8.9E+03	3.2E+03
A-value (OD)				
Mouse 1	X	X	0.2	1.1
Mouse 2	X	1.0	1.4	1.3
Mouse 3	X	1.4	1.7	2.5

When anti-coprostanol (analyte) IgG were assayed in the sera – Figure 70 right-hand side and Table 22 – very similar titres to the ones obtained for anti-isolithocholic acid antibodies were found (similar A-values). The contrary was observed regarding the C-values, which present 100- to 200-fold higher values when coprostanol standards are used. Interesting is the increment observed in the coprostanol C-value when the immunogen is switch from insoluble to soluble (from the 2nd to the 3rd boost) and the apparent decrease afterwards (4th boost) should be regarded carefully as it might just result from the poor fitting of the coprostanol curve. As depicted in Figure 70 (right-hand side), the highest standard used – 10,000 µg/L coprostanol – shows still a considerable higher absorbance and higher standards would have been required to establish a proper comparison between the immunizations. Yet, this was not possible due to the fact that more concentrated

standards contained high percentages of organic solvent (isopropanol), above 10%, leading to poor curves.

Nevertheless, a trend seems to arise from the data: the soluble immunogen improves the affinity towards isolithocholic acid as it decreases affinity towards similar compounds like coprostanol.

Coprostanol seems to bind like a cross-reactant to the anti-isolithocholic acid IgGs rather than binding to specific anti-coprostanol IgGs, which probably were not produced. Or even if they were, the levels of expression were too low to be detected. This hypothesis is supported by the same A-values for both compounds and different ones when the C-value is considered.

To sum up:

No affinity maturation was observed within the immunization process, as shown by the obtained C-values;

The soluble antigen seems to produce a faster growth of antibody-producing B cells in all the mice;

The immune system is different from individual to individual and these results show it clearly: the three mice showed different immune responses towards the same immunogen and immunization plan. Yet, the C-values are very much alike and did not change significantly along the immunization timeframe in none of them.

i.a. Cross-reactivity of the sera

Chemically-related sterols and steroids were also tested for cross-reactivities with the three mice after the 4th boost. The outcome was very alike for the three mice and it is illustrated in Figure 71 using serum from mouse immunized 3 (diluted 1:100,000) as an example.

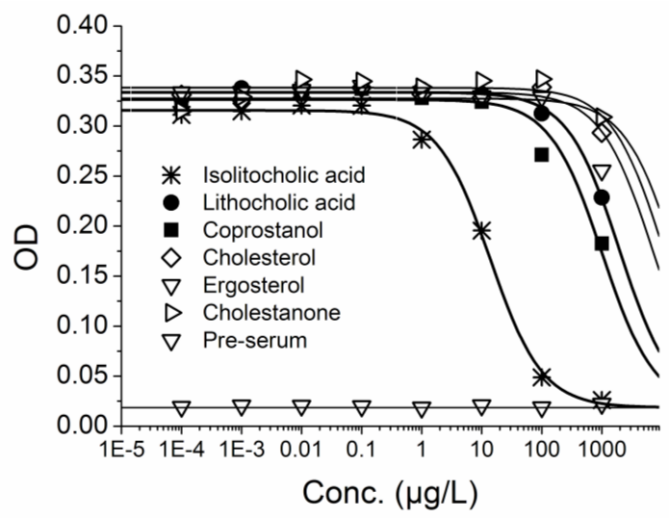

Figure 71. Several sterols and steroids tested for cross-reactivity with the serum from mouse 3 after the 4th boost. All compounds were tested using also the pre-immunized serum and one example (using isolithocholic acid standards) is depicted on the figure. Stigmasterol was also tested (not shown) with similar results to cholesterol.

Coprostanol seems to present the highest cross-reactivity of all the tested compounds, which means that the hydroxyl group position at C3 is of paramount importance for the recognition, as previously hypothesised while selecting the hapten to prepare the immunogen. The curves obtained for lithocholic acid support this conclusion, as the only difference from isolithocholic acid is the position of the hydroxyl in C3, and it has a higher C-value than coprostanol. The other C3-alcohols (cholesterol, stigmasterol and ergosterol) show a very similar outcome: no remarkable inhibition, probably due to the double bond in ring B, which produces a change in the molecule geometry, and therefore on the antibody-antigen binding. The C3-ketone, as expected, does not bind to the antibodies in the sera at all, thus stressing the importance of the hydroxyl group for the antibody recognition.

To sum up:

The hydroxyl group in C3 is crucial for the antibody recognition, including the stereochemistry. The side chain on C17 also seems to play a relevant role as shown by the differences between the isolithocholic acid and the coprostanol recognition.

i.b. Optimisation of the C-value

The lowest C-value at the end of the immunization, after the 4th boost, was obtained using higher dilution of the sera and HRP-conjugate (1:100,000 and 1:1,000,000 respectively) and increasing the incubation time of the sera to 3h30min while reducing the HRP-conjugate incubation time to 20 min. The lowest C-values obtained were between 1 and 10 µg/L isolithocholic acid and an example of such curves is illustrated in Figure 72.

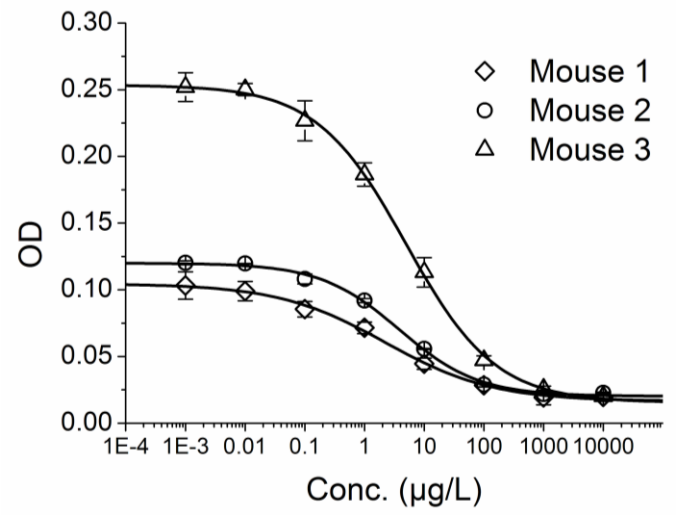

Figure 72. Optimised ELISA using the mice sera after the 4th boost and isolithocholic acid standards (x-axis). The C-values for the represented curves are 2.2 µg/L, 3.8µg/L and 4.9 µg/L, for mouse 1, mouse 2 and mouse 3, respectively.

The seconds bleeds after the 4th boost (54 days after the 1st venipuncture), showed slightly higher C-values for the three mice (5.4; 6.1; 9.1 µg/L for M1, M2 and M3 respectively) when analysed side-by-side with the first bleed of this boost (curves displayed in Figure 72). The A-values were about the same except for mouse 1, which in the second bleeding had a rather higher one, A = 0.14. This shows that the affinity and the titre do not seem to change significantly 59 days after boosting the animals with the immunogen and also that immunity status is kept for an extended time. The animals were just boosted once more (5th boost) shortly before proceeding to the splenectomy and subsequent fusion of the B-cell with the myeloma cell line.

ii. Faeces

During this immunization, it was shown for the first time that faeces can be used to monitor the immunization course as a trustworthy alternative to serum samples.

This represents a major breakthrough in laboratory animals' welfare as in future immunizations no venipuncture would be needed. Faeces samples can be collected

and used for the testing, leaving the animals untouched during the whole process. The most common venipuncture in mice is performed in the tail vein or in the orbital sinus, leading very often to tail loss and blindness, respectively. Faeces are much easier to obtain and the extraction method here described is simple and cost-effective, thus offering an alternative to blood collection.

This presence of anti-hapten specific antibodies in the faeces was observed in the last part of the immunization after a fortuity laboratory mistake while extracting faeces for LC-MS/MS measurements of cholesterol and coprostanol levels. The faeces were extracted with Milli-Q water instead of the organic solvent – of no use for LC-MS/MS measurements. These water extracts were not rejected but checked alongside with sera in an ELISA plate. Similar curves to the ones with sera were obtained. Two colleagues, performing immunizations to produce antibodies against ochratoxin A (OTA) and triacetone triperoxide (TATP)[332] – observed afterwards the same outcome. The detailed results will be published soon[333] and here a short overview is given.

The faeces extracts provided similar inhibition curves, i.e. comparable shapes and C-values, to the ones obtained with the immunized mice sera as illustrated by Figure 73. The faeces curve depicts results from a mixed faeces sample of the three animals; the displayed serum curve originates from one single mouse since no significant differences were found between the animals except for the antibody titre. Besides, the animals were kept together in a single cage from the beginning of the immunization making it difficult to collect the faeces of the individual mice. Yet, the two colleagues running the OTA and TATP immunizations showed that no differences existed between the faeces and the serum from each single mouse, caged separately from the others.[333]

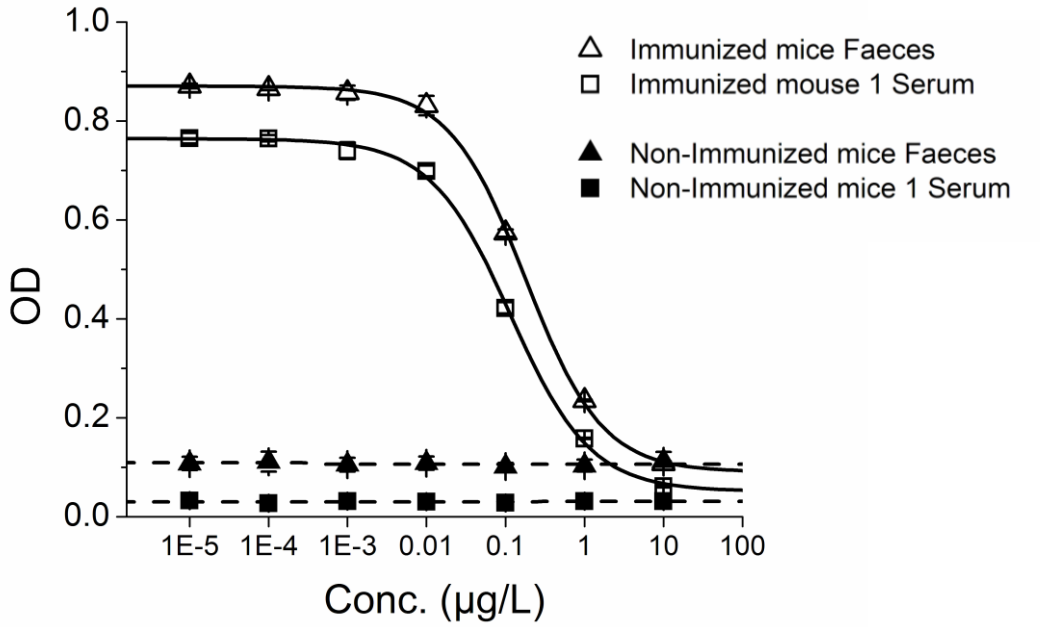

Figure 73. Calibration curves obtained using mice sera (squares) and faeces (triangles) from immunized (open shapes) and non-immunized mice (solid shapes). The solid lines represent the calibration curves: C-value = 0.17 µg/L (faeces) and 0.12 µg/L (serum). Isolithocholic acid standards were used (x-axis).

When faeces from TATP and progesterone immunized mice were tested with isolithocholic acid standards no inhibition was observed, providing extra confidence about the presence of anti-hapten specific antibodies in the faeces.

A question arose during the experiments regarding the class of immunoglobulins present in the faeces. It is well known that the gut secrets high amounts of immunoglobulin A (IgA)[334,335] but when an anti-IgA coating antibody was used for testing the faeces, no inhibition was observed. Thus, the class of immunoglobulin is most likely IgG, which has been previously reported to be present in the faeces.[336,337] Whether these IgGs originate from the general immune system or from the gut local immune system remains unclear. The gut immune system operates rather independently from the general immune system, responding to pathogenic invasions locally.[338,339] As the immunization was carried out intraperitoneally it is unlikely, but not impossible, that a local production of IgG took place. Some new trends in vaccination include colon-immunization to achieve systemic protection against certain antigens[340] showing that an IgG pathway linking the two immune systems exists.[339,341]

Additional data were obtained by comparing two coating antibodies: an anti-IgG whole molecule (H&L), i.e. a secondary antibody that recognises epitopes in the heavy or in the light chain, with an anti-IgG F(c), an antibody that binds the mouse antibodies via their F_c region. The results from the sera and the faeces were different: higher titres were obtained when the anti-IgG whole molecule was used in the case of the faeces while for the sera the anti-F(c) provide the highest signal, as illustrated in Figure 74.

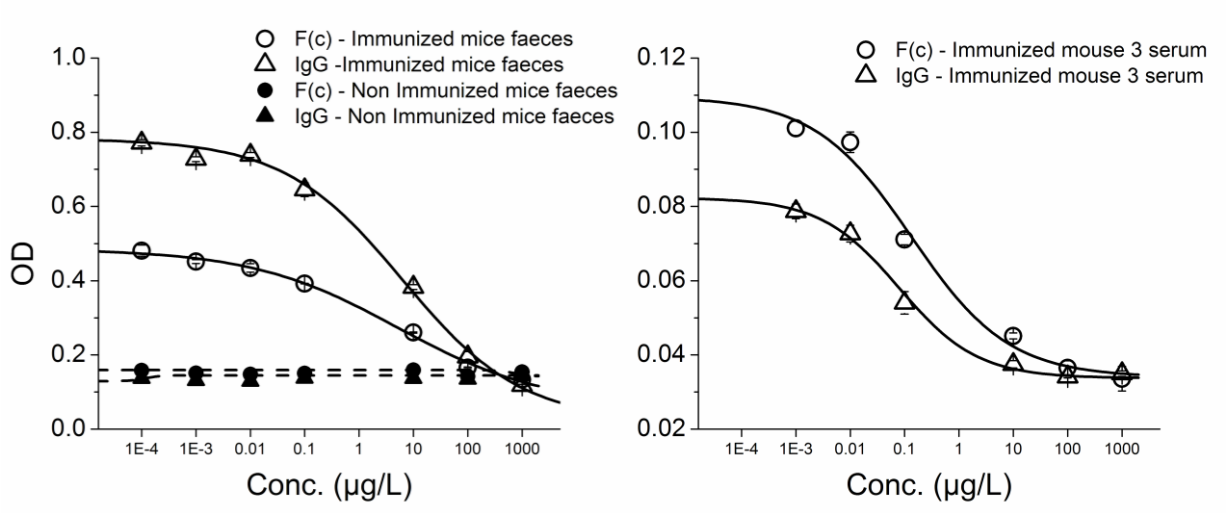

Figure 74. Calibration curves obtained using the hapten isolithocholic acid. The comparison between two coating antibodies is shown: Anti-mouse IgG, H&L, "whole molecule" (triangles) and anti-mouse IgG F(c) (circles). The open shapes represent immunized animals and the solid shapes non-immunized ones. Left: faeces extracts; right: mouse serum.

Presumably, the IgGs present in the serum and in the faeces have some differences, otherwise the binding to the coating antibodies should observe the same trends. Either they have indeed a different origin or the shuttle mechanism[342] between the intestine and the systemic circulation produces some changes on the constant region of the IgGs (F(c)), like different glycosylations of the peptide chain for example. The question is still to be answered as the shuttle mechanism is not yet well understood, remaining a topic for immunologists,[341,343-345] and some research about the FcRn receptor (the MHC-class I-like neonatal Fc receptor) is still to be done. Thought it seems clear that the FcRn receptor plays a role in transporting circulating IgG throughout the intestine endothelium (transcytosis) as well as backwards, recycling IgG and IgG-antigen complexes.[337,346] Indeed the FcRn receptor is a key homeostatic regulator for IgG controlling its transport

(bidirectional) across several epithelial barriers in mammals to affect both systemic and mucosal immunity.[335-337,339]

To sum up:

Aqueous extracts of mouse faeces provide similar results to the ones obtained from serum samples, except for the absolute IgG titre which is considerably lower in the faeces extracts.

No selective IgA was found in the animal faeces.

The tracking of the immune response of mice is a very frequent task in both immunology and immunochemistry, and the novel approach represents a considerable progress as it permits early and frequent testing for the development of specific antibody titre in several animals immunized in parallel.

For future studies, optimised storage and extraction protocols should be developed together with strategies for sampling in groups of mice. Yet, collecting faeces instead of sampling blood allows for a daily monitoring of the immunization progress in mice without hurting or even touching the animals.

In the 3R concept (replacement, reduction, refinement) of animal protection,[347,348] this represents a "refinement" with the potential to improve laboratory animal welfare considerably.

iii. Sterol and stanol levels *in vivo*

Because affinity maturation did not seem to occur all along this immunization, as described in immunology textbooks,[196,202] some explanations had to be advanced and tested. The most logical one is related with the cholesterol metabolism itself: what happens if an animal is producing an antibody against an endogenous molecule such as a bile acid? Could this immunization have produced something similar to an autoimmune disease? And if that molecule is a metabolite of cholesterol, will not the organism try to compensate that disequilibrium in order to replace the lipid balance?

Cholesterol is a vital molecule for life, playing important physiological roles starting at very basic functions like cells membranes support. Its metabolism is very complex and it is down- and up-regulated by several tissues and organs being the liver a major player in the process.[349] Cholesterol is converted to cholic acid in the

liver of mammals, which is further converted into isolithocholic acid (ILA) by bacteria in the gut.[330,350]

If anti-ILA IgGs are present in the serum, then it is likely that higher amounts of (serum) cholesterol will be deviated into this pathway so to replace physiological levels of isolithocholic acid, meanwhile depleted by the anti-ILA IgG. To test this hypothesis, the (free) cholesterol level in the serum was measured in 17 sera from ILA-immunized mice and 17 sera from mice immunized with a non-endogenous molecule (TATP – triacetone triperoxide). The results are displayed as a box-plot in Figure 75.

Cholesterol concentrations' averages are significantly different between the two groups (one-way ANOVA, at 0.05 confidence level) while no significant differences exist between the two groups variances.

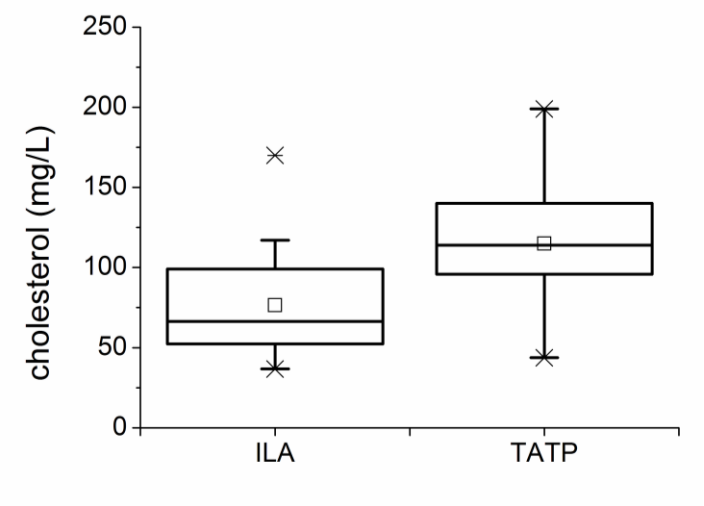

Figure 75. Box-plot showing the distribution of free cholesterol in two groups of mice sera: one immunized with an ILA (isolithocholic acid)-BSA conjugate and another immunized with a TATP (triacetone triperoxide)-BSA conjugate. Seventeen sera were analysed per group.

Even though a difference in cholesterol concentrations unequivocally exists between the two groups, it cannot be attributed to the ILA immunization as the experiments were not performed under controlled conditions.

Several reasons could have contributed for these differences: 1) the two immunizations were carried out in different labs, with different animals and different diets; 2) The glucose values were not measured in the sera samples; 3) The time when the blood was collected as well as the time (and amounts) of the last feeding should have been registered. Since the experiment was not planned this data is

missing and therefore the results should be regarded with some care. In any case, they were too interesting to be omitted here.

What is more, a decrease of free-cholesterol concentrations in sera was observed between the first and the fourth boost in all the ILA-immunized mice. Mouse one presented a reduction of 15%, mouse two 32% and mouse three 96%. It can be an effect related to the immunization or not – last time the animals ate, the moment of the bleedings. Anyhow, if these percentages of cholesterol reduction are correlated with the respective maximal OD obtained by ELISA after the 4th immunization (0.992, 1.185 and 2.4, respectively) – rough amount of anti-ILA IgGs in the sera – a coefficient of correlation of 0.995 is obtained.

The faeces of the mice also show interesting upshots. Animals immunized with the ILA-BSA conjugate show higher coprostanol concentrations in their faeces (by 3-fold) then in both, non-immunized animals and a mouse immunized with a progesterone conjugate. The faecal cholesterol on the other hand seems to be only slightly reduced in those ILA-immunized mice (to 80%). Consequently the ratio cholesterol/coprostanol show significant differences between the immunized animals and non-immunized animals – Figure 76.

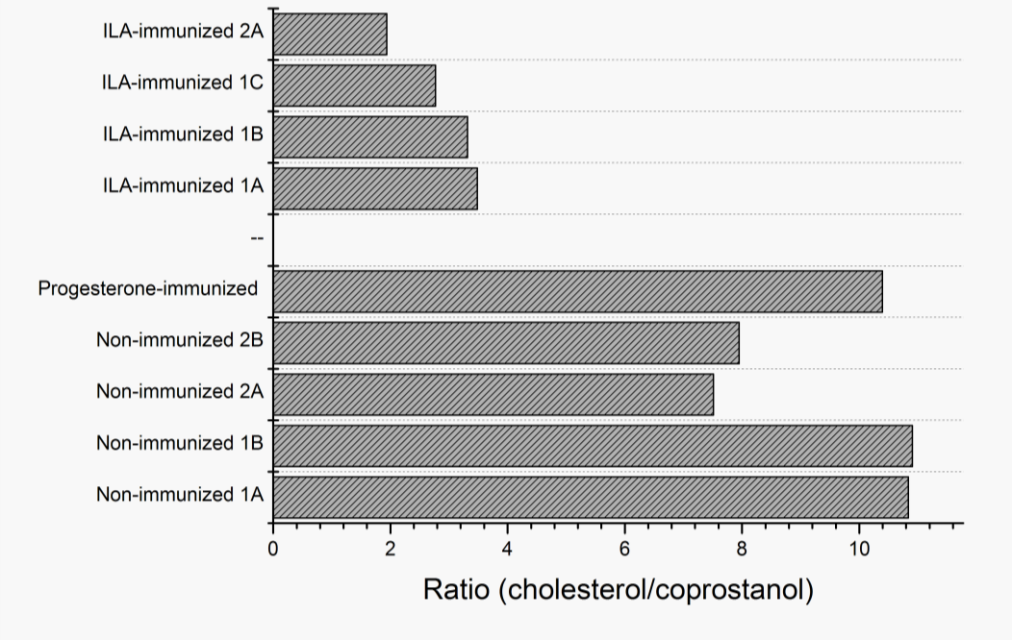

Figure 76. Ratio cholesterol/coprostanol concentrations in mice faeces extracts. The mice immunized with isolithocholic acid (ILA) are represented on the top: 2A – second faeces collection; 1C, 1B, 1C – first faeces collection but extracted independently and on different days. The extracts from non-immunized mice as well as a progesterone immunized mice are represented on the lower part of the graph: 1A, 1B – first faeces collection, extracted independently and on different days; 2A, 2B – second faeces collection extracted independently.

If cholesterol is being displaced from the blood stream into the liver, to compensate a bile acid depletion, then it is also likely that the level of its metabolite coprostanol will be increased in the faeces. The coprostanol concentrations in immunized mice faeces were between 650 µg/g and 800 µg/g while in non-immunized faces they lay in the interval 200 µg/g to 300 µg/g.

After splenectomy of mouse 2, the one used to produce the hybridoma cell line, a strange anatomic aspect was also observed: the spleen was over-sized (according to Hybrotec staff) and its size was not much smaller than the mouse liver! An overproduction of B-cells, caused by constant exposure to a self-antigen (ILA) would explain this spleen oversize.

10.1.5. Hybridoma screening

Screening hybridoma supernatants (HybS) is a very complex, expensive and time-consuming procedure, requiring a considerable workforce. Numerous ELISAs were performed for testing supernatants during the screening process. Herein only the highlights are reported, together with some limitations and technical difficulties encountered during the proceedings.

The very first problem one has to face when screening HybS is their low volume (~100 µL) and the low antibody concentrations in it. This is a major drawback in the beginning as signals (OD) are very low and, on one hand the number of microtitre plates to be tested had to be reduced fast (for logistical reasons), on the other hand the risk of losing the hybridoma producing the right antibody has to be avoided. Therefore, a criterion was established to distinguish between positive clones, possible positive clones and clearly negative ones. Per each microtitre plate containing the supernatant, the OD average and the standard deviation (SD) were calculated and clones with an OD value higher than the average+2*SD were classified as positive. The possible positive clones were the ones with OD equal or above the threshold average+1*SD, and some others which, though not fulfilling this criterion, were also allowed to grow until testing negative in the next supernatant collection.

The second problem was the optimisation of the direct and indirect ELISA for screening of supernatants. The assays were optimised using sera, which is a completely different matrix than supernatants. One good example was the high number supernatants testing (false-)positive but originated from wells where no

living cells were present. Because the sera have a high amount of antibodies and other proteins, the surface of the plate wells is blocked while with supernatants the surface is more exposed and available to non-specific binding of the tracer and thus producing a positive signal. A solution of casein 0.5% (m/v) in PBS was sufficient to overcome this problem but the previous tests with the sera only required a 0.05% concentration to block the well surfaces.

The third and last problem worth a mention was the intermittence of positive/negative results observed for some of the clones, i.e. testing positive for a supernatant at a certain date, negative the next one and again positive thereafter. These clones were mostly passed through until the end of the process.

i. Hybridoma selection

From the 500 tested HybS, 467 (~94%) were discharged (frozen) one month after the cell fusion. Supernatants from the dismissed hybridomas never tested positive, neither in direct nor indirect ELISA, at four different dates: 16, 20, 25 and 30 days after the fusion.

The remaining 33 hybridomas were tested once more (36 days after fusion) and the positive ones (23) expanded in 24-well plates. From that point onwards only the indirect assay was used, because the direct assay showed very feeble signals overall. While some supernatants gave very high signals in the indirect assay (above OD = 1, when the background was only 0.020), no signals were observable in the direct format.

The amplification in 24-well plates provided higher volumes of supernatants (~ 1mL) allowing further tests after the binding/not binding to the ILA-OVA conjugate (positive/negative decision only). These HybS amplifications (23) were ergo tested for:

- binding to ILA-OVA conjugate and ILA-BSA conjugate (immunogen) when the plate was coated with 3.5 µg/mL of each conjugate;
- inhibition by ILA using 3 standards (0, 0.1 and 10 µg/L);
- inhibition by coprostanol (COP) using 3 standards (0, 0.1 and 10 µg/L).

Only 19 HybS tested positive and the results are presented in Figure 77. From that point onwards, a clone was classified as positive if the signal was higher than the one obtained for the negative control (non-immunized mice serum). An inhibition, though using only three standards (0, 0.1 and 10 µg/L), was said to be present if the obtained ELISA curve presented a clear decreasing trend with an ILA or COP concentration increment.

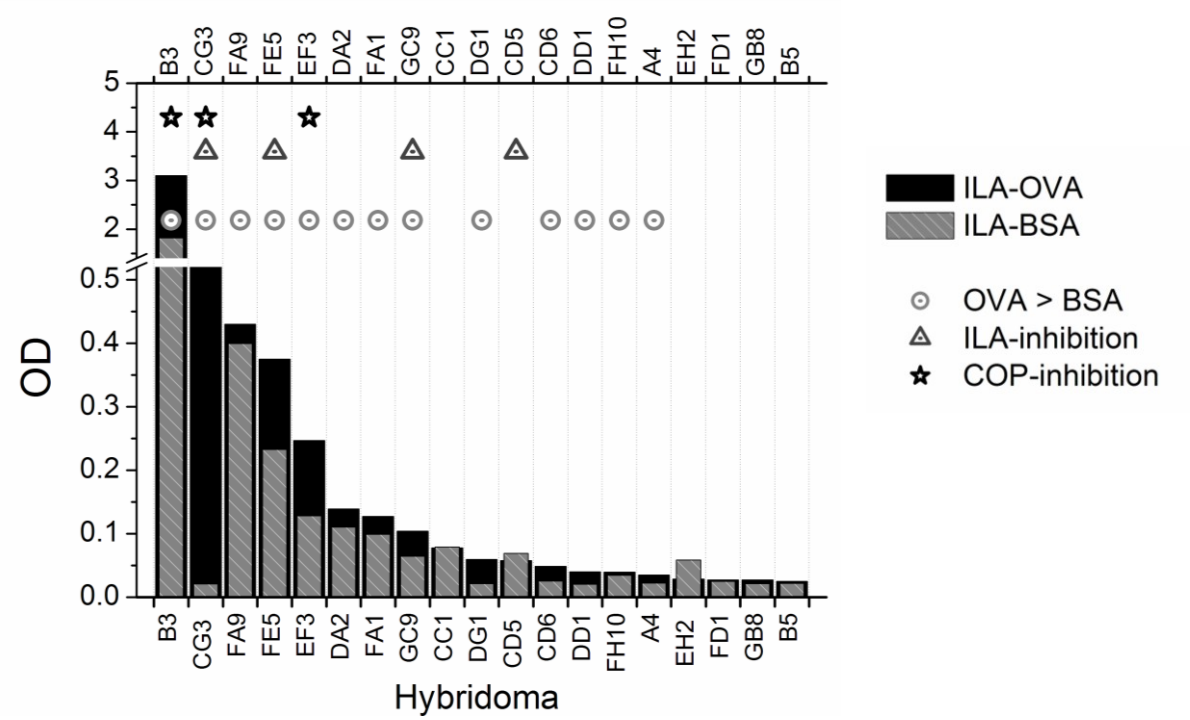

Figure 77. Hybridoma supernatants (HybS) screening after amplification of positive clones in 24-well plates (36 days after the fusion). The hybridoma codes are represented on the x-axis and the bars show the signal (OD) obtained when a microtitre plate row was coated: with the isolithocholic acid-ovalbumin conjugate – ILA-OVA – (black bars) and with the immunogen – ILA-BSA – (striped grey bars). The HybS showing higher signal with ISO-OVA than with ISO-BSA are marked with a grey open circle (OVA>BSA); the ones showing inhibition with isolithocholic acid standards are marked with a dark-grey open triangle (ILA-inhibition) and the supernatants showing inhibition using coprostanol standards indicated by the black stars (COP-inhibition).

Independently of showing or not inhibition, the positive hybridomas were either further amplified – if there were just a few cells inside the wells – or directly recloned in a 96-well plate.

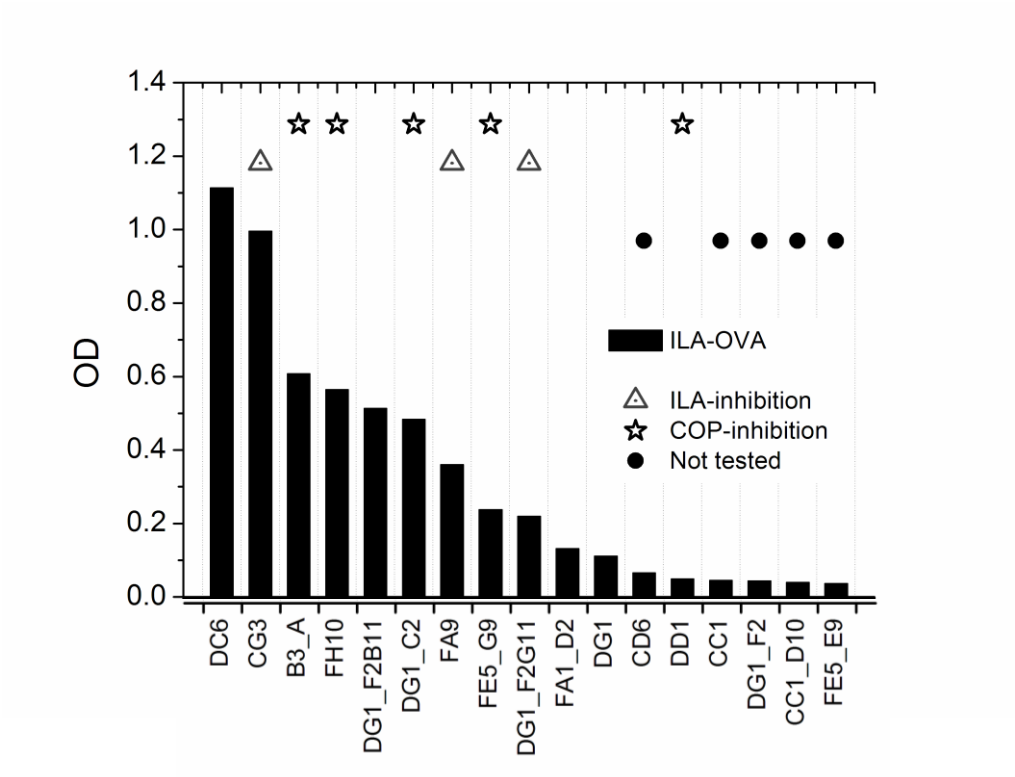

Figure 78. Positive hybridoma supernatants (HybS) after amplification and recloning (marked by a "_" followed by another code) 49 days after fusion. The black bars represent the signal in the indirect ELISA using the ILA-OVA conjugate The supernatants showing inhibition with isolithocholic acid standards are identified by a dark-grey open triangle (ILA-inhibition) and the ones showing inhibition using coprostanol standards signalised by the black stars (COP-inhibition). The black circles identified low-volume supernatant (100µL), thus not tested for inhibition.

The supernatants represented in Figure 78 were also tested using the direct ELISA being the Hyb B3_4 the only one testing positive. Clones showing possible inhibition are displayed in Figure 79.

All positive hybridomas were amplified or recloned and further tested.

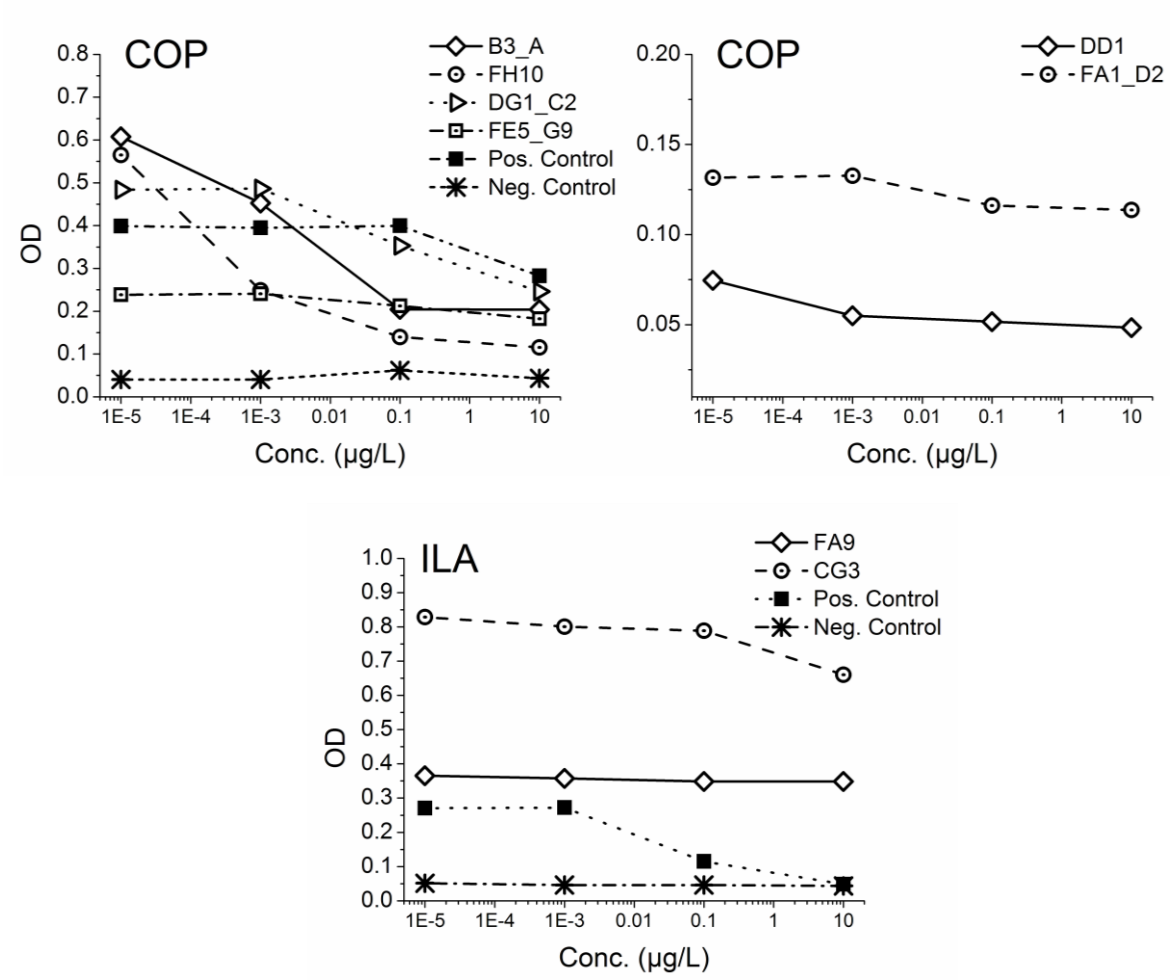

Figure 79. HybS showing possible inhibition using coprostanol (COP) – upper graphs – and using isolithocholic acid (ILA) standards – lower graph. The supernatants were collected 49 days after fusion. The coprostanol data is represented in two graphs because of the differences on the scale.

Some hybridomas showed promising results (B3_A, DG1_C2, FH10) at this point, with even better coprostanol inhibition profiles than the sera itself. After amplification and recloning, 70 days after the fusion, only 5 clones tested positive and only one (B3_A) showed a clear inhibition using coprostanol standards (Figure 80).

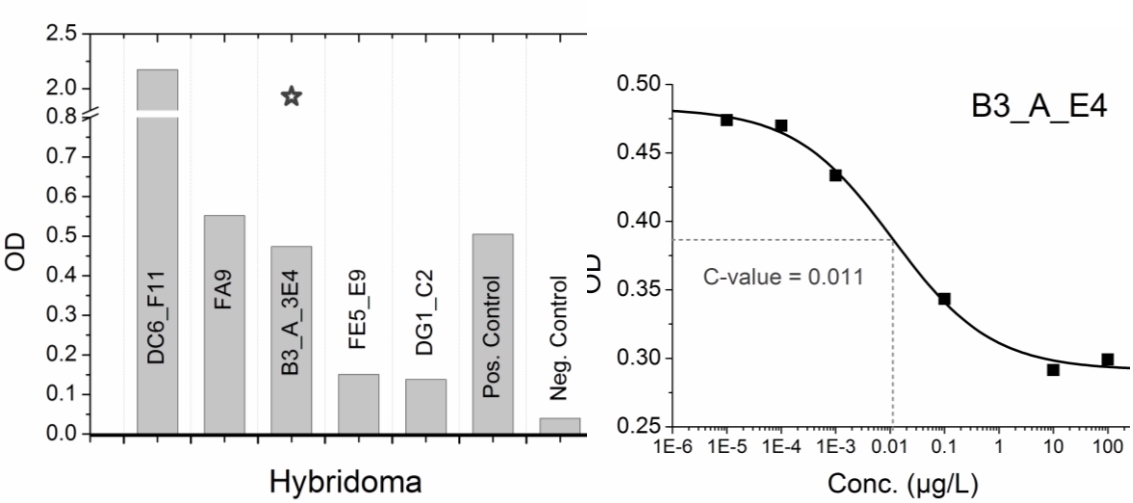

Figure 80. Positive hybridomas 70 days after fusion. Left graph: the signals of the positive hybridomas are indicated by the bars alongside with the positive control (serum from mouse 2) and the negative control (non-immunized mouse serum). The star marks the only clone showing inhibition behaviour using coprostanol standards (B3_A_3EA). Right graph: ELISA curve obtained for clone B3_A_E4 using coprostanol standards.

If only clone B3_A_3E4 shows inhibition, the remaining ones should be binding something else than the analyte. A possibility is that these clones are producing antibodies that bind to some epitopes in OVA, as the plates were coated with the ILA-OVA conjugate. To test that hypothesis, a plate was coated with equal concentrations of OVA, the ILA-OVA conjugate, BSA and the ILA-BSA conjugate (the used immunogen), and the different supernatants tested. The results are summarised in Figure 81 and they show that hybridoma DC6_F11 is producing antibodies which strongly bind to OVA and the ILA-OVA conjugate. This explains why supernatant from this hybridoma tested always positive in the indirect ELISA, from the very beginning of the screening process, with very high signal; and never tested positive on the direct assay (as no OVA is present). Obviously, this HybS could never show inhibition either with ILA or coprostanol. Still, and from Figure 81, one can see that the antibodies secreted from this hybridoma are binding to a rather related epitope OVA/BSA, as it is also binding to BSA. Interesting is the positive control (serum from mouse 2) which does not bind to OVA and shows very high signal for the well coated with BSA, the carrier protein in the immunogen.

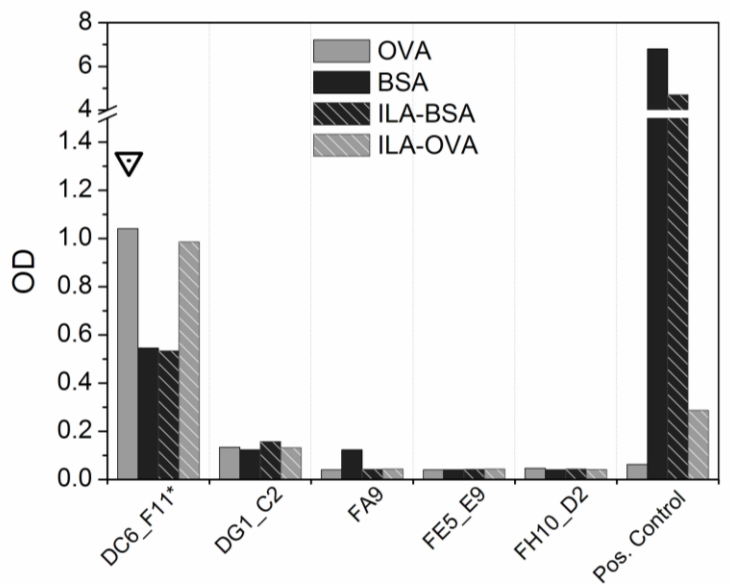

Figure 81. Hybridoma supernatants (70 days after fusion) tested for binding ovalbumin (OVA), bovine serum albumin (BSA) and the respective conjugates with isolithocholic acid (ILA-OVA, ILA-BSA). The ILA-BSA conjugate is the immunogen used to immunize the mouse. The positive control (Pos. Control) was a serum from mouse 2 obtained after the 4th boost. Clone B3_A_3EA was not tested due to insufficient HybS volume. (*) Clone DC6_F11 was tested after dilution 1:5 in PBS buffer. The open triangle indicates that inhibition was observed using OVA and OVA-ILA conjugate.

To determine if an antibody against OVA was about to be obtained, a new supernatant from DC6_F11 was tested on a plate coated with four different concentrations of OVA, ILA-OVA conjugate, BSA and the ILA-BSA conjugate. Here, the higher the concentration of the coating protein/protein conjugate; the higher the signal if anti-protein specific antibodies are present.

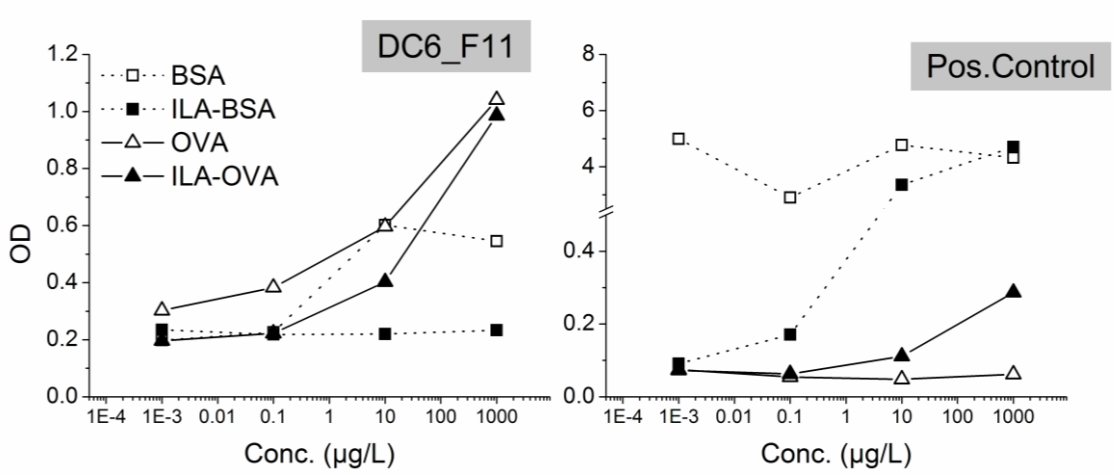

Figure 82. Clone DC6_F11 supernatant (diluted 1:5 in PBS) incubated in a microtitre plate coated with four different concentrations of proteins/protein conjugates: bovine serum albumin (BSA), ovalbumin (OVA) and the respective isolithocholic acid conjugates (ILA-BSA and ILA-OVA). The right-graph represents the same experiment using serum from immunized mouse 2 after 4th boost .

Hybridoma DC6_F11 seems to produce antibodies which recognise OVA (Figure 82). It also binds to the ILA-OVA conjugate, though with lower affinity, probably due to OVA-epitope changes caused by the ILA coupling.

Additionally, the OVA epitope recognised by these antibodies must have some similarities with one in BSA, as this later also shows some binding at the two highest concentrations. The conjugation of BSA with ILA seems to be detrimental for the epitope recognition by the antibody. The serum (positive control) from the killed mouse was also included in Figure 82 to mainly show that it did not bind to OVA even at very high concentration (tested here at 1:10,000).

Remark: The results from BSA with the serum should be regarded with care as the apparent lack of inhibition is the results of a saturation effect. High concentrations of the serum were necessary here to show the non-binding to the native OVA while binding to the ILA-OVA conjugate.

All hybridomas were frozen in liquid nitrogen (77 days after fusion) for a period of one month and plated again in culture afterwards. After one week in culture, the supernatants were tested again and some results were very awkward:

– B3_A_3EA did not show inhibition using coprostanol standards and even the signal was very low (OD ~ 0.1).

Consequently, the former hybridoma line B3_A was allowed to grow and it was again recloned. Three clones tested clearly positive (OD: 1.1; 0.94 and 0.84) – 109 days after the fusion – and were expanded in 24-well plates. None of them showed inhibition and the signals in subsequent tests were very feeble as can be seen in the last test performed 130 days after the fusion (Figure 83).

– The hybridomas FH10 tested alternately positive and negative along the screening process. Some positive clones were at this point positive but once amplified tested always negative when ILA-OVA and ILA-BSA conjugates were used.

– The hybridomas FA9 gave some very high signals (above OD = 1) and once recloned some clones still tested positive for both conjugates ILA-BSA and ILA-

OVA. They never tested positive in the direct ELISA and it was never clear to what they were binding.

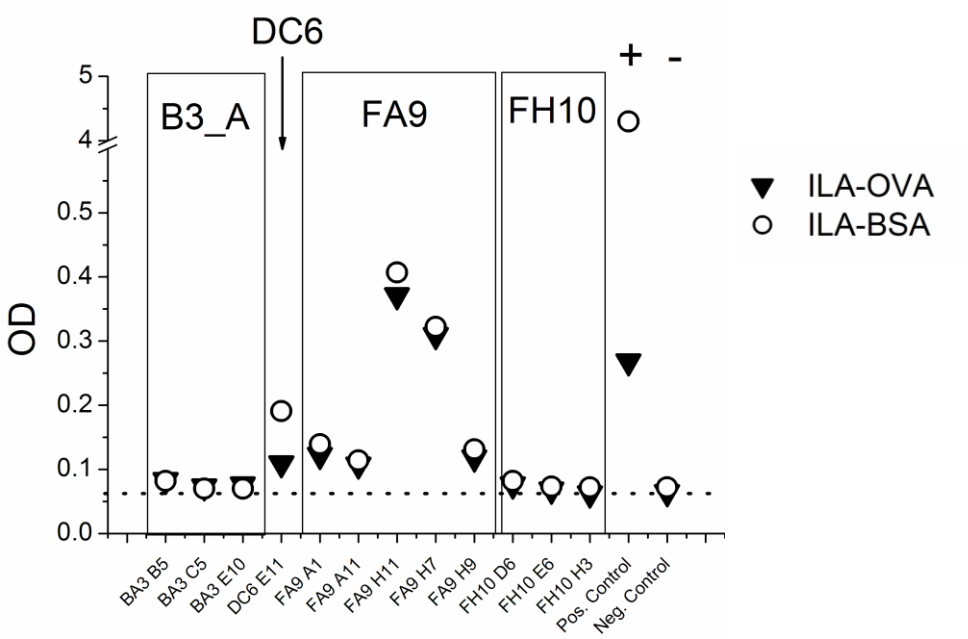

Figure 83. Hybridoma supernatant screening (130 days after the fusion) on a plate coated with represent isolithocholic acid-ovalbumin (ILA-OVA) conjugate – bold triangles; and with the isolithocholic acid-bovine serum albumin (ILA-BSA) conjugate – open circles. The dotted-horizontal line represents the signal obtained with the negative control (non-immunized mouse serum) which is also indicated by a minus; the positive control (immunized mouse 2 serum) is represented by the plus.

Probably the most intriguing Hyb, DC6_E11, which was binding to OVA and showing some inhibition (Figure 82) does not express the same behaviour any longer (Figure 83). Strangely, the signals which were always very high (please refer to Figure 81, where the supernatant was diluted 1:5) are now very feeble even when the supernatant is used without dilution (Figure 83).

It remains also unclear whether the results from Figure 80 were a fruitful coincidence or if something did happen to the secreting hybridoma B3_A_3EA.

10.2. Reference method for sterols, stanols and bile acids

10.2.1. APCI-MS/MS

For a better understanding of the results, an overview of the compounds' structures is again presented.

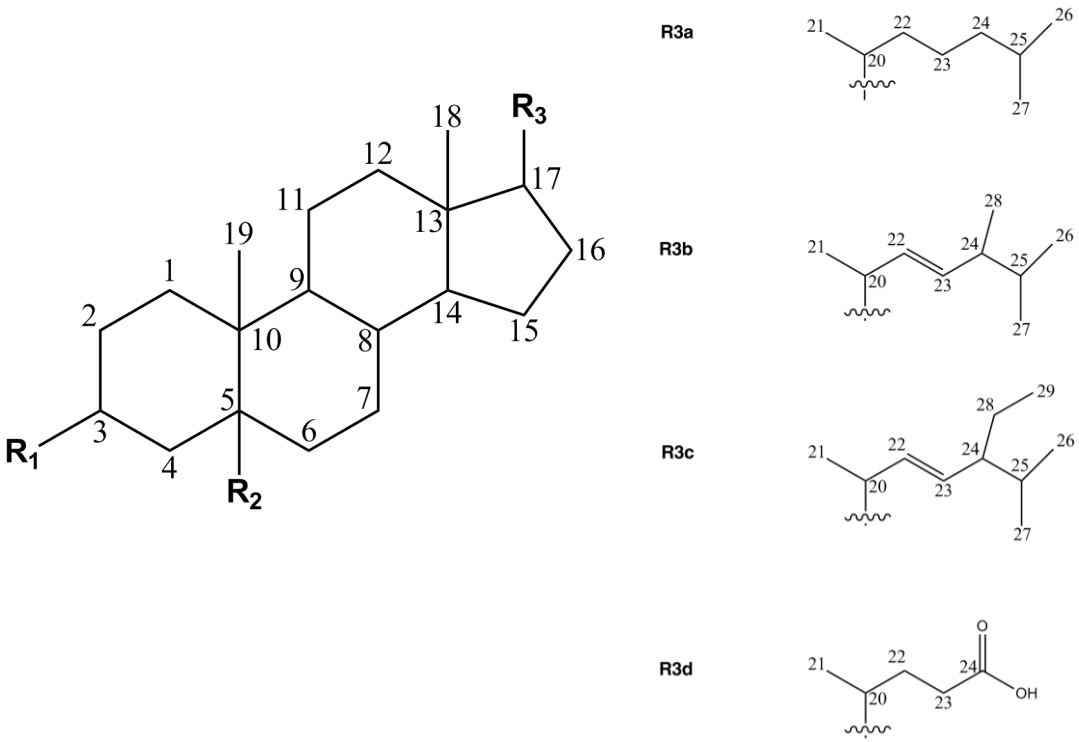

Compound	R1 (C3)	R2 (C5)	R3 (C17)	C-C Double bond(s) position
Coprostanol	β - OH	β - H	β – R3a	-
Cholestanol	α - OH	β - H	β – R3a	-
Cholesterol	β - OH	-	β – R3a	C5 – C6
Ergosterol	β - OH	-	β – R3b	C5 – C6 C7 – C8 C22 – C23
Stigmasterol	β - OH	-	β – R3c	C5 – C6 C22 – C23
Isolithocholic acid	β - OH	β - H	β – R3d	-
Lithocholic acid	α - OH	β - H	β – R3d	-
Cholestanone	O	β - H	β – R3a	-
Cholestan	H	β - H	β – R3a	-

Figure 84. Chemical structures of the sterols, stanols and bile acids under analysis.

i. Scan Spectra

Whatever conditions were used to acquire the spectra (in scan mode), after APCI ionisation, the molecular ion $[M+H]^+$ was never present for all compounds containing the hydroxyl group on C3. Indeed, the pseudomolecular ion present in these spectra is the result of a neutral loss of a molecule of water – $[M-H_2O+H]^+$ – as already reported for steroids,[351] some cholesterol derivatives[352,353] and cholesterol oxidation products.[354,355] The presence of an excess of H^+ ions in the ionisation interface allows the formation of a very stable small molecule and a charged pseudomolecular ion, a typical feature for alcohols ionised under soft ionisation techniques such as APCI.[356]

A coprostanol scan spectrum – Figure 85 – shows the pseudomolecular ion $[M-H_2O+H]^+$ (m/z = 374.1) as the most intense peak. The isotopic mass distribution, given in the insert figure, is in line with the theoretical ones obtained with ChemDraw: 100.0%, 29.2% and 4.1%, from the lowest to the highest m/z. Moreover, the same trend was observed for all the compound analysed except for cholestanone, the scan spectrum of which shows additionally the molecular ion $[M+H]^+$.

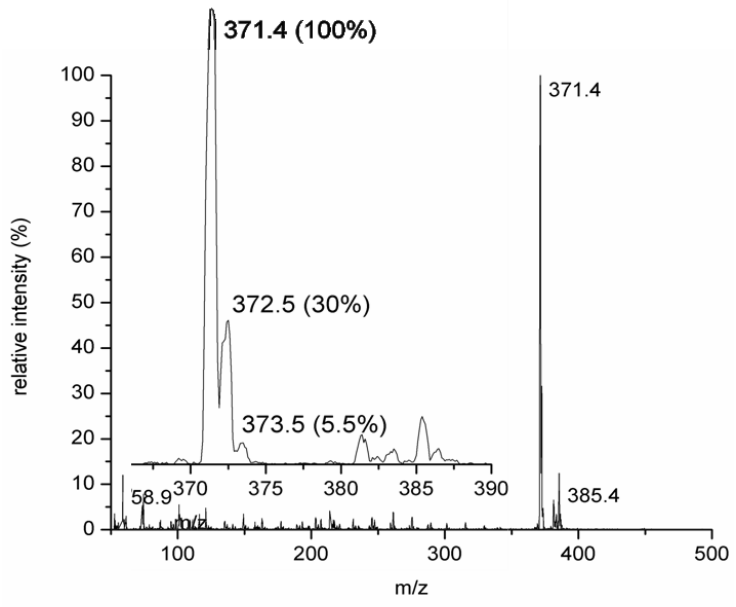

Figure 85. Coprostanol scan obtained after injecting 25 µL of a 1 mg/L standard into the HPLC system. The signal is represented as relative intensity, corresponding 100% to 1.2x10^7 cps (counts per second). The insert picture gives a detailed view of the isotopic mass abundances.

ii. Product scans

The product scans show a high number of fragments when compared to less complex structures as the xanthines, for example. Not surprisingly, the fragmentation pattern is the same for the entire group under analysis, as a direct result of the common cyclopenta[a]phenanthrene skeleton. Slight differences can however be observed on the relative intensity of the different fragment ions, which are the result of small differences in chemical structure.

The most intense fragments encountered in the product scans are included in Table 23 as are the collision energies used to obtain them. Two product scans, coprostanol and isolithocholic acid, are shown to illustrate the pattern of fragmentation obtained for the sterols/stanols and the bile acids (Figure 86).

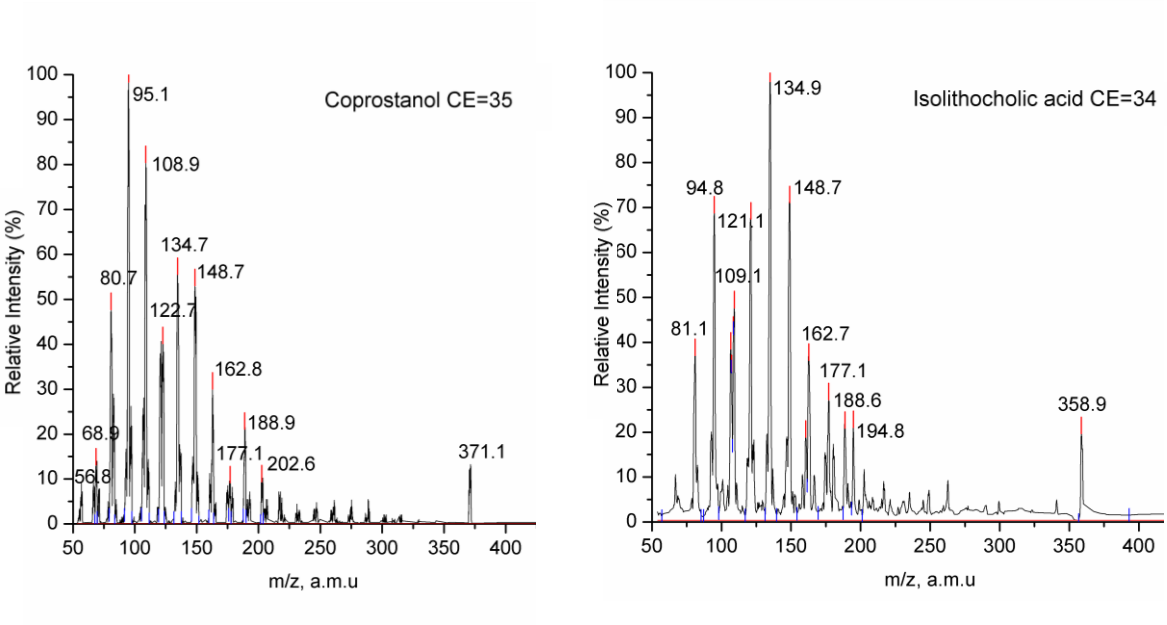

Figure 86. Products scan of m/z 371.1 (coprostanol) and m/z 358.9 (isolithocholic acid) obtained using a collision energy of 35 eV and 34 eV, respectively.

Table 23. Fragments obtained for the sterols, stanols and bile acids after applying the indicated collision energy. The intensity of each fragment is included in brackets and the precursor ion pointed out by the asterisk (*).

Compound (chemical formula)	Exact mass [u]	precursor ion (*m/z*)	Collision energy [eV]	Product ions (*m/z*) with the highest intensities
Coprostanol	388.371	371.4 $[M+H-H_20]^+$	35	95 (100%); 109 (95%); 135 (72%); 81 (68%); 149 (63%); 123 (59%);163 (36%); 371 (28%)*
Cholestanol	388.371	371.4 $[M+H-H_20]^+$	35	95 (100%); 109 (87%); 135 (72%); 149 (59%); 81 (57%); 123 (43%); 163 (31%); 371 (16%)*
Stigmasterol	412.371	395.3 $[M+H-H_20]^+$	42	147 (100%); 83 (97%); 95 (73%); 161 (62%); 109 (61%); 81 (60%); 135 (60%); 187 (52%); 107 (50%); 173 (48%); 69 (47%); 396 (27%)*
Cholesterol	386.355	369.3 $[M+H-H_20]^+$	38	147 (100%); 161 (85%); 95 (78%); 135 (76%); 109 (73%); 81 (48%); 149 (45%); 107 (39%); 121 (37%); 119 (30%); 175 (29%); 123 (27%);369 (16%)*
Cholestanone	386.355	369.4 $[M+H-H_20]^+$	42	95 (100%); 147 (90%); 135 (85%); 109 (82%); 81 (80%); 107 (67%); 121 (57%); 161 (57%); 133 (52%); 105 (48%); 119 (48%); 175 (25%); 369 (12%)*
Cholestanone	386.355	387.5 $[M+H]^+$	32	95 (100%); 369 (97%)*; 109 (84%); 161 (71%); 147 (70%); 123 (60%); 135 (55%); 149 (53%); 121 (42%); 187 (39%); 81 (38%); 175 (35%); 107 (34%); 387 (25%)‡
Ergosterol	396.339	379.4 $[M+H-H_20]^+$	40	69 (100%); 145 (55%); 159 (51%); 95 (42%); 83 (39%); 147 (36%); 133 (32%); 107 (35%); 199 (32%); 109 (29%); 123 (28%); 185 (28%); 121 (24%); 173 (24%); 379 (35%)*
Isolithocholic acid	376.298	359.4 $[M+H-H_20]^+$	35	135 (100%); 149 (57%); 163 (43%); 121 (36%); 95 (29%); 107 (29%); 177 (28%); 109 (24%); 195 (24%); 81 (19%); 359 (18%)*
Lithocholic acid	376.298	359.4 $[M+H-H_20]^+$	34	135 (100%); 149 (78%); 109 (66%); 121 (60%); 95 (48%); 163 (42%); 107 (36%); 189 (36%); 195 (36%); 81 (30%); 177 (29%); 123 (24%); 359 (30%)*

The C17-C20 bond is the primary fragmentation site as illustrated by the solid black line in Figure 87. Several secondary fragmentation sites are represented by dashed lines and identified by a roman numeral, whose resulting ions are described in the table beneath the figure. Fragmentation I, II and IV had been observed by other authors and comprehensively described.[352] Herein, fragmentation IV and III are

additionally suggested leaving however ring A and D fragmentations pattern out of the discussion. In fact, the fragments produced by cleavage between C1-C2/C4-C5 (ring A) and C13-C17/C14-C15 (Ring D) have the same mass (m/z 217) so as the ones resulting from C1-C10/C4-C5 (ring A) and C13-C17/C15-C16 (ring C) – m/z 231.

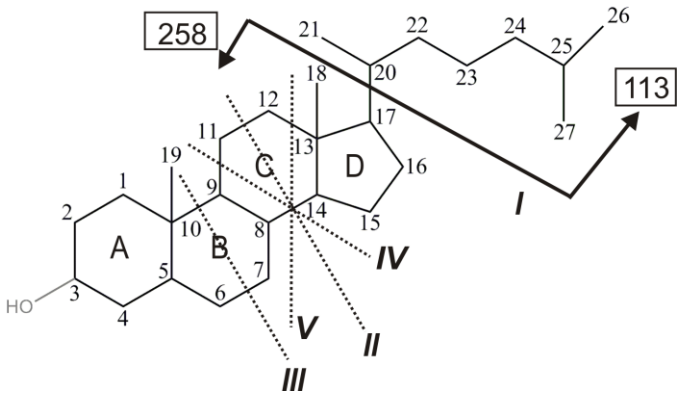

		Coprostanol *Cholestanol* *Isolithocholic acid* *Lithocholic acid*		*Stigmasterol* *Cholesterol*		*Cholestanone*		*Ergosterol*	
	Bonds	Product ion (m/z)	Fragment	Product ion (m/z)	Fragment	Product ion (m/z)	Fragment	Product ion (m/z)	Fragment
II	C11–C12 C8–C14	163	$C_{12}H_{19}$	161	$C_{12}H_{17}$	161	$C_{12}H_{17}$	159	$C_{12}H_{15}$
		95	C_7H_{11}	95	C_7H_{11}	95	C_7H_{11}	95	C_7H_{11}
III	C9–C10 C6–C7	149	$C_{11}H_{17}$	149	$C_{11}H_{17}$	149	$C_{11}H_{17}$	147	$C_{11}H_{15}$
		109	C_8H_{13}	107	C_8H_{11}	107	C_8H_{11}	107	C_8H_{11}
IV	C9–C11 C8–C14	149	$C_{11}H_{17}$	147	$C_{11}H_{15}$	147	$C_{11}H_{15}$	145	$C_{11}H_{13}$
		109	C_8H_{13}	109	C_8H_{13}	109	C_8H_{13}	109	C_8H_{13}
V	C12–C13 C8–C14	177	$C_{13}H_{21}$	175	$C_{13}H_{19}$	175	$C_{13}H_{19}$	173	$C_{13}H_{17}$
		81	$C_{16}H_9$	81	$C_{16}H_9$	81	$C_{16}H_9$	81	$C_{16}H_9$

Figure 87. Fragmentation pattern illustrated using coprostanol as example. The table details the resulting fragments.

Worth to mention is the fact that a small difference within two quasi-consecutive collision energies bring about rather different spectra, mainly vis-à-vis the precursor ion. As illustrated below for isolithocholic acid – Figure 88) – an increment of 2 eV (from 30 to 32 eV) reduces the precursor ion by roughly 65%. Furthermore, a pattern can be observed for the m/z values higher than 175: the higher the collision energy the lower the relative intensity of the ions; being the opposite valid for the lower masses, as one would actually expect.

Exceptional behaviour seems to be the one from the two ions resulting by ring B cleavage, m/z 149 and m/z 109, which show almost no connection between the fragment intensity and the applied collision energy (in the short values range presented in Figure 88)[a].

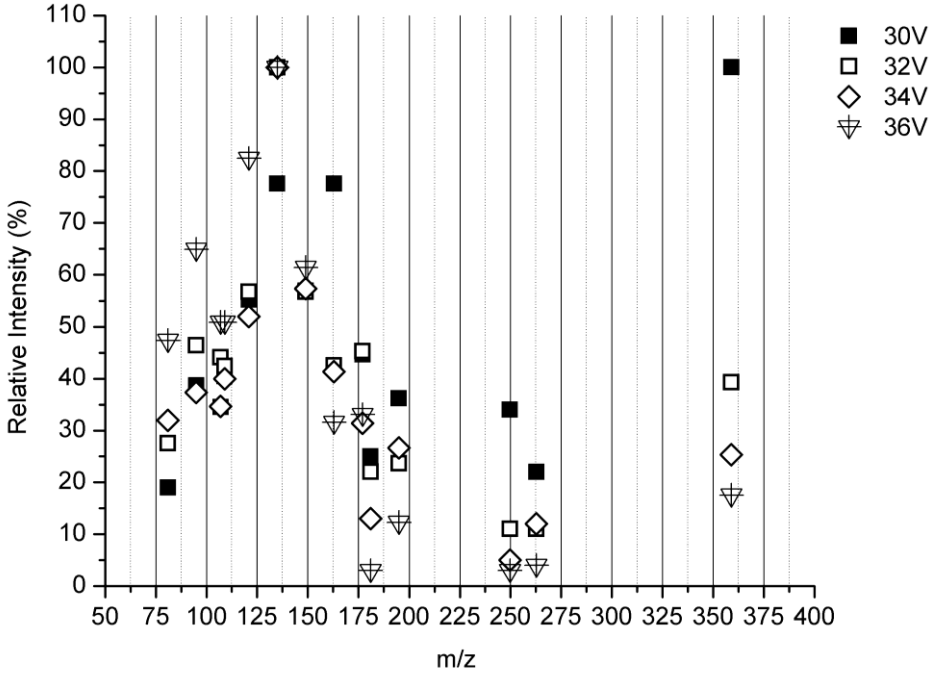

Figure 88. Influence of the collision energy on the relative intensity of the fragments from m/z 359.4 (isolithocholic acid). The values indicated on the top right-hand side of the picture are the collision energies tested.

iii. Multiple reaction monitoring (MRM)

Two MRM transitions were used per compound: one for quantitation (MRM-Q) and a second one as confirmation transition (MRM-C). As a rule, the two most intense transitions were selected for the method except in cases where a less intense transition provides however a better signal-to-noise (S/N) ratio. Some collision energies used for the MRMs are slightly lower than the ones presented in Table 23, to allow a noticeable presence of the precursor ion (relative intensity between 20% and 30%).

[a] *When higher collision energies (CE) were used, the relative intensities of these two fragments do change. The statement is thus just valid for the short CE range presented here.*

iv. MS Parameter optimisation

Nebulizing current (NC), entrance potential (EP), declustering potential (DP), source temperature (T), curtain gas (CUR) and ion source gas (GS) were optimised by acquiring first in Scan mode and thereafter using SIR mode.

The results presented in Figure 89 and Figure 90 were obtained using scan mode, after extracting the correspondent precursor ion for each compound. The obtained peak was automatically integrated using the Analyst Software and the areas normalised to the maximum value (100%) for each compound and for each parameter. As an example, the maximum values for the coprostanol peak areas are the following: NC = $1.27x10^8$; DP = $1.17x10^8$; EP = $1.01x10^8$; T = $1.06x10^8$; CUR = $1.06x10^8$; GS = $8.29x10^7$. As can be observed, only GS maximum presented a somehow lower value and this can be explained by the fact that this parameter was the last being studied, after three days of consecutive injections. Indeed slightly lower signals for this parameter were observed for all the compounds. For comparison purposes, a bar graph was included in Figure 89 (bottom), where the absolute signal is presented for the different ions. All the experiments were performed using a multi-compound standard mixture containing 1 mg/L of each compound.

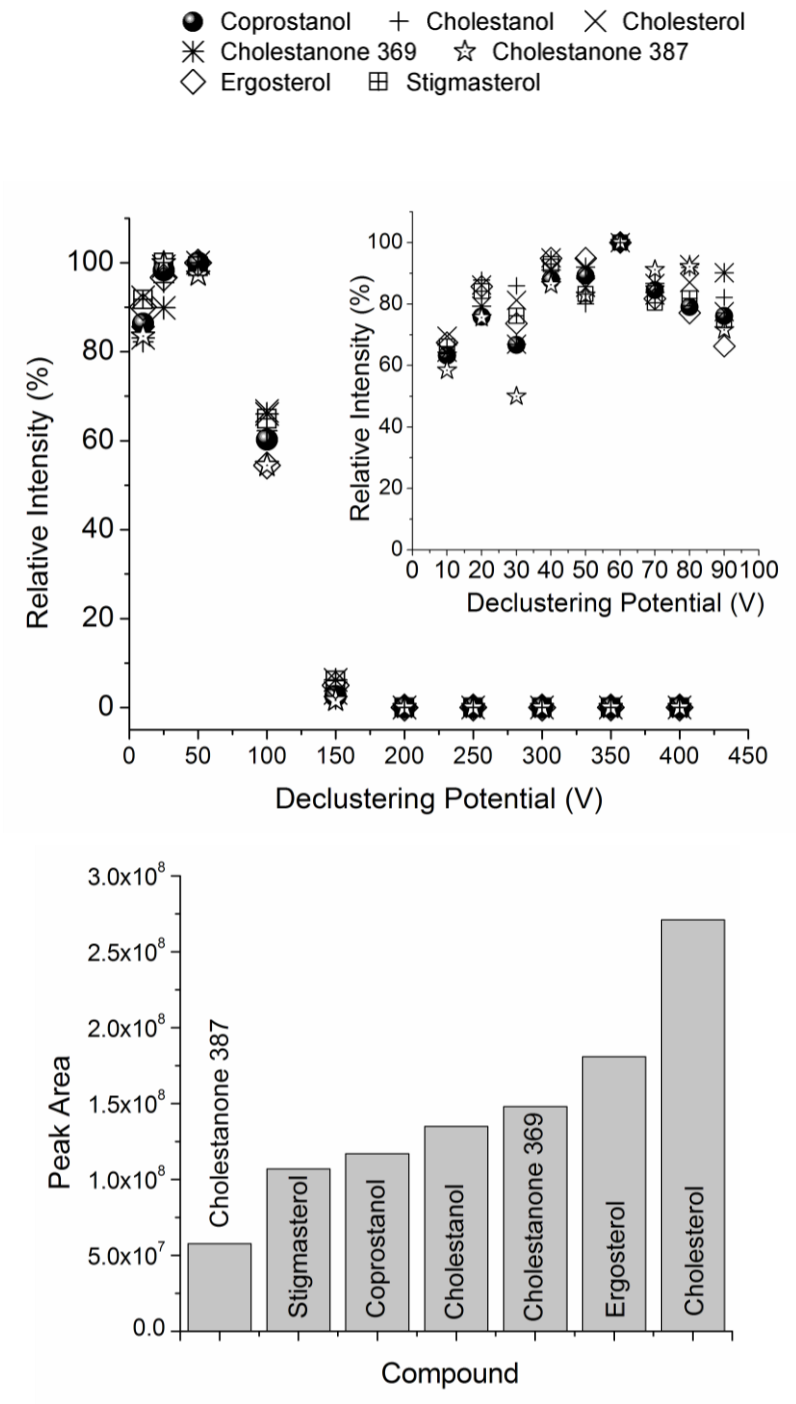

Figure 89. Effect of the declustering potential on the peak areas (top graph). The absolute values corresponding to 100% of the relative intensities for each compound are presented on the graph on the bottom. For further details please refer to the text Seite 208.

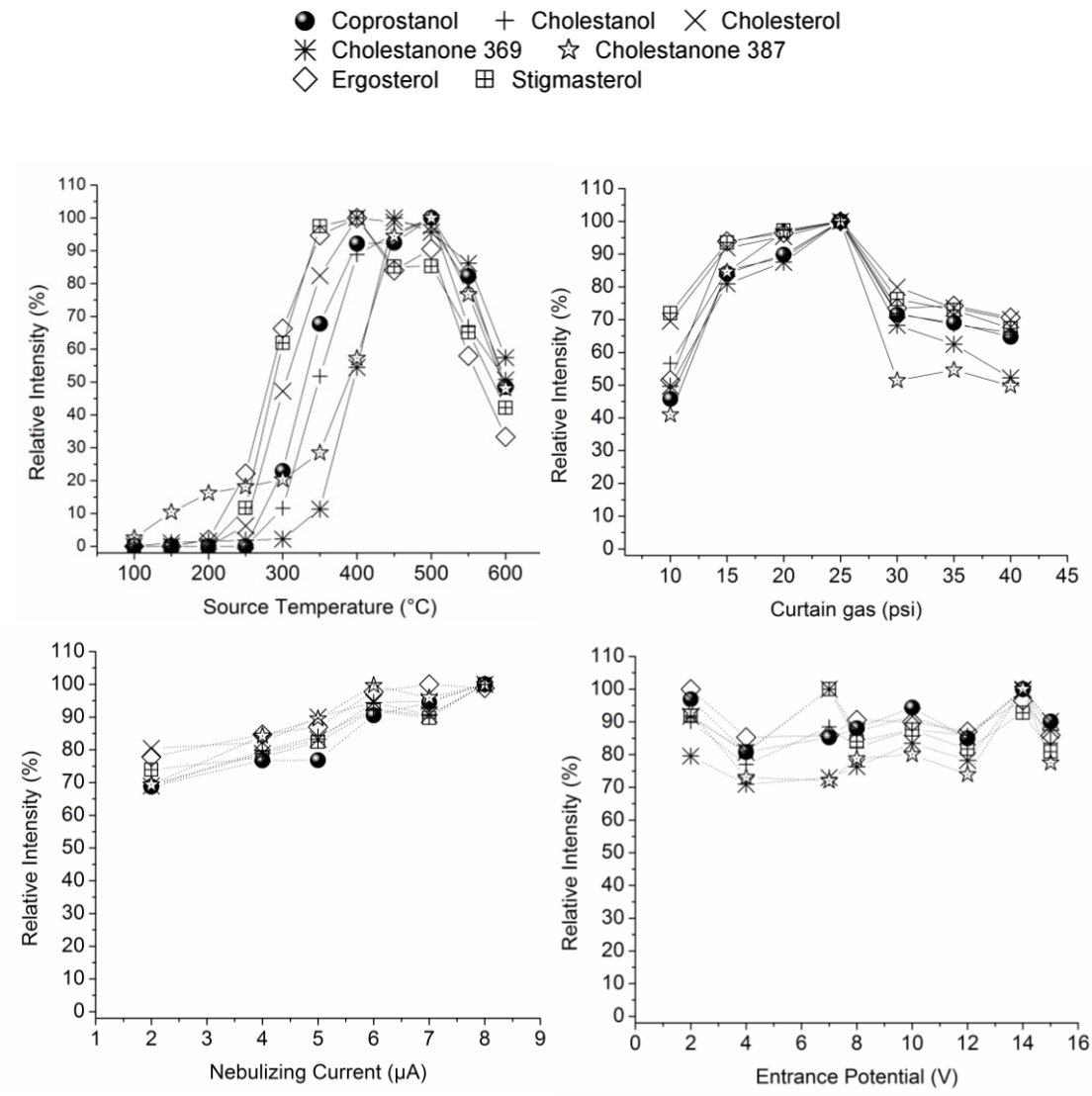

Figure 90. Effect of several parameters on the signal intensity (peak area). Please refer to the text Seite 208 for detailed description about the presented data.

The source temperature has a manifest effect on the signals. Below 200 °C only the cholestanone $[M+H]^+$ ion can be detected and the most favourable temperature for the majority seems to be between 400 and 500 °C.

Alcohols seem to require lower temperatures than the ketone, and among them the ones with the double bound C5-C6 (Stigmasterol, Ergosterol and Cholesterol) need lower temperatures.

Ergosterol and Stigmasterol signals (both compounds have double bounds between C5-C6 and C22-C23) go side-by-side concerning the source temperature, being that the signal of Ergosterol (which has an additional double bond C7-C8) drops

faster when the temperatures overpass the threshold of 500 °C. Both compounds reach the maximum signal at 350 °C while the unsaturated structures, without double bonds, require at least 450 °C. And this temperature appears to be a good compromise for the entire batch analysed.

A little difference can also be noticed between the isomers coprostanol and cholestanol. Higher temperatures are needed for the 3α isomer (Cholestanol) to achieve the same signal as the 3β isomer (coprostanol).

Declustering potentials between 40 and 80 V provide the highest intensities and above 150 V a signal was quasi not observed (Figure 90). The nebulizing current seems to be irrelevant for values higher than 6 µA while the entrance potential experiment shows an unclear outcome. Regarding the curtain gas, the best signal for all the compounds was found to be 25 psi.

10.2.2. Chromatographic separation

i. Column selection

The reversed-phase chromatography was performed using a C18 column SepServ, 100 x 4 mm, 5 µm (hereafter abbreviated SEP) after testing two other columns: UltraSep ES C18 Phen1, 250 mm × 3 mm, 5 µm (hereafter Phen) and a monolithic column 50 mm × 2.0 mm (hereafter Monolithic).

The Phen column provides acceptable separation but longer chromatographic runs than the ones obtained with the SEP column. Additionally the backpressure of the Phen column was considerably high when isopropanol was included in the mobile phase B: at 98% B (methanol:isopropanol, 1:1) the pressure was ~ 205 bar against ~ 135 bar when using methanol alone.

Attempts were made to reduce the viscosity of the mobile phase, thus reducing the overall backpressure, as well as the replacement of the tightly-packed column by a monolithic one. The highly-permeable monolithic structure generates indeed very low back pressure (30 bar for the same gradient used with the Phen, with isopropanol as mobile phase) and very short runs (< 10 min) but did not resolve two consecutive peaks – coprostanol and cholestanol – at the baseline (Resolution = 0.75). Additionally, monolithic columns work optimally using higher flow rates (> 0.5 mL/min) which are known to be detrimental for APCI ionisation, favoured by the lowest flow possible. Keeping the particle size (5 µm) and reducing the column size (by 15 cm) and diameter (by 1 mm) was the encountered solution to reduce the

backpressure, the run and equilibration times, without losing resolution in isomers separation. Hence the SEP column was selected.

ii. Organic phase

Methanol alone could not elute the compounds out of the Phen column. And isopropanol alone does not allow the separation between the isomers coprostanol and cholestanol. A mixture 1:1 (v/v) methanol:isopropanol brought about the best resolution without overlong run times (< 40 min).

When acetonitrile was employed, a good separation was obtained but the peaks widths at half-height were very broad (between 80 s and 95 s) showing its arduousness to displace the compounds from the stationary phase. Cholestanone, the one compound lacking the alcohol group, is however the exception and it shows an acceptable peak width at half-height (32 sec). What is more, the retention times were exceedingly long making the chromatography utterly unfeasible for routine purposes (elution times: coprostanol = 59 min; cholestanol = 89 min; cholesterol = 69 min; cholestanone = 29.4 min). The acetonitrile option could have been further explored but back there when the experiments were conducted, the solvent shortage and high prices led to its replacement by the aforementioned alcohol mixture.

iii. Additives

The chromatographic separation of sterols and stanols was not significantly altered by the additives tested (ammonium acetate, acetic acid and formic acid).

No improvements on separation were observed when the additives were added only to the water phase. But when they were added to the organic phase, minor improvements were observed in the cholestanone/cholesterol resolution, mainly by using a mixture ammonium acetate 5 mM + 0.05% (v/v) acetic acid (Rs Additives = 4.80; Rs without = 4.53). A dissimilar effect was observed for coprostanol/cholestanol, the resolution of which drops slightly from 4.08 to 3.90 when additives are added. For the bile acid, as can be observed in Figure 91, the presence of additives is compulsory, proving the presence of the acid to be advantageous for the separation between the two isomers. Being organic acids themselves, with pKa~4.8, they do need addition of an acid to ensure a mobile phase pH~3, at least (99% of the non-ionised form).

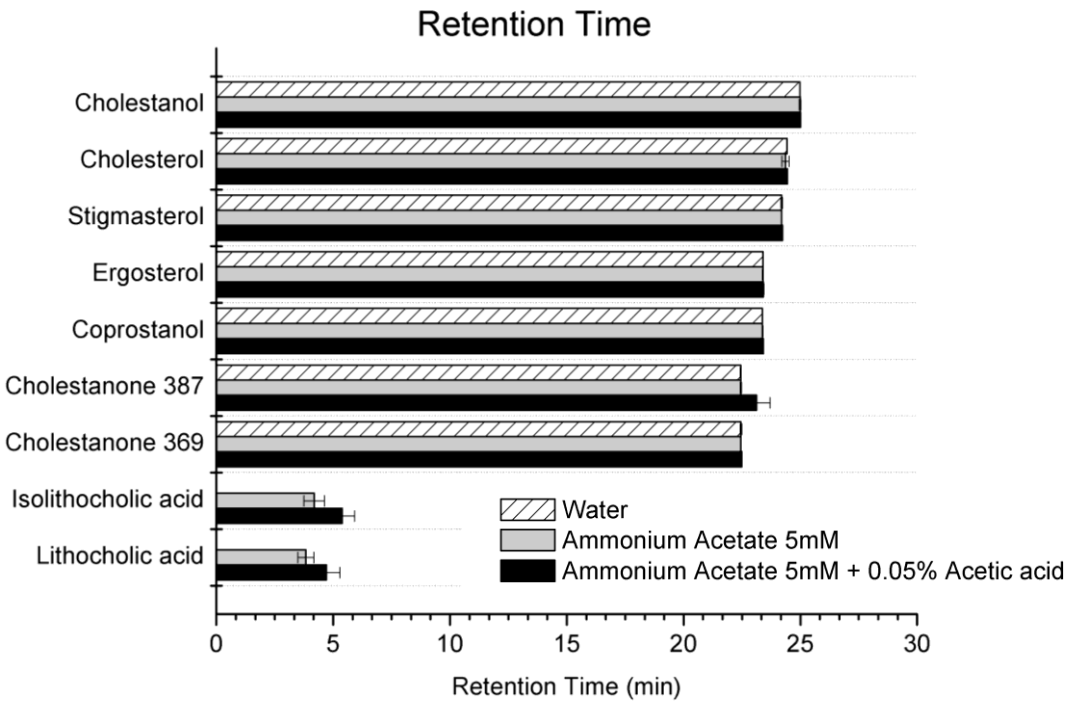

Figure 91. Retention time of the analytes using three different aqueous mobile phases. The retention times are an average value of 5 consecutive injections. All the experiments were carried out on the same day, one after the other, starting with water and ending with the acetic acid mobile phase.

Noteworthy was the unchangeable intensity of the MS signal whether additives are being used or not. Ionisation in positive mode is usually enhanced when proton abundance is provided by additives like ammonium acetate in the mobile phase. This does not apply here and the reason might probably be the low percentage of water in the mobile phase at the compounds' elution time (2%).

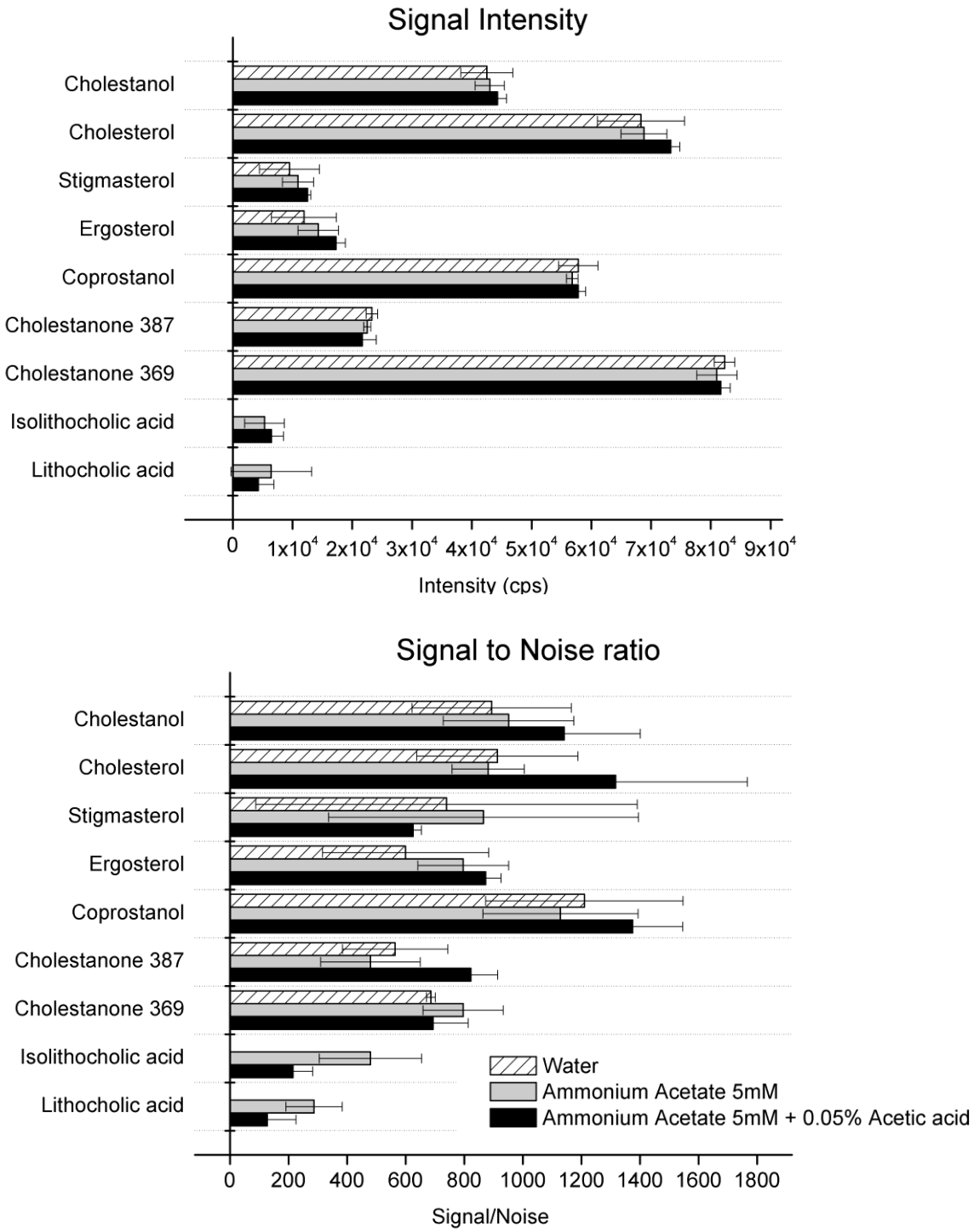

Figure 92. Average signal intensity (in counts per second, cps) variation with the mobile phase composition (top graph). On the bottom the average signal-to-noise ratios obtained for the same injections (n = 5 consecutive injection per mobile phase, 1 mg/L standard, 25 µL injection volume).

Very high standard deviations were observed for the signal-to-noise ratios (n = 5) making it difficult to draw any reliable statement. Nonetheless the variation must be caused by noise variation between the injections as the signal intensity does not show discernible differences (Figure 92). The signal-to-noise ratios were calculated

as depicted in Figure 93: the noise was taken, for all the compounds, between 19.0 and 19.5 minutes while the signal was calculated at the peak apex with a time window of 0.1 minutes.

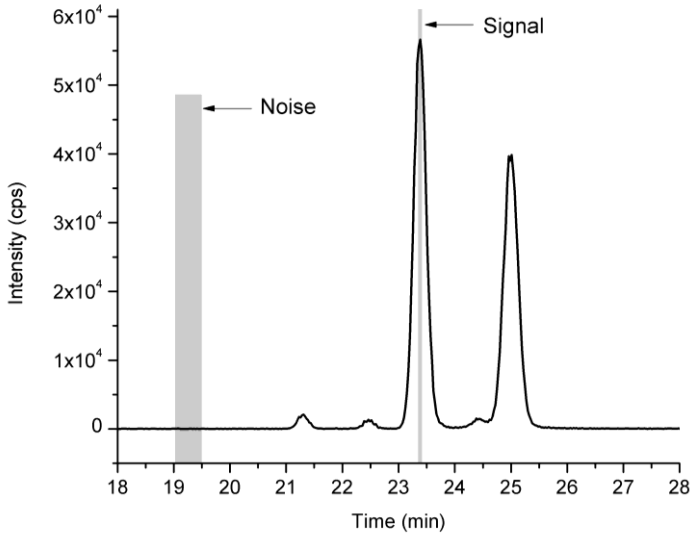

Figure 93. Coprostanol chromatogram showing how the signal and noise were obtained for the calculation of the ratio S/N. The second peak is the isomer cholestanol.

To sum up:

The additives are essential for a successful separation of the bile acids but not for the sterols and stanols.

Neither an improvement nor an inconvenience is attributable to the additive regarding the MS signals. Whenever bile acids are to be quantified, additives should be included in the mobile phase; otherwise, the use of water alone is adequate.

iv. Column temperature

As the column oven temperature increases, the faster the compounds will move throughout the column, thus lessening to some extent the peak resolution. Temperature affects more noticeable the coprostanol/cholestanol resolution than the cholesterol/cholestanone one. The resolution between the first pair of peaks decreases about 22% when the column oven temperature is increased from 50 to 60 °C, whereas cholesterol/cholestanone resolution seems to remain unaffected. Temperatures below 50 °C, mainly at 40 °C, led to high backpressures and too long

analysis time (when using the Phen column). A compromise between resolution and throughput was selected by setting the thermostat to 50 °C.

v. Gradient and flow rate

Two final gradients were established. The first one starting with 80% of the organic mobile phase and with a flow rate set at 0.300 mL/min; and a second gradient starting with 20% of the organic phase at 0.400 mL/min (gradients are described in Table 24). The main advantage of gradient 2 is that it allows a slightly better separation of the bile acids. But as expected, the higher flow rate has a deleterious effect in the APCI signals' intensity, as can be observed in Figure 94 . If sensitivity is at stake for stanols and sterols, then gradient 1 is highly recommended.

Table 24. Gradients used to separate stanol, sterols and bile acids. Mobile phase A is water containing Ammonium acetate 5 mM and 0.05% (v/v) acetic acid; mobile phase B is a 50:50 (v/v) mixture of methanol and isopropanol.

	Gradient 1	Gradient 2
Time [min]	% Mobile phase B	% Mobile phase B
0	80	20
3	80	20
10	80	40
15	98	98
30	98	98
30.1	80	20
40	80	20
Flow [µL/min]	300	400

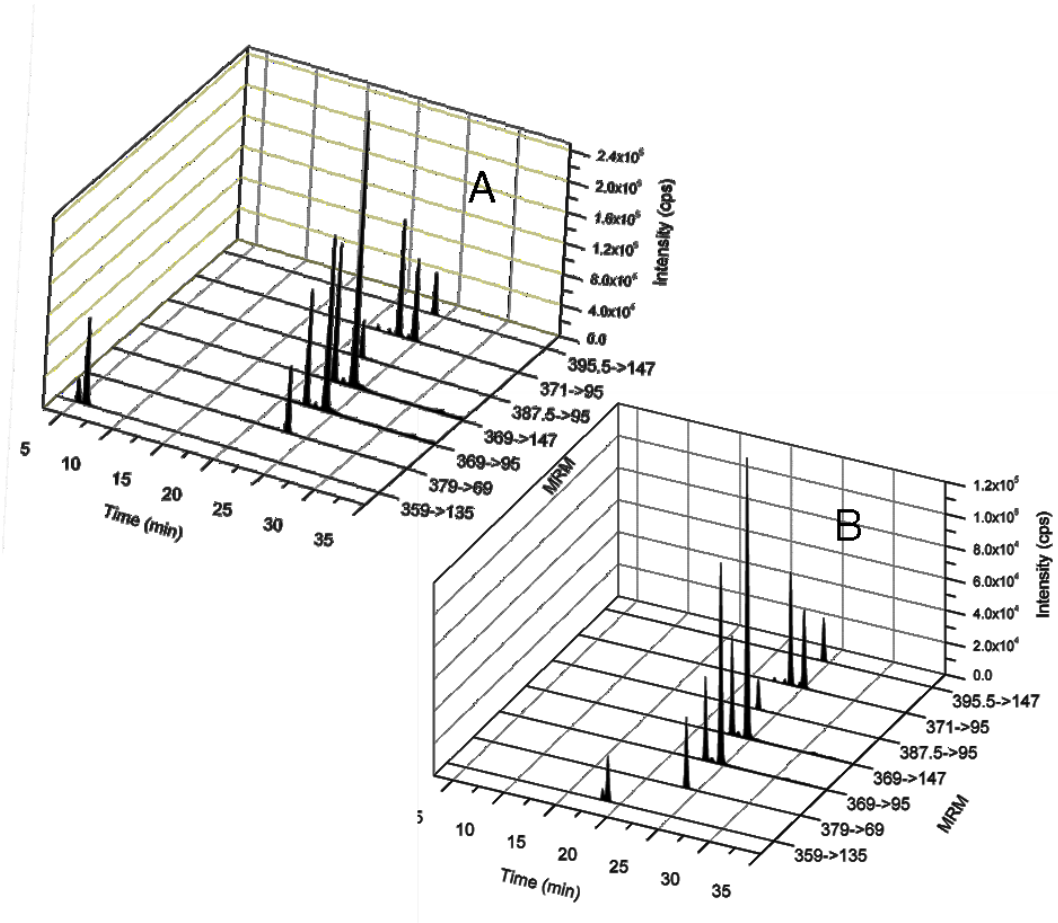

*Figure 94. Chromatograms obtained using MRM acquisition (one transition per compound) and the two gradients described in Table 24: Gradient 1 (**A**) and Gradient 2 (**B**). Isolithocholic and lithocholic acid (359>135), ergosterol (379>69), cholesterol and cholestanone (369>95), cholestanone (387.5>95), coprostanol and cholestanol (371>95), stigmasterol (395.5>147).*

vi. Chromatographic resolution

Detection in MRM mode usually does not require a good separation. An exception however comes about when isomers with identical fragmentation patterns are at play. This is the case here, where stereoisomers and functional group isomers are involved. A detailed view of the achieved isomers' separation is given in Figure 95, when gradient 2 is used. Moreover, gradient 1 provides an equivalent resolution for all isomeric pairs with the exception for bile acid, whose resolution is lower. The peak resolutions are presented in Table 25. Stigmasterol and ergosterol were deliberately excluded from the table to improve readability.

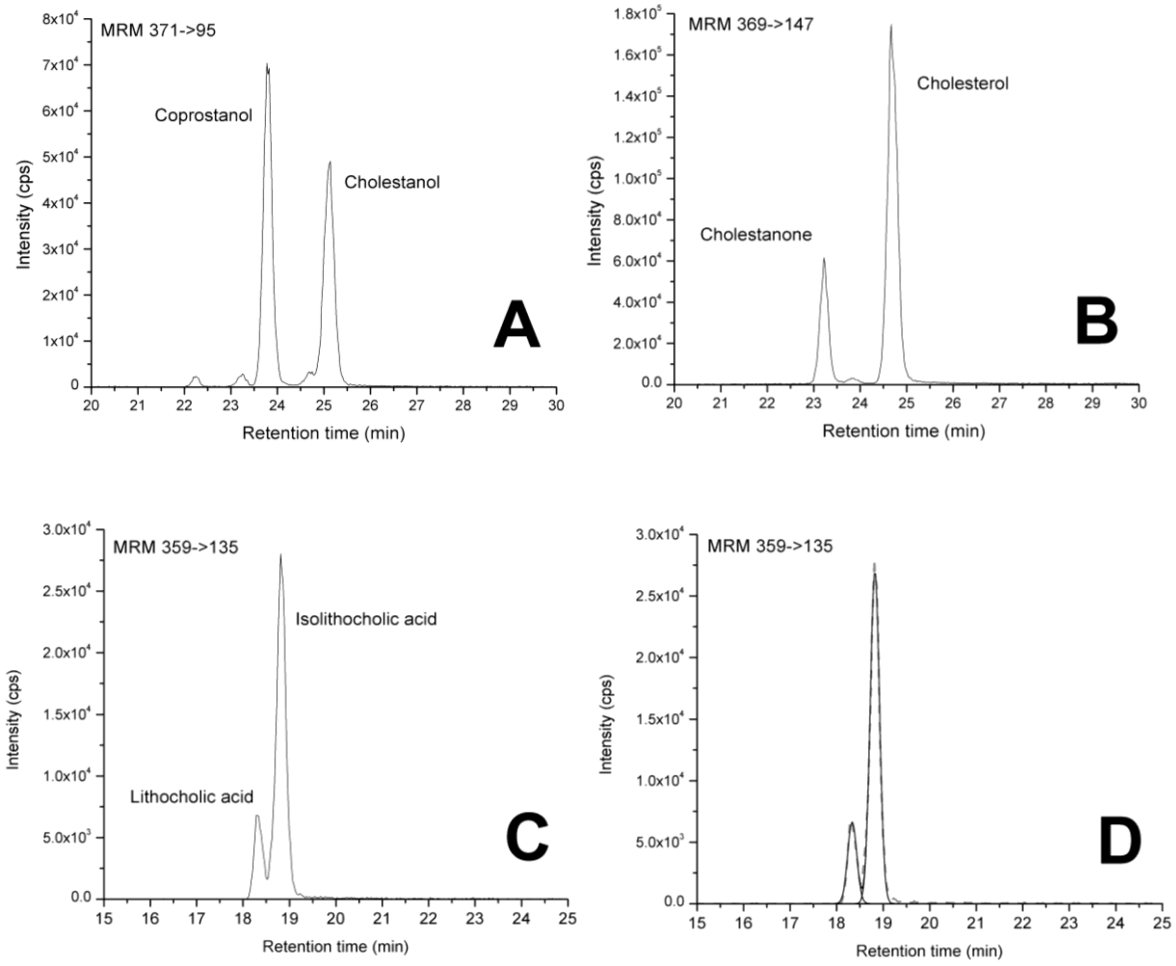

Figure 95. Chromatograms showing in details the isomers separation: A – coprostanol and cholestanol; B – cholestanone and cholesterol; C – isolithocholic and lithocholic acids; D – same as C after fitting individually the peaks with a Gauss curve.

Table 25. Chromatographic data for the 3 pairs of isomers using two different gradients. Details on the calculations and equation are provided in the material and methods section (9.2.2.ii - Chromatographic resolution, page 168).

Gradient 1

	LA[j]	ILA[k]	Cholestan-one	Cholesterol	Coprostanol	Cholestanol
Retention time [min]	18.24	18.82	23.22	24.67	23.83	25.11
Peak width at half-height [min]	0.18	0.2	0.2	0.24	0.2	0.24
Plates number (N)	54915	49118	74809	61182	76198	62499
Height equivalent to one theoretical plate	5492	4912	7481	6118	7620	6250
Capacity factor (K')	5.72	5.93	7.55	8.09	7.78	8.25
Selectivity factor (α)		1.04		1.07	1.06	
Peak width at baseline (W)	0.5	0.5	0.55	0.65	0.8	0.6
Resolution (Rs)	1.16		2.42		1.84	
Purnell Resolution (PRs)	1.7		3.64		3.52	

Gradient 2

	LA	ILA	Cholestan-one	Cholesterol	Coprostanol	Cholestanol
Retention time [min]	5.25	5.99	22.32	24.22	23.21	24.8
Peak width at half-height [min]	0.25	0.28	0.23	0.25	0.24	0.26
Plates number (N)	2386	2570	53052	50747	54122	49835
Height equivalent to one theoretical Plate	239	257	5305	5075	5412	4984
Capacity factor (K')	0.93	1.21	7.22	7.92	7.55	8.13
Selectivity factor (α)		1.29		1.1	1.08	
Peak width at baseline (W)	0.6	0.88	0.7	0.8	0.75	0.7
Resolution (Rs)	1		2.53		2.19	
Purnell Resolution (PRs)	1.56		4.42		3.7	

T0 (non-retained solute) = 2.93 min (Gradient 1); 2.72 min (gradient 2).

[j] *LA – Lithocholic acid.*
[k] *ILA – Isolithocholic acid.*

vii. Quantitation

A calibration curve using 8 or 9 standards was established, per each compound, using the method of least squares. All but cholestanone were fitted using a linear fitting as illustrated by Figure 96.

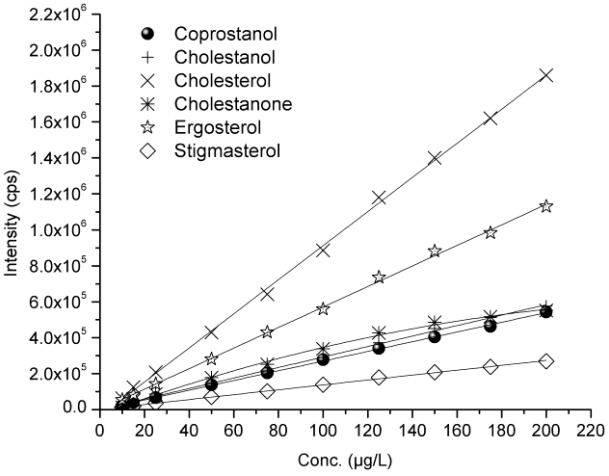

Compound	R^2	Slope	Intercept
Coprostanol	0.9992	2699.5	168.15
Cholestanol	0.9989	1236.6	2915.2
Cholesterol	0.9990	9479.5	-35466
Ergosterol	0.9986	5711.9	-257.63
Stigmasterol	0.9986	1359.7	1779.0
Cholestanone	0.9970	$y = -8x^2 + 4518.6x - 25945$	

Figure 96. Calibration curves for sterols and stanols.

10.2.3. Extraction methods

i. Membrane-assisted liquid-liquid extraction (MALLE)

Sterols and stanols can be extracted from the water phase into the receiving organic-phase (isopropanol) through a polyethylene membrane.

Two different densities were successfully tested: low-density polyethylene (LDPE) and high-density polyethylene (HDPE), though with different outcomes.

LPDE membranes show better recovery rates, as illustrated by the higher signals in Figure 97. The main drawback of these membranes is the often observed leakage of solvent into the water phase.

It should be borne in mind that MALLE is an equilibrium technique[327] and therefore recovery rates close to 100% should not be expected. In any case, the obtained recovery values were not enough to reach the desirable quantitation limit for coprostanol: at least 0.1 µg/L. Recovery rates between 5% and 10% were obtained

when the LDPE membranes were used and between 1% and 6% for the HDPE membranes.

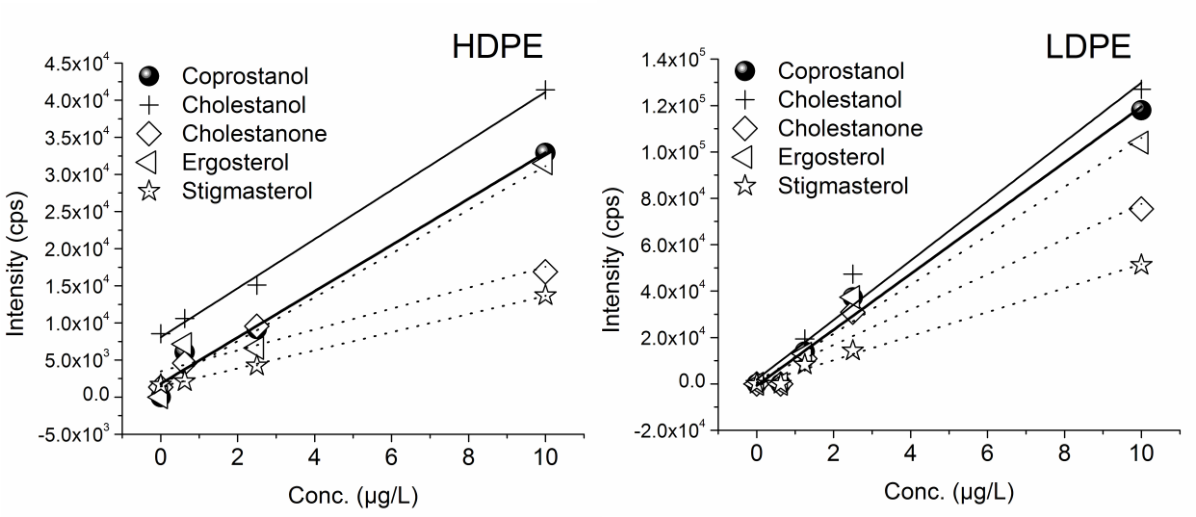

HDPE				LDPE			
	slope	Intercept	R^2		slope	Intercept	R^2
Coprostanol	3111	1824	0.9789	Coprostanol	12025	-732	0.9847
Cholestanol	3306	8061	0.9956	Cholestanol	12794	1957	0.9654
Cholestanone	1407	3490	0.8730	Cholestanone	7595	1603	0.9489
Stigmasterol	1220	1430	0.9980	Stigmasterol	5173	-113	0.9883
Ergosterol	2949	1644	0.9427	Ergosterol	10555	535	0.9710

Figure 97. Membrane-assisted liquid-liquid microextraction using high-density polyethylene (HDPE) and low-density polyethylene membranes (LDPE). Four standards were used to establish the HDPE calibration curves and five for the LDPE. The slopes and the correlation coefficients of the linear calibrations are summarised in the inserted table.

In an attempt to increase analytes' recovery the variables pH and ionic strength of the sample were studied using LDPE membrane and spiked tap water. Acid pH showed better recovery rates than neutral or alkaline ones (Figure 98). Surprisingly, the addition of NaCl seems to have no effect (or even being detrimental) for most of the compounds studied, as already observed for compounds used as UV filters in solar lotions extracted using the same technique.[327] These results should be looked at very carefully because the experiment was just performed once and the data is not enough to sketch a conclusive statement. Nevertheless, the pH effect was observed in all the extraction techniques tested beforehand and not described in this thesis: liquid-liquid extraction, liquid-liquid microextraction[357] and single-drop extraction.[358]

The variable temperature was not evaluated because the experimental setup did not permit it, mainly the option not to use stir-bar ("flea") inside the sample flasks. Without it, the sample could not be agitated on a hot-plate magnetic-stirrer device and evaluate for temperature effect.

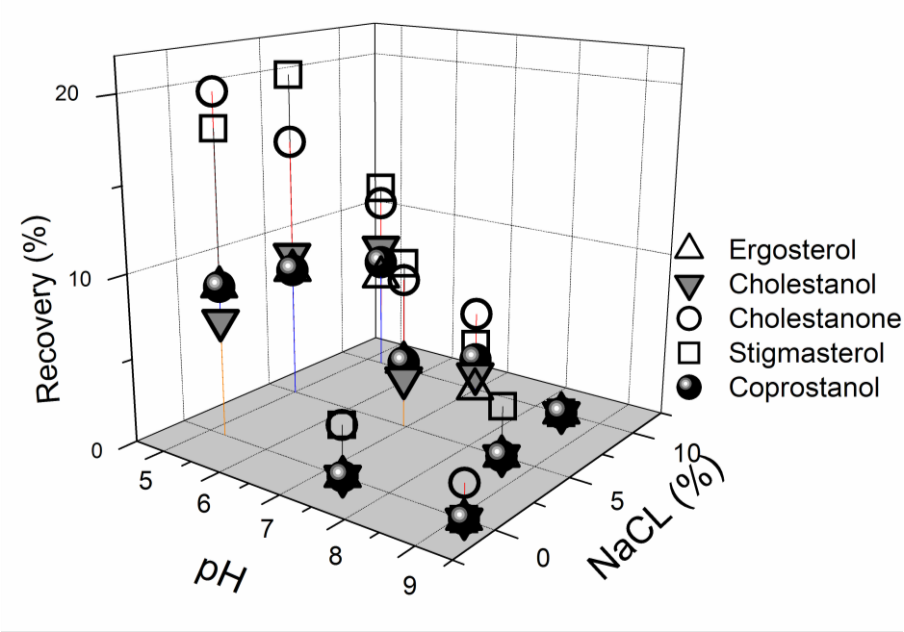

Figure 98. Influence of the pH and salt (NaCl) adding in the recovery rate of the analytes. The pH values tested were 5, 7 and 9 and for each of them three concentration of NaCl were tested: 0%, 5% and 10% (m/v).

Other factors could have been further explored but the main drawbacks were still to be solved beforehand: repeatability of membranes preparation (size, sealing and cutting), adsorption of the analytes on the outer membrane and solvent leakages.

LPDE membranes were the ones where leakages happened more often, barely any of the membranes retained the 200 µL solvent placed inside them before the extraction. Another solvent – a water immiscible one – could have been a possible solution but then the advantages of using a membrane interface would have become pointless, as the solvent could be in direct contact with the sample and recovered afterwards.

Even if the repeatability problem concerning the membrane preparation would be solved, together with the leakages/diffusion of the solvent into the water, the adsorption of very non-polar compounds on polyethylene membranes seems unavoidable. New polymers can be tested in the future for similar non-polar compounds and further variables optimised, following what has been successfully done for less polar substances like UV filters in water samples.[327]

ii. Dispersive liquid-liquid microextraction (DLLME)

Alcohols cannot be used as dispersive solvent for DLLME of sterols and stanols. The solubility of these analytes in the alcohols, tested as dispersive solvent (ethanol and isopropanol), is most likely the reason for the incomplete transfer into the organic phase (n-hexane). Cholesterol seems to an exception, it presented recoveries around 90% when ethanol was used as dispersive solvent[l]. Other authors observed the same behaviour for cholesterol in food samples but unfortunately they did not include other compounds in their study to allow for a comparison.[328]

The extraction solvent was selected after testing some others: carbon tetrachloride, dichloromethane, octanol, n-butanol, ethyl acetate and 2,2,4-trimethylpentane. The first two solvents – carbon tetrachloride and dichloromethane – having densities higher than water, required a special extraction tube as the one depicted in Figure 99. Besides the wearisome handling of these tubes during the extraction, mainly caused by their fragile bottom, the extracting solvent recovery from the bottom using a glass Pasteur pipette was sometimes difficult. Thus, solvents with lower densities than water, low melting points (< -70 °C) and immiscible with water at the concentrations used, were finally selected. Octanol produces very good recovery rates (similar to the ones obtained with n-hexane) but has a major drawback: too long evaporation time – extending for more than one hour – and consequently high consumption of nitrogen. Also the phase separation cannot be performed using temperature (-20 °C) because octanol itself will freeze. Yet, at room temperature octanol can be rather efficiently and completely recovered from the sample surface.

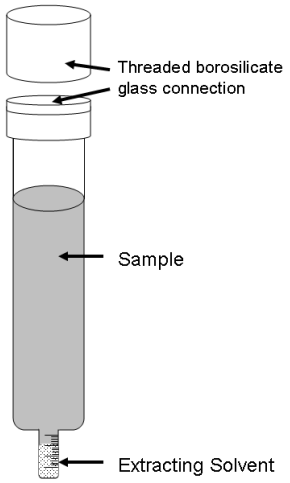

Figure 99. Extraction tube used for DLLME with extraction solvents having higher densities than water.

With n-butanol and ethyl acetate poor recoveries were obtained overall mostly because the 200 µL volume added before the extraction could not be completely recovered after the freezing step. These two solvents are not completely immiscible

[l] *20 mL of a sterols standards 1.5 µg/L in Milli-Q water, 1 mL ethanol, 200 µL carbon tetrachloride.*

with water and frequently an emulsion interface was produced, particularly in water/n-butanol mixtures.

Hence, n-hexane was the selected extracting solvent: It has low solubility in water (13 mg/L at 20°C), density 0.6548 kg/L and a melting point of – 95 °C. After extracting and freezing the samples, exactly 200 µL of n-hexane was always recovered from the extraction vial.

As dispersive solvents, besides the aforementioned ethanol and isopropanol, only acetonitrile was tested. The good results obtained with acetonitrile (Figure 100) discouraged further testing with other commonly utilised dispersive solvents, as acetone for example.[359,360]

The volume of the dispersive solvent seems not to affect upon most of the compounds with the exception of ergosterol (Figure 100 – top left-hand side). Nonetheless the presence of the dispersive solvent is required to achieve acceptable recoveries in fairly short extraction times. The minimum extraction time tested was one hour, yet several authors reported comparably shorter times (a few minutes)[328,359,361] while using higher amounts of dispersive solvent (in the mL range). As for the dispersive solvent, ergosterol extraction efficiency is improved by increasing the extraction time, being in this case the difference very significant.

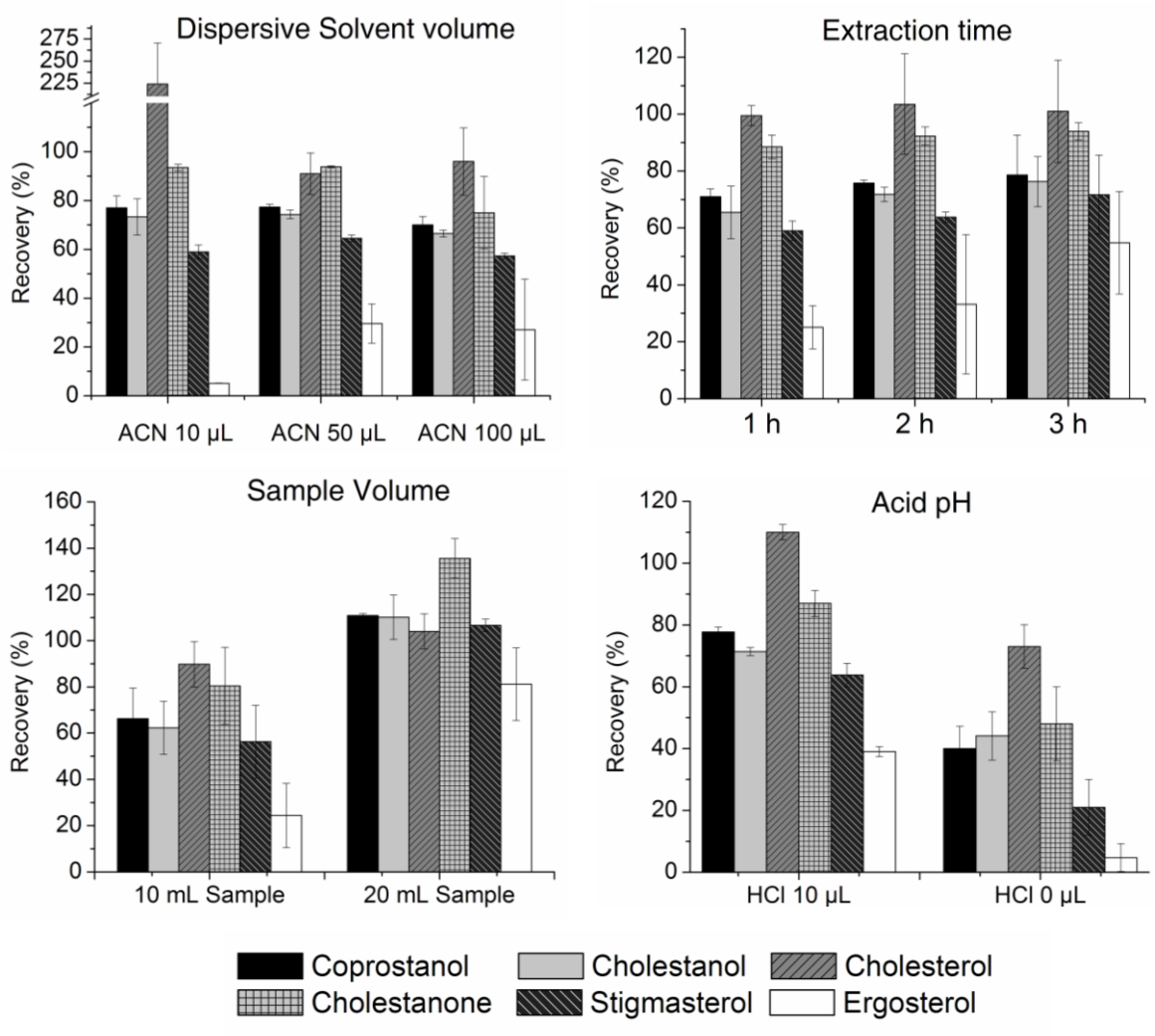

Figure 100. Factor optimisation for dispersive liquid-liquid microextraction (DLLME): dispersive solvent volume, extraction time, sample volume and acid pH. Each column represents the average value of the recovery (n = 3) and the error bars the associated standard deviation of the mean.

The sample volume graph – Figure 100 left-hand side, bottom – should not be looked at isolated but in association with the extraction solvent volume used: 200 µL in all cases. Better results were obtained using 20 mL of sample and 200 µL n-hexane; the same outcome would have probably been obtained if 100 µL n-hexane had been used to extract just 10 mL sample.

In general, all compounds' recovery is improved when the samples are acidified with 10 µL HCl 20%. This trend was observed no matter which kind of liquid-liquid extraction technique was used.

Salt-addition is evidently not possible as adding a solute like NaCl into the water causes a freezing-point depression, making impracticable the phase separation by freezing.

Cholesterol shows always the highest standard deviation (low repeatability) among the studied compounds. Even though measures had been taken to avoid contamination, including the use of gloves in every step of the extraction process, the ubiquitous distribution of cholesterol seems to play a role on the final results variations.

The final conditions used for extracting the water samples and standards are described in the methods section (9.2.3.ii, page 173).

Several standards (Milli-Q water spiked with the analytes) and spiked surface waters, from different origins in Berlin, were extracted and the obtained recoveries displayed in Figure 101 and Figure 102.

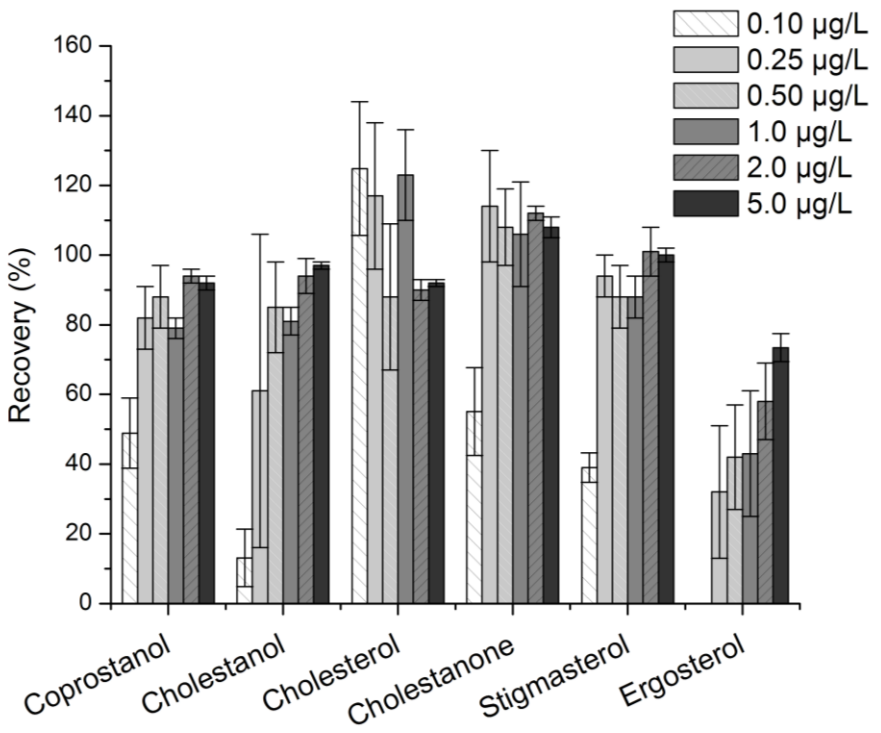

Figure 101. Spiked Milli-Q water samples extracted by DLLME. Several standards were prepared in Milli-Q water (0.10 µg/L – 5.0 µg/L) and split in three aliquots each prior to extraction. The bars represent the average of the three extracted standards and the error bar the associated standard deviation.

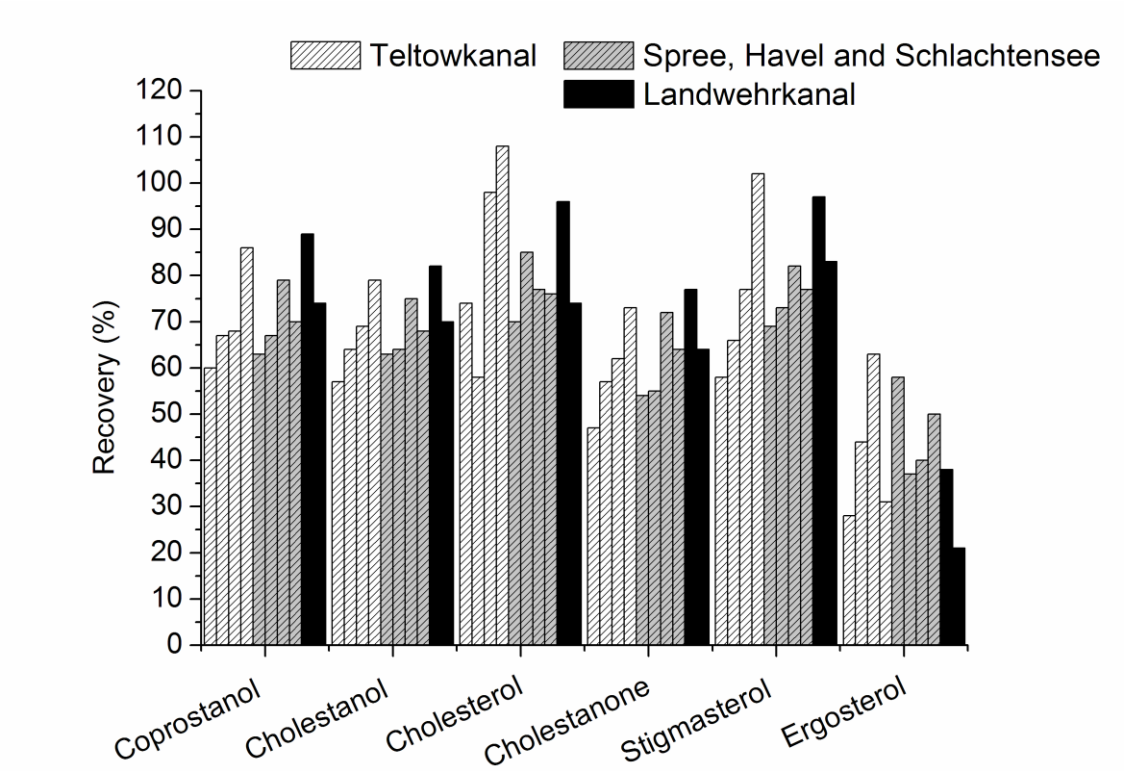

Figure 102. Spiked real samples with 1 µg/L sterols/stanols mixture. Several surface water samples, from different locations in Berlin, were spiked with 1 µg/L standard and extracted using DLLME. Each bar represents a spiked sample.

PART III

Environmental monitoring of surface waters

11. Water sampling campaigns (PART III)

Several water campaigns were carried out; some small-scale ones were used to study matrix effects or validate the caffeine immunoassay and are not included in this section. Although wastewaters were out of the scope of this thesis, some tests had to be performed mainly due to some matrix effect/interference found near a wastewater discharge point in Teltowkanal. Extending the scope of the developed caffeine immunoassay to wastewater requires further studies and optimisation.

The climate conditions on the sampling day were obtained from the Deutscher Wetterdienst (climatological data online).[362] The watercourses' flows, STP locations, discharged points and effluent volumes were obtained from Berliner Wasserbetriebe (BWB) and their published data.[363]

11.1. Surface waters

11.1.1. Previous screening for matrix mineral characterisation

Six grab samples were collected on the 10th and the 11th of December 2007 from diverse watercourses and lakes in Berlin – Figure 103. The matrix characterisation was performed by a reference laboratory (Metal analysis, Inorganic Reference materials, BAM, Berlin).

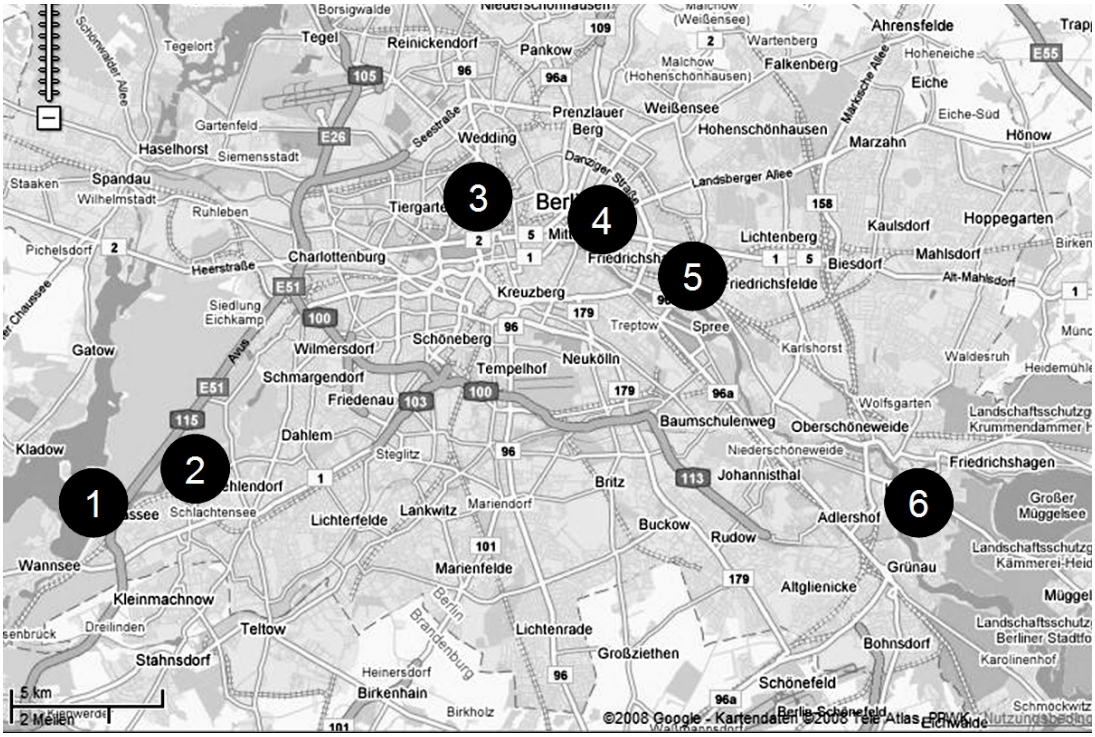

Figure 103. Water sampling spots of the water screening of the 10th and 11th of December 2007. The map was obtained from Googlemaps on the 15.01.2008. Samples origin: (1) Havel; (2) Schlachtensee; (3), (4) and (5) Spree; (6) Teltowkanal.

Remarkable differences were not noticed between the samples regarding either the calcium concentration (ranging from 96 to 105 mg/L), or the electric conductivity (from 645 to 695 µS/cm). The results are described in detail in Table 26.

Table 26. Results of the elements and anions of six water samples from different origins in Berlin. n.d. – not detectable.*

	sample 1 (Havel)	sample 2 (Schlachtensee)	sample 3 (Spree)	sample 4 (Spree)	sample 5 (Spree)	sample 6 (Teltowkanal)
	(mg/L)	(mg/L)	(mg/L)	(mg/L)	(mg/L)	(mg/L)
Element						
Al	0.012	0.009	0.027	0.016	0.013	0.058
Cu	0.002	0.003	0.002	0.006	0.002	0.010
Fe	0.077	0.006	0.25	0.22	0.15	0.18
Hg	n.d.*	n.d.	n.d.	n.d.	n.d.	n.d.
Mn	0.12	0.003	0.13	0.12	0.11	0.11
Se	n.d.	n.d.	n.d.	n.d.	n.d.	n.d.
Zn	0.009	0.004	0.007	0.006	0.004	0.004
Ca	95.80	81.77	102.45	103.52	104.27	104.55
K	8.81	9.09	6.95	6.95	6.80	6.48
Mg	12.19	10.82	14.14	13.97	14.00	13.95
Na	38.94	39.34	32.17	33.03	31.41	30.76
Anion						
F^-	0.15	0.16	0.17	0.17	0.18	0.16
Cl^-	60.7	81.5	51.6	52.9	52.0	50.3
SO_4^{2-}	141.3	120.4	182.1	183.8	178.9	174.7
NO_3^-	6.3	2.2	3.3	3.1	2.6	2.4
NO_2^-	8.0	6.1	7.5	7.5	7.7	5.9
PO_4^{3-}	0.4	< 0,3	0.4	1.2	0.3	< 0,3
pH	6.3	6.4	6.3	6.5	6.6	6.1
Elect. Conductivity (µS/cm)	683	645	695	697	692	671

The samples were analysed for the several xanthines in order to understand the distribution of the caffeine metabolites in the water compartment. As this preliminary study already shows (please refer to Figure 104) the main caffeine metabolite, paraxanthine (~90% of caffeine is metabolised to paraxanthine by humans)[307,364]

shows a residual presence in water. Paraxanthine is not very often included in the monitoring programs but when it is the case, its concentration were always well below the caffeine' ones.[365,366] The removal efficient of paraxanthine, in wastewater treatment plants does not differ from the caffeine one[367] and, considering that paraxanthine concentration in the affluent is much higher than the caffeine one; then the reason for such low concentration in surface and groundwater samples – here and in reported data[365,366] – is probably due to stability differences between both compounds when in the environmental compartments.

Interesting are also the figures observed for theophylline and theobromine: although both are minor metabolites of caffeine, they have as well their own direct input in the environment via tea and chocolate, respectively. Yet, their concentrations are also very low, with theophylline being even undetected in five out of the six samples analysed. Again, even if the reason for this has not yet been unveiled, the similarities between the three chemical structures (paraxanthine, theophylline and theobromine) and dissimilarities with caffeine itself should be considered: the three metabolites are dimethylated while caffeine is tri-methylated, without any available secondary amine for N-conjugated elimination by humans. As aforesaid, no further explanations can be given besides speculation as some work is still to be done for clarifying the reasons behind these surprising observations. Unfortunately at the time this previous monitoring study was performed the method for the metabolite xanthine was not ready and these data is lacking here.

The antibiotic sulfamethoxazole was part of a student master thesis and since it was monitored using the same SPE-LC-MS/MS method the results were included in Figure 104. Sulfamethoxazole, as other pharmaceutical active compounds, are present in water at very low concentration, sometimes even undetected; but sulfamethoxazole concentration do correlate well with a higher concentrated compound, and thus easier to detect and quantify: caffeine.

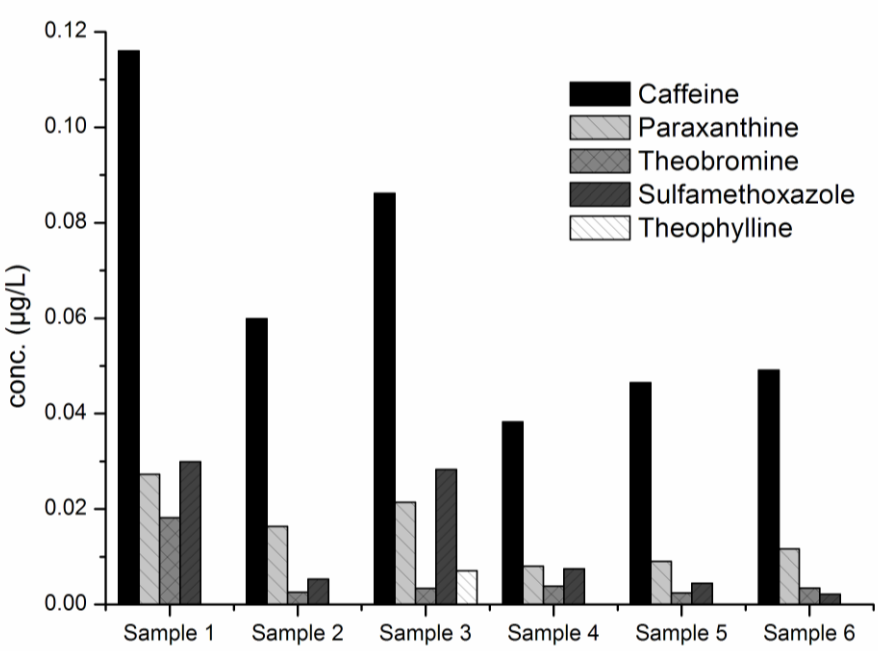

Figure 104. Concentration of xanthines and the antibiotic sulfamethoxazole in six water samples from different watercourses in Berlin, measured by SPE-LC-MS/MS.

The samples were also quantified using the immunoassay (ELISA), directly and after solid-phase extraction (SPE). The high solubility of caffeine in water permits recovering the SPE extracts' residue in 100% water and thus performing the immunoassay unconcerned over the presence of organic solvents. The correlation between SPE-LC-MS/MS and ELISA has previously been disclosed (7.6 Monitoring caffeine in water samples, page 142) and Figure 105 is only included here to bring out the fact that a 1000-fold sample concentration prior to ELISA can further improve the correlation of results with the LC-MS/MS. Even without SPE, the results are pretty encouraging if one keeps in mind that 3 orders of magnitude difference, in terms of concentration, are being compared.

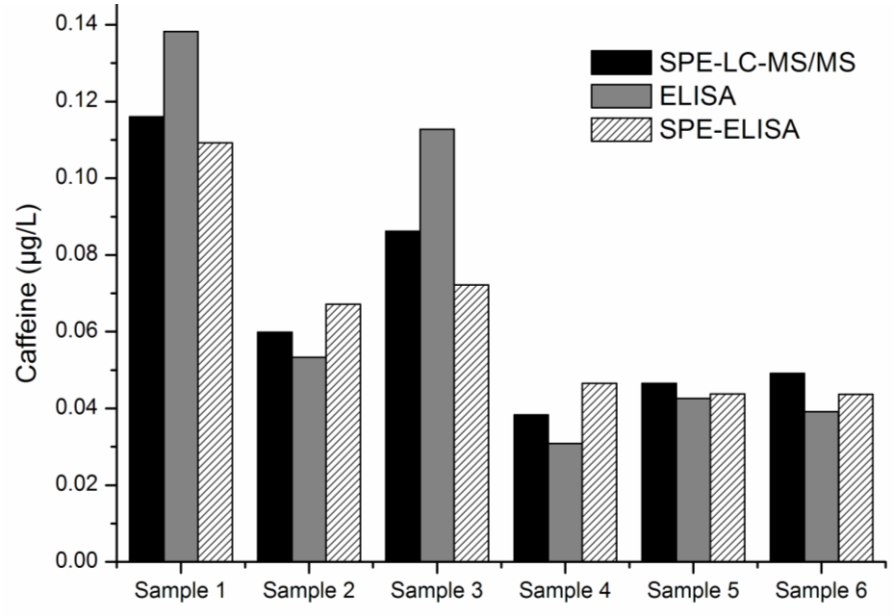

Figure 105. Caffeine concentration in six surface water samples by two different methods: SPE-LC-MS/MS and ELISA, with and without pre-concentration (SPE).

This previous screening showed that the surface waters' mineral composition in central Berlin is very alike. And caffeine was the most concentrated xanthine in all the samples analysed while its metabolites unexpectedly revealed lower concentrations. Xanthine itself was not analysed during this water screening.

11.1.2. Berlin Water Screening (BWS)

In June 2009 a large water screening was conducted for 4 weeks involving large amounts of samples, different research projects, several analysts and the entire immunochemical methods group (BAM) manpower. A total of 20 surface water spots were selected, from several watercourses in Berlin: Teltowkanal, Spree, Havel, Wannsee, Dahme and Erpe (Neuenhagener Muehlenfliess). Some of the spots were deliberately selected downstream and upstream of sewage treatment plants (STP) discharging points, to evaluate their contribution to caffeine input into surface waters. The sampling spots, as well as the sampling dates, are described in Table 27 and can be seen on the map represented in Figure 106.

Table 27. Berlin water screening (June 2009) – sampling spots and dates of the 20 analysed samples. STP stands for Sewage Treatment Plant.

Sample	Sampling spot	Observation	Sampling date
1	Teltowkanal – Wegedornstraße	downstream of STP Wassmannsdorf	02.06.2009
2	Teltowkanal – BAM	downstream of STP Wassmannsdorf	02.06.2009
3	Teltowkanal – Kleingartensiedlung	downstream of STP Wassmannsdorf	02.06.2009
4	Teltowkanal – Emil-Schulz-Bruecke	uptream of STP Ruhleben	09.06.2009
5	Teltowkanal – Krahmersteg	downstream of STP Ruhleben	09.06.2009
6	Teltowkanal – Hafen Steglitz	downstream of STP Ruhleben	09.06.2009
7	Teltowkanal – Autobahnbruecke	uptream of STP Stahnsdorf	09.06.2009
8	Teltowkanal – Schleuse Kleinmachnow	downstream of STP Stahnsdorf	09.06.2009
9	Teltowkanal – Friedensbruecke	downstream of STP Stahnsdorf	09.06.2009
10	Großer Wannsee – Scabellstraße		16.06.2009
11	Havel – Heerstraße		16.06.2009
12	Havel – Eiswerderufer	Before the influx to the Spree	16.06.2009
13	Spree Ruhleben – An der Spreeschanze	Before the influx to the Havel	16.06.2009
14	Spree Bellevue – Bundesratufer		16.06.2009
15	Spree Treptower Park – Molecule Man		16.06.2009
16	Spree – Spindlersfelder Straße	Behind the confluence of the Dahme and the Mueggelspree	23.06.2009
17	Mueggelspree – Mueggelseedamm	Before the influx of the Erpe	23.06.2009
18	Dahme – Oberspreestraße	Before influx into the Spree	23.06.2009
19	Neuenhagener Muehlenfliess (Erpe) Muehlenstraße	downstream of STP Muenchehofe	23.06.2009
20	Neuenhagener Muehlenfliess (Erpe) Friedrichshagener Chaussee	upstream of STP Muenchehofe	23.06.2009

Figure 106. (Next page) Berlin water screening (June 2009) – The sampling spots are represented by the yellow spheres with the respective sample number inside, the Sewage Treatment Plants (STP) location are marked with red spheres and their discharge points identified with the bold-black lines. The map was downloaded from Wikipedia on the 21st of October 2010 without any further modifications.

(http://de.wikipedia.org/wiki/Datei:Karte_der_Berliner_Wasserstraßen.png)

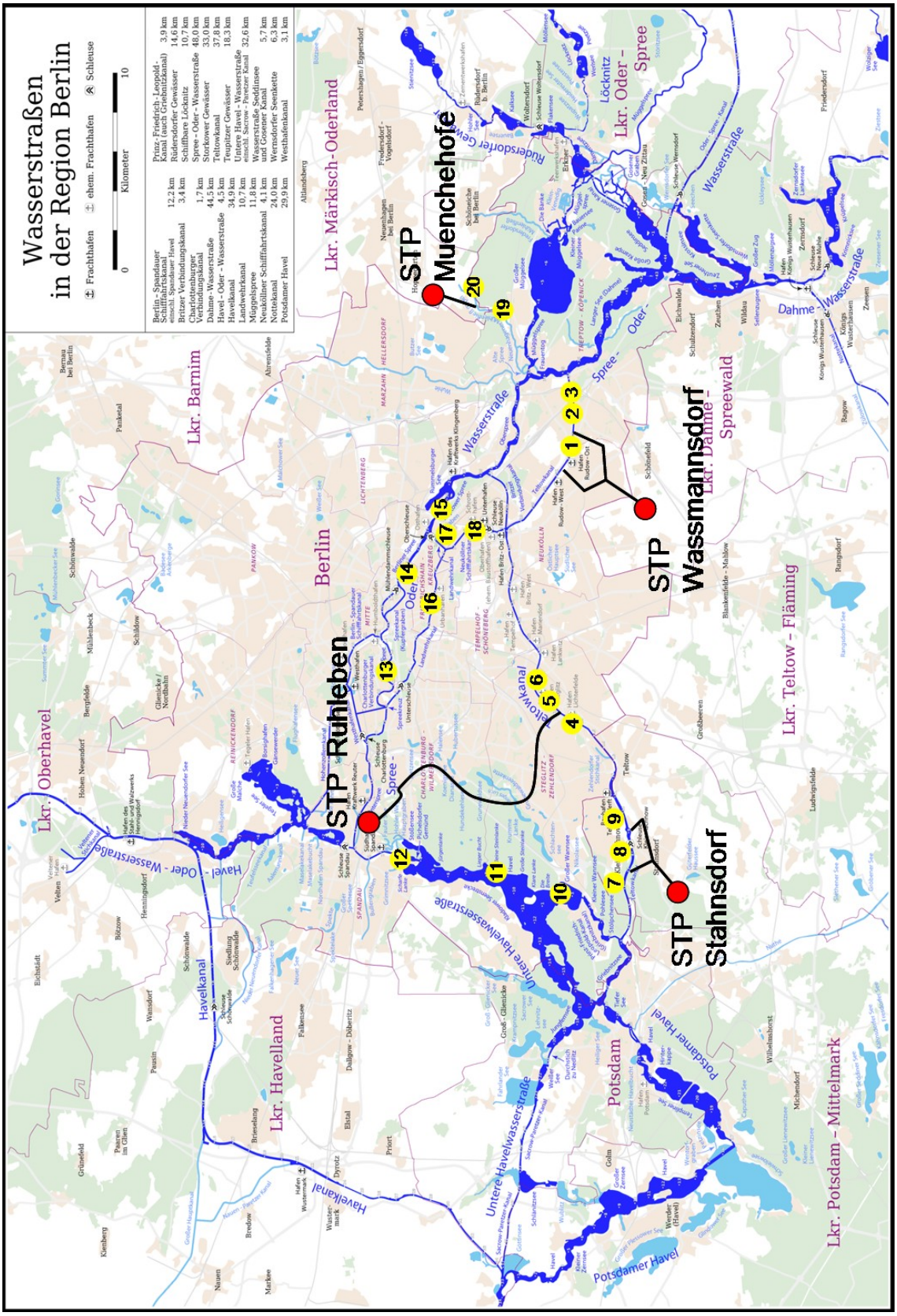
Wasserstraßen
in der Region Berlin
Frachthafen
ehem. Frachthafen
Schleuse
0
Kilometer
10
Berlin-Spandauer Schiffahrtskanal 12,2 km
einschl. Spandauer Havel
Britzer Verbindungskanal 3,4 km
Charlottenburger Verbindungskanal 1,7 km
Dahme-Wasserstraße 44,5 km
Havel - Oder - Wasserstraße 4,5 km
Havelkanal 34,9 km
Landwehrkanal 10,7 km
Müggelspree 11,8 km
Neuköllner Schiffahrtskanal 4,1 km
Nottekanal 24,0 km
Potsdamer Havel 29,9 km
Prinz-Friedrich-Leopold-Kanal (auch Griebnitzkanal) 3,9 km
Rüdersdorfer Gewässer 14,6 km
Schiffbare Löcknitz 10,7 km
Spree - Oder - Wasserstraße 48,0 km
Storkower Gewässer 33,0 km
Teltowkanal 37,8 km
Teupitzer Gewässer 18,3 km
Untere Havel - Wasserstraße einschl. Sacrow - Paretzer Kanal 32,6 km
Wasserstraße Saalmühlsee Wernsdorfer Seenkette 5,7 km
Wernsdorfer Seenkette 6,3 km
Westhafenkanal 3,1 km
STP Ruhleben
STP Muenchehofe
STP Wassmannsdorf
STP Stahnsdorf
Berlin
Lkr. Oberhavel
Lkr. Barnim
Lkr. Märkisch-Oderland
Lkr. Havelland
Lkr. Potsdam - Mittelmark
Lkr. Teltow - Fläming
Lkr. Dahme - Spreewald
Lkr. Oder - Spree
Havel - Oder - Wasserstraße
Havelkanal
Teltowkanal
Untere Havelwasserstraße
Potsdamer Havel
Spree - Oder - Wasserstraße
Dahme - Wasserstraße
Rüdersdorfer Gewässer
Löcknitz
Potsdam

The xanthines distribution in this water screening (BWS) showed dissimilarities to the previous one: even if caffeine is still the most dominant xanthine in most of the samples, the distribution of its metabolites revealed new and interesting features (Figure 107). The reason for this seems to be the fact that this time spots near sewage treatment plants (STP) discharging points were included along with other surface water without treated wastewater (direct) input. These samples (STP) show indeed very interesting insights on xanthines' stability in waters. As can be immediately seen in Figure 107, xanthine is the major component in the first 3 samples (all from Teltowkanal, downstream of STP Wassmannsdorf, collected on the same day). And its presence was exclusively detected in surface waters with a direct treated wastewater input, independently of the contamination level of the sample (known from other colleagues' results and caffeine itself). Calculating the concentrations ratios caffeine/xanthine, the samples can be backtracked to the sampling spot: Teltowkanal (STP Wassmannsdorf) – 0.3 ± 0.05; Teltowkanal (STP Ruhleben) – 2.8 ± 0.5; Teltowkanal (STP Stahnsdorf) – 6.4 ± 1.5. These samples were not collected within the same day (Table 27, page 235) and a possible explanation for these differences is the time mediating the treated wastewater discharge and the sampling itself. If xanthine half-live in water is very short (assuming a couple of hours) this would explain the differences found and also why xanthine was never detected in the remaining water samples. In any case, stability studies will be very welcome for a comprehensive understanding of the whole picture.

Paraxanthine shows a different outcome. Unlike xanthine, its entrance into the environment is exclusively through caffeine metabolism[368,369] and, analytically it has a lower limit of detection by SPE-LC-MS/MS allowing to estimate its concentration in all the 20 samples analysed. Regarding the concentration ratio caffeine/paraxanthine, one can not backtrack the origin of the sample as it could be made for xanthine. When samples are sorted by this ratio caffeine/paraxanthine, samples with STP input are flanked below and above by other surface waters without it, and no trend can be found. Nevertheless what can be observed in those samples with higher caffeine concentration is a highest ratio caffeine/paraxanthine: all samples in Figure 107 with caffeine concentrations above 0.3 µg/L, i.e., the immediately visible concentration peaks (samples 8, 9, 11, 13, 19, 20), present an average ratio of 20 ± 3.6 while the ones below the 0.3 µg/L caffeine threshold have an average of 7.2 ± 2.3. The previous screening (11.1.1, page 229), performed with

surface waters without wastewater input and caffeine concentration about 0.12 µg/L, has a caffeine/paraxanthine ratio of 4.4 ± 0.5.

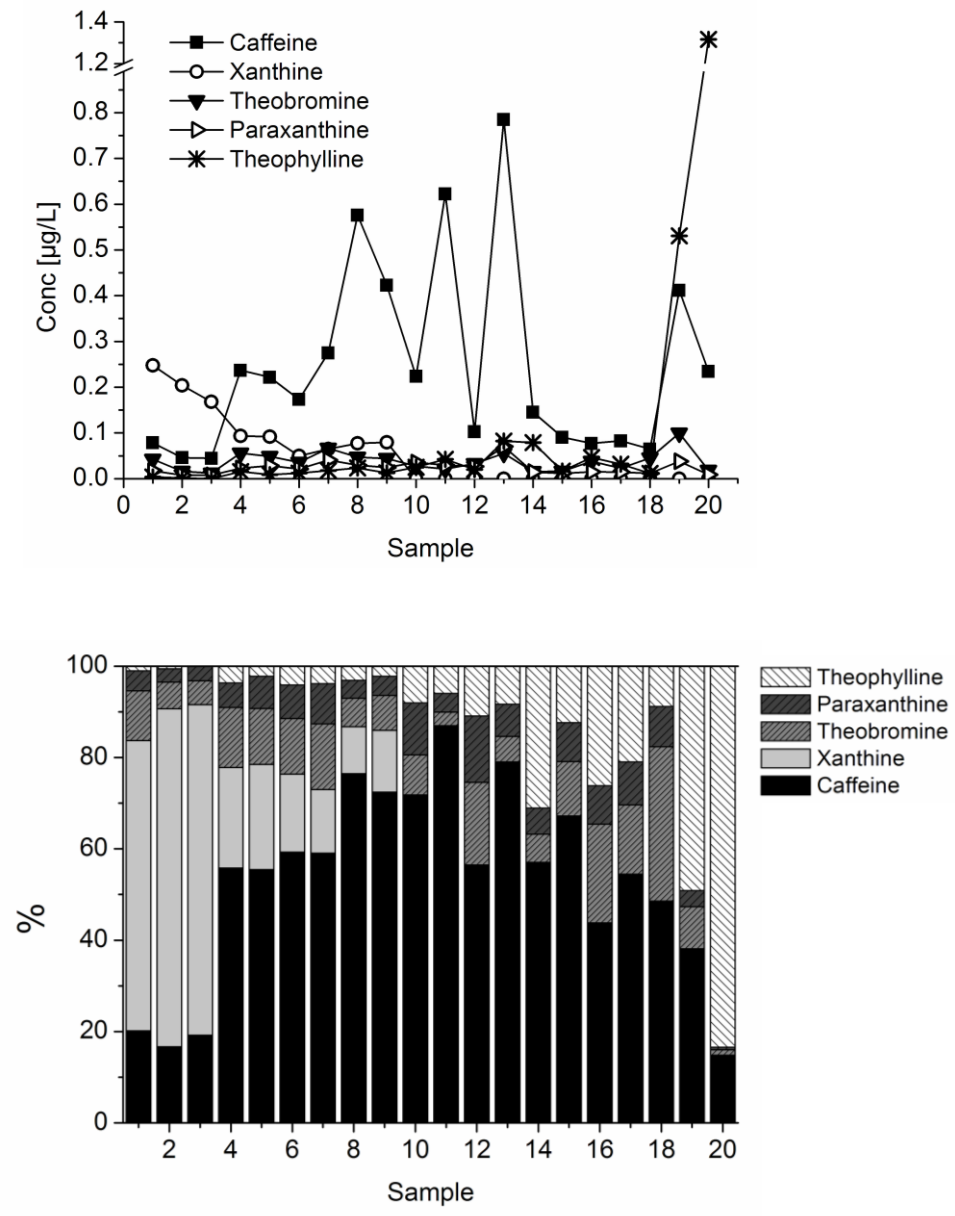

Figure 107. Results of the BWS (June 2009): Upper graph – Xanthines' concentrations in surface waters; and lower graph – Contribution of each individual xanthine in the overall xanthine content per sample, in percentage. Sample 20 present a very awkward result for theophylline, but no logical reason was found to explain it.

In the same samples coprostanol and carbamazepine (an antiepileptic) were also measured and the results are summarised in Figure 108. A good correlation between caffeine and coprostanol concentrations was found and some interesting feature arose out of the data: sample eleven (11) for example shows increased caffeine and coprostanol concentration but not carbamazepine ones, showing that

probably untreated combined wastewater (wastewater and rainwater) has reached the Havel. While in the previous sampling days (02.06.2009 and 09.06.2009) no rainfall was registered, the day before collecting samples 10 to 15, 12.2 mm of rainfall were measured in Berlin-Tempelhof. The same reason can explain the concentration peaks observed for sample 19, which was collected after intense rainfall in the previous two days (17.1 mm and 4.6 mm, respectively). Once the affluent volume exceeds the capacity of the STP, as after intense rainfall, a part of the affluent is discharged untreated in several spots in Berlin.[363] This also explains the peak of theophylline observed in sample 19 (Figure 107), meaning that some amounts of this xanthine did not pass through sewage treatment.

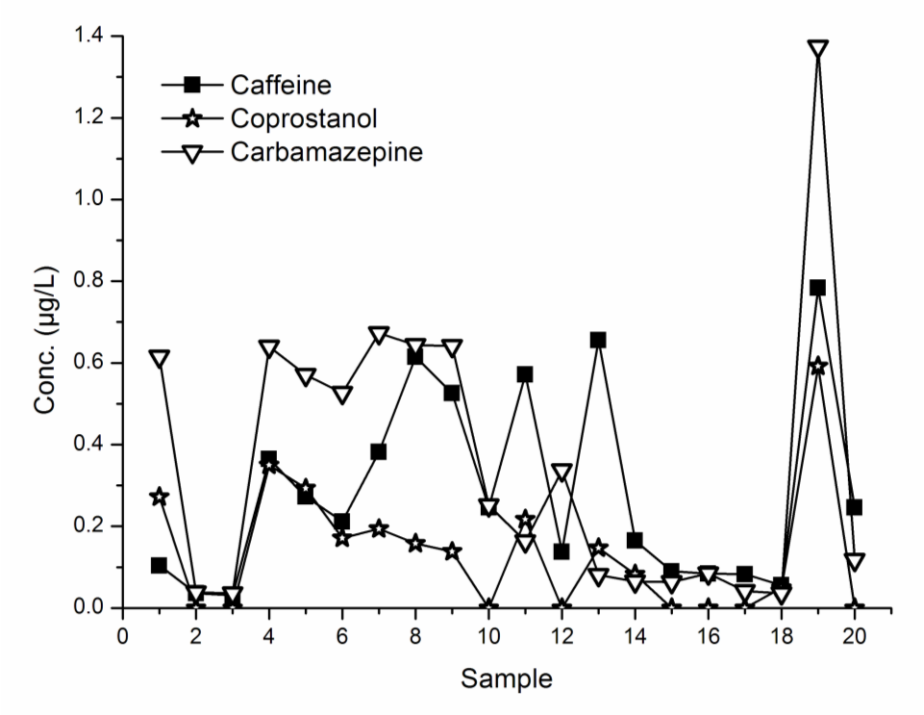

Figure 108. Caffeine, coprostanol and carbamazepine concentration in the samples collected during the BWS (June 2009).

As the results show, caffeine and coprostanol present alike outcome concerning human contamination input into surface waters. Caffeine is present in highest concentrations and additionally can be analysed faster (using ELISA) and with lower limit of detection than coprostanol. Therefore, for the huge amount of samples measured during the screening hereafter described, caffeine was selected as the indicator of the contamination level of the watercourses.

11.1.3. Teltowkanal (TK)

i. Teltowkanal screening 1

The samples were collected on the 1st of October 2008 along the Teltowkanal (Berlin), every 0.5 km, from kilometer 37 to kilometer 27 – sampling from east to west. The samples were analysed all together in a single plate by ELISA.

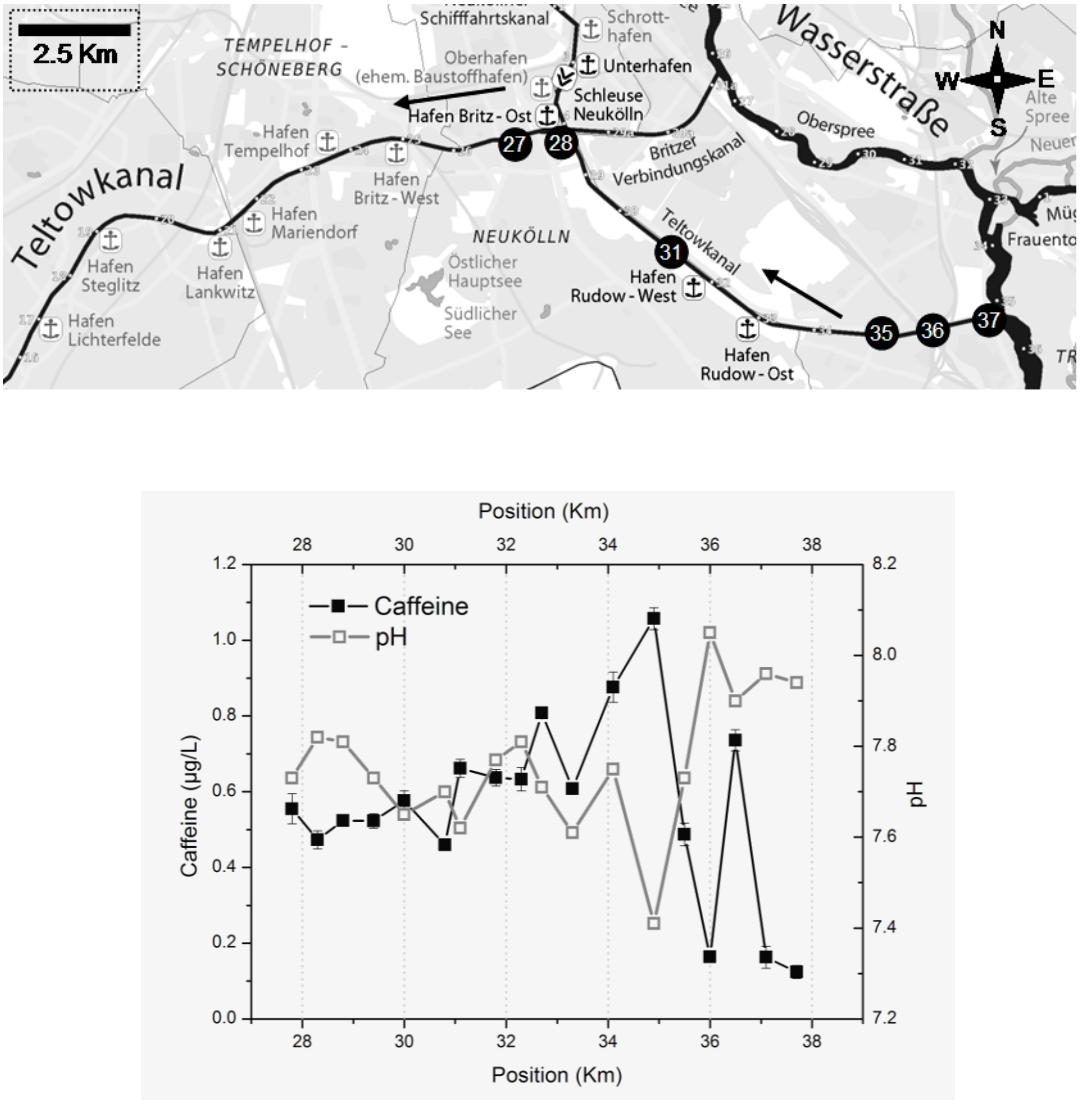

Figure 109. Caffeine concentrations in Teltowkanal, in October 2008. A sample was collected every 0.5 km from km 37 to km 27 – black spheres – following the channel flow as indicated by the bold-arrows on the map on top. Bottom graph: The samples' pH is represented by the grey open-squares connected with a line in the same colour; caffeine concentrations are depicted as black bold-squares, connected by a black line.

The sampling aimed at evaluating the impact of the STP discharge in the Teltowkanal. The STP Wassmannsdorf is discharging its treated effluent between km36 and km35, the point where caffeine concentration increases sharply (Figure 109) and the pH value decreases, illustrating chemically that impact. The effluent is discharged at 2.3 m^3/s and it is entering the Teltowkanal (0.77 m^3/s), at 1.99 m^3/s.[363]m Easy to understand is the impact caused by such high amount of effluent in a low-flow channel. Some compensation is however introduced a few meters downstream by the entrance of groundwater into the channel. An out-of-service water treatment plant (WTP) is still pumping groundwater into the channel with an average flow of 0.24 m^3/s and hence diluting the effluent. The Britzer Verbindungkannal (1.50 m^3/s) – connecting the Spree to the Teltowkanal – is additionally helping to reduce the effluent impact as can be seen in the samples' results from the first kilometres of the Teltowkanal (samples 29 – 27, Figure 109).

ii. Teltowkanal screening 2

The second water sampling in Teltowkanal was planed in order to show if major day-to-day variations exist regarding caffeine concentrations and consequently the contamination level of the channel.

Grab samples were collected every week day from the 2nd of November 2009 until the 22nd of March 2010, between 1p.m. and 2 p.m – except when the channel was partially frozen and during holidays. One sample was collected 400 m upstream of the STP Wassmannsdorf discharge point and the second one 200 m downstream. The upstream sampling spot was frozen between the 6th of January and the 19th February 2010; hence some samples were not collected during this time. Also, during Christmas holidays (19th December 2009 to the 6th of January 2010) samples were not collected. The ELISA was performed once a week and samples were placed at 4°C until analysis. The sampling was organised and performed together with a PhD colleague, Arnold Bahlmann, who was measuring the anti-epileptic drug carbamazepine within his PhD project. The carbamazepine data are herein presented and discussed with the author's permission.

[m] *Data from the summer 2003.*

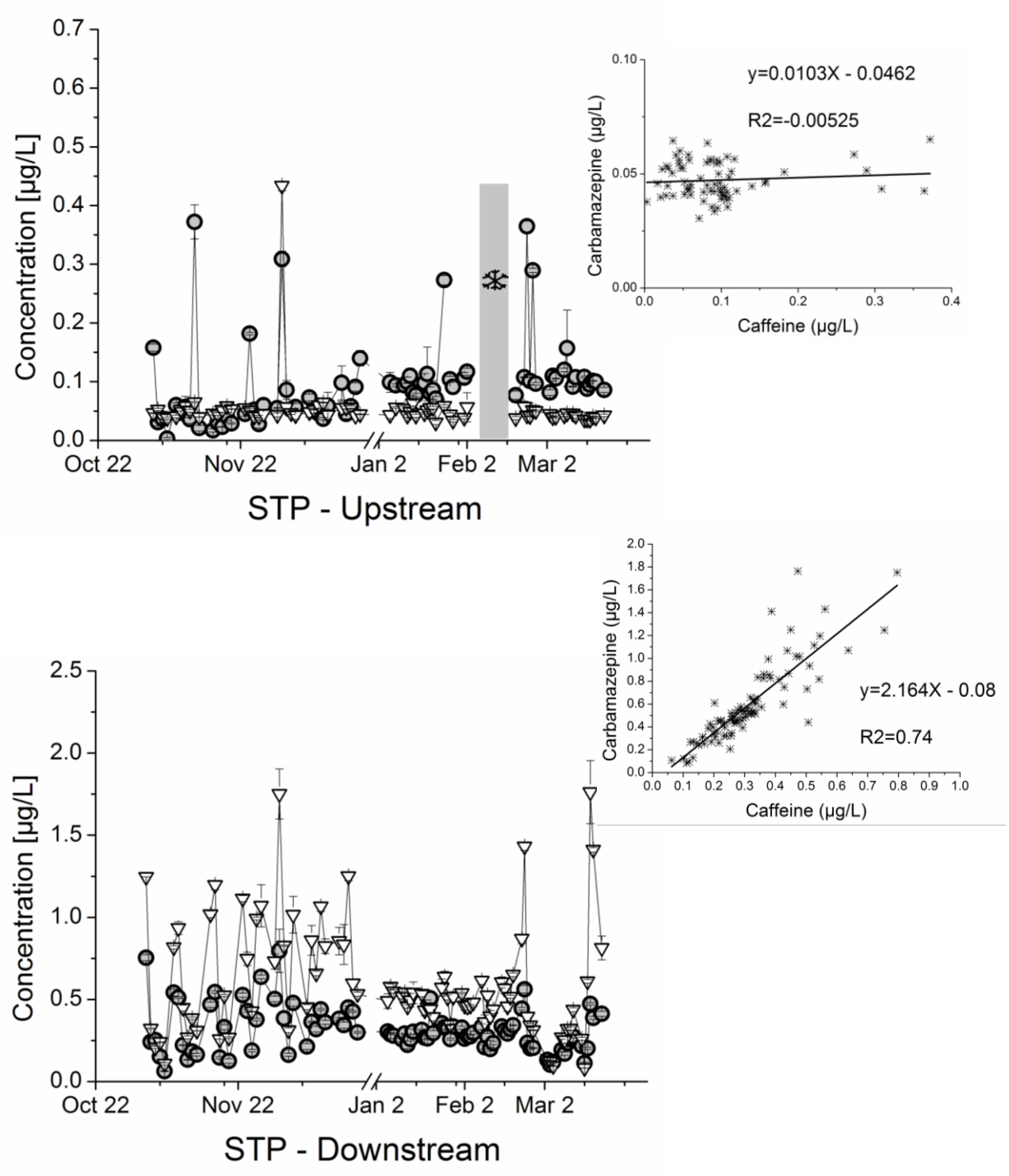

Figure 110. Caffeine (black bold circles) and Carbamazepine (open triangles) concentration in Teltowkanal, downstream and upstream of STP Wassmannsdorf discharging spot, from the 2nd of November 2009 until the 22nd of March 2010. The upper graph represents the samples collected 400 m upstream of the STP affluent and the lower one the samples collected 200 m downstream. The break in the x-axis represents the Christmas holidays, when samples were not collected; Sample between the 2nd February and 18th February 2010 were not collected upstream as the sampling site was frozen. The inserts in both graphs depict the respective caffeine (x-axis)/ carbamazepine (y-axis) linear correlation; upstream: y = 0.0103x -0.046 (R^2 = -0.0052); downstream: y = 2.164x – 0.08 (R^2 = 0.74).

Not surprisingly the caffeine results downstream of the STP correlate well with another human contamination marker: carbamazepine (R^2 = 0.74), with this last presenting almost always the highest concentrations. This was expected as caffeine is efficiently removed (>95%) by STP[67,370] whereas carbamazepine is not (<30%).[370]

Contrary, the downstream results were somehow unanticipated, with higher caffeine concentration and some odd concentration peaks. One of those caffeine concentration peaks appears together with a high carbamazepine concentration (1st of December 2009, Figure 110), which is probably due to a flow inversion on the channel or due to a boat passing by shortly before the sampling moment. That day the caffeine concentration downstream (0.80 µg/L) was rather high, thus supporting the hypothesis of a flow inversion. An explanation for the remaining samples, with very high caffeine concentration unaccompanied by the carbamazepine ones, it is not so clear. A possible flow of non-treated wastewater nearby would explain these values but no spot was identified within the timeframe of this thesis. Curious is the fact that these peaks appeared exclusively on Mondays and Tuesday, which may be nothing but an insignificant coincidence.

Another interesting feature of this Teltowkanal sampling is that it allowed showing something often unmentioned in environmental chemistry studies: the influence of climate conditions on the final analytical results. Frequently the climate conditions, before and during the sampling, are neither provided nor taken into account during results interpretation. As shown in Figure 111, the rainfall seems to influence somehow the final caffeine concentrations: days with intense rainfall are accompanied by high caffeine concentration downstream, whereas upstream concentrations peaks only occurred in days with none or very little precipitation.

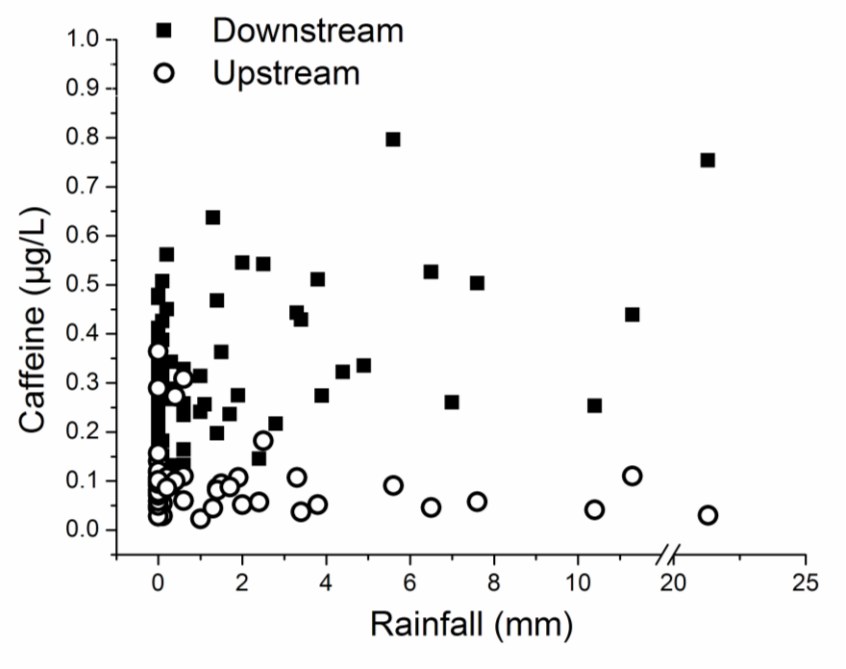

Figure 111. Caffeine concentrations variation in Teltowkanal, downstream (bold squares) and upstream (open circles) of the STP Wassmannsdorf discharging point and the rainfall (x-axis) registered in the day where the sample were collected.

As most of Berlin has a combined system for collecting wastewater and run-off rain waters,[363] it is reasonable that in days with intense rainfall the STP, reaching its treatment capacity, discharges untreated combined-wastewaters into the channel. This topic is discussed further on afterward using a superior example of the rainfall influence on caffeine concentration using the model Landwehrkanal (11.1.4 - Landwehrkanal, page 245).

11.1.4. Landwehrkanal (LWK)

Within-day variations on caffeine concentrations were studied using samples from Landwehrkanal, which contrary to the Teltowkanal does not have flow input from STP effluents. A grab sample was collected every morning (8.00h – 11.00h) and every evening (20.00h – 24.00h) at a single sampling spot: Planufer, near the Urbanhafen (52.495121° N13.41082° E35 m). The sampling was performed daily from the 9th November 2009 until the 16th December 2010, unremitting and including weekend days.

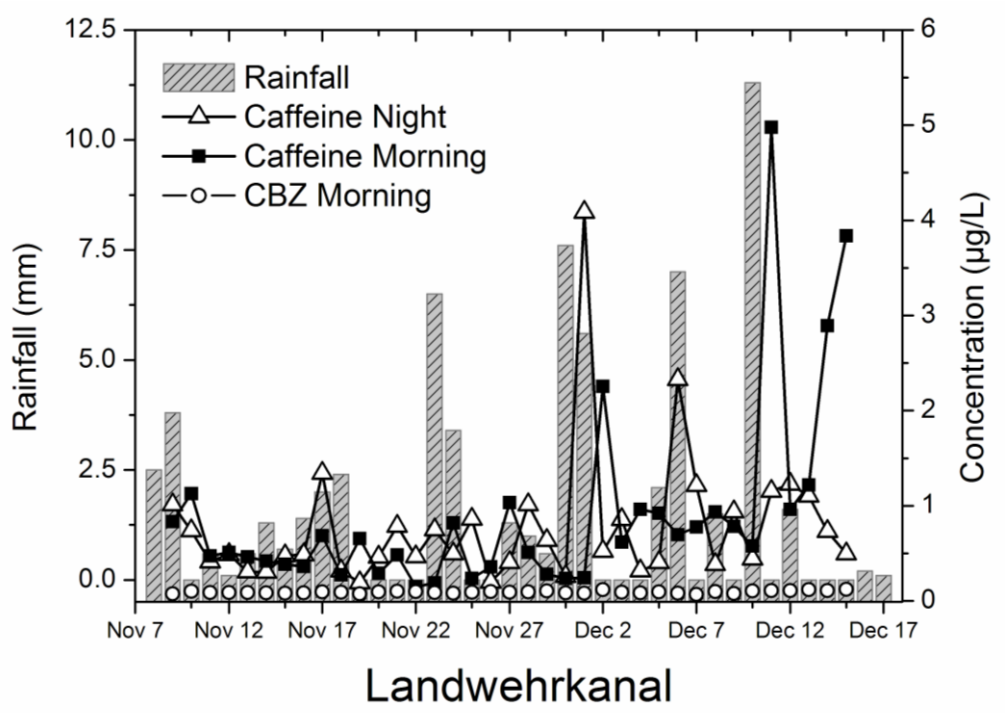

Figure 112. Caffeine concentrations in Landwehrkanal – within day variation. Carbamazepine (CBZ) concentrations found in the morning samples are also included. The bars represent the daily rainfall in millimetres (mm).

The caffeine concentrations' mean in the morning (0.904 ± 1.014) is slightly higher than at night (0.773 ± 0.700), but the difference is not statistically significant (paired sample *t*-test, at 0.05 level and 36 DOF). Interesting to observe in Figure 112 is the steadiness of the caffeine concentration in the morning and at night until the end of November.

Different is the picture after the beginning of December, when several caffeine concentration peaks occur, either in the morning or in the evening. The graph in Figure 112 also includes the rainfall amount on each day and a connection seems to exist between the high amount of rainfall[n] and the caffeine peak during December. The houses' wastewaters and run-off rainwater (from the buildings) flow into a unique system in the central neighbourhoods of Berlin; when the volume of this combined wastewater arriving into the STP exceeds their capacity, as in case of intense rainfall, a part of this combined wastewater is deviated untreated into the Landwehrkanal and the Spree.[363] This explains the high caffeine concentrations observed after intense rainfall in December but leaves a question open: why did the concentrations not increase after intense rainfall on the 23rd and the 24th of November? A possible explanation for such a nonconforming observation is the

[n] *The daily rainfall was calculated from 5.55 a.m. – 5.50 a.m. of the next day.*

strong winds observed on that day. On those two days, wind from southwest and west, respectively, with 35 km/h were registered, while on the remaining sampling days the maximal speed ever registered was 20 km/h. Considering that the samples were always collected on the same spot, the strong winds can explain why in those particular days caffeine concentration were not as odd as the ones observed in December after the same rainfall amounts.

The message to take from these results is: if one took a grab sample on the morning of the 1st of December or the next morning, the results will be completely different: 0.245 µg/L and 2.26 µg/L caffeine, respectively. Thus, stressing the need to produce on-line monitoring systems for quantifying particular analytes (as caffeine) and therefore detect contamination events. A comprehensive study about this combined sewers overflows to surface waters was published in 2006 by the Swiss Federal Office for Agriculture (Agroscope), Buerge *et al.*, stressing that caffeine is a "gold-marker" to determine the level of surface waters' contamination after intense rainfall in Switzerland.[68]

Figure 113. Detailed view of the Landwehrkanal (Berlin) showing the combined rainwater-wastewater discharging point (bold triangles) in cases of storm and intense rainfall. The sampling spot is indicated by the grey-arrow.

Another interesting feature arising from Figure 112 is the low and fairly constant carbamazepine concentration found in the samples. Its concentrations vary from 0.070 µg/L to 0.125 µg/L, a very short range when compared with the one found in the Teltowkanal samples (downstream of STP: 0.080 µg/L – 1.76 µg/L) and caffeine itself in Landwehrkanal. Then, it is very likely that a source of non-treated wastewater is present somewhere in the Landwehrkanal.

Despite the already mentioned occasional high concentrations of caffeine, a constant input is likely to be present considering the "steady-state" caffeine concentrations. They are often much higher than the ones found downstream of the STP in the Teltowkanal. Whether this is due to some leakages on the wastewater system or some direct wastewater streaming into the channel remains uncertain. An attempt to identify some direct wastewater flows was done by organizing a sampling campaign along the Landwehrkanal on the 12th of December.

The sampling was performed on the 12th of December 2009 and the climate conditions (daily average) are summarised in Table 28. During the sampling campaign (15.10h first sample – 16.40h the last one) it was snowing and raining with temperatures from 0 °C to 1°C, humidity 100% and wind from Northwest. The samples were collected from west to east as indicated in Figure 114, from sample 1 to sample 12, in duplicate.

Table 28. Climate condition on the 12th of December 2009 registered in Berlin-Tempelhof by the Deutscher Wetterdienst.[362]

Day averages

Temperature (°C)			Relative Humidity [%]	Wind speed [m/sec]	Sunshine [hours]	Rainfall [mm]	Atmosp. Pressure [mbar]
Min.	Med.	Max.					
-1.3	1.3	3.2	93.4	6.1	0	1.6	1020.7

Sampling period

Time	Temperature [°C]	Wind speed [m/sec]	Rainfall [mm]
14.00h	2.4	7	0.3
15.00h	2.6	4	0.3
16.00h	1.1	17	1.9
17.00h	1.3	22	0.5

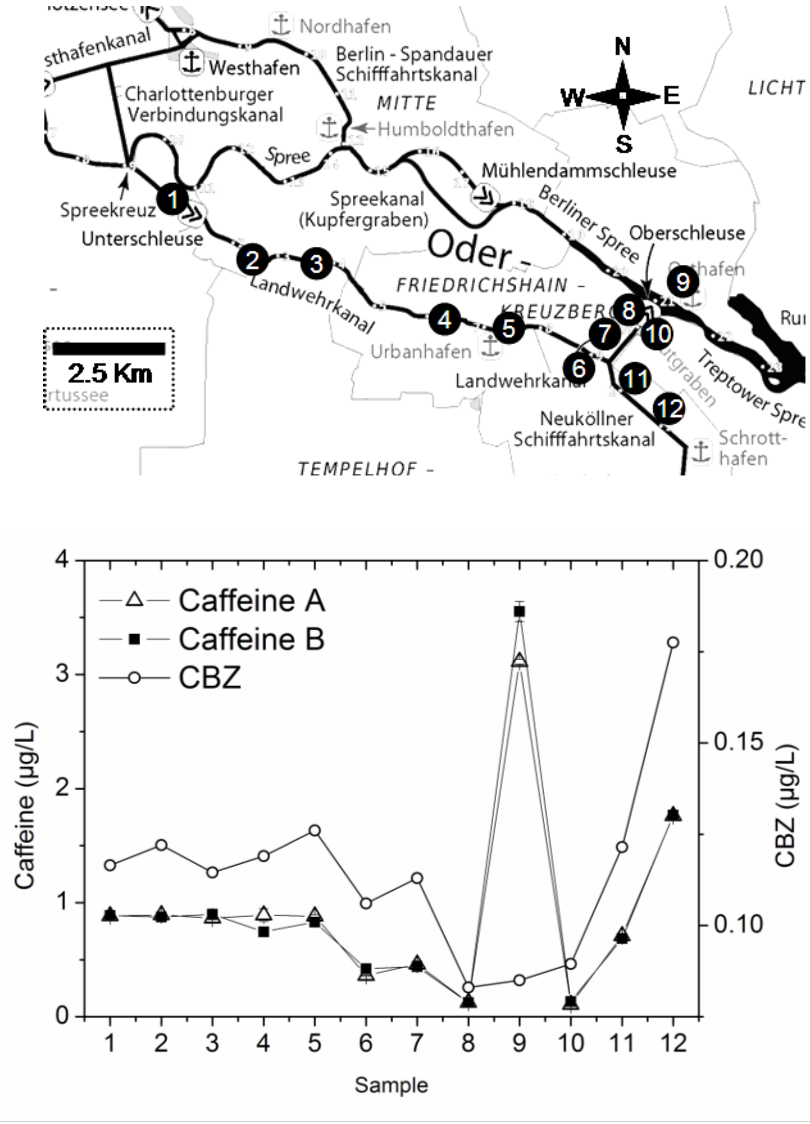

Figure 114. Landwehrkanal sampling on the 12th of December 2009. Twelve samples were collected at the spots indicated by the black spheres on the map, with the respective sample number inside. The caffeine concentrations are presented on the graph (reads on the left y-axis) as well as the carbamazepine (CBZ) ones (reads on the right y-axis). Per spot two different samples were collected and the results are represented by Caffeine A and Caffeine B in the graph. Remark: The left y-axis (Caffeine) has a different scale than the right one (CBZ, carbamazepine) to allow a better comparison between the concentration trends of both compounds.

From sample one (1) to sample five (5), alike caffeine concentrations were found in all samples. The lower concentrations found in sample six (6) and seven (7) are most likely caused by the confluence of the Neukoellner Kanal and the Landwehrkanal branch which connects it to the Spree. The Neukoellner kanal (0.30 m^3/s) stream to the Landwehrkanal (1.03 m^3/s) as it does the branch (0.73 m^3/s) connecting it to the Spree (~ 8.16 m^3/s at that spot), causing a dilution effect in the mentioned sampling spots. Sample nine (9) was collected at the confluence of Landwehrkanal and Spree and shows a very interesting result: caffeine

concentration is very high while carbamazepine stays steady. These results originate another sampling campaign involving the water police of Berlin and such results are not presented here. Near sampling spot 9 very high concentration of caffeine where found when compared with the other Spree samples. The area is well known by intense after-hours activities with the most popular Berlin techno clubs being located directly on the Spree in the area around that sampling spot. Additionally, some boats working as restaurants and bars are around the area and might as well contribute to these findings. Samples 11 and 12 show already the increasing trend on both compounds (caffeine and carbamazepine) concentration caused by the Teltowkanal stream (3.00 m^3/s) into the Neukoellner Kanal (0.30 m^3/s).

The question whether there are non-declared wastewater discharge into the Landwehrkanal or some leakage in the combined wastewater system is still to be answered. But what is clear from the results is that from one day to another, or even from the morning to the night, the Landwehrkanal can show a completely different level of contamination and caffeine is a very helpful indicator of it.

A curiosity: Although no statistical significant differences exist between the days, Tuesday was the day with the highest caffeine mean concentration (0.73 ± 0.34 µg/L) and Sunday with the lowest (0.60 ± 0.36 µg/L). This can easily be explain by some consumption habits, being Monday a day where people probably ingest more caffeine-containing beverages than they do on Saturdays.

11.2. Drinking water

Several drinking water samples (33) were collected in different neighbourhoods in Berlin: one sample from Adlershof, Altglienicke, Charlottenburg, Koenigs Wusterhausen, Marzahn, Mitte, Neukoeln, Pankow, Reinickendorf, Rudow, Spandau, Steglitz, Tempelhof, Treptower Park, Zehlendorf; two samples from Koepenick, Schoeneberg, Wedding; and three samples from Prenzlauer Berg, Kreuzberg, Friedrichshain and Lichtenberg. The samples were collected by co-workers of the BAM on the 25th of November 2009 and analysed the next day. Caffeine was under the 0.005 µg/L in most of the samples except the ones from Kreuzberg (0.016 µg/L ± 0.008; 0.012 µg/L ± 0.004; 0.026 µg/L ± 0.008), Tempelhof (0.018 µg/L ± 0.008), Neukoelln (0.013 µg/L ± 0.003), Schoeneberg (0.009 µg/L ± 0.004), Wedding (0.016 µg/L ± 0.008) and Koenigs Wusterhausen (0.056 µg/L ± 0.009). The drinking water distributed to the neighbourhoods of Kreuzberg, Tempelhof, Neukoeln and Schoenberg has the same origin, which justifies similar concentration of caffeine in drinking water. The same is valid for Wedding which is supplied by the water from Tegeler See. Koenigs Wusterhausen receives waters from a treatment plant on the Mueggelsee.

The samples were analysed in triplicate and on two different days. Nevertheless the results should be regarded with care as just one sample per spot was taken and further samplings are needed to conclude about the presence of caffeine in Berlin drinking waters.

Several drinking water samples from the BAM tap (Adlershof) were collected in different dates along 2008 and 2009, none of them ever testing positive for caffeine.

12. Conclusions and outlook

12.1. Conclusions

Caffeine and coprostanol were quantified in several water samples in Berlin. Analytical methods for caffeine quantitation are widely available but none has the high-throughput, cost-effectiveness and sensitivity of the new developed immunoassay.

The new caffeine immunoassay was established using a commercial monoclonal antibody and a *de novo* synthesised tracer. Sixty-six samples can be analysed per plate within 2 hours, making the assay suitable for high-throughput routine caffeine screening. A LOD of 0.001 µg/L could be experimentally verified and concentrations above 0.025 µg/L (LOQ) can be quantified with a relative concentration error below 20%.

The high selectivity of the chosen antibody allowed caffeine quantitation not only in surface water samples but also in several beverages, shampoos, caffeine tablets, and human saliva. The antibody's low cross-reactivity towards caffeine's major metabolite, paraxanthine (0.08%), concedes for further uses of the assay, particularly as a tool for single-point caffeine measurements in clinical chemistry, doping control, veterinary medicine and cognitive studies.

The coupling ratio of the enzyme tracer was studied in detail and it was shown that it plays a minor role on the overall sensitivity of the assay. More systematic studies are needed to draw a definite conclusion regarding the influence of the tracer coupling ratios in hapten-based immunoassays.

Matrix effects, mainly caused by calcium concentration variability and salinity differences, could be minimised by using a high salinity buffer with an electric conductivity of around 15 mS/cm. When selecting an appropriate assay buffer, the analyte matrix should be the major concern. In the case of surface waters, buffers with high salinity are strongly recommended in order to counterbalance salinity differences between samples, which hinder the sample-to-sample repeatability and deleteriously affect the accuracy of the assay.

Splitting the assay into two short calibration ranges ensured higher precision for both of them, when compared with the classic logarithmic spacing between standards, usually used for immunoassays. Moreover, extending this practice of reducing the calibration range is very likely to increase accuracy in immunoassays used in environmental chemistry.

Contrary to caffeine, anti-coprostanol antibodies are neither commercially available nor described in scientific literature. Attempts to obtain an anti-coprostanol monoclonal antibody were made, with relevant conclusions coming out of the immunization process as well as the hybridoma screening method.

As hypothesised, the C3-hydroxyl group in stanol-related compounds was essential for the antibody recognition. Therefore, future strategies for raising antibodies against such molecules should leave free the C3-hydroxyl group in the final immunogen. Within the timeline of this thesis, similar results were obtained by others using a similar hapten – lithocholic acid, corroborating this statement.[229] The side chain on C17 should not, however, be neglected. The polyclonal antiserum showed clearly a difference between coprostanol and isolithocholic acid recognition by the antibodies.

Although isolithocholic acid is an endogenous molecule (self), it induced a strong secondary immune response in mice. The first polyclonal antiserum against isolithocholic was obtained and it showed very low cross-reactivities against its isomer lithocholic acid. Lithocholic acid was recently recognised as a key compound involved in colon cancer.cancer.[371] Clinical data for its isomer isolithocholic acid are still to be produced. Should an assay be required in the near future, the obtained polyclonal serum could possibly serve the purpose.

An unexpected finding of this thesis is that the immune response in a mouse could be monitored non-invasively by using the animal faeces. Aqueous extracts of mouse faeces provided equivalent results to the ones obtained from serum samples, except for the absolute IgG titre. Collecting faeces instead of sampling blood allows for a daily monitoring of the immunization progress in mice without hurting or even touching the animals. In the 3R concept (replacement, reduction, refinement) of animal protection,[347,348] this represents a “refinement” with the potential to improve laboratory animal welfare considerably.

A chromatographic reference method was also developed for coprostanol and structurally related compounds in water samples. The ionisation of coprostanol was possible by using Atmospheric Pressure Chemical Ionisation (APCI) prior to mass spectrometric detection. Coprostanol could be quantified in surface water samples above 0.1 µg/L and after a sample concentration step. The samples were concentrated using a simple and inexpensive developed method: dispersive-liquid-liquid microextraction. Being a liquid-liquid based extraction, samples did not need to be previously filtered, which is a significant advantage for non-polar compounds like coprostanol, known to adsorb to particulate and colloidal matter. Furthermore, the method could easily be extended to coprostanol extraction in sediment and soils, a common application that still lacks a straightforward extraction method.

The results of the surface water's monitoring campaigns showed a very broad range of analytes' concentration. Their values varied from day to day and even according to the time of the day at which the sample were collected (morning or evening). Climate conditions, mainly rainfall, also had an influence on the contamination status of surface waters, thus stressing the need to use on-line sensors for continuous measurements. The proposed caffeine immunoassay has a great potential to construct a prospective on-line immunosensor.

12.2. Outlook

Future strategies for coprostanol *in vivo* immunization should consider 1) the use of a completely new (synthetic) hapten, containing the same side chain; or 2) immunizations using a liposome-based formulation. This last option seems indeed very promising: past immunizations using cholesterol liposomes (containing lipid A) proved very successful in murine models.[214] In addition, there is no need to look for a mimetic hapten, since coprostanol can be directly incorporated in the liposome.

Methods for high-throughput screening of hybridomas are needed. The available methodologies are labour-intensive, time-consuming, costly, have low sensitivity and high risks of losing the desired hybridoma-secreting clone. The screening is indeed one of the recognised process bottlenecks together with the cell fusion technology from the 1970s.[234] Could not B cells be immortalised by other means than somatic fusion? Some viruses and parasites are known for effectively invading immune cells and to put their cell machinery working *ad aeternum*.[372] The parasite *Theileria parva* has been recognised to grant quasi immortality to mast cells.[373,374] Could this parasite also invade B cells to produce continuous secreting cell lines?

13. Appendices

13.1. Appendix I – Detailed mechanism of the conjugation using a carbodiimide

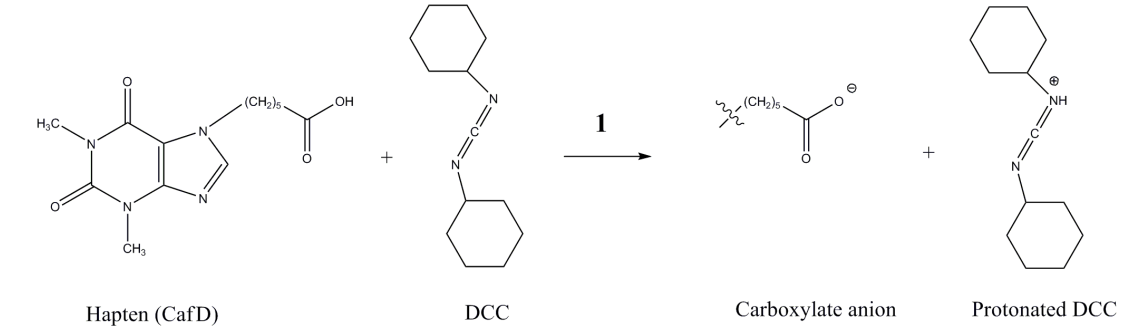

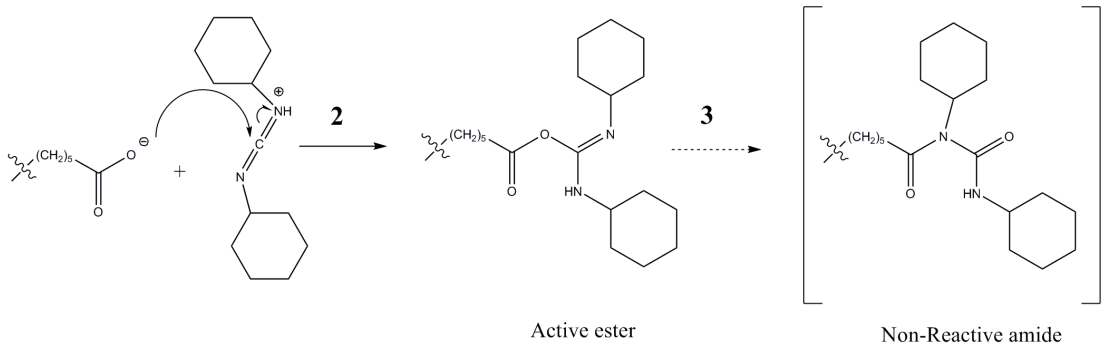

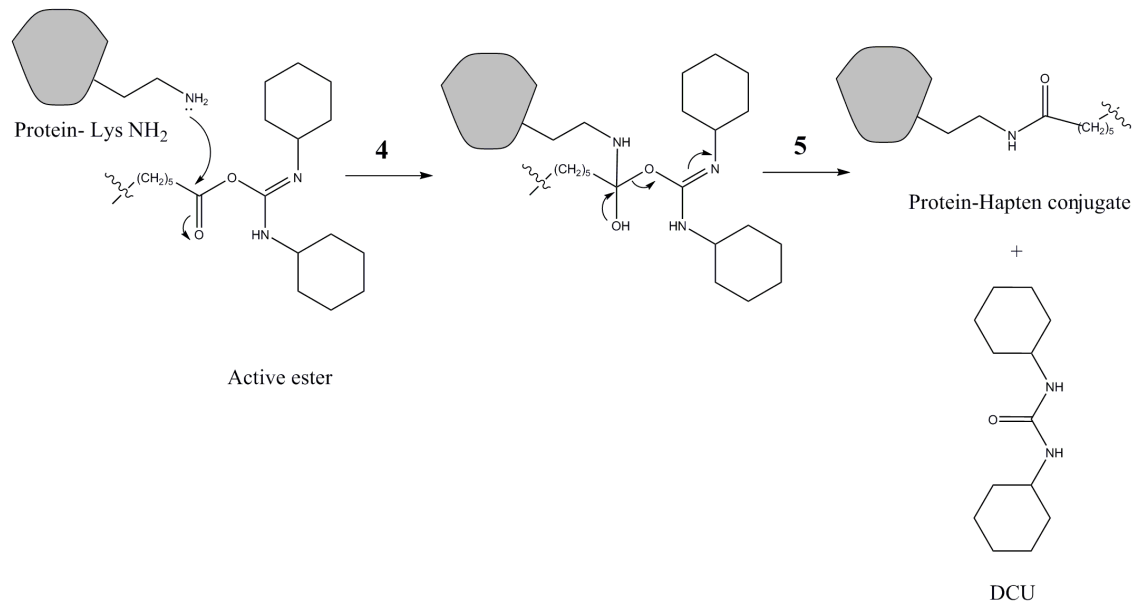

1. *DCC (N,N'-dicyclohexylcarbodiimide) reacts with the hapten carboxylic acid groups to form a carboxylate anion by proton transfer to the nitrogen of DCC;* ***2.*** *The carboylate anion adds to the protonated DCC forming an active ester. This active ester is very unstable and can originate several products, including the original acid when water is present;* ***3.*** *a non-reactive N-acylurea or even react with another hapten carboxylic group to give an acid anhydride which can react further to give the desired amide (not shown).* ***4.*** *The carboxyl carbon of the active ester will then be attack by the nucleophile nitrogen from a lysine residue of the protein producing the covalent bond 5. between the hapten and the protein with the elimination of dicyclohexylurea (DCU).*

13.2. Appendix II – A brief Immunological Glossary

Adapted from several textbooks[163,194,196,199,202,375]

Adjuvant – a substance that non-specifically enhances the immune response to an antigen.

Affinity – a measure of the binding strength between an antigenic determinant (epitope) and its antibody binding side. The stronger the binding, the higher the affinity. Antibodies produced in a secondary (memory) immune response usually present higher affinities than those of the primary response.

Affinity maturation – the increase in average antibody affinity frequently seen during a secondary immune response.

Allelic exclusion – occurs when the use of a gene from the maternal or paternal chromosome prevents the use of the other. This phenomenon is observed with antibody and T cell receptor genes.

Antibody – a molecule produced in response to antigen that combines specifically with the antigen that induced its formation.

Antigen – a molecule that generates an immunological response and reacts with antibody and the specific receptor on T and B cells

Antigen presentation – the process by which certain cells in the body (antigen-presenting cells) express antigen on their cell surfaces in a form recognizable by lymphocytes.

Antigen processing – the conversion of an antigen into a form in which it can be recognise by lymphocytes.

Autoimmunity – immune recognition and reaction against the individual's own cells/tissues.

Avidity – the functional combining strength of an antibody with its antigen related to both the affinity of the reaction between the epitopes and paratopes, and the valences of the antibody and antigen.

B cells – lymphocytes that develop in the bone marrow in adults and produce antibodies.

C domains – the constant domains of antibody and the T cell receptor. These domains do not contribute to the antigen binding.

Carrier – an immunogenic molecule or part of a molecule that is recognised by T cells in an antibody response. It is usually used coupled to hapten to induce immune response toward the hapten.

Central lymphoid organs – lymphoid organs primarily involved in the production and maturation of immune cells. They include the bone marrow and the thymus.

Clonal deletion – the loss of lymphocytes of a particular specificity due mainly to contact with self-antigens.

Clone – a group of genetically identical cells or organisms descended from a single common ancestor.

Clone selection principal – the prevalent theory stating that the specificity and diversity of an immune response are the result of selection by antigen of specifically reactive clones from a large repertoire of preformed lymphocytes, each with individual specificities.

Conjugate – A reagent that is formed by covalently coupling two molecules together, such as a hapten coupled to a carrier protein as BSA.

Constant regions – The relatively invariable part of immunoglobulin heavy and light chains.

Cross-reactivity – the ability of an antibody, specific for one antigen, to react with a slightly different antigen.

Epitope – the part of an antigen that contacts the antigen binding site of an antibody (paratope). Small molecules (haptens) are believed to have a single epitope.

Fab – the part of an antibody molecule that contains the antigen-combining site consisting of light chain and part of the heavy chain; it is produced by enzymatic digestion with papain, which cuts at the hinge region.

Fc – the portion of an antibody that is responsible for binding to antibody receptor in cells and activation of the complement (in vivo) and binding to the microtitre plate in immunoassays.

Freund's adjuvant – is a non-specific stimulator of the immune response. When mixed with an antigen it helps to deposit or sequester the injected material. It causes a dramatic increase in the resultant antibody response. Freund's Complete Adjuvant is a water-in-oil emulsion and killed mycobacteria, used for initial injections of antigen into animals to enhance the immune response, while the incomplete adjuvant does not contain mycobacteria, and is used for further boosts.

Hapten – a small molecule that can act as an epitope, but is incapable by itself of eliciting an antibody response unless bound to a carrier protein or large antigenic molecule.

Hybridoma – cell line created in vitro by fusing two different cell types, usually lymphocytes with a tumour cell.

Hypervariable region – the most variable areas of the V domain of immunoglobulins. These regions are clustered at the distal portion of the V domain and contribute to the antigen-binding site.

Immunogenic – having the ability to evoke B cell and/or T cell mediated immune reaction.

Immunoglobulins – the serum antibodies, including IgG, IgM, IgA, IgE and IgD.

Induced fit – a description of the way in which an antigen can alter the normal tertiary structure of the binding site on a receptor following binding, by displacing amino acids.

Lipid A – is a lipid component of an endotoxin held responsible for toxicity of Gram-negative bacteria. It is used as an adjuvant in immunizations, mostly in liposome-based formulations.

Lysosyme – an enzyme secreted by mononuclear phagocytes that hydrolyses bonds present in bacterial cells walls.

Macrophage – a large and versatile immune cell derived from monocytes, which is responsible for phagocytosis of microbes and immuno-complexes.

Myeloma – a lymphoma produced from cells of the B cell lineage that can invade the bone.

Paratope – the antibody binding site where the antigen binds. It is the antibody-combining site to the antigen epitope.

Plasma cell – an antibody-producing B cell that has reached the end of its differentiation pathway.

Primary lymphoid tissues – lymphoid organs in which lymphocytes complete their initial maturation steps; they include the foetal liver, adult bone marrow and thymus.

Primary response – the immune response (cellular or humoral) following an initial encounter with a particular antigen.

Recombination – a process by which genetic information is rearranged during meiosis; this process also occurs during the somatic rearrangements of DNS that occur in the formation of genes encoding antibody molecules and T cell receptors.

Repertoire – set of cells or molecules in the immune systems.

Secondary Lymphoid organs – organs where the immune cells interact with the antigenic stimulus, thus initiating adaptive immune responses (e.g. tonsils, spleen, lymphoid nodules, digestive system).

Secondary response – the immune response that follow a second or subsequent encounter with a particular antigen.

Somatic mutation – a process occurring during B cell maturation and affecting the antibody gene region that permits refinement of antibody specificity.

T cells – lymphocytes that differentiate primary in the thymus and are central to the control and development of immune responses.

Tolerance – a state of specific immunological unresponsiveness.

14. Acknowledgements

I would like to express my debt and my gratitude to the many colleagues and friends who have helped me, in fruitful discussions, lab assistance and many other ways. Their contributions have varied widely. In some instances, they have been of direct assistance in particular experiments, but in other cases they have been stimulating in a more indirect way, often over a period of years, influencing my general thinking and helping me to clarify my views. Thank you for making this work possible.

First of all, I would like to express my gratitude to the BAM Federal Institute for Materials Research and Testing for the opportunity I was given, the financial support, the excellent research facilities but, above all, for the freedom I could enjoy in my research work.

I am indebted to Rudolf Schneider and Michael Weller for their continuous support, fruitful discussions and encouragement, which were invaluable for the successful completion of this thesis. Thank you for sending me miles away and taking me back to earth on a reasonable time. Ulrich Panne is gratefully acknowledged for his long-lasting support, enthusiasm and for his cheerful words in the right moments.

This project would never come to an end without the direct help and advice from experts in fields which were completely unknown to me when I started this journey. I express my profound gratitude to Franziska Emmerling (BAM) for the x-ray measurements, crystallography tips and fruitful discussion; Ana Descalzo-Lopez (BAM/ UC Madrid) for the organic synthesis advice, patience and motivation; Dietmar Pfeifer (BAM) for the NMR measurements; Detlef Lück (BAM) for skilful characterisation of the sample matrix; Wolfram Bremser (BAM) for his dazzling advice in statistics; Sebastian Hein (BAM) for the DSC measurements. Christine Lenz and Jörg Schenk (Hybrotec) are acknowledged for the outstanding cooperation during the antibodies production. I greatly appreciated the discussions with Elise Siegert (Charité) and Diana Aga (University at Buffalo, SUNY) and I thank them for their time.

My sincere thanks go to many colleagues for scientific discussions, advice and direct assistance in the lab. Their contributions, ideas and suggestions were greatly appreciated. Kristin Petsch and Sabine Flemig, who were often my third and fourth hand in the lab, without their assistances, I could not have managed the experimental work. Andreas Lehmann is acknowledged for his advice on the LC-MS/MS, Dagmar Schütt and Cornelia Brünn for their introduction in the ELISA world, Nadine Hoffmann for her valuable help in the sterol extraction methods and Denise Thurmann for helping me during the ELISA validation.

I am deeply grateful to my PhD colleagues Astrid Walter, Arnold Bahlmann, Friedmar Delißen and Jörg Polte for hearing me, giving me inputs and sharing my daily frustrations and successes.

My gratefulness to my students Martin Nichczynski, Dennis Pleiner and Heike Pecher for their commitment and painstaking contribution to this project. I would take the opportunity to apologise for some of the frustration I might have infringed on them.

Juliane Schaefer, Christin Heinrich and Anka Kohl are acknowledged for managing, on a short time, the (apparently) impossible.

I would like to address my gratitude to the many colleagues and friends who read all or parts of the manuscript and suggested improvements. I would mention in particular Rudolf Schneider, Michael Weller, Julien Sialelli, Elise Siegert, Julia Grandke, Ana Descalzo-Lopez, Astrid Walter, Valeria Zazzu and Wolfram Bremser. None of the above-named persons can be held responsible for mistakes, misrepresentation of the facts, misspellings or any other failings in this work, for which I accept alone the responsibility.

Bernd Brunner is warmly acknowledged for stimulating discussions and non-scientific reading suggestions.

My sincere thanks to the many friends who directly supported me along this journey. A special thanks to Adriana Osório, Ana Descalzo-Lopez, Anita Osorio-

Choi, Astrid Walter, Bernd Brunner, Bill Lourenco, Catarina Costa, Catarina Tacanho, Célia Silva, Dana Schloeffel, Duarte Nóbrega, Elise Siegert, Eloi Prat i Morgades, Friedmar Delißen, Gonçalo Sousa Pinto, Horst Droste, José Eduardo Lima, José Liberal, Julien Sialelli, Kitty Solaris, Maria de Fatima Alpendurada, Matthias Nikolaidis, Matty-Ben Urmersbach, Michal Perry, Nuno Che, Olivia Funnel, Palmetto, Paulo Cravo, Rodrigo Leite de Oliveira, Rudolf Schneider, Sónia Queirós, and “mamma” Valeria Zazzu.

Maria de Fatima Alpendurada, for introducing me to science, providing me with her wise advice and sharing her unconventional view of the world.

Last but by no means least, I would like to thank my family and close relatives for general education and the opportunity to start and pursue a career in science.

I am particularly indebted to my parents for their never-ending encouragement and for teaching me what love means. A very special thank to my beloved sister Pinó for her support and craziness. My aunts Paula and Maria are specially acknowledged for the motivating words, supporting emails and long-lasting meaningless phone calls.

I am aware of the fact that there are many more and these words cannot express the gratitude and respect I feel for all of those.

Yours, João

15. Literature

1. EPA (1999). *25 years of safe drinking water act: history and trends*. EPA 816-R-99-007, Office of Water – U.S. Environmental Protection Agency.

2. EPA (2000). *Drinking water: past, present and future*. EPA 816-F-00-002, Office of water – U.S. Environmental Protection Agency.

3. EPA (2000). *The history of drinking water treatment*. EPA-816-F-00-006, Office of Water – U.S. Environmental Protection Agency.

4. Johnson S. (2006). *The Ghost Map: The Story of London's Most Terrifying Epidemic – and How it Changed Science, Cities and the Modern World*. Riverhead books, New York.

5. Newsom S.W.B. (2006). *Pioneers in infection control: John Snow, Henry Whitehead, the Broad Street pump, and the beginnings of geographical epidemiology*. Journal of Hospital Infection 64: pp 210-216.

6. Koch T., Denike K. (2009). *Crediting his critics' concerns: Remaking John Snow's map of Broad Street cholera, 1854*. Social Science & Medicine 69: pp 1246-1251.

7. Bates A.J. (2000). *Water as consumed and its impact on the consumer – do we understand the variables?* Food and Chemical Toxicology 38: pp S29-S36.

8. Shapin S. (2006). *Sick City – maps and mortality in the time of cholera,* The New Yorker, November 6th, page 24.

9. Scherf H., Winkle S. (2005). *Heine über die Cholera 1832 in Paris und Börnes Choleraphobie*. Hamburger Ärzteblatt pp 8-11.

10. Okun D.A. (1999). *Identifying Future Drinking Water Contaminants.* In: *Historical Overview of Drinking Water Contaminants and Public Water Utilities, pp* 22-32, National Academy of Sciences, Washington D.C.

11. Wargo J. (1998). *Our children's toxic legacy – How science and law fail to protect us from pesticides,* 2nd ed. Yale University Press, New Haven.

12. Engelhardt H. (2004). *One century of liquid chromatography from Tswett's columns to modem high speed and high performance separations*. Journal of Chromatography B: 800: pp 3-6.

13. Tswett M. (1906). *On a New Category of Adsorption Phenomena and their Application to Biochemical Analysis (translation from the Russian). The original paper is hardly found and the English translation has been published by G. Hesse and H. Weil in 1954 (Woelm Mitteilungen AL8, M. Woelm, Eschwege)*. The Proceedings of the Warsaw Society of Natural Sciences, Sect XIV (6).

14. Sakodyns K. (1972). The Life and Scientific Works of Michael Tswett. Journal of Chromatography A 73: pp 303-360.

15. Kirkland J.J. (1971). *Modern Practice of Liquid Chromatography,* John Wiley & Sons, New York.

16. Bartle K.D., Myers P. (2002). *History of gas chromatography*. Trac – Trends in Analytical Chemistry, 21: pp 547-557.

17. James A.T., Martin A.J.P. (1954). *Gas-Liquid Chromatography – the Separation, Micro-Estimation and Identification of Hydrocarbons, Alkyl Halides, Alcohols, Aldehydes, Ketones, Esters and Ethers*. Biochemical Journal 57: pp R5-R6.

18. Glaze W.H., Peyton G.R., Saleh F.Y., Huang F.Y. (1979). *Analysis of Disinfection By-Products in Water and Waste-Water*. International Journal of Environmental Analytical Chemistry 7: pp 143-160.

19. Cantor K.P., Lynch C.F., Hildesheim M.E., Dosemeci M., Lubin J., Alavanja M., Craun G. (1999). *Drinking water source and chlorination byproducts in Iowa. III. Risk of brain cancer*. American Journal of Epidemiology 150: pp 552-560.

20. Cantor K.P. (1997). *Drinking water and cancer*. Cancer Causes & Control 8: pp 292-308.

21. Waller K., Swan S.H., DeLorenze G., Hopkins B. (1998). *Trihalomethanes in drinking water and spontaneous abortion*. Epidemiology 9: pp 134-140.

22. Nieuwenhuijsen M.J., Toledano M.B., Eaton N.E., Fawell J., Elliott P. (2000). *Chlorination disinfection byproducts in water and their association with adverse reproductive outcomes: a review*. Occupational and Environmental Medicine 57: pp 73-85.

23. Michaud J. (2010). *Eighty-Five from the Archive: Rachel Carson (containing the original text from "Silent Spring" published in the issue of June 16, 1962)*. The New Yorker, April 22nd.

24. Carson R. (2000 (first edition from 1962)). *Silent Spring* 13th ed. *(The first edition was published in 1962 by Houghton Mifflin).* Penguin Classics, London.

25. Sumpter J.P. (2005). *Endocrine disrupters in the aquatic environment: An overview*. Acta Hydrochimica et Hydrobiologica 33: pp 9-16.

26. White R., Jobling S., Hoare S.A., Sumpter J.P., Parker M.G. (1994). *Environmentally Persistent Alkylphenolic Compounds Are Estrogenic*. Endocrinology 135: pp 175-182.

27. Mills L.J., Chichester C. (2005). *Review of evidence: Are endocrine-disrupting chemicals in the aquatic environment impacting fish populations?* Science of the Total Environment 343: pp 1-34.

28. Black D.A., Howell W.M. (1979). *North-American Mosquitofish, Gambusia affinis – Unique Case in Sex-Chromosome Evolution*. Copeia pp 509-513.

29. Howell W.M., Black D.A., Bortone S.A. (1980). *Abnormal Expression of Secondary Sex Characters in a Population of Mosquitofish, Gambusia affinis holbrooki – Evidence for Environmentally-Induced Masculinization*. Copeia pp 676-681.

30. Parks L.G., Lambright C.S., Orlando E.F., Guillette L.J., Ankley G.T., Gray L.E. (2001). *Masculinization of female mosquitofish in kraft mill effluent-contaminated Fenholloway River water is associated with androgen receptor agonist activity*. Toxicological Sciences 62: pp 257-267.

31. Durhan E.J., Lambright C., Wilson V., Butterworth B.C., Kuehl D.W., Orlando E.E., Guillette L.J., Gray L.E., Ankley G.T. (2002). *Evaluation of androstenedione as an androgenic component of river water downstream of a pulp and paper mill effluent*. Environmental Toxicology and Chemistry 21: pp 1973-1976.

32. Guillette L.J., Crain D.A., Gunderson M.P., Kools S.A.E., Milnes M.R., Orlando E.F., Rooney A.A., Woodward A.R. (2000). *Alligators and endocrine disrupting contaminants: A current perspective*. American Zoologist 40: pp 438-452.

33. Hignite C., Azarnoff D.L. (1977). *Drugs and Drug Metabolites as Environmental Contaminants – Chlorophenoxyisobutyrate and Salicylic-Acid in Sewage Water Effluent*. Life Sciences 20: pp 337-341.

34. Richardson M.L., Waggott A. (1981). *Occurrence and Fate of Certain Triphenylmethane Blue Dyestuffs in the Aquatic Environment*. Ecotoxicology and Environmental Safety 5: pp 424-436.

35. Richardson M.L., Bowron J.M. (1985). *The Fate of Pharmaceutical Chemicals in the Aquatic Environment*. Journal of Pharmacy and Pharmacology 37: pp 1-12.

36. Heberer T., Stan H.J. (1996). Determination of clofibric acid and N-(phenylsulfonyl)-sarcosine in sewage, river and drinking water. Proceddings of the 26th International Symposium on Environmental Analytical Chemistry, pp. 113-123. Vienna, Austria. Published by Gordon and Breach Science Publishers, New York.

37. Heberer T., Stan H.J. (1997). *Determination of clofibric acid and N-(phenylsulfonyl)-sarcosine in sewage, river and drinking water*. International Journal of Environmental Analytical Chemistry 67: pp 113-123.

38. Ternes T.A. (1998). *Occurrence of drugs in German sewage treatment plants and rivers*. Water Research 32: pp 3245-3260.

39. Kolpin D.W., Furlong E.T., Meyer M.T., Thurman E.M., Zaugg S.D., Barber L.B., Buxton H.T. (2002). *Pharmaceuticals, hormones, and other organic wastewater contaminants in US streams, 1999-2000: A national reconnaissance*. Environmental Science & Technology 36: pp 1202-1211.

40. ISI Web of Knowledge™ (2010). Thomson Reuters.

41. Zühlke S., Dünnbier U., Heberer T. (2007). *Investigation of the behavior and metabolism of pharmaceutical residues during purification of contaminated ground water used for drinking water supply*. Chemosphere 69: pp 1673-1680.

42. Wilken R.D., Ternes T.A., Heberer T. (2000). *Pharmaceuticals in sewage, surface and drinking water in Germany*. Security of Public Water Supplies 66: pp 227-240.

43. Reddersen K., Heberer T., Dünnbier U. (2002). *Identification and significance of phenazone drugs and their metabolites in ground- and drinking water*. Chemosphere 49: pp 539-544.

44. Kim S.D., Cho J., Kim I.S., Vanderford B.J., Snyder S.A. (2007). *Occurrence and removal of pharmaceuticals and endocrine disruptors in South Korean surface, drinking, and waste waters*. Water Research 41: pp 1013-1021.

45. Guo Y.C., Krasner S.W. (2009). *Occurrence of Primidone, Carbamazepine, Caffeine, and Precursors for N-Nitrosodimethylamine in Drinking Water Sources Impacted by Wastewater*. Journal of the American Water Resources Association 45: pp 58-67.

46. Focazio M.J., Kolpin D.W., Barnes K.K., Furlong E.T., Meyer M.T., Zaugg S.D., Barber L.B., Thurman E.M. (2008). *A national reconnaissance for pharmaceuticals and other organic wastewater contaminants in the United States – II) Untreated drinking water sources*. Science of The Total Environment 402: pp 201-216.

47. Busetti F., Linge K.L., Heitz A. (2009). *Analysis of pharmaceuticals in indirect potable reuse systems using solid-phase extraction and liquid chromatography-tandem mass spectrometry*. Journal of Chromatography A 1216: pp 5807-5818.

48. Simazaki D., Fujiwara J., Manabe S., Matsuda M., Asami M., Kunikane S. (2008). *Removal of selected pharmaceuticals by chlorination, coagulation-sedimentation and powdered activated carbon treatment*. Water Science and Technology 58: pp 1129-1135.

49. Loos R., Wollgast J., Huber T., Hanke G. (2007). *Polar herbicides, pharmaceutical products, perfluorooctanesulfonate (PFOS), perfluorooctanoate (PFOA), and nonylphenol and its carboxylates and ethoxylates in surface and tap waters around Lake Maggiore in Northern Italy*. Analytical and Bioanalytical Chemistry 387: pp 1469-1478.

50. Kruawal K., Sacher F., Werner A., Muller J., Knepper T.P. (2005). *Chemical water quality in Thailand and its impacts on the drinking water production in Thailand*. Science of The Total Environment 340: pp 57-70.

51. Boulikas T., Vougiouka M. (2004). *Recent clinical trials using cisplatin, carboplatin and their combination chemotherapy drugs (Review)*. Oncology Reports 11: pp 559-595.

52. Curtis L., Turner A., Vyas N., Sewell G. (2010). *Speciation and Reactivity of Cisplatin in River Water and Seawater*. Environmental Science & Technology 44: pp 3345-3350.

53. Ravindra K., Bencs L., Van Grieken R. (2004). *Platinum group elements in the environment and their health risk*. Science of The Total Environment 318: pp 1-43.

54. Kümmerer K. (2009). *The presence of pharmaceuticals in the environment due to human use – present knowledge and future challenges*. Journal of Environmental Management 90: pp 2354-2366.

55. Kümmerer K. (2001). *Drugs in the environment: emission of drugs, diagnostic aids and disinfectants into wastewater by hospitals in relation to other sources – a review*. Chemosphere 45: pp 957-969.

56. EMeA (2006). Guideline on the environmental risk assessment of medical products for human use. Office for Pre-Authoritarion Evaluation of Medicines for Human use, European Medicines Agency (EMeA), London.

57. Titz A., Doll P. (2009). *Actor modelling and its contribution to the development of integrative strategies for management of pharmaceuticals in drinking water*. Social Science & Medicine 68: pp 672-681.

58. START (2007). – Strategien zum Umgang mit Arzneimittelwirkstoffen in Trinkwasser (http://www.start-project.de, last accessed September 14th, 2010).

59. Knoblauch J.A. (2009). *Europe leads effort to push for design of "green" drugs* Environmental Health News (http://wwwenvironmentalhealthnewsorg/ehs/news/benign-drugs-by-design, last accessed September 15th, 2010).

60. Ternes T.A., Joss A., Siegrist H. (2004). *Scrutinizing pharmaceuticals and personal care products in wastewater treatment*. Environmental Science & Technology 38: pp 392a-399a.

61. Larsen T.A., Gujer W. (1996). *Separate management of anthropogenic nutrient solutions (human urine)*. Water Science and Technology 34: pp 87-94.

62. Heberer T. (2002). *Occurrence, fate, and removal of pharmaceutical residues in the aquatic environment: a review of recent research data*. Toxicology Letters 131: pp 5-17.

63. Poiger T., Buser H.R., Müller M.D., Balmer M.E., Buerge I.J. (2003). *Occurrence and fate of organic micropollutants in the environment: Regional mass balances and source apportioning in surface waters based on laboratory incubation studies in soil and water, monitoring, and computer modeling*. Chimia 57: pp 492-498.

64. Zukowska B., Breivik K., Wania F. (2006). *Evaluating the environmental fate of pharmaceuticals using a level III model based on poly-parameter linear free energy relationships*. Science of The Total Environment 359: pp 177-187.

65. Jones O.A.H., Voulvoulis N., Lester J.N. (2002). *Aquatic environmental assessment of the top 25 English prescription pharmaceuticals*. Water Research 36: pp 5013-5022.

66. EPA (2009). ECOSAR™ – part of the package EPI Suite™ available in http://www.epa.gov/opptintr/exposure/pubs/episuite.htm, September 2010: United States Environmental Protection Agency.

67. Buerge I.J., Poiger T., Müller M.D., Buser H.R. (2003). *Caffeine, an anthropogenic marker for wastewater contamination of surface waters*. Environmental Science & Technology 37: pp 691-700.

68. Buerge I.J., Poiger T., Müller M.D., Buser H.R. (2006). *Combined sewer overflows to surface waters detected by the anthropogenic marker caffeine*. Environmental Science & Technology 40: pp 4096-4102.

69. Buerge I.J., Kahle M., Buser H.R., Müller M.D., Poiger T. (2008). *Nicotine derivatives in wastewater and surface waters: Application as chemical markers for domestic wastewater*. Environmental Science & Technology 42: pp 6354-6360.

70. Buerge I.J., Buser H.R., Kahle M., Müller M.D., Poiger T. (2009). *Ubiquitous Occurrence of the Artificial Sweetener Acesulfame in the Aquatic Environment: An Ideal Chemical Marker of Domestic Wastewater in Groundwater*. Environmental Science & Technology 43: pp 4381-4385.

71. Cleuvers M. (2005). *Initial risk assessment for three beta-blockers found in the aquatic environment*. Chemosphere 59: pp 199-205.

72. EMeA (2007). European Medicines Agency recommends restricted use of nimesulide-containing medicinal products (EMEA/432604/2007). European Medicines Agency (EMeA), London.

73. EMeA (2009). Questions and answers on the outcome of the review of nimesulide-containing medicines (EMEA/263700/2008). European Medicines Agency (EMeA), London.

74. EU (2008). Directive 2008/105/EC of the European Parliament and of the Council of 16 December 2008 on environmental quality standards in the field of water policy, pp. 95-98. Official Journal of the European Communities L84/ 24.12.2008.

75. EU (2000). Directive 2000/60/EC of the European Parliament and of the Council of 23 October 2000 establishing a framework for Community action in the field of water policy, pp. 1-72. Official Journal of the European Communities L327/ 22.12.2000.

76. Leeming R., Ball A., Ashbolt N., Nichols P. (1996). *Using faecal sterols from humans and animals to distinguish faecal pollution in receiving waters*. Water Research 30: pp 2893-2900.

77. Mudge S.M., Lintern D.G. (1999). *Comparison of Sterol Biomarkers for Sewage with other Measures in Victoria Harbour, B.C., Canada*. Estuarine, Coastal and Shelf Science 48: pp 27-38.

78. Venkatesan M.I., Maldonado C., Bayona J.M. (1996). *Sewage markers in the sediments of Santa Monica San Pedro basins, California*. Abstracts of Papers of the American Chemical Society 212: page 33.

79. Tyagi P., Edwards D.R., Coyne M.S. (2008). *Use of sterol and bile acid biomarkers to identify domesticated animal sources of fecal pollution*. Water Air and Soil Pollution 187: pp 263-274.

80. Eganhouse R.P., Hill R.J., Leventhal J., Aizenshtat Z., Baedecker M.J., Claypool G., Goldhaber M., Peters K. (2004).In: *Molecular markers and their use in environmental organic geochemistry, pp* 143-158, The Geochemical Society Special Publications, Elsevier.

81. Eganhouse R.P., Olaguer D.P., Gould B.R., Phinney C.S. (1988). *Use of molecular markers for the detection of municipal sewage sludge at sea*. Marine Environmental Research 25: pp 1-22.

82. Glassmeyer S.T., Furlong E.T., Kolpin D.W., Cahill J.D., Zaugg S.D., Werner S.L., Meyer M.T., Kryak D.D. (2005). *Transport of chemical and microbial compounds from known wastewater discharges: Potential for use as indicators of human fecal contamination*. Environmental Science & Technology 39: pp 5157-5169.

83. Servais P., Garcia-Armisen T., George I., Billen G. (2007). *Fecal bacteria in the rivers of the Seine drainage network (France): sources, fate and modelling*. Science of The Total Environment 375: pp 152-167.

84. Peeler K.A., Opsahl S.P., Chanton J.P. (2006). *Tracking anthropogenic inputs using caffeine, indicator bacteria, and nutrients in rural freshwater and urban marine systems*. Environmental Science & Technology 40: pp 7616-7622.

85. Sankararamakrishnan N., Guo Q.Z. (2005). *Chemical tracers as indicator of human fecal coliforms at storm water outfalls*. Environment International 31: pp 1133-1140.

86. Young T.A., Heidler J., Matos-Perez C.R., Sapkota A., Toler T., Gibson K.E., Schwab K.J., Halden R.U. (2008). *Ab initio and in situ comparison of caffeine, triclosan, and triclocarban as indicators of sewage-derived microbes in surface waters*. Environmental Science & Technology 42: pp 3335-3340.

87. Venkatesan M.I., Mirsadeghi F.H. (1992). *Coprostanol as sewage tracer in McMurdo Sound, Antarctica*. Marine Pollution Bulletin 25: pp 328-333.

88. Tyagi P., Edwards D.R., Coyne M.S. (2007). *Use of selected chemical markers in combination with a multiple regression model to assess the contribution of domesticated animal sources of fecal pollution in the environment*. Chemosphere 69: pp 1617-1624.

89. Shah V.G., Dunstan R.H., Geary P.M., Coombes P., Roberts M.K., Von Nagy-Felsobuki E. (2007). *Evaluating potential applications of faecal sterols in distinguishing sources of faecal contamination from mixed faecal samples*. Water Research 41: pp 3691-3700.

90. Rogers P.J., Dernoncourt C. (1998). *Regular caffeine consumption: A balance of adverse and beneficial effects for mood and psychomotor performance*. Pharmacology Biochemistry and Behavior 59: pp 1039-1045.

91. Barone J.J., Roberts H.R. (1996). *Caffeine consumption*. Food and Chemical Toxicology 34: pp 119-129.

92. Fredholm B.B., Battig K., Holmen J., Nehlig A., Zvartau E.E. (1999). *Actions of caffeine in the brain with special reference to factors that contribute to its widespread use*. Pharmacological Reviews 51: pp 83-133.

93. Mandel H.G. (2002). *Update on caffeine consumption, disposition and action*. Food and Chemical Toxicology 40: pp 1231-1234.

94. Weigel S., Berger U., Jensen E., Kallenborn R., Thoresen H., Hühnerfuss H. (2004). *Determination of selected pharmaceuticals and caffeine in sewage and seawater from Tromsø/Norway with emphasis on ibuprofen and its metabolites*. Chemosphere 56: pp 583-592.

95. Seitzinger S.P., Styles R.M., Lauck R., Mazurek M.A. (2003). *Atmospheric pressure mass spectrometry: A new analytical chemical characterization method for dissolved organic matter in rainwater*. Environmental Science & Technology 37: pp 131-137.

96. Ferreira A.P. (2005). *Caffeine as an environmental indicator for assessing urban aquatic ecosystems*. Cadernos de Saúde Pública 21: pp 1884-1892.

97. Ferreira A.P., De Lourdes C., Da Cunha N. (2005). *Anthropic pollution in aquatic environment: Development of a caffeine indicator*. International Journal of Environmental Health Research 15: pp 303-311.

98. Seiler R.L., Zaugg S.D., Thomas J.M., Howcroft D.L. (1999). *Caffeine and pharmaceuticals as indicators of waste water contamination in wells*. Ground Water 37: pp 405-410.

99. Rodil R., Moeder M. (2008). *Development of a method for the determination of UV filters in water samples using stir bar sorptive extraction and thermal desorption-gas chromatography-mass spectrometry*. Journal of Chromatography A 1179: pp 81-88.

100. Hintemann T., Schneider C., Schöler H.F., Schneider R.J. (2006). *Field study using two immunoassays for the determination of estradiol and ethinylestradiol in the aquatic environment*. Water Research 40: pp 2287-2294.

101. Heberer T., Schmidt-Baeumler K., Stan H.-J. (1998). *Occurrence and Distribution of Organic Contaminants in the Aquatic System in Berlin. Part I: Drug Residues and other Polar Contaminants in Berlin Surface and Groundwater*. Acta Hydrochimica et Hydrobiologica 26: pp 272-278.

102. Glassmeyer S.T., Shoemaker J.A. (2005). *Effects of chlorination on the persistence of pharmaceuticals in the environment*. Bulletin of Environmental Contamination and Toxicology 74: pp 24-31.

103. Santos J.L., Aparicio I., Alonso E. (2007). *Occurrence and risk assessment of pharmaceutically active compounds in wastewater treatment plants. A case study: Seville city (Spain)*. Environment International 33: pp 596-601.

104. Bartelt-Hunt S.L., Snow D.D., Damon T., Shockley J., Hoagland K. (2009). *The occurrence of illicit and therapeutic pharmaceuticals in wastewater effluent and surface waters in Nebraska*. Environmental Pollution 157: pp 786-791.

105. Lin A.Y.C., Yu T.H., Lin C.F. (2008). *Pharmaceutical contamination in residential, industrial, and agricultural waste streams: Risk to aqueous environments in Taiwan*. Chemosphere 74: pp 131-141.

106. Choi K., Kim Y., Park J., Park C.K., Kim M., Kim H.S., Kim P. (2008). *Seasonal variations of several pharmaceutical residues in surface water and sewage treatment plants of Han River, Korea*. Science of The Total Environment 405: pp 120-128.

107. Metcalfe C.D., Miao X.S., Koenig B.G., Struger J. (2003). *Distribution of acidic and neutral drugs in surface waters near sewage treatment plants in the lower Great Lakes, Canada*. Environmental Toxicology and Chemistry 22: pp 2881-2889.

108. Verenitch S.S., Lowe C.J., Mazumder A. (2006). *Determination of acidic drugs and caffeine in municipal wastewaters and receiving waters by gas chromatography-ion trap tandem mass spectrometry*. Journal of Chromatography A 1116: pp 193-203.

109. Barnes K.K., Kolpin D.W., Furlong E.T., Zaugg S.D., Meyer M.T., Barber L.B. (2008). *A national reconnaissance of pharmaceuticals and other organic wastewater contaminants in the United States – I) Groundwater*. Science of The Total Environment 402: pp 192-200.

110. Hummel D., Loffler D., Fink G., Ternes T.A. (2006). *Simultaneous determination of psychoactive drugs and their metabolites in aqueous matrices by liquid chromatography mass spectrometry*. Environmental Science & Technology 40: pp 7321-7328.

111. Murtaugh J.J., Bunch R.L. (1967). *Sterols as a Measure of Fecal Pollution*. Journal Water Pollution Control Federation 39: pp 404-409.

112. Grimalt J.O., Fernandez P., Bayona J.M., Albaiges J. (1990). *Assessment of Fecal Sterols and Ketones as Indicators of Urban Sewage Inputs to Coastal Waters*. Environmental Science & Technology 24: pp 357-363.

113. Savichtcheva O., Okabe S. (2006). *Alternative indicators of fecal pollution: Relations with pathogens and conventional indicators, current methodologies for direct pathogen monitoring and future application perspectives*. Water Research 40: pp 2463-2476.

114. Fattore E., Benfenati E., Marelli R., Cools E., Fanelli R. (1996). *Sterols in sediment samples from Venice Lagoon, Italy*. Chemosphere 33: pp 2383-2393.

115. Field K.G., Samadpour M. (2007). *Fecal source tracking, the indicator paradigm, and managing water quality*. Water Research 41: pp 3517-3538.

116. Bjorkhem I., Gustafsson J.-A. (1971). *Mechanism of Microbial Transformation of Cholesterol into Coprostanol*. European Journal of Biochemistry 21: pp 428-432.

117. Bjorkhem I., Gustawsson J.-A., Wrange O. (1973). *Microbial Transformation of Cholesterol into Coprostanol – Properties of a 3-Oxo-Delta-4-Steroid-5-Beta-Reductase*. European Journal of Biochemistry 37: pp 143-147.

118. Tyagi P., Edwards D.R., Coyne M.S. (2009). *Fecal Sterol and Bile Acid Biomarkers: Runoff Concentrations in Animal Waste-Amended Pastures*. Water Air and Soil Pollution 198: pp 45-54.

119. Choi S.M., Kwan S.Y., Wong C.M. (1996). *Studies of Coprostanol (5[beta]-Cholestan-3[beta]-ol) in Environmental Samples by Tandem Mass Spectrometry*. Microchemical Journal 53: pp 54-64.

120. Hurst W.J., Martin R.A. (1993). *The Quantitative-Determination of Caffeine in Beverages Using Capillary Electrophoresis*. Analusis 21: pp 389-391.

121. Zou J.K., Li N. (2006). *Simple and environmental friendly procedure for the gas chromatographic-mass spectrometric determination of caffeine in beverages*. Journal of Chromatography A 1136: pp 106-110.

122. Hawthorne S.B., Miller D.J., Pawliszyn J., Arthur C.L. (1992). *Solventless Determination of Caffeine in Beverages Using Solid-Phase Microextraction with Fused-Silica Fibers*. Journal of Chromatography 603: pp 185-191.

123. McCusker R.R., Goldberger B.A., Cone E.J. (2003). *Caffeine content of specialty coffees*. Journal of Analytical Toxicology 27: pp 520-522.

124. Andrews K.W., Schweitzer A., Zhao C., Holden J.M., Roseland J.M., Brandt M., Dwyer J.T., Picciano M.F., Saldanha L.G., Fisher K.D., Yetley E., Betz J.M., Douglass L. (2007). *The caffeine contents of dietary supplements commonly purchased in the US: analysis of 53 products with caffeine-containing ingredients*. Analytical and Bioanalytical Chemistry 389: pp 231-239.

125. Pellegrini M., Marchei E., Rossi S., Vagnarelli F., Durgbansh A., Garcia-Algar S., Vall O., Pichini S. (2007). *Liquid chromatography/electrospray ionization tandem mass spectrometry assay for determination of nicotine and metabolites, caffeine and arecoline in breast milk*. Rapid Communications in Mass Spectrometry 21: pp 2693-2703.

126. Ohnsmann J., Quintas G., Garrigues S., de la Guardia M. (2002). *Determination of caffeine in tea samples by Fourier transform infrared spectrometry*. Analytical and Bioanalytical Chemistry 374: pp 561-565.

127. Armenta S., Garrigues S., de la Guardia M. (2005). *Solid-phase FT-Raman determination of caffeine in energy drinks*. Analytica Chimica Acta 547: pp 197-203.

128. Llorent-Martinez E.J., Garcia-Reyes J.F., Ortega-Barrales P., Molina-Diaz A. (2005). *Solid-phase ultraviolet sensing system for determination of methylxanthines*. Analytical and Bioanalytical Chemistry 382: pp 158-163.

129. Zen J.M., Ting Y.S. (1997). *Simultaneous determination of caffeine and acetaminophen in drug formulations by square-wave voltammetry using a chemically modified electrode*. Analytica Chimica Acta 342: pp 175-180.

130. Ly S.Y., Jung Y.S., Kim M.H., Han I.K., Jung W.W., Kim H.S. (2004). *Determination of caffeine using a simple graphite pencil electrode with square-wave anodic stripping voltammetry*. Microchimica Acta 146: pp 207-213.

131. Riahi S., Faridbod F., Ganjali M.R. (2009). *Caffeine Sensitive Electrode and Its Analytical Applications*. Sensor Letters 7: pp 42-49.

132. Burkhardt M.R., Soliven P.P., Werner S.L., Vaught D.G. (1999). *Determination of submicrogram-per-liter concentrations of caffeine in surface water and groundwater samples by solid-phase extraction and liquid chromatography*. Journal of AOAC International 82: pp 161-166.

133. Conley J.M., Symes S.J., Kindelberger S.A., Richards S.A. (2008). *Rapid liquid chromatography-tandem mass spectrometry method for the determination of a broad mixture of pharmaceuticals in surface water*. Journal of Chromatography A 1185: pp 206-215.

134. Pedrouzo M., Reverte S., Borrull F., Pocurull E., Marce R.M. (2007). *Pharmaceutical determination in surface and wastewaters using high-performance liquid chromatography-(electrospray)-mass spectrometry*. Journal of Separation Science 30: pp 297-303.

135. Cook C.E., Tallent C.R., Amerson E.W., Myers M.W., Kepler J.A., Taylor G.F., Christensen H.D. (1976). *Caffeine in Plasma and Saliva by a Radioimmunoassay Procedure*. Journal of Pharmacology and Experimental Therapeutics 199: pp 679-686.

136. Zysset T., Wahllander A., Preisig R. (1984). *Evaluation of Caffeine Plasma-Levels by an Automated Enzyme-Immunoassay (Emit) in Comparison with a High-Performance Liquid-Chromatographic Method*. Therapeutic Drug Monitoring 6: pp 348-354.

137. Miceli J.N., Aravind M.K., Ferrell W.J. (1984). *Analysis of Caffeine – Comparison of the Manual Enzyme Multiplied Immunoassay (Emit), Automated Emit, and High-Performance Liquid-Chromatography Procedures*. Therapeutic Drug Monitoring 6: pp 344-347.

138. Helgeson C., Hu M., Chegwidden K., Collins C., Singh P., Jaklitsch A. (1983). *A Homogeneous Enzyme-Immunoassay for Caffeine in Serum*. Clinical Chemistry 29: pp 1275-1275.

139. Pearson S., Smith J.M., Marks V. (1984). *Measurement of Plasma Caffeine Concentrations by Substrate Labeled Fluoroimmunoassay*. Annals of Clinical Biochemistry 21: pp 208-212.

140. Wong P., Leylandjones B., Wainer I.W. (1995). *A Competitive Enzyme-Linked-Immunosorbent-Assay for the Determination of N-Acetyltransferase (Nat2) Phenotypes*. Journal of Pharmaceutical and Biomedical Analysis 13: pp 1079-1086.

141. Fickling S.A., Hampton S.M., Teale D., Middleton B.A., Marks V. (1990). *Development of an Enzyme-Linked-Immunosorbent-Assay for Caffeine*. Journal of Immunological Methods 129: pp 159-164.

142. Verenitch S.S., Mazumder A. (2008). *Development of a methodology utilizing gas chromatography ion-trap tandem mass spectrometry for the determination of low levels of caffeine in surface marine and freshwater samples*. Analytical and Bioanalytical Chemistry 391: pp 2635-2646.

143. Viglino L., Aboulfadl K., Mahvelat A.D., Prevost M., Sauve S. (2008). *On-line solid phase extraction and liquid chromatography/tandem mass spectrometry to quantify pharmaceuticals, pesticides and some metabolites in wastewaters, drinking, and surface waters*. Journal of Environmental Monitoring 10: pp 482-489.

144. Chaler R., Simoneit B.R.T., Grimalt J.O. (2001). *Bile acids and sterols in urban sewage treatment plants*. Journal of Chromatography A 927: pp 155-160.

145. Moliner-Martinez Y., Herraez-Hernandez R., Molins-Legua C., Campins-Falco P. (2010). *Improving analysis of apolar organic compounds by the use of a capillary titania-based column: Application to the direct determination of faecal sterols cholesterol and coprostanol in wastewater samples*. Journal of Chromatography A 1217: pp 4682-4687.

146. Readman J.W., Fillmann G., Tolosa I., Bartocci J., Mee L.D. (2005). *The use of steroid markers to assess sewage contamination of the Black Sea*. Marine Pollution Bulletin 50: pp 310-318.

147. Hjulstrom B., Isaksson S. (2009). *Identification of activity area signatures in a reconstructed Iron Age house by combining element and lipid analyses of sediments*. Journal of Archaeological Science 36: pp 174-183.

148. Lu B.Y., Zhang Y., Wu X.Q., Shi H. (2007). *Separation and determination of diversiform phytosterols in food materials using supercritical carbon dioxide extraction and ultraperformance liquid chromatography-atmospheric pressure chemical ionization-mass spectrometry*. Analytica Chimica Acta 588: pp 50-63.

149. Elhmmali M.M., Roberts D.J., Evershed R.P. (2000). *Combined analysis of bile acids and sterols/stanols from riverine particulates to assess sewage discharges and other fecal sources*. Environmental Science & Technology 34: pp 39-46.

150. Froehner S., Maceno M., Martins R.F. *Sediments as a potential tool for assessment of sewage pollution in Barigui River, Brazil*. Environmental Monitoring and Assessment 170: pp 261-272.

151. Cathum S., Sabik H. (2001). *Determination of steroids and coprostanol in surface water, effluent and mussel using gas chromatography-mass spectrometry*. Chromatographia 53: pp S394-S399.

152. Jayasinghe L.Y., Marriott P.J., Carpenter P.D., Nichols P.D. (1998). *Application of pentafluorophenyldimethylsilyl derivatization for gas chromatography-electron-capture detection of supercritically extracted sterols*. Journal of Chromatography A 809: pp 109-120.

153. Isobe K.O., Tarao M., Zakaria M.P., Chiem N.H., Minh L.Y., Takada H. (2002). Quantitative application of fecal sterols using gas chromatography-mass spectrometry to investigate fecal pollution in tropical waters: Western Malaysia and Mekong Delta, Vietnam. Environmental Science & Technology 36: pp 4497-4507.

154. Shah V.K.G., Dunstan H., Taylor W. (2006). *An efficient diethyl ether-based soxhlet protocol to quantify faecal sterols from catchment waters*. Journal of Chromatography A 1108: pp 111-115.

155. Gilli G., Rovere R., Traversi D., Schiliro T., Pignata C. (2006). *Faecal sterols determination in wastewater and surface water*. Journal of Chromatography B 843: pp 120-124.

156. Piocos E.A., de la Cruz A.A. (2000). *Solid phase extraction and high performance liquid chromatography with photodiode array detection of chemical indicators of human fecal contamination in water*. Journal of Liquid Chromatography & Related Technologies 23: pp 1281-1291.

157. Yalow R.S., Berson S.A. (1970). *Radioimmunoassay of Gastrin*. Gastroenterology 58: pp 1-14.

158. Suri C.R., Boro R., Nangia Y., Gandhi S., Sharma P., Wangoo N., Rajesh K., Shekhawat G.S. (2009). *Immunoanalytical techniques for analyzing pesticides in the environment*. Trac – Trends in Analytical Chemistry 28: pp 29-39.

159. Meulenberg E.P., Peelen G.O.H., Lukkien E., Koopal K. (2005). *Immunochemical detection methods for bioactive pollutants*. International Journal of Environmental Analytical Chemistry 85: pp 861-870.

160. Bahlmann A., Weller M.G., Panne U., Schneider R.J. (2009). *Monitoring carbamazepine in surface and wastewaters by an immunoassay based on a monoclonal antibody*. Analytical and Bioanalytical Chemistry 395: pp1809–1820.

161. Marquette C.A., Blum L.J. (2006). *State of the art and recent advances in immunoanalytical systems*. Biosensors & Bioelectronics 21: pp 1424-1433.

162. Wood W.G. (2008). *Immunoassays & Co.: Past, Present, Future? – A Review and Outlook from Personal Experience and Involvement over the Past 35 Years*. Clinical Laboratory 54: pp 423-438.

163. Gosling J.P. (2000). *Immunoassays*, Oxford University Press, New York.

164. Farré M., Brix R., Barceló D. (2005). *Screening water for pollutants using biological techniques under European Union funding during the last 10 years*. Trac – Trends in Analytical Chemistry 24: pp 532-545.

165. Hock B., Dankwardt A., Kramer K., Marx A. (1995). *Immunochemical Techniques – Antibody-Production for Pesticide Analysis – a Review*. Analytica Chimica Acta 311: pp 393-405.

166. Krämer P.M., Martens D., Forster S., Ipolyi I., Brunori C., Morabito R. (2007). *How can immunochemical methods contribute to the implementation of the Water Framework Directive?* Analytical and Bioanalytical Chemistry 387: pp 1435-1448.

167. Carvalho J.J., Weller M.G., Panne U., Schneider R.J. (2010). *A highly sensitive caffeine immunoassay based on a monoclonal antibody*. Analytical and Bioanalytical Chemistry 396: pp 2617-2628.

168. De Masi F., Chiarella P., Wilhelm H., Massimi M., Belinda B., Ansorge W., Sawyer A. (2005). *High throughput production of mouse monoclonal antibodies using antigen microarrays*. Proteomics 5: pp 4070-4081.

169. Morais S., Carrascosa J., Mira D., Puchades R., Maquieira A. (2007). *Microimmunoanalysis on standard compact discs to determine low abundant compounds*. Analytical Chemistry 79: pp 7628-7635.

170. Ekins R.P. (1960). *The Estimation of Thyroxine in Human Plasma by an Electrophoretic Technique*. Clinica Chimica Acta 5: pp 453-459.

171. Ekins R. (1976). *ELISA – Replacement for Radioimmunoassays*. Lancet 2: pp 569-570.

172. Ballesteros B., Barceló D., Dankwardt A., Schneider P., Marco M.-P. (2003). *Evaluation of a field-test kit for triazine herbicides (SensioScreen(R) TR500) as a fast assay to detect pesticide contamination in water samples*. Analytica Chimica Acta 475: pp 105-115.

173. Brun E.M., Garcés-García M., Puchades R., Maquieira A. (2004). *Enzyme-linked immunosorbent assay for the organophosphorus insecticide fenthion. Influence of hapten structure*. Journal of Immunological Methods 295: pp 21-35.

174. Schneider C., Schöler H.F., Schneider R.J. (2004). *A novel enzyme-linked immunosorbent assay for ethynylestradiol using a long-chain biotinylated EE2 derivative*. Steroids 69: pp 245-253.

175. Schneider C., Schöler H.F., Schneider R.J. (2005). *Direct sub-ppt detection of the endocrine disruptor ethinylestradiol in water with a chemiluminescence enzyme-linked immunosorbent assay*. Analytica Chimica Acta 551: pp 92-97.

176. Wang X.H., Liu T., Xu N., Zhang Y., Wang S. (2007). *Enzyme-linked immunosorbent assay and colloidal gold immunoassay for ochratoxin A: investigation of analytical conditions and sample matrix on assay performance*. Analytical and Bioanalytical Chemistry 389: pp 903-911.

177. Schneider P., Hammock B.D. (1992). *Influence of the Elisa Format and the Hapten Enzyme Conjugate on the Sensitivity of an Immunoassay for S-Triazine Herbicides Using Monoclonal-Antibodies*. Journal of Agricultural and Food Chemistry 40: pp 525-530.

178. Weller M.G., Weil L., Niessner R. (1992). *Increased Sensitivity of an Enzyme-Immunoassay (Elisa) for the Determination of Triazine Herbicides by Variation of Tracer Incubation-Time*. Mikrochimica Acta 108: pp 29-40.

179. Shu T.W., Wen J.G., Yi R.G., Guo N.Z. (2007). *Preparation of a multi-hapten antigen and broad specificity polyclonal antibodies for a multiple pesticide immunoassay*. Analytica Chimica Acta 587: pp 287-292.

180. Chen L.J., Zeng G.M., Zhang Y., Tang L., Huang D.L., Liu C., Pang Y., Luo J. (2010) *Trace detection of picloram using an electrochemical immunosensor based on three-dimensional gold nanoclusters*. Analytical Biochemistry 407: pp 172-179.

181. Coetsier C., Lin L.M., Roig B., Touraud E. (2007). *Integrated approach to the problem of pharmaceutical products in the environment: an overview*. Analytical and Bioanalytical Chemistry 387: pp 1163-1166.

182. Franek M., Diblikova I., Cernoch I., Vass M., Hruska K. (2006). *Broad-specificity immunoassays for sulfonamide detection: Immunochemical strategy for generic antibodies and competitors*. Analytical Chemistry 78: pp 1559-1567.

183. Hennion M.-C., Barceló D. (1998). *Strengths and limitations of immunoassays for effective and efficient use for pesticide analysis in water samples: A review*. Analytica Chimica Acta 362: pp 3-34.

184. Schneider R.J. (2003). *Environmental immunoassays*. Analytical and Bioanalytical Chemistry 375: pp 44-46.

185. Deng A.P., Himmelsbach M., Zhu Q.Z., Frey S., Sengl M., Buchberger W., Niessner R., Knopp D. (2003). *Residue analysis of the pharmaceutical diclofenac in different water types using ELISA and GC-MS*. Environmental Science & Technology 37: pp 3422-3429.

186. Tschmelak J., Kumpf M., Proll G., Gauglitz G. (2004). *Biosensor for seven sulphonamides in drinking, ground, and surface water with difficult matrices*. Analytical Letters 37: pp 1701-1718.

187. Adrian J., Pinacho D.G., Granier B., Diserens J.M., Sanchez-Baeza F., Marco M.P. (2008). *A multianalyte ELISA for immunochemical screening of sulfonamide, fluoroquinolone and beta-lactam antibiotics in milk samples using class-selective bioreceptors*. Analytical and Bioanalytical Chemistry 391: pp 1703-1712.

188. Morais S., Tortajada-Genaro L.A., Arnandis-Chover T., Puchades R., Maquieira A. (2009). *Multiplexed Microimmunoassays on a Digital Versatile Disk*. Analytical Chemistry 81: pp 5646-5654.

189. Jornet D., Gonzalez-Martinez M.A., Puchades R., Maquieira A. *Antibiotic immunosensing: Determination of sulfathiazole in water and honey*. Talanta 81: pp 1585-1592.

190. Blake D.A., Yu H.N., James E.A., Li X., Blake R.C. (2005). *Field portable and autonomous immunosensors for the detection of environmental contaminants, edited by* B. J. Merkel, Book and A. Hasche-Berger: Uranium in the Environment: Mining Impact and Consequences: *pp* 87-95. Springer, Berlin.

191. Shankaran D.R., Gobi K.V.A., Miura N. (2007). *Recent advancements in surface plasmon resonance immunosensors for detection of small molecules of biomedical, food and environmental interest*. Sensors and Actuators B: Chemical 121: pp 158-177.

192. Hatcher P.G., McGillivary P.A. (1979). *Sewage Contamination in the New-York Bight – Coprostanol as an Indicator*. Environmental Science & Technology 13: pp 1225-1229.

193. Gagné F., Blaise C., Lachance B., Sunahara G.I., Sabik H. (2001). *Evidence of coprostanol estrogenicity to the freshwater mussel Elliptio complanata*. Environmental Pollution 115: pp 97-106.

194. Male D., Brostoff J., Roth D.B., Roitt I. (2006). *Immunology*, 7th ed. Elsevier, Philadelphia.

195. Defresne M.P. (1998). *Chapter XVI – The mouse model,* edited by P. P. Pastoret, P. Griebel, H. Bazin and A. Govaerts: Handbook of vertebrate immunology, *pp* 563-594. Academic Press, San Diego.

196. Playfair J., Brancroft G. (2004). *Infection and Immunity*, 2nd ed. Oxford University Press, New York.

197. Feige M.J., Nath S., Catharino S.R., Weinfurtner D., Steinbacher S., Buchner J. (2009). *Structure of the Murine Unglycosylated IgG1 Fc Fragment*. Journal of Molecular Biology 391: pp 599-608.

198. Banfield M.J., King D.J., Mountain A., Brady R.L. (1997). *V-L:V-H domain rotations in engineered antibodies: Crystal structures of the Fab fragments from two murine antitumor antibodies and their engineered human constructs*. Proteins-Structure Function and Bioinformatics 29: pp 161-171.

199. Ward P.A. (1999). Monoclonal Antibody Production, The National Academies Press, Washington D.C.

200. Hermanson G.T. (2008). *Bioconjugate Techniques,* 2nd ed. Academic Press (Elsevier), San Diego.

201. Singh K.V., Kaur J., Varshney G.C., Raje M., Suri C.R. (2004). *Synthesis and characterization of hapten-protein conjugates for antibody production against small molecules*. Bioconjugate Chemistry 15: pp 168-173.

202. Shepherd P., Dean C. (2000). *Monoclonal Antibodies – a pratical approach.* Oxford University Press, New York.

203. Darwish I.A., Al-Obaid A.R.M., Al-Malaq H.A. (2009). *New highly sensitive enzyme immunoassay for the determination of pravastatin in human plasma*. Talanta 79: pp 1478-1483.

204. Harris J.R., Markl J. (2000). *Keyhole limpet hemocyanin: Molecular structure of a potent marine immunoactivator*. European Urology 37: pp 24-33.

205. Lipman N.S., Jackson L.R., Trudel L.J., Weis-Garcia F. (2005). *Monoclonal versus polyclonal antibodies: Distinguishing characteristics, applications, and information resources*. ILAR Journal 46: pp 258-268.

206. Pohanka M. (2009). *Monoclonal and polyclonal antibodies production – preparation of potent biorecognition element*. Journal of Applied Biomedicine 7: pp 115-121.

207. Chiarella P., Fazio V.M. (2008). *Mouse monoclonal antibodies in biological research: strategies for high-throughput production*. Biotechnology Letters 30: pp 1303-1310.

208. de Castro L.N., Timmis J. (2002). *Chapter 7 – Case studies*. Artificial immune system: A new computational intelligence approach: *pp* 269. Springer, London.

209. Alving C.R., Swartz G.M. (1991). *Antibodies to cholesterol, cholesterol conjugates and liposomes – implications for atherosclerosis and autoimmunity*. Critical Reviews in Immunology 10: pp 441-453.

210. Alving C.R., Swartz G.M., Wassef N.M., Ribas J.L., Herderick E.E., Virmani R., Kolodgie F.D., Matyas G.R., Cornhill J.F. (1996). *Immunization with cholesterol-rich liposomes induces anti-cholesterol antibodies and reduces diet-induced hypercholesterolemia and plaque formation*. Journal of Laboratory and Clinical Medicine 127: pp 40-49.

211. Landsteiner K. (1962). *The Specificity of Serological Reactions, 2nd Edition (first edition from 1936*). Harvard University Press, New York.

212. Bailey JM B.R., Tomar R (1964). *Immunization with a Synthetic Cholesterolester Antigen and Induced Atherosclerosis in Rabbits.* Nature 201: pp 407-408.

213. Swartz G.M., Gentry M.K., Amende L.M., Blanchettemackie E.J., Alving C.R. (1988). *Antibodies to Cholesterol*. Proceedings of the National Academy of Sciences of the United States of America 85: pp 1902-1906.

214. Biro A., Cervenak L., Balogh A., Lorincz A., Uray K., Horvath A., Romics L., Matko J., Furst G., Laszlo G. (2007). *Novel anti-cholesterol monoclonal immunoglobulin G antibodies as probes and potential modulators of membrane raft-dependent immune functions*. Journal of Lipid Research 48: pp 19-29.

215. Veres A., Fust G., Smieja M., McQueen M., Horvath A., Yi Q.L., Biro A., Pogue J., Romics L., Karadi I., Singh M., Gnarpe J., Prohaszka Z., Yusuf S. (2002). *Relationship of anti-60 kDa heat shock protein and anti-cholesterol antibodies to cardiovascular events*. Circulation 106: pp 2775-2780.

216. Karasavvas N., Beck Z., Tong J., Matyas G.R., Rao M., McCutchan F.E., Michael N.L., Alving C.R. (2008). *Antibodies induced by liposomal protein exhibit dual binding to protein and lipid epitopes*. Biochemical and Biophysical Research Communications 366: pp 982-987.

217. Horvath A., Biro A. (2003). *Anti-cholesterol antibodies in human sera*. Autoimmunity Reviews 2: pp 272-277.

218. Horvath A., Banhegyi D., Biro A., Ujhelyi E., Veres A., Horvath L., Prohaszka Z., Bacsi A., Tarjan V., Romics L., Horvath I., Toth F.D., Fust G., Karadi I. (2001). *High level of anticholesterol antibodies (ACHA) in HIV patients. Normalization of serum ACHA concentration after introduction of HAART*. Immunobiology 203: pp 756-768.

219. Beck Z., Balogh A., Kis A., Izsepi E., Cervenak L., Laszlo G., Biro A., Liliom K., Mocsar G., Vamosi G., Fust G., Matko J. (2010). *New cholesterol-specific antibodies remodel HIV-1 target cells' surface and inhibit their in vitro virus production*. Journal of Lipid Research 51: pp 286-296.

220. Alving C.R, Kenner J., Swartz Jr. G.M., Madsen, J.W. (2001). US Patent 6224902: Vaccines against sterols. EntreMed, Inc. (Rockwille), May 1st.

221. Rittershaus C. (2007). *Vaccines for Cholesterol Management*. World Journal of Surgery 31: pp 690-694.

222. Matyas G.R., Wassef N.M., Rao M., Alving C.R. (2000). *Induction and detection of antibodies to squalene*. Journal of Immunological Methods 245: pp 1-14.

223. Phillips C.J., Matyas G.R., Hansen C.J., Alving C.R., Smith T.C., Ryan M.A.K. (2009). *Antibodies to squalene in US Navy Persian Gulf War veterans with chronic multisymptom illness*. Vaccine 27: pp 3921-3926.

224. Matyas G.R., Rao M., Alving C.R. (2002). *Induction and detection of antibodies to squalene II. Optimization of the assay for murine antibodies*. Journal of Immunological Methods 267: pp 119-129.

225. Asa P.B., Cao Y., Garry R.F. (2000). *Antibodies to squalene in gulf war syndrome*. Experimental and Molecular Pathology 68: pp 55.

226. Del Giudice G., Fragapane E., Bugarini R., Hora M., Henriksson T., Palla E., O'Hagan D., Donnelly J., Rappuoli R., Podda A. (2006). *Vaccines with the MF59 adjuvant do not stimulate antibody responses against squalene*. Clinical and Vaccine Immunology 13: pp 1010-1013.

227. Matyas G.R., Rao M., Pittman P.R., Burge R., Robbins I.E., Wassef N.M., Thivierge B., Alving C.R. (2004). *Detection of antibodies to squalene III. Naturally occurring antibodies to squalene in humans and mice*. Journal of Immunological Methods 286: pp 47-67.

228. Fox C.B. (2009). *Squalene Emulsions for Parenteral Vaccine and Drug Delivery*. Molecules 14: pp 3286-3312.

229. Ikegawa S., Yamamoto T., Miyashita T., Okihara R., Ishmata S., Sakai T., Chong R.H., Maeda M., Hofmann A.F., Mitamura K. (2008). *Production and Characterization of a Monoclonal Antibody to Capture Proteins Tagged with Lithocholic Acid*. Analytical Sciences 24: pp 1475-1480.

230. Sheedy C., Roger MacKenzie C., Hall J.C. (2007). *Isolation and affinity maturation of hapten-specific antibodies*. Biotechnology Advances 25: pp 333-352.

231. Zafir-Lavie I., Michaeli Y., Reiter Y. (2007). *Novel antibodies as anticancer agents*. Oncogene 26: pp 3714-3733.

232. Yamashita M., Katakura Y., Shirahata S. (2007). *Recent advances in the generation of human monoclonal antibody*. Cytotechnology 55: pp 55-60.

233. da Silva F.A., Corte-Real S., Gonçalves J. (2008). *Recombinant antibodies as therapeutic agents – Pathways for modeling new biodrugs*. Biodrugs 22: pp 301-314.

234. Köhler G., Milstein C. (1975). *Continuous Cultures of Fused Cells Secreting Antibody of Predefined Specificity*. Nature 256: pp 495-497.

235. Chartrain M., Chu L. (2008). *Development and Production of Commercial Therapeutic Monoclonal Antibodies in Mammalian Cell Expression Systems: An Overview of the Current Upstream Technologies*. Current Pharmaceutical Biotechnology 9: pp 447-467.

236. Moran E., O'Keeffe M., O'Connor R., Larkin A.M., Murphy P., Clynes M. (2002). *Methods for generation of monoclonal antibodies to the very small drug hapten, 5-benzimidazolecarboxylic acid*. Journal of Immunological Methods 271: pp 65-75.

237. Sellrie F., Schenk J.A., Behrsing O., Drechsel O., Micheel B. (2007). *Cloning and characterization of a single chain antibody to glucose oxidase from a murine hybridoma*. Journal of Biochemistry and Molecular Biology 40: pp 875-880.

238. Stuckas H., Messerschmidt K., Putzler S., Baumann O., Schenk J.A., Tiedemann R., Micheel B. (2009). *Detection and Characterization of Gamete-Specific Molecules in Mytilus edulis Using Selective Antibody Production*. Molecular Reproduction and Development 76: pp 4-10.

239. Tsoneva I., Tomov T., Panova I., Strahilov D. (1980). *Effective production by electrofusion of hybridomas secreting monoclonal antibodies against Hc-antigen of Salmonella*. Bioelectrochemistry and Bioenergetics 24: pp 41-49.

240. Nagata S., Yamamoto K., Ueno Y., Kurata T., Chiba J. (1991). *Preferential Generation of Monoclonal IgG-Producing Hybridomas by Use of Vesicular Stomatitis Virus-Mediated Cell Fusion*. Hybridoma 10: pp 369-378.

241. Pasqualini R., Arap W. (2004). *Hybridoma-free generation of monoclonal antibodies*. Proceedings of the National Academy of Sciences of the United States of America 101: pp 257-259.

242. Pasqualini R., Arap W. (2004). International Patent WO/2004/092220: Method for ex vivo hybridoma-free production of polyclonal and monoclonal antibodies and generation of immortalized cell populations. The University of Texas (Austin), October 28th.

243. Killard A.J., Deasy B., Okennedy R., Smyth M.R. (1995). *Antibodies – Production, Functions and Applications in Biosensors*. Trac – Trends in Analytical Chemistry 14: pp 257-266.

244. Puck T.T., Marcus P.I. (1955). *A rapid method for viable cell titration and clone production with HeLa cells in tissue culture: the use of X-irradiated cells to supply conditioning factors*. Proceedings of the National Academy of Sciences of the United States of America 41: pp 432–437.

245. Cervino C., Weber E., Knopp D., Niessner R. (2008). *Comparison of hybridoma screening methods for the efficient detection of high-affinity hapten-specific monoclonal antibodies*. Journal of Immunological Methods 329: pp 184-193.

246. Browne S.M., Al-Rubeai M. (2007). *Selection methods for high-producing mammalian cell lines*. Trends Biotechnol 25: pp 425-432.

247. Rieger M., Cervino C., Sauceda J.C., Niessner R., Knopp D. (2009). *Efficient Hybridoma Screening Technique Using Capture Antibody Based Microarrays*. Analytical Chemistry 81: pp 2373-2377.

248. Pedersen M.K., SØrensen N.S., Heegaard P.M.H., Beyer N.H., Bruun L. (2006). *Effect of different hapten-carrier conjugation ratios and molecular orientations on antibody affinity against a peptide antigen*. Journal of Immunological Methods 311: pp 198-206.

249. Corbett C.R., Elias M.D., Simpson L.L., Yuan X.Y., Cassan R.R., Ballegeer E., Kabani A., Plummer F.A., Berry J.D. (2007). *High-throughput homogeneous immunoassay readily identifies monoclonal antibody to serovariant clostridial neurotoxins*. Journal of Immunological Methods 328: pp 128-138.

250. Sasaki K., Glass T.R., Ohmura N. (2005). *Validation of accuracy of enzyme-linked immunosorbent assay in hybridoma screening and proposal of an improved screening method*. Analytical Chemistry 77: pp 1933-1939.

251. Weller M.G. (1992). *Strukturelle und kinetische Untersuchungen zur Entwicklung und Optimierung von Hapten-Enzymimmunoassays (ELISAs) am Beispiel der Bestimmung von Triazinherbiziden.* PhD Thesis, Technische Universitaet Muenchen.

252. Canziani G.A., Klakamp S., Myszka D.G. (2004). *Kinetic screening of antibodies from crude hybridoma samples using Biacore*. Analytical Biochemistry 325: pp 301-307.

253. Daigo K., Sugita S., Mochizuki Y., Iwanari H., Hiraishi K., Miyano K., Kodama T., Hamakubo T. (2006). *A simple hybridoma screening method for high-affinity monoclonal antibodies using the signal ratio obtained from time-resolved fluorescence assay*. Analytical Biochemistry 351: pp 219-228.

254. Mann C.J. (2007). *Rapid isolation of antigen-specific clones from hybridoma fusions*. Nature Methods 4: pp 8-9.

255. Moretti P., Behr L., Walter J.G., Kasper C., Stahl F., Scheper T. (2010). *Characterization and improvement of cell line performance via flow cytometry and cell sorting*. Engineering in Life Sciences 10: pp 130-138.

256. Frey A., Meckelein B., Externest D., Schmidt M.A. (2000). *A stable and highly sensitive 3,3',5,5'-tetramethylbenzidine-based substrate reagent for enzyme-linked immunosorbent assays*. Journal of Immunological Methods 233: pp 47-56.

257. Cook C.E., Twine M.E., Myers M., Amerson E., Kepler J.A., Taylor G.F. (1976). *Theophylline radioimmunoassay: synthesis of antigen and characterization of antiserum.* Research Communications in Chemical Pathology & Pharmacology 13: pp 497-505.

258. Bruker (2001). *SMART, SAINST and SADABS.* Bruker AXS Inc., Madison, Wisconsin, USA.

259. Sheldrick G.M. (2001). *SHELXTL Version 5.0.* Bruker AXS Inc. , Madison, Wisconsin, USA.

260. Tatake J.G., Knapp M.M., Ressler C. (1991). *Synthesis and Characterization of Protein and Polylysine Conjugates of Sulfamethoxazole and Sulfanilic Acid for Investigation of Sulfonamide Drug Allergy*. Bioconjugate Chemistry 2: pp 124-132.

261. Chaudhry M.Q. (2000). *Chapter 6 – Standards and Immunogens, edited by* J. P. Gosling: Immunoassays – Practical Approach. Oxford University Press, New York.

262. Fox M.A., Whitesell J.K. (1997). *Organic Chemistry*, 2nd ed. Jones and Bartlett, New York.

263. Kuipers M.E., Swart P.J., Hendriks M., Meijer D.K.F. (1995). *Optimization of the Reaction Conditions for the Synthesis of Neoglycoprotein-AZT Monophosphate Conjugates*. Journal of Medicinal Chemistry 38: pp 883-889.

264. Staros J.V., Wright R.W., Swingle D.M. (1986). *Enhancement by N-Hydroxysulfosuccinimide of Water-Soluble Carbodiimide-Mediated Coupling Reactions*. Analytical Biochemistry 156: pp 220-222.

265. Pedron J., Maldiney R., Brault M., Miginiac E. (1996). *Monitoring of hapten-protein coupling reactions by capillary zone electrophoresis: Improvement of abscisic acid-bovine serum albumin coupling and determination of molar coupling ratios*. Journal of Chromatography A 723: pp 381-388.

266. Poitevin M., Morin A., Busnel J.-M., Descroix S., Hennion M.-C., Peltre G. (2007). *Comparison of different capillary isoelectric focusing methods – use of "narrow pH cuts" of carrier ampholytes as original tools to improve resolution*. Journal of Chromatography A 1155: pp 230-236.

267. Barrangou L.M., Daubert C.R., Allen Foegeding E. (2006). *Textural properties of agarose gels. I. Rheological and fracture properties*. Food Hydrocolloids 20: pp 184-195.

268. Eaton A.D., Clesceri L.S., Rice E.W., Greenberg A.E. (2005). *Standard Methods for the Examination of Water and Wastewater*, 21st Edition. American Public Health Association, Washington DC.

269. FDA (2001). Guidance for Industry – Bioanalytical Method Validation, pp. 1-22. U. S. Food and Drug Administration.

270. Kaus R. (1998). *Detection limits and quantitation limits in the view of international harmonization and the consequences for analytical laboratories*. Accreditation and Quality Assurance 3: pp 150-154.

271. Vogelgesang J., Hadrich J. (1998). *Limits of detection, identification and determination: a statistical approach for practitioners*. Accreditation and Quality Assurance 3: pp 242-255.

272. Kuselman I., Sherman F. (1999). *Assessment of limits of detection and quantitation using calculation of uncertainty in a new method for water determination*. Accreditation and Quality Assurance 4: pp 124-128.

273. Linnet K., Kondratovich M. (2004). *Partly nonparametric approach for determining the limit of detection*. Clinical Chemistry 50: pp 732-740.

274. Faber N.M., Boque R. (2006). *On the calculation of decision limits in doping control*. Accreditation and Quality Assurance 11: pp 536-538.

275. Faber N.M. (2008). *The limit of detection is not the analyte level for deciding between "detected" and "not detected"*. Accreditation and Quality Assurance 13: pp 277-278.

276. Huber W. (2003). *Basic calculations about the limit of detection and its optimal determination*. Accreditation and Quality Assurance 8: pp 213-217.

277. Huber W. (2002). *Do we need a limit of determination?* Accreditation and Quality Assurance 7: pp 256-257.

278. Desimoni E., Brunetti B., Cattaneo R. (2004). *Comparing some operational approaches to the limit of detection*. Annali Di Chimica 94: pp 555-569.

279. Ekins R.P. (1981). *The precision profile: its use in RIA assessment and design*. The Ligand Quarterly 4: pp 33-44.

280. Heberer T. (2002). *Tracking persistent pharmaceutical residues from municipal sewage to drinking water*. Journal of Hydrology 266: pp 175-189.

281. Lucchi G., Chambon C., Truntzer C., Pecqueur D., Ducoroy P., Schwartz C., Nicklaus S., Morzel M. (2009). *Mass-Spectrometry Based Characterisation of Infant Whole Saliva Peptidome*. International Journal of Peptide Research and Therapeutics 15: pp 177-185.

282. Hoetelmans R.M.W., van Essenberg M., Profijt M., Meenhorst P.L., Mulder J.W., Beijnen J.H. (1998). *High-performance liquid chromatographic determination of ritonavir in human plasma, cerebrospinal fluid and saliva*. Journal of Chromatography B 705: pp 119-126.

283. Chi J.D., Jayewardene A.L., Stone J.A., Motoya T., Aweeka F.T. (2002). *Simultaneous determination of five HIV protease inhibitors nelfinavir, indinavir, ritonavir, saquinavir and amprenavir in human plasma by LC/MS/MS*. Journal of Pharmaceutical and Biomedical Analysis 30: pp 675-684.

284. Zarei H.A., Lavasani M.Z., Iloukhani H. (2008). *Densities and Volumetric Properties of Binary and Ternary Liquid Mixtures of Water (1) + Acetonitrile (2) + Dimethyl Sulfoxide (3) at Temperatures from (293.15 to 333.15) K and at Ambient Pressure (81.5 kPa)*. Journal of Chemical & Engineering Data 53: pp 578-585.

285. del Carmen Grande M., Juliá J.A., Barrero C.R., Marschoff C.M., Bianchi H.L. (2006). *The (water + acetonitrile) mixture revisited: A new approach for calculating partial molar volumes*. The Journal of Chemical Thermodynamics 38: pp 760-768.

286. Ladenson R.C., Crimmins D.L., Landt Y., Ladenson J.H. (2006). *Isolation and characterization of a thermally stable recombinant anti-caffeine heavy-chain antibody fragment*. Analytical Chemistry 78: pp 4501-4508.

287. Alonso-Salces R.M., Guillou C., A. Berrueta L. (2009). *Liquid chromatography coupled with ultraviolet absorbance detection, electrospray ionization, collision-induced dissociation and tandem mass spectrometry on a triple quadrupole for the on-line characterization of polyphenols and methylxanthines in green coffee beans*. Rapid Communications in Mass Spectrometry 23: pp 363-383.

288. Huck C.W., Guggenbichler W., Bonn G.K. (2005). *Analysis of caffeine, theobromine and theophylline in coffee by near infrared spectroscopy (NIRS) compared to high-performance liquid chromatography (HPLC) coupled to mass spectrometry*. Analytica Chimica Acta 538: pp 195-203.

289. Bianco G., Abate S., Labella C., Cataldi T.R.I. (2009). *Identification and fragmentation pathways of caffeine metabolites in urine samples via liquid chromatography with positive electrospray ionization coupled to a hybrid quadrupole linear ion trap (LTQ) and Fourier transform ion cyclotron resonance mass spectrometry and tandem mass spectrometry*. Rapid Communications in Mass Spectrometry 23: pp 1065-1074.

290. Carvalho J.J., Emmerling F., Schneider R.J. (2007). *7-(5-Carboxypentyl)-1,3-dimethyl-xanthine monohydrate*. Acta Crystallographica Section E-Structure Reports Online 63: O3718-U2211.

291. Derollez P., Correia N.T., Danede F., Capet F., Affouard F., Lefebvre J., Descamps M. (2005). *Ab initio structure determination of the high-temperature phase of anhydrous caffeine by X-ray powder diffraction*. Acta Crystallographica Section B-Structural Science 61: pp 329-334.

292. Edwards H.G.M., Lawson E., deMatas M., Shields L., York P. (1997). *Metamorphosis of caffeine hydrate and anhydrous caffeine*. Journal of the Chemical Society-Perkin Transactions 2: pp 1985-1990.

293. Allen F.H. (2002). *The Cambridge Structural Database: a quarter of a million crystal structures and rising*. Acta Crystallographica Section B-Structural Science 58: pp 380-388.

294. Sutor D.J. (1958). *The Structures of the Pyrimidines and Purines: VI. The Crystal Structure of Theophylline*. Acta Crystallographica 11: pp 83-87.

295. Walsh G. (2002). *Proteins – Biochemistry and Structure.* John Wiley & Sons. West Sussex.

296. Nichczynski M. (2007). *Aufbau und Optimierung eines Immunoassays zur Bestimmung von Koffein in Oberflächengewässern.* Diploma Thesis. Fachbereich II (Mathematik, Physik, Chemie) – Technische Fachhochschule Berlin, Berlin.

297. Biocompare database (2007) http://www.biocompare.com/, Searching for" anti-caffeine", accessed January,19th.

298. Herman R.A., Scherer P.N., Shan G. (2008). *Evaluation of logistic and polynomial models for fitting sandwich-ELISA calibration curves*. Journal of Immunological Methods 339: pp 245-258.

299. Findlay J.W.A., Dillard R.F. (2007). *Appropriate calibration curve fitting in ligand binding assays*. AAPS Journal 9: pp E260-E267.

300. Little J.A. (2004). *Comparison of curve fitting models for ligand binding assays*. Chromatographia 59: pp S177-S181.

301. Shah V., Midha K., Findlay J., Hill H., Hulse J., McGilveray I., McKay G., Miller K., Patnaik R., Powell M., Tonelli A., Viswanathan C.T., Yacobi A. (2000). *Bioanalytical Method Validation—A Revisit with a Decade of Progress*. Pharmaceutical Research 17: pp 1551-1557.

302. Akaike H. (1974). *New Look at Statistical-Model Identification*. IEEE Transactions on Automatic Control 19: pp 716-723.

303. Wahllander A., Mohr S., Paumgartner G. (1990). *Assessment of Hepatic-Function – Comparison of Caffeine Clearance in Serum and Saliva during the Day and at Night*. Journal of Hepatology 10: pp 129-137.

304. Jost G., Wahllander A., von Mandach U., Preisig R. (1987). *Overnight salivary caffeine clearance: a liver function test suitable for routine use*. Hepatology 7: pp 338-344.

305. McDonagh J.E., Nathan V.V., Bonavia I.C., Moyle G.R., Tanner A.R. (1991). *Caffeine clearance by enzyme multiplied immunoassay technique: a simple, inexpensive, and useful indicator of liver function*. Gut 32: pp 681-684.

306. Newton R., Broughton L.J., Lind M.J., Morrison P.J., Rogers H.J., Bradbrook I.D. (1981). *Plasma and Salivary Pharmacokinetics of Caffeine in Man*. European Journal of Clinical Pharmacology 21: pp 45-52.

307. Carrillo J.A., Christensen M., Ramos S.I., Alm C., Dahl M.L., Benitez J., Bertilsson L. (2000). *Evaluation of caffeine as an in vivo probe for CYP1A2 using measurements in plasma, saliva, and urine*. Therapeutic Drug Monitoring 22: pp 409-417.

308. Haskell C.F., Kennedy D.O., Wesnes K.A., Scholey A.B. (2005). *Cognitive and mood improvements of caffeine in habitual consumers and habitual non-consumers of caffeine*. Psychopharmacology 179: pp 813-825.

309. Tarantino G., Conca P., Capone D., Gentile A., Polichetti G., Basile V. (2006). *Reliability of total overnight salivary caffeine assessment (TOSCA) for liver function evaluation in compensated cirrhotic patients*. European Journal of Clinical Pharmacology 62: pp 605-612.

310. Brice C., Smith A. (2001). *Caffeine levels in saliva: associations with psychosocial factors and behavioural effects*. Human Psychopharmacology: Clinical and Experimental 16: pp 507-521.

311. Caffeine Source Reference (2009). http://www.energyfiend.com/the-caffeine-database. Accessed March 19th.

312. McCusker R.R., Goldberger B.A., Cone E.J. (2006). *Caffeine content of energy drinks, carbonated sodas, and other beverages*. Journal of Analytical Toxicology 30: pp 112-114.

313. Pena A., Lino C., Silveira M.I.N. (2005). *Survey of caffeine levels in retail beverages in Portugal*. Food Additives & Contaminants: Part A: Chemistry, Analysis, Control, Exposure & Risk Assessment 22: pp 91-96.

314. Roehrs T., Roth T. (2008). *Caffeine: Sleep and daytime sleepiness*. Sleep Medicine Reviews 12: pp 153-162.

315. Brauerei Beck & Co. (2009). http://www.becks.de/. Accessed September 23rd.

316. Chin J.M., Merves M.L., Goldberger B.A., Sampson-Cone A., Cone E.J. (2008). *Caffeine Content of Brewed Teas*. Journal of Analytical Toxicology 32: pp 702-704.

317. Bunker M.L., Mcwilliams M. (1979). *Caffeine Content of Common Beverages*. Journal of the American Dietetic Association 74: pp 28-32.

318. *SciFinder.* (2007). CAS, American Chemical Society, Columbus.

319. PubChem (2007). National Center for Biotechnology Information (NCBI).

320. Dion C., Montagne P., Bene M.C., Faure G. (2004). *Measurement of faecal immunoglobulin a levels in young children*. Journal of Clinical Laboratory Analysis 18: pp 195-199.

321. Schenk J.A., Matyssek F., Micheel B. (2004). *Interleukin 4 increases the antibody response against Rubisco in mice*. In Vivo 18: pp 649-652.

322. Elder P.A., Gaynor P.T., Lewis J.G., Bodger P.S., Bason L.M. (1997). *Generation of monoclonal progesterone antibodies by electrofusion techniques*. Bioelectrochemistry and Bioenergetics 43: pp 35-40.

323. Heftmann E. (2004). *Part A: Fundamentals and techniques. Chromatography 6th edition – fundamentals and applications of chromatography and related differential migration methods*. Elsevier, Amsterdam.

324. Foley J.P. (1991). *Resolution Equations for Column Chromatography*. Analyst 116: pp 1275-1279.

325. Purnell J.H. (1960). *The Correlation of Separating Power and Efficiency of Gas-Chromatographic Columns*. Journal of the Chemical Society pp 1268-1274.

326. Purnell J.H., Jones J.R., Wattan M.H. (1987). *Theory and Practice of Coupled Gas-Chromatographic Columns*. Journal of Chromatography 399: pp 99-109.

327. Rodil R., Schrader S., Moeder M. (2009). *Non-porous membrane-assisted liquid-liquid extraction of UV filter compounds from water samples*. Journal of Chromatography A 1216: pp 4887-4894.

328. Daneshfar A., Khezeli T., Lotfi H.J. (2009). *Determination of cholesterol in food samples using dispersive liquid-liquid microextraction followed by HPLC-UV*. Journal of Chromatography B: 877: pp 456-460.

329. Rezaee M., Assadi Y., Hosseinia M.R.M., Aghaee E., Ahmadi F., Berijani S. (2006). *Determination of organic compounds in water using dispersive liquid-liquid microextraction*. Journal of Chromatography A 1116: pp 1-9.

330. Deo A.K., Bandiera S.M. (2008). *Biotransformation of lithocholic acid by rat hepatic microsomes: Metabolite analysis by liquid chromatography/mass spectrometry*. Drug Metabolism and Disposition 36: pp 442-451.

331. Hofmann A.F. (1999). *The continuing importance of bile acids in liver and intestinal disease*. Archives of Internal Medicine 159: pp 2647-2658.

332. Walter M.A., Pfeifer D., Kraus W., Emmerling F., Schneider R.J., Panne U., Weller M.G. (2010). *Triacetone Triperoxide (TATP): Hapten Design and Development of Antibodies*. Langmuir 26: pp 15418-15423.

333. Carvalho J.J., Walter M.A., Baermann Y., Weller M.G., Panne U., Schenk J.A., Schneider R.J. (2011). *Non-invasive Monitoring of Selective Immunoglobulins in Mice by Sampling of Faeces*. Bioscience, Biotechnology, and Biochemistry (submitted, February 2011).

334. Vetvik H., Grewal H.M.S., Haugen I.L., Ahren C., Haneberg B. (1998). *Mucosal antibodies can be measured in air-dried samples of saliva and feces*. Journal of Immunological Methods 215: pp 163-172.

335. Hansen G.H., Niels-Christiansen L.L., Immerdal L., Danielsen E.M. (2006). *Antibodies in the small intestine: mucosal synthesis and deposition of anti-glycosyl IgA, IgM, and IgG in the enterocyte brush border*. American Journal of Physiology-Gastrointestinal and Liver Physiology 291: pp G82-G90.

336. Lencer W.I., Blumberg R.S. (2005). *A passionate kiss, then run: exocytosis and recycling of IgG by FcRn*. Trends in Cell Biology 15: pp 5-9.

337. Montoyo H.P., Vaccaro C., Hafner M., Ober R.J., Mueller W., Ward E.S. (2009). *Conditional deletion of the MHC class I-related receptor FcRn reveals the sites of IgG homeostasis in mice*. Proceedings of the National Academy of Sciences of the United States of America 106: pp 2788-2793.

338. Yoshida M., Masuda A., Kuo T.T., Kobayashi K., Claypool S.M., Takagawa T., Kutsumi H., Azuma T., Lencer W.I., Blumberg R.S. (2006). *IgG transport across mucosal barriers by neonatal Fc receptor for IgG and mucosal immunity*. Springer Seminars in Immunopathology 28: pp 397-403.

339. Baker K., Qiao S.W., Kuo T., Kobayashi K., Yoshida M., Lencer W.I., Blumberg R.S. (2009). *Immune and non-immune functions of the (not so) neonatal Fc receptor, FcRn*. Seminars in Immunopathology 31: pp 223-236.

340. Mitchell L.A., Galun E. (2003). *Rectal immunization of mice with hepatitis A vaccine induces stronger systemic and local immune responses than parenteral immunization*. Vaccine 21: pp 1527-1538.

341. Spiekermann G.M., Finn P.W., Ward E.S., Dumont J., Dickinson B.L., Blumberg R.S., Lencer W.I. (2002). *Receptor-mediated immunoglobulin G transport across mucosal barriers in adult life: Functional expression of FcRn in the mammalian lung*. Journal of Experimental Medicine 196: pp 303-310.

342. Yoshida M., Claypool S.M., Wagner J.S., Mizoguchi E., Mizoguchi A., Roopenian D.C., Lencer W.I., Blumberg R.S. (2004). *Human neonatal Fc receptor mediates transport of IgG into luminal secretions for delivery of antigens to mucosal dendritic cells*. Immunity 20: pp 769-783.

343. Yoshida M., Claypool S.M., Wagner J.S., Mizoguchi E., Mizoguchi A., Roopenian P.C., Lencer W.I., Blumberg R.S. (2004). *Human neonatal Fc receptor mediates transport of IgG into luminal secretions for delivery of antigens to mucosal dendritic cells*. Gastroenterology 126: pp A104-A104.

344. Ober R.J., Martinez C., Vaccaro C., Zhou J., Ward E.S. (2004). *Visualizing the site and dynamics of IgG salvage by the MHC class I-related receptor, FcRn*. Journal of Immunology 172: pp 2021-2029.

345. Ober R.J., Martinez C., Lai X., Zhou J., Ward E.S. (2004). *Exocytosis of IgG as mediated by the receptor, FcRn: an analysis at the single-molecule level*. Proceedings of the National Academy of Sciences of the United States of America 101: pp 11076-11081.

346. Kim J., Hayton W.L., Robinson J.M., Anderson C.L. (2007). *Kinetics of FcRn-mediated recycling of IgG and albumin in human: pathophysiology and therapeutic implications using a simplified mechanism-based model*. Clinical Immunology 122: pp 146-155.

347. Balls M., Goldberg A.M., Fentem J.H., Broadhead C.L., Burch R.L., Festing M.F., Frazier J.M., Hendriksen C.F., Jennings M., van der Kamp M.D., Morton D.B., Rowan A.N., Russell C., Russell W.M., Spielmann H., Stephens M.L., Stokes W.S., Straughan D.W., Yager J.D., Zurlo J., van Zutphen B.F. (1995). *The three Rs: the way forward: the report and recommendations of ECVAM Workshop*. Alternatives to laboratory animals 23: pp 838-866.

348. Russell W.M.S., Burch R.L. (1959). *Part One: The Scope of Humane Technique.* The Principles of Humane Experimental Technique. On-line publication: http://altweb.jhsph.edu/pubs/books/humane_exp/het-toc. Altweb - the Alternatives to Animal Testing Web Site, Johns Hopkins Bloomberg School of Public Health, Baltimore. Accessed February 12nd, 2010.

349. Stedronsky E.R. (1994). *Interaction of bile acids and cholesterol with non-systemic agents having hypocholesterolemic properties (Review)*. Biochimica et Biophysica Acta 1210: pp 255-287.

350. Deo A.K., Bandiera S.M. (2008). *Identification of human hepatic cytochrome P450 enzymes involved in the biotransformation of cholic and chenodeoxycholic acid*. Drug Metabolism and Disposition 36: pp 1983-1991.

351. Kobayashi Y., Saiki K., Watanabe F. (1993). *Characteristics of Mass Fragmentation of Steroids by Atmospheric-Pressure Chemical-Ionization Mass-Spectrometry*. Biological & Pharmaceutical Bulletin 16: pp 1175-1178.

352. Rossmann B., Thurner K., Luf W. (2007). *MS-MS fragmentation patterns of cholesterol oxidation products*. Monatshefte für Chemie 138: pp 436-444.

353. Burkard I., Rentsch K.M., von Eckardstein A. (2004). *Determination of 24S-and 27-hydroxycholesterol in plasma by high-performance liquid chromatography-mass spectrometry*. Journal of Lipid Research 45: pp 776-781.

354. Razzazi-Fazeli E., Kleineisen S., Luf W. (2000). *Determination of cholesterol oxides in processed food using highperformance liquid chromatography-mass spectrometry with atmospheric pressure chemical ionisation*. Journal of Chromatography A 896: pp 321-334.

355. Raith K., Brenner C., Farwanah H., Muller G., Eder K., Neubert R.H.H. (2005). *A new LC/APCI-MS method for the determination of cholesterol oxidation products in food*. Journal of Chromatography A 1067: pp 207-211.

356. de Hoffmann E., Strobant V. (2001). *Chapter 6 – Fragmentation Reactions.* Mass Spectrometry – Principles and Application, 2nd ed, *page* 223. John Wiley & Sons, London.

357. Psillakis E., Kalogerakis N. (2003). *Developments in liquid-phase microextraction*. Trac - Trends in Analytical Chemistry 22: pp 565-574.

358. López-Jiménez F.J., Rubio S., Pérez-Bendito D. (2008). *Single-drop coacervative microextraction of organic compounds prior to liquid chromatography: Theoretical and practical considerations*. Journal of Chromatography A 1195: pp 25-33.

359. Bernardo M., Gonçalves M., Lapa N., Mendes B. (2010). *Determination of alkylphenols in eluates from pyrolysis solid residues using dispersive liquid-liquid microextraction*. Chemosphere 79: pp 1026-1032.

360. Hashemi P., Beyranvand S., Mansur R.S., Ghiasvand A.R. (2009). *Development of a simple device for dispersive liquid-liquid microextraction with lighter than water organic solvents: Isolation and enrichment of glycyrrhizic acid from licorice*. Analytica Chimica Acta 655: pp 60-65.

361. Farahani H., Norouzi P., Dinarvand R., Ganjali M.R. (2007). *Development of dispersive liquid-liquid microextraction combined with gas chromatography-mass spectrometry as a simple, rapid and highly sensitive method for the determination of phthalate esters in water samples*. Journal of Chromatography A 1172: pp 105-112.

362. Deutscher Wetterdienst. Climatological data online: http://www.dwd.de/ .Federal Ministry of Transport, Building and Urban Affairs. Accessed during 2009 and 2010.

363. Moeller K., Burgschweiger J. (2008). Wasserversorgungkonzept für Berlin und für das von den BWB versorgte Umland (Entwicklung bis 2040). Report. May, Berliner Wasserbetriebe, Berlin.

364. Cazeneuve C., Pons G., Rey E., Treluyer J.M., Cresteil T., Thiroux G., Dathis P., Olive G. (1994). *Biotransformation of Caffeine in Human Liver-Microsomes from Fetuses, Neonates, Infants and Adults*. British Journal of Clinical Pharmacology 37: pp 405-412.

365. Wu C.X., Witter J.D., Spongberg A.L., Czajkowski K.P. (2009). *Occurrence of selected pharmaceuticals in an agricultural landscape, Western Lake Erie basin*. Water Research 43: pp 3407-3416.

366. Teijon G., Candela L., Tamoh K., Molina-Diaz A., Fernandez-Alba A.R. (2010). *Occurrence of emerging contaminants, priority substances (2008/105/CE) and heavy metals in treated wastewater and groundwater at Depurbaix facility (Barcelona, Spain)*. Science of The Total Environment 408: pp 3584-3595.

367. Huerta-Fontela M., Galceran M.T., Martin-Alonso J., Ventura F. (2008). *Occurrence of psychoactive stimulatory drugs in wastewaters in north-eastern Spain*. Science of The Total Environment 397: pp 31-40.

368. Hakooz N.M.K. (2009). *Caffeine Metabolic Ratios for the In Vivo Evaluation of CYP1A2, N-acetyltransferase 2, Xanthine Oxidase and CYP2A6 Enzymatic Activities*. Current Drug Metabolism 10: pp 329-338.

369. Ullrich D., Compagnone D., Munch B., Brandes A., Hille H., Bircher J. (1992). *Urinary Caffeine Metabolites in Man – Age-Dependent Changes and Pattern in Various Clinical Situations*. European Journal of Clinical Pharmacology 43: pp 167-172.

370. Matamoros V., Arias C., Brix H., Bayona J.M. (2007). *Removal of pharmaceuticals and personal care products (PPCPs) from urban wastewater in a pilot vertical flow constructed wetland and a sand filter*. Environmental Science & Technology 41: pp 8171-8177.

371. Debruyne P.R., Bruyneel E.A., Li X.D., Zimber A., Gespach C., Mareel M.M. (2001). *The role of bile acids in carcinogenesis*. Mutation Research – Fundamental and Molecular Mechanisms of Mutagenesis 480: pp 359-369.

372. Dobbelaere D., Heussler V. (1999). *Transformation of leukocytes by Theileria parva and T. annulata*. Annual Review of Microbiology 53: pp 1-42.

373. Heussler V.T., Machado J., Fernandez P.C., Botteron C., Chen C.G., Pearse M.J., Dobbelaere D.A.E. (1999). *The intracellular parasite Theileria parva protects infected T cells from apoptosis*. Proceedings of the National Academy of Sciences of the United States of America 96: pp 7312-7317.

374. Dobbelaere D.A.E., Fernandez P.C., Heussler V.T. (2000). *Theileria parva: taking control of host cell proliferation and survival mechanisms*. Cellular Microbiology 2: pp 91-99.

375. Goding J. (1996). *Monoclonal Antibodies: Principles and Practice*, 3rd ed. Academic Press, London.

SELBSTÄNDIGKEITSERKLÄRUNG

Hiermit erkläre ich, dass ich die vorliegende Arbeit selbständig verfasst und keine anderen als die angegebenen Quellen und Hilfsmittel verwendet habe. Ich versichere, dass diese Arbeit in dieser oder anderer Form noch keiner anderen Prüfungsbehörde vorgelegt wurde. Der Inhalt der geltenden Promotionsordnung der Mathematisch-Naturwissenschaftlichen Fakultät I der Humboldt Universität zu Berlin vom 01. September 2005 ist mir bekannt.

Berlin, den 24. Februar 2011

José João Dias Carvalho